



CAN UNCLASSIFIED



DRDC | RDDC  
technologysciencetechnologie

# Propeller Optimization for Noise Reduction

Chris Arisman  
Lloyd's Register Applied Technology Group

Prepared by:  
Lloyd's Register Applied Technology Group  
237 Brownlow Ave. Suite 200  
Dartmouth (Nova Scotia) B3B 2C7  
Canada  
Report No.: TR-21-24 Rev.03  
Control Number: 19.28074.1125  
PSPC Contract Number: W7707-186266/001/HAL  
Technical Authority: Matthew Gauthier, Defence Scientist  
Contractor's date of publication: February 2022

**Terms of Release:** This document is approved for public release.

The body of this CAN UNCLASSIFIED document does not contain the required security banners according to DND security standards. However, it must be treated as CAN UNCLASSIFIED and protected appropriately based on the terms and conditions specified on the covering page.

**Defence Research and Development Canada**

**Contract Report**  
DRDC-RDDC-2022-C195  
May 2022

CAN UNCLASSIFIED

## CAN UNCLASSIFIED

### IMPORTANT INFORMATIVE STATEMENTS

This document was reviewed for Controlled Goods by Defence Research and Development Canada using the Schedule to the *Defence Production Act*.

Disclaimer: This document is not published by the Editorial Office of Defence Research and Development Canada, an agency of the Department of National Defence of Canada but is to be catalogued in the Canadian Defence Information System (CANDIS), the national repository for Defence S&T documents. Her Majesty the Queen in Right of Canada (Department of National Defence) makes no representations or warranties, expressed or implied, of any kind whatsoever, and assumes no liability for the accuracy, reliability, completeness, currency or usefulness of any information, product, process or material included in this document. Nothing in this document should be interpreted as an endorsement for the specific use of any tool, technique or process examined in it. Any reliance on, or use of, any information, product, process or material included in this document is at the sole risk of the person so using it or relying on it. Canada does not assume any liability in respect of any damages or losses arising out of or in connection with the use of, or reliance on, any information, product, process or material included in this document.

© Her Majesty the Queen in Right of Canada (Department of National Defence), 2022

© Sa Majesté la Reine en droit du Canada (Ministère de la Défense nationale), 2022

CAN UNCLASSIFIED

---

# Propeller Optimization for Noise Reduction

**Report for:** Matthew Gauthier

---

**Name of company:** DRDC Atlantic

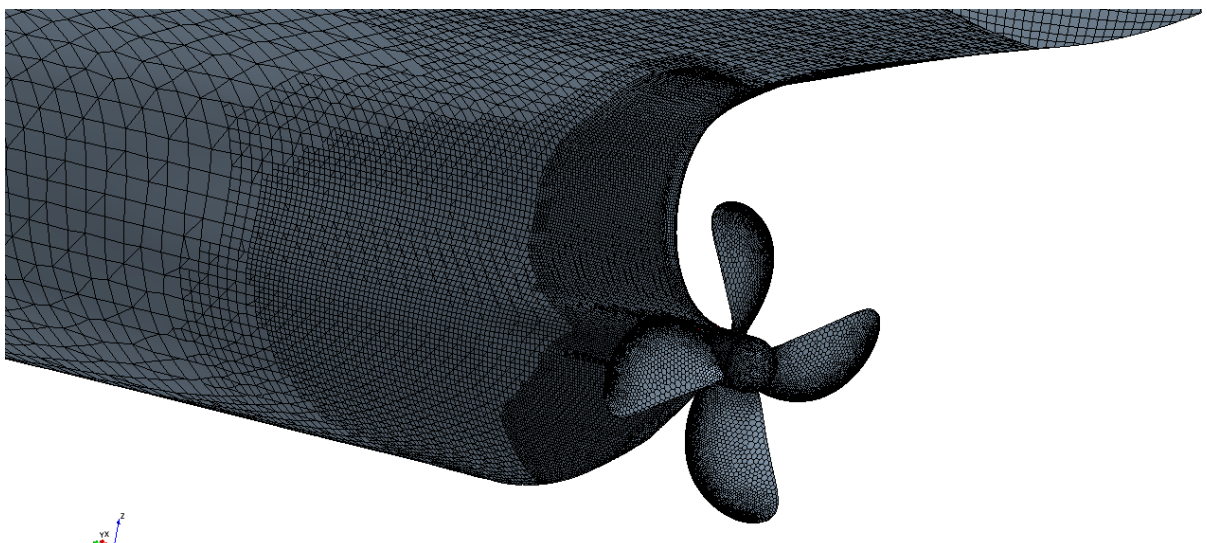
---

**Report no:** TR-21-24 Rev03

---

17 February 2022

---



**Prepared for:  
Matthew Gauthier  
DRDC Atlantic  
9 Grove Street  
Dartmouth, NS  
Canada  
B3A 3C5**

**Control Number:  
19.28074.1125**

**Authored by:  
C. Arisman<sup>1</sup>  
<sup>1</sup>Lloyd's Register Applied Technology Group**

**Martec Limited is a member of the Lloyd's Register Group, doing business as the Applied  
Technology Group**

---

# Revision Control

Revision	Revision Date
Interim Report	31 March 2021
Final Report	29 July 2021
Rev 02	10 November 2021
Rev 03	17 February 2022

---

# Proprietary Notice

This report was prepared under **W7707-186266/001/HAL** for **DRDC Atlantic**.

The information contained herein may be used and/or further developed by **DRDC Atlantic** for their purposes only.

Complete use and disclosure limitations are contained in **W7707-186266/001/HAL**.


---

# Signature Page

Propeller Optimization for Noise Reduction

Prepared by:  \_\_\_\_\_ Date: 17 February 2022


Chris Arisman  
Research Engineer, Explosion and Fluid Dynamics

Reviewed by:  \_\_\_\_\_ Date: 17 February 2022

Derrick Alexander  
Lead Technical Specialist, Explosion and Fluid Dynamics

Reviewed by:  \_\_\_\_\_ Date: 17 February 2022

Tamunoiyala S. Koko  
Team Leader, Risk & Reliability

Approved by:  \_\_\_\_\_ Date: 17 February 2022

Dave Whitehouse, P.Eng.  
Technical Manager

---

# Executive Summary

It is of interest to Transport Canada and Defense Research and Development Canada (DRDC) Atlantic to show a general approach for reducing the noise radiated by commercial shipping vessels. The objective of this task is to undertake propeller optimization design studies for two typical commercial vessels, operating in the west coast of Canada, to determine potential underwater radiated noise reduction benefits.

This report details the calculation methodology used to obtain the ship wake fields for both ships: a 159,000 DWT tanker and a ferry. The ship wake fields are required to account for the effect of the ship wake on the propeller noise calculation and are an integral component in the optimization routine. The ship wake fields are calculated using a coupled Computational Fluid Dynamics (CFD) and a potential flow approach. Results of the optimization study for both vessels are included in Appendix A and B for the 159,000 DWT tanker and the ferry respectively.

In addition to the optimization, CFD simulations of the vessels are conducted for comparison to speed-power predictions. These simulations utilize a sliding mesh methodology for the propeller. The ferry shows better agreement between the CFD and the speed power predictions, with a difference of 8% for the shaft power. The tanker shows a difference of 20% in the shaft power, but the results show oscillations in the forward speed and free surface wake, suggesting that simulation setup refinements may be required to achieve better predictions.



---

# Contents

<b>1.</b>	<b>Introduction .....</b>	<b>1</b>
<b>2.</b>	<b>Wake Field Prediction.....</b>	<b>2</b>
2.1.	Coupling Methodology.....	2
2.2.	Procal Setup .....	2
2.3.	Star-CCM+ Setup .....	2
2.4.	159,000 DWT Tanker.....	3
2.4.1.	Procal Conditions, Geometry, and Mesh .....	3
2.4.2.	Star-CCM+ Conditions, Geometry and Mesh .....	3
2.5.	Ferry .....	5
2.5.1.	Procal Conditions, Geometry, and Mesh .....	5
2.5.2.	Star-CCM+ Conditions, Geometry and Mesh .....	6
2.6.	Results .....	8
2.6.1.	159,000 DWT tanker.....	8
2.6.2.	Ferry .....	9
<b>3.</b>	<b>Speed Power Predictions .....</b>	<b>11</b>
3.1.	Star-CCM+ Setup .....	11
3.2.	Conditions, Geometry, and Mesh .....	11
3.2.1.	159,000 DWT Tanker .....	11
3.2.2.	Ferry .....	17
3.3.	Results .....	21
3.3.1.	159,000 DWT Tanker .....	22
3.3.2.	Ferry .....	23
<b>4.</b>	<b>Conclusion .....</b>	<b>25</b>
<b>5.</b>	<b>References .....</b>	<b>26</b>

## Appendix A 159,000 DWT Propeller Optimization Report

## Appendix B Ferry Propeller Optimization Report

# List of Figures

Figure 2-1: 159,000 DWT tanker propeller geometry and mesh, contours indicate relative face area .....	3
Figure 2-2: 159,000 DWT tanker geometry .....	4
Figure 2-3: 159,000 DWT tanker mesh .....	5
Figure 2-4: Ferry propeller geometry and mesh, contours indicate relative face area .....	6
Figure 2-5: Ferry geometry .....	7
Figure 2-6: Ferry hub geometry .....	7
Figure 2-7: Ferry mesh .....	8
Figure 2-8: 159,000 DWT tanker wake results, design draught (normalized velocity contours) .....	9
Figure 2-9: 159,000 DWT tanker wake results, ballast draught (normalized velocity contours) .....	9
Figure 2-10: Ferry wake results, design draught (normalized velocity contours) .....	10
Figure 3-1: 159,000 DWT tanker CFD domain .....	12
Figure 3-2: 159,000 DWT tanker mesh .....	13
Figure 3-3: 159,000 DWT tanker hull wall Y+ .....	14
Figure 3-4: 159,000 DWT tanker propeller geometry .....	15
Figure 3-5: 159,000 DWT tanker propeller mesh .....	16
Figure 3-6: 159,000 DWT tanker propeller wall Y+ .....	16
Figure 3-7: Ferry CFD domain .....	17
Figure 3-8: Ferry Bay mesh .....	18
Figure 3-9: Ferry hull wall Y+ .....	19
Figure 3-10: Ferry propeller geometry .....	20
Figure 3-11: Ferry propeller mesh .....	21
Figure 3-12: Ferry propeller wall Y+ .....	21
Figure 3-13: 159,000 DWT tanker free surface .....	22
Figure 3-14: 159,000 DWT tanker propeller axial velocity .....	23
Figure 3-15: Ferry free surface .....	24
Figure 3-16: Ferry propeller axial velocity .....	24

# List of Tables

Table 2-1: Generic propeller characteristics .....	3
Table 2-2: 159,000 DWT tanker ship particulars .....	4
Table 2-3: Ferry propeller characteristics .....	6
Table 2-4: Ferry ship particulars .....	7
Table 3-1: 159,000 DWT Tanker Comparisons .....	22
Table 3-2: Ferry speed power comparisons .....	23

## 1. Introduction

In a previous task, Defence Research and Development Canada (DRDC) Atlantic, in collaboration with Transport Canada, undertook a redesign of the ORCA-Class ship propellers to improve the noise characteristics of the vessel. The project was seen as an opportunity for Transport Canada to show a general approach for silencing commercial shipping. A design optimization study was carried out to increase the cavitation inception speed of the vessel and thereby reduce the underwater noise generation. This resulted in the development of a new propeller design with an improved cavitation inception speed for the ORCA class ship propellers. The current task seeks to undertake similar design optimization studies for typical commercial ships operating in the West Coast of Canada, in order to determine potential underwater radiated noise (URN) reduction benefits that can be achieved for such vessels.

This report details the ship wake field calculation methodology and results for two vessels: a 159,000 DWT tanker and a ferry. An additional report summarizing the propeller optimization results are included in Appendix A and B for the 159,000 DWT tanker and the ferry respectively.

In addition to the optimization, a CFD simulation of the vessels was conducted using a sliding mesh methodology for the propeller. The results of these simulations were compared to speed-power predictions performed by Maritime Research Institute Netherlands (MARIN).

## 2. Wake Field Prediction

This section details the coupling methodology used to compute the wake fields for use in the propeller optimization. Wake fields were computed using Computational Fluid Dynamics (CFD) simulations utilizing Star-CCM+ coupled with potential flow simulations utilizing Procal for the propeller. The general coupling methodology is described in Section 2.1, the Procal setup in Section 2.2, the Star-CCM+ setup in Section 2.3, geometry and numerical setup for the 159,000 DWT tanker and ferry in Sections 2.4 and 2.5 respectively, and the results presented in Section 2.6.

### 2.1. Coupling Methodology

The wake field was simulated by coupling a CFD code, Star-CCM+ 2020.1 (build 15.02.007) [1], with a potential flow code, Procal v2218 [2], through the use of java macros. The flow around the hull was simulated in Star-CCM+ with the propeller forces obtained from Procal. An outline of the coupling routine is as follows:

1. Simulate the propeller in Procal with a nominal wake field
2. Extract the propeller forces from Procal for use in Star-CCM+
3. Simulate the flow around the hull with Star-CCM+
4. Extract the wake field from Star-CCM+ for use in Procal
5. Update the Procal simulation with the new wake field
6. Repeat steps 2 through 5 until wake field is converged

The routine is considered converged when the wake field changes by less than 2% between iterations. The difference is defined as the sum of the absolute difference of each individual point in the wake field:

$$\sum^n \frac{|W_{ni} - W_{ni-1}|}{|W_{ni-1}|} \times 100\% < 2.0\% \quad 2-1$$

where  $n$  is the number of wake field entries,  $W$ , and  $i$  is the iteration number.

### 2.2. Procal Setup

The propeller forces were sampled in both space and time to arrive at an average field for use in the CFD simulation. Forces were averaged in time over one rotation of the propeller with samples being taken every 6 degrees of rotation for a total of 60 positions. In space, the propeller field was sampled in 10 equally spaced radial positions every 10 degrees for a total of 100 sample points in the propeller disk.

### 2.3. Star-CCM+ Setup

In the Star-CCM+ simulation, the propeller forces were incorporated using a virtual disk model with a volume equivalent to the swept volume of the propeller. The forces from the Procal simulation were applied to the virtual disk domain using a momentum source to capture the influence of the propeller. Turbulence was modelled using the k-omega SST turbulence model [3] with the all y+ wall treatment. Simulations were carried out until steady state. Self-propulsion is not modelled in these cases, the ship was assumed to be moving at a fixed forward speed during the entire procedure. Second order schemes were used for the spatial discretization. Seawater properties were taken at 15°C.

## 2.4. 159,000 DWT Tanker

The Procal setup specific to the 159,000 DWT Tanker provided by the operator [4] is described in Section 2.4.1 and the Star-CCM+ setup in Section 2.4.2.

### 2.4.1. Procal Conditions, Geometry, and Mesh

The information provided by the operator was insufficient to fully model the propeller for the ship. MARIN therefore provided the geometry for a Wageningen B-series propeller with the same size and thrust characteristics as the tanker propeller. The propeller geometry and mesh are shown in Figure 2-1 and the characteristics are listed in Table 2-1. Thirty panels were used in both directions for the blade mesh.

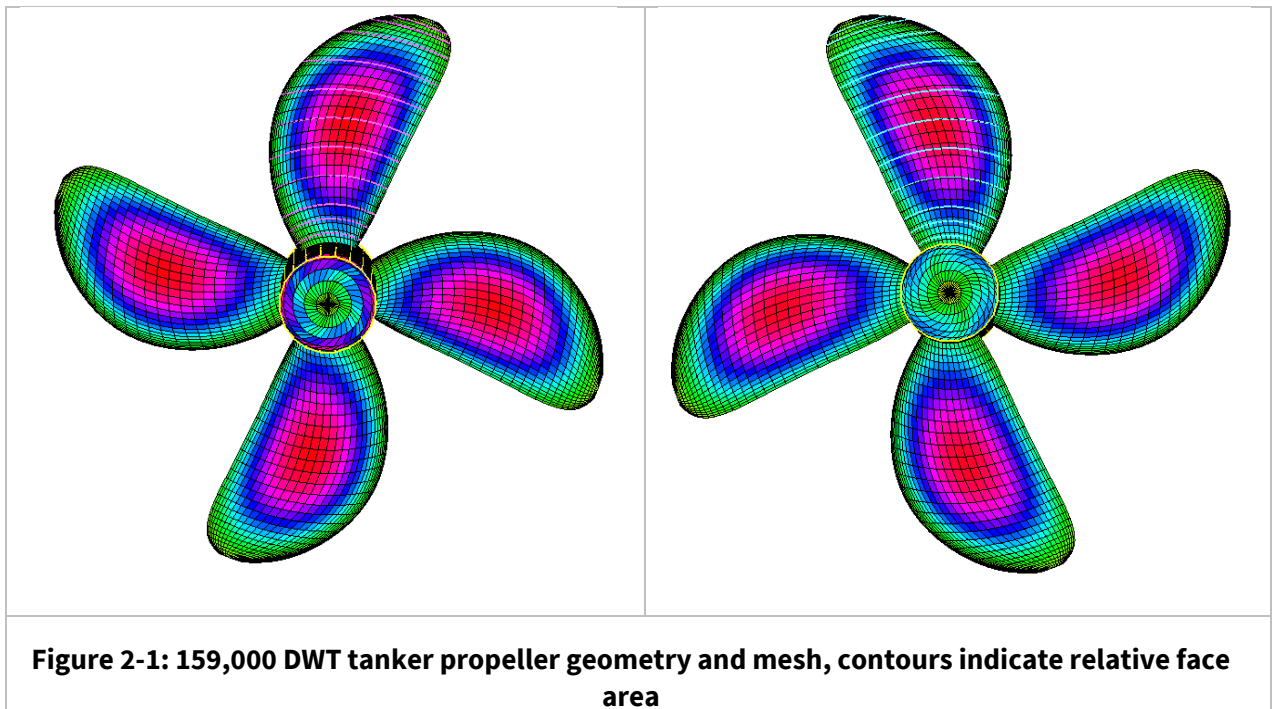


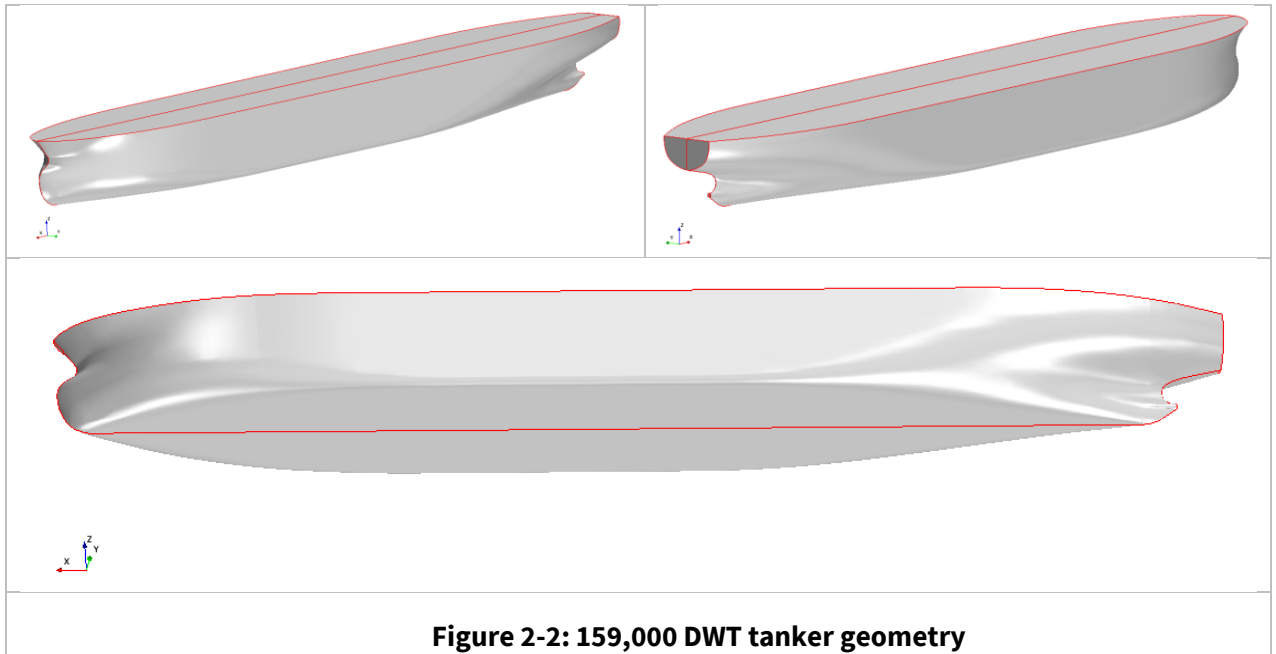
Figure 2-1: 159,000 DWT tanker propeller geometry and mesh, contours indicate relative face area

Table 2-1: Generic propeller characteristics

Characteristics	Value
Diameter (m)	8.2
Hub Diameter (m)	1.38
RPM	91

### 2.4.2. Star-CCM+ Conditions, Geometry and Mesh

The hull geometry for the 159,000 DWT tanker was modelled from the lines plan provided by the operator [4] and is shown in Figure 2-2. The ship particulars are listed in Table 2-2.



**Figure 2-2: 159,000 DWT tanker geometry**

The ship particulars including the length between perpendiculars (Lpp) and length at the waterline (Lwl) for the 159,000 DWT tanker are shown in Table 2-2.

**Table 2-2: 159,000 DWT tanker ship particulars**

Characteristic	Value
Lpp (m)	264
Lwl (m)	269
Mass (kg)	$1.704 \times 10^8$

Two draught configurations were considered:

- Design: draught = 16.0 m, trim = 0 m
- Ballast: draught = 9.24 m, trim = -2.78

Both draughts were simulated at a forward speed of 12 knots.

The CFD domain was 1136 m in length, 1136 m wide, and 726 m tall and was meshed using hexahedral elements with a minimum cell dimension of 0.27 m resulting in a grid that consisted of approximately 2.7 million cells. Cells were concentrated around the hull and the aft of the ship in the wake region. Inflation layers were added to the propeller virtual disk domain to ensure a good transition between domains with minimal numerical diffusion. Representative views of the mesh are shown in Figure 2-3.

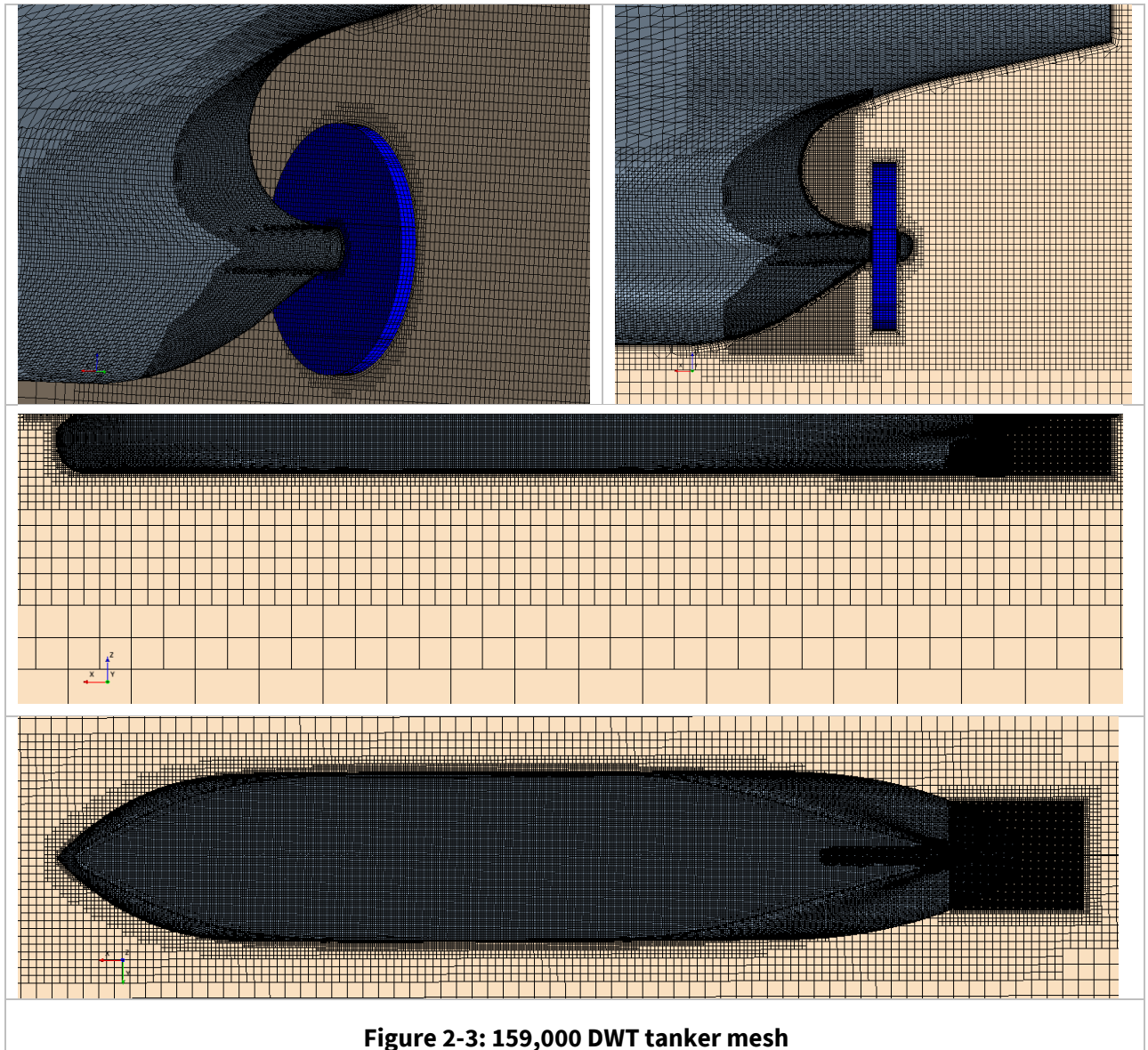


Figure 2-3: 159,000 DWT tanker mesh

## 2.5. Ferry

The Procal setup specific to the ferry is described in Section 2.5.1 and the Star-CCM+ setup in Section 2.5.2

### 2.5.1. Procal Conditions, Geometry, and Mesh

The ferry propeller model was provided by MARIN based on the information provided by the operator. While the actual propeller is a variable pitch propeller, only a single pitch was considered in this work. The propeller geometry and mesh are shown in Figure 2-4 and the characteristics are listed in Table 2-3. Thirty panels were used in both directions for the blade mesh. The propeller blade pitch was assumed constant.

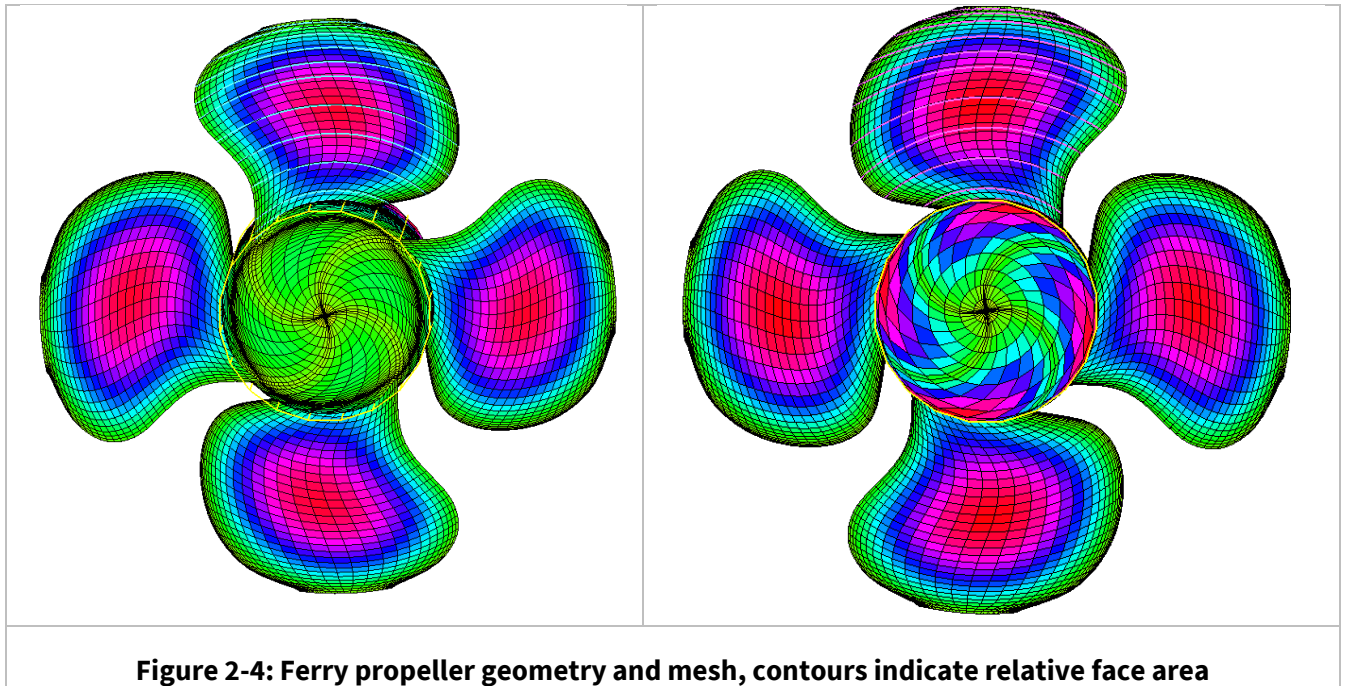


**Figure 2-4: Ferry propeller geometry and mesh, contours indicate relative face area**

**Table 2-3: Ferry propeller characteristics**

Characteristics	Value
Diameter (m)	3.81
Hub Diameter (m)	0.76
RPM	195

### 2.5.2. Star-CCM+ Conditions, Geometry and Mesh

The hull geometry for the ferry was modelled from the lines plan provided by the operator [5] and is shown in Figure 2-5. The ship particulars are listed in Table 2-4. The ferry has two propellers, one for each direction of travel. The front, stationary propeller geometry was not modelled. It is not expected that the front propeller will strongly influence the wake results for the rear propeller.



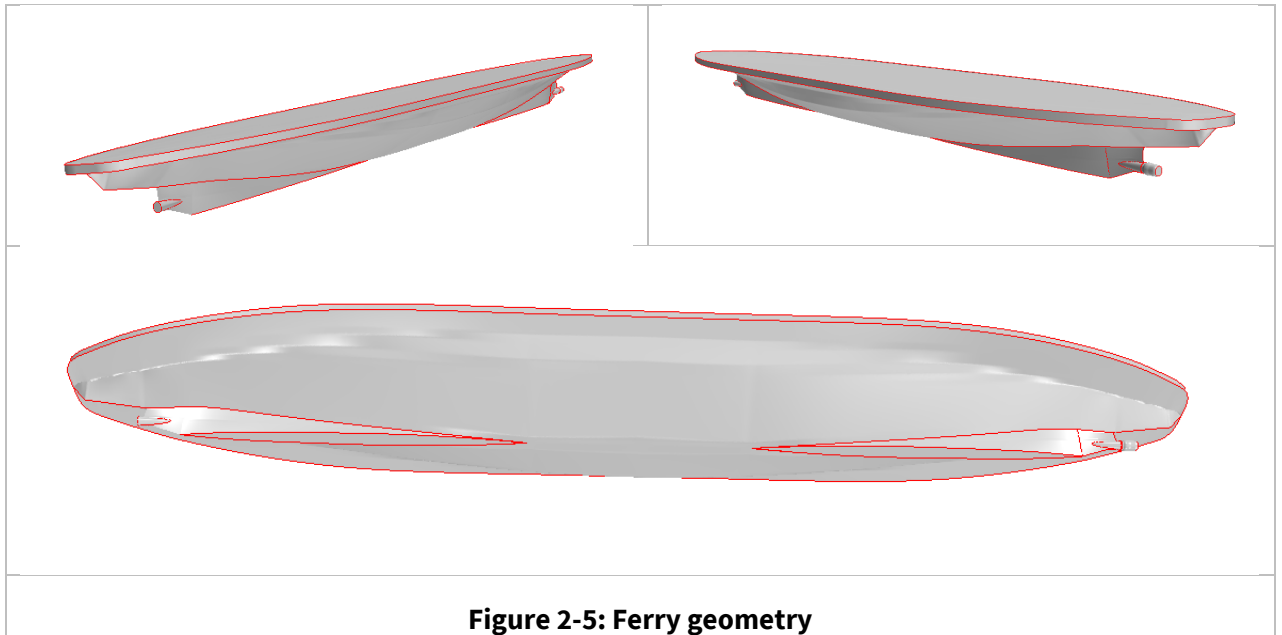


**Figure 2-5: Ferry geometry**

**Table 2-4: Ferry ship particulars**

Characteristic	Value
Lpp (m)	127.2
Mass (kg)	5,595,220

The propeller hub was modelled in Star-CCM+ based on the drawings provided by the operator [6] and is shown in Figure 2-6. Approximations of the curves had to be made as they were not clearly dimensioned on the drawing.

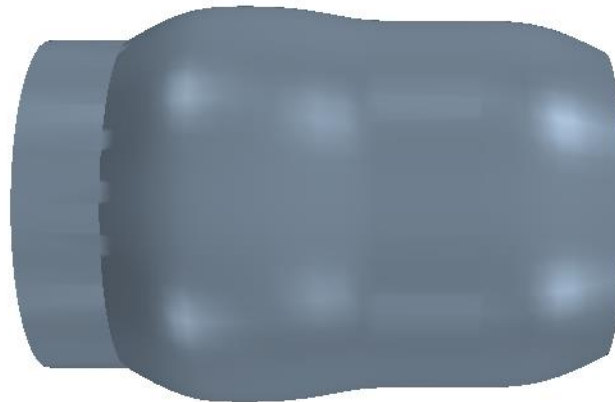
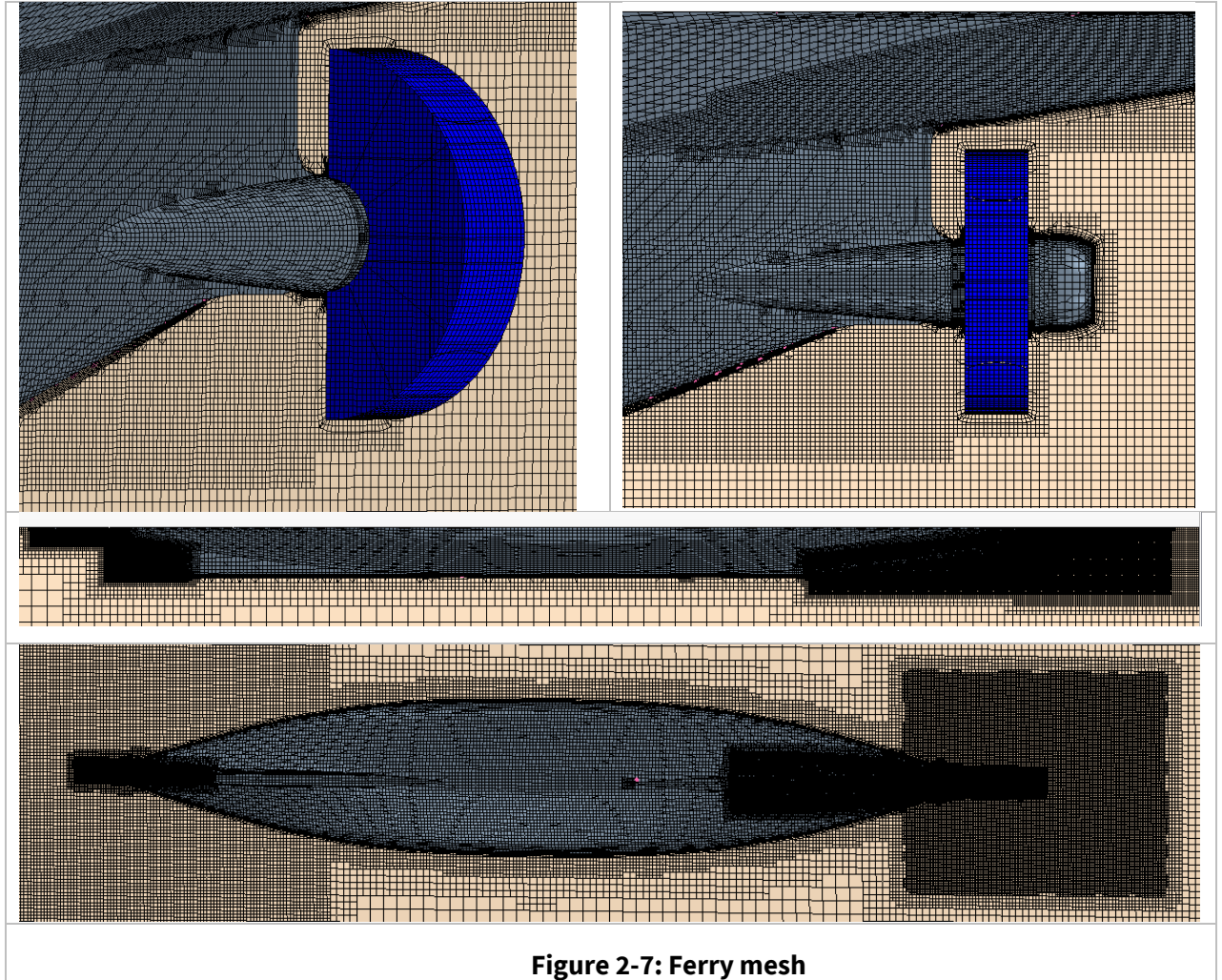


**Figure 2-6: Ferry hub geometry**

The wake field was calculated at the design draught of 5.92 m and speed of 20.5 knots.

The CFD domain was 1136 m in length, 1136 m wide, and 726 m tall and was meshed using hexahedral elements with a minimum cell dimension of 0.27 m resulting in a grid that consists of approximately 2.7 million cells. Cells were concentrated around the hull and the aft of the ship in the wake region. Inflation layers were added to the propeller virtual disk domain to ensure a good transition between domains with minimal numerical diffusion. Representative views of the mesh are shown in Figure 2-7.

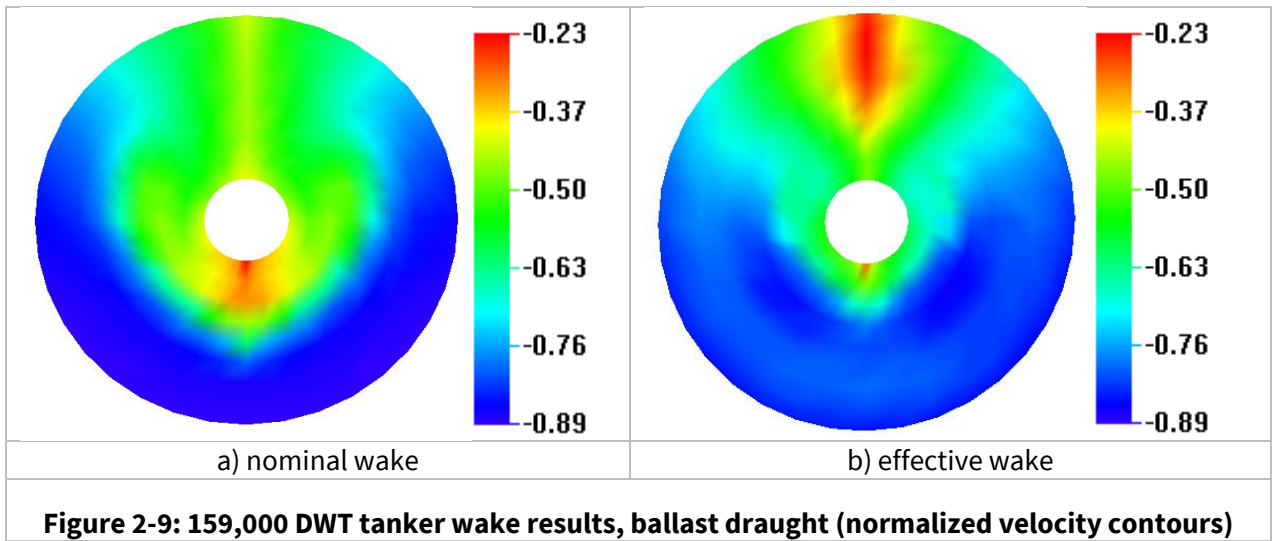
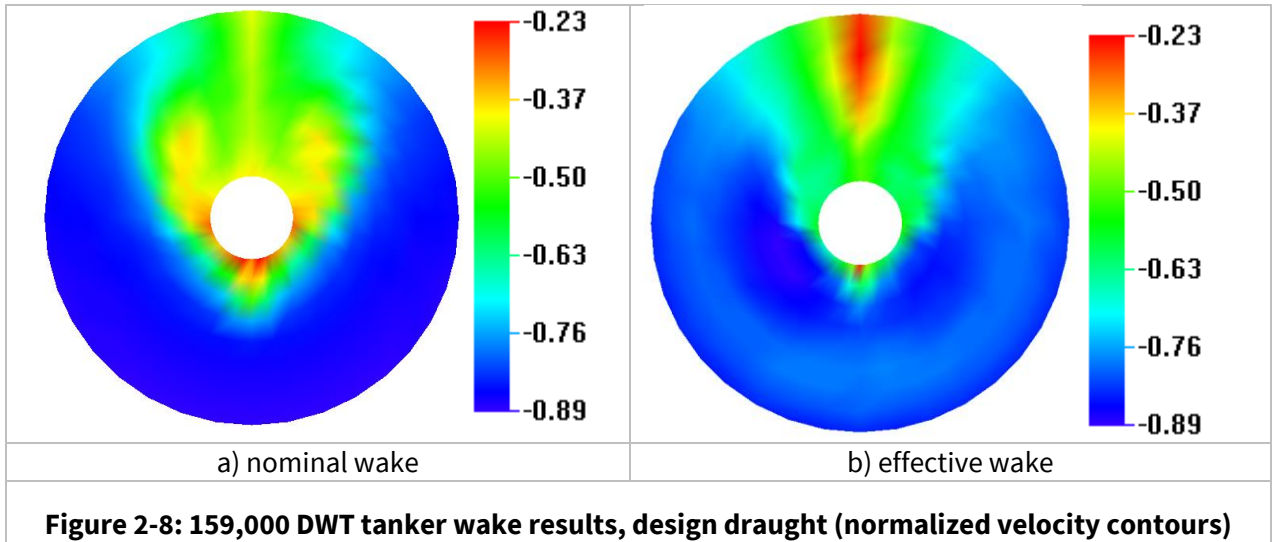


## 2.6. Results

Wake field results for the 159,000 DWT tanker and ferry are presented in Sections 2.6.1 and 2.6.2 respectively.

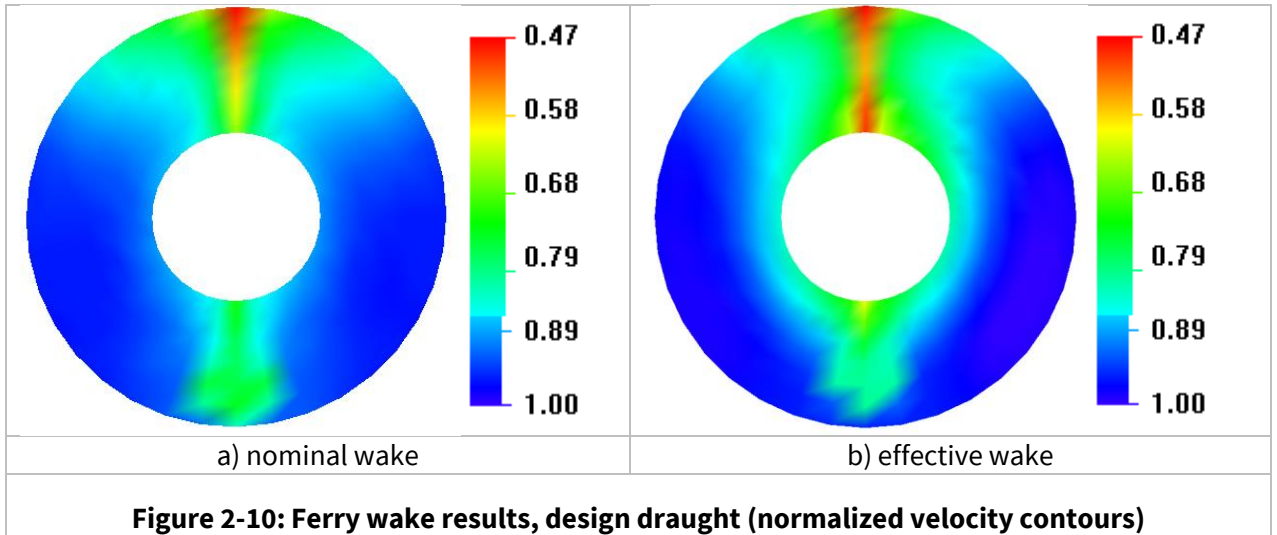
### 2.6.1. 159,000 DWT tanker

Wake field results for the design draught are shown in Figure 2-8 and the ballast draught in Figure 2-9. Included in the figures are the nominal and effective wakes. The images are oriented from the stern looking forward. The nominal wake is the inflow to the propeller plane when the propeller is not modelled. The effective wake is the wake with the propeller operating and accounts for the interaction between the propeller and the hull. Note that the effective wake is the CFD calculated wake minus the propeller induced velocities from Procal. Wake values are normalized by the ship speed of 12 knots.



### 2.6.2. Ferry

Wake field results for the design draught are shown in Figure 2-10. Wake values are normalized by the ship speed of 20.5 knots.



### 3. Speed Power Predictions

In addition to the wake fields, a speed-power simulation was performed. This was done for one set of conditions with the results compared to the predictions made using the Holtrop-Mennen method, detailed in Appendix A and B for the 159,000 DWT tanker and ferry respectively.

#### 3.1. Star-CCM+ Setup

The speed-power simulation was performed using Star-CCM+ 2020.1 (build 15.02.007). The propeller motion was modelled using a sliding mesh methodology. In the sliding mesh method, the propeller domain is modelled separate from the ship domain and is rotated independently. To accomplish this, the mesh interface between the propeller domain and overall domain is allowed to slide with the cells on either side being mapped and quantities interpolated across the interface. Turbulence was modelled using the  $k-\omega$  SST (Menter) RANS model.

The ship was allowed to translate forward/backward with fixed heave and pitch. This was done to simplify the numerical and meshing setups and reduce the run time of the simulations. The simulation therefore corresponds to a specific loading condition that would result in the fixed pitch and heave. The propeller rotation rate was fixed at the design rate and the ship was allowed to accelerate due to the thrust from the propeller. The simulation was run until the ship reached a steady speed. Since the simulations are being run to steady forward speed, the specific values of the moments of inertia were not required as they only dictate how quickly the ship accelerated and did not influence the final result.

The general simulation setup is summarized as follows:

- Transient RANS with  $k-\omega$  SST (Menter) model.
- Star-CCM+'s all  $y^+$  wall function used on all physical walls.
- 2nd order discretization.
- Free surface modeled with volume of fluid approach.
- Numerical wave damping at domain boundaries to prevent wake wave reflections.
- Ship motion modeled using one degree of freedom model.
- Propeller motion modeled using sliding mesh interface.

#### 3.2. Conditions, Geometry, and Mesh

Simulation setup specific to the 159,000 DWT tanker and the ferry are described in Sections 3.2.1 and 3.2.2 respectively.

##### 3.2.1. 159,000 DWT Tanker

For the 159,000 DWT tanker the propeller rotation rate was set to 91 RPM. The design draught was 16.0 m on even keel. The Holtrop-Mennen method predicted a forward speed of 7.97 m/s (15.5 knots) at these conditions (see Appendix A).

The 159,000 DWT tanker CFD domain was 1336 m in length, 1136 m wide, and 726 m tall and is shown in Figure 3-1. Velocity inlet boundary conditions were used for the inflow, top, and sides, symmetry for the bottom, and pressure outlet for the outflow. The hull and propeller walls were no-slip and used Star-CCM+'s All  $y^+$  wall function, which switches between a low  $y^+$  and high  $y^+$  mode depending on the cell near wall spacing.

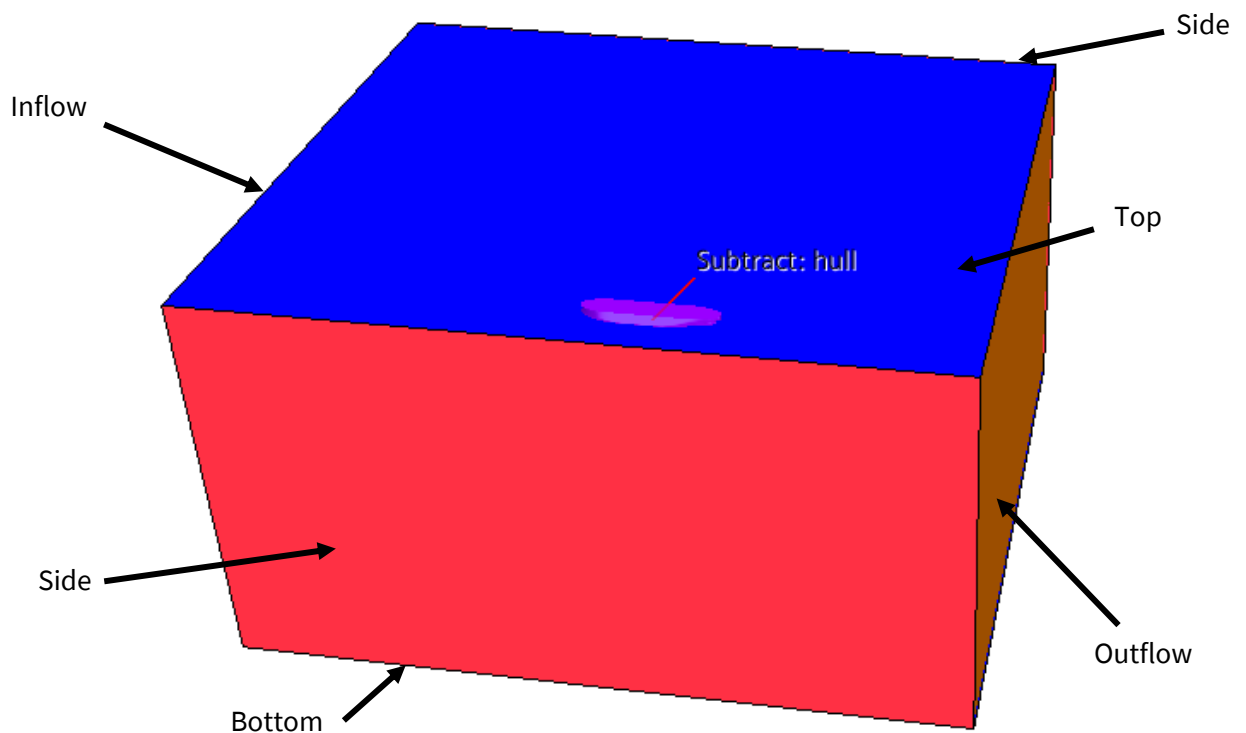


**Figure 3-1: 159,000 DWT tanker CFD domain.**

The same hull model from Section 2.4.2 was used. Star-CCM+'s trimmer style (hexahedral dominant) mesh was used for the overall domain mesh. Refinement regions were added around the hull and at the aft and stern. The free surface was also refined utilizing thin, flat cells to properly resolve the ship wake. The minimum cell dimension in the free surface was 0.71 m. A minimum cell dimension of 0.069 m was used around the hull. Prism layers around the hull were extruded from a first cell height of 0.005 m to an overall prism layer thickness of 0.28 m. A total of 9 prism layers were used. The overall domain consisted of a total of 4.2 million cells. Representative images of the mesh are shown in Figure 3-2.

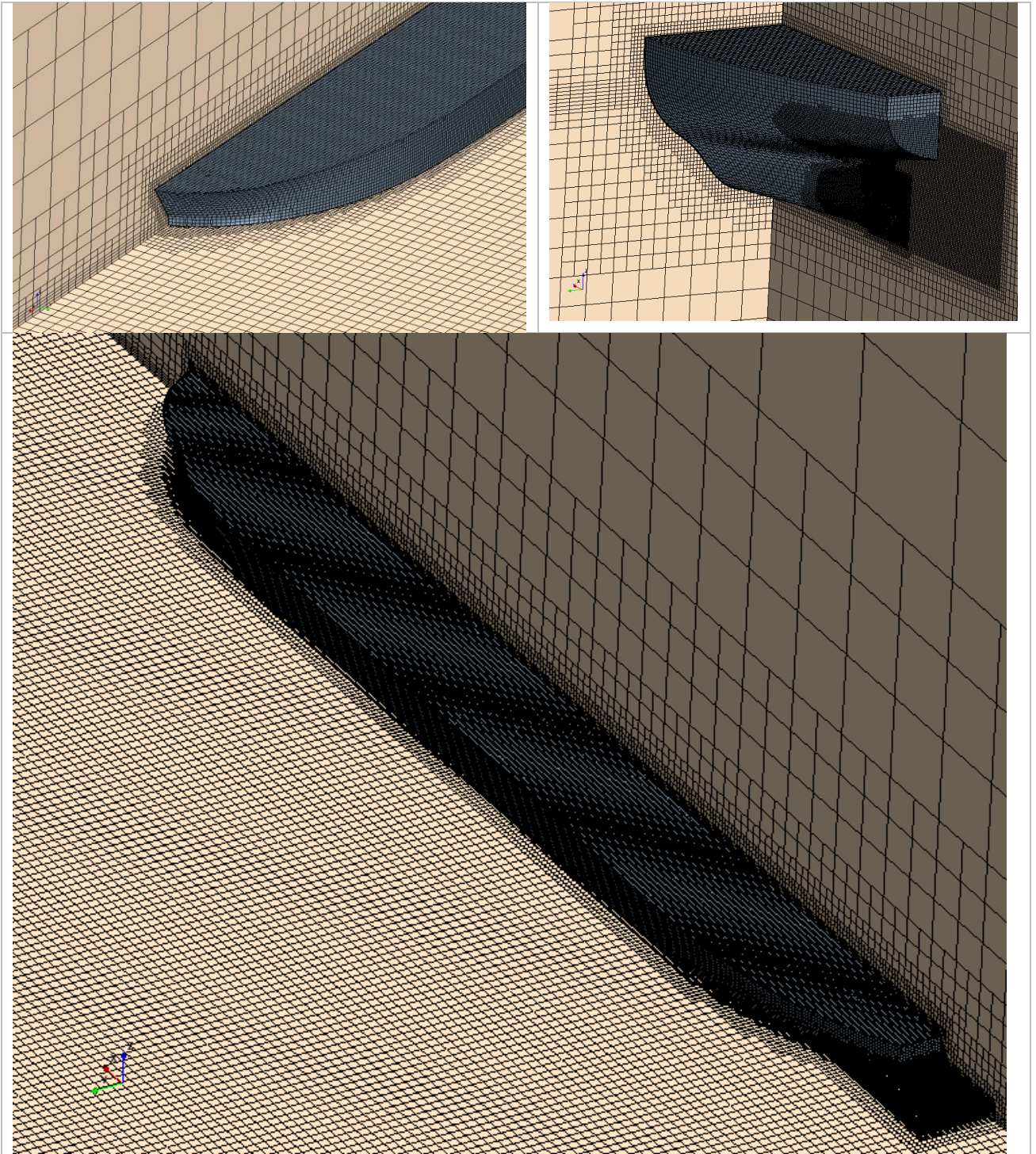


**Figure 3-2: 159,000 DWT tanker mesh.**

A histogram of the wall  $y^+$  values for the hull once the ship had reached a steady speed is shown in Figure 3-3. The bulk of the  $y^+$  values were between 200 – 400 and 1 - 70 which is acceptable for the All  $Y^+$  wall function used.

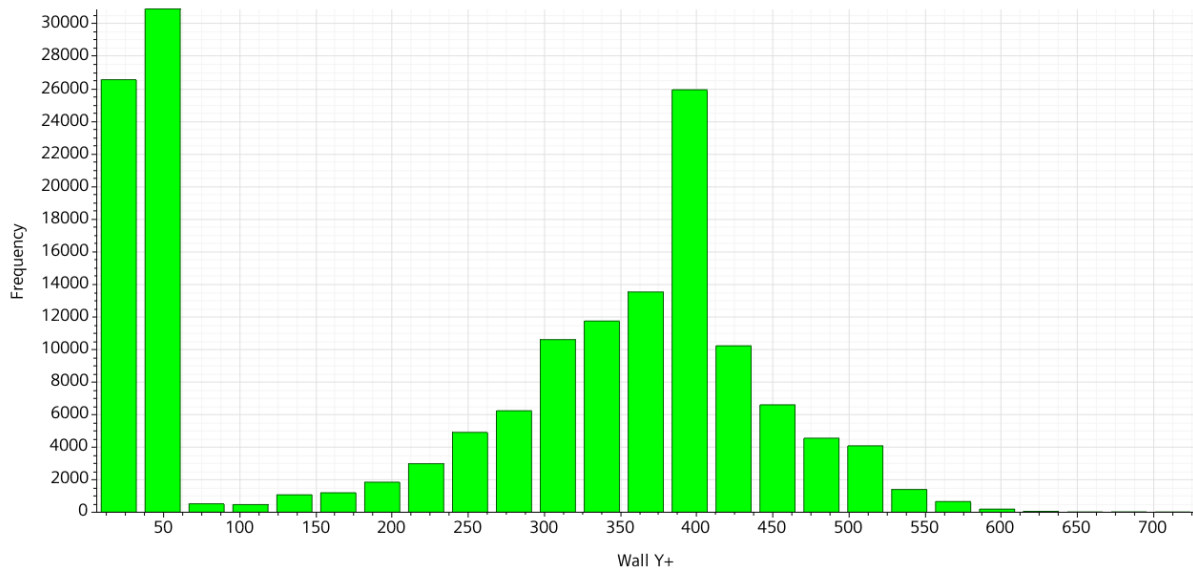


**Figure 3-3: 159,000 DWT tanker hull wall Y+.**

The propeller geometry can be seen in Figure 3-4. The propeller domain was based on the propeller radius,  $R_{prop}$ , with a domain radius equal to  $1.5 R_{prop}$ . The domain extended 1.2 m upstream of the propeller center and 2.4 m downstream.



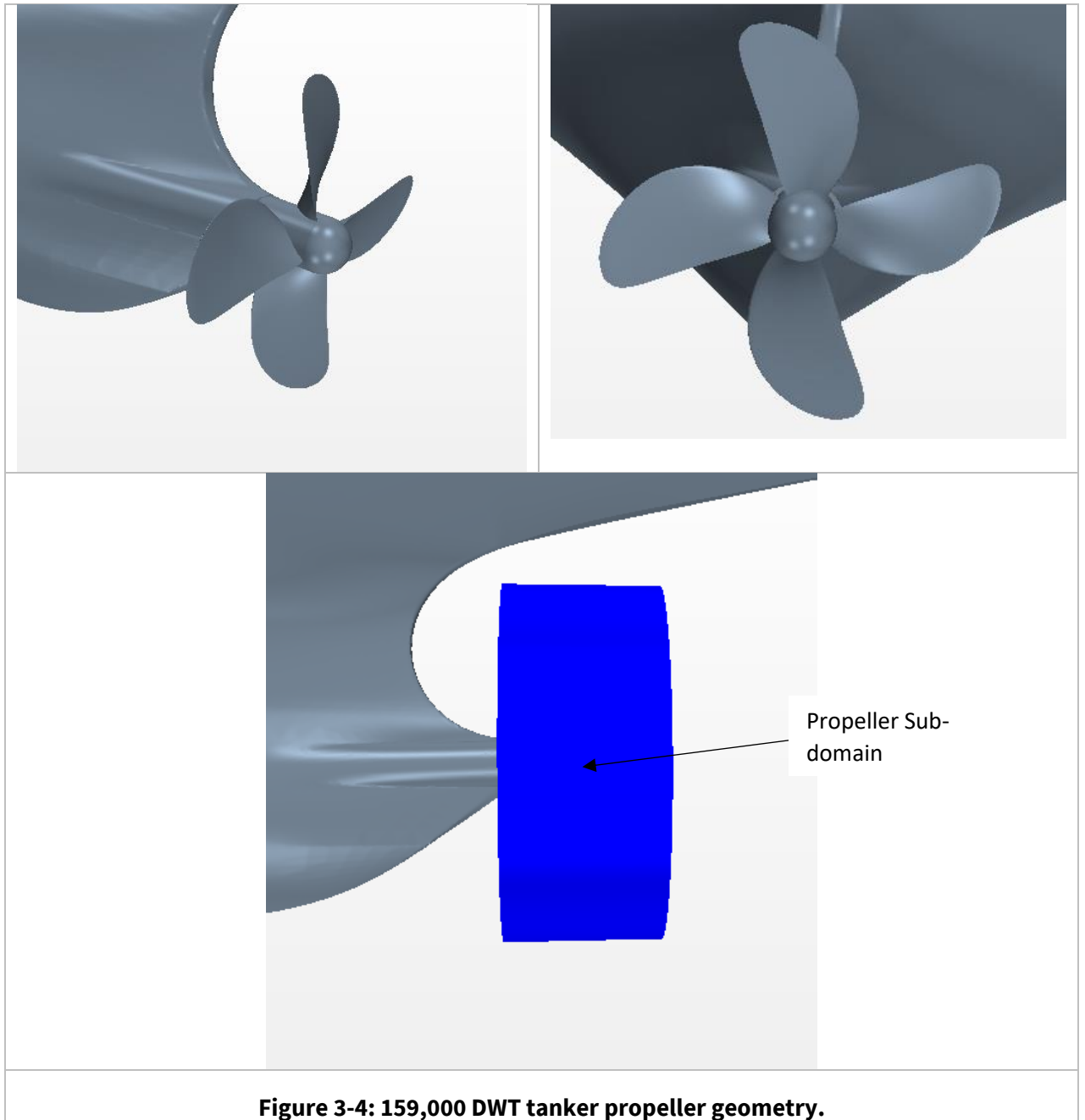


**Figure 3-4: 159,000 DWT tanker propeller geometry.**

The propeller sub-domain mesh was generated using a trimmer style (hexahedral dominant) mesh. The propeller target cell dimension was 0.064 m with a minimum cell dimension of 0.004 m. In order to capture the boundary layer effects, prism layers were extruded with a first cell height of 0.002 m and a total thickness of 0.04 m. A total of 5 prism layers were utilized. The shaft was meshed with a minimum cell dimension of 0.04 m and two prism layers with a total thickness of 0.02 m. The minimum cell dimension around the interface was set to be 0.14 m in an attempt to ensure a good transition between the overall domain and the rotating sub-domain. A total of 9 prism layers were used. The propeller domain consisted of a total of 1.5 million cells. Representative images of the mesh are shown in Figure 3-5.

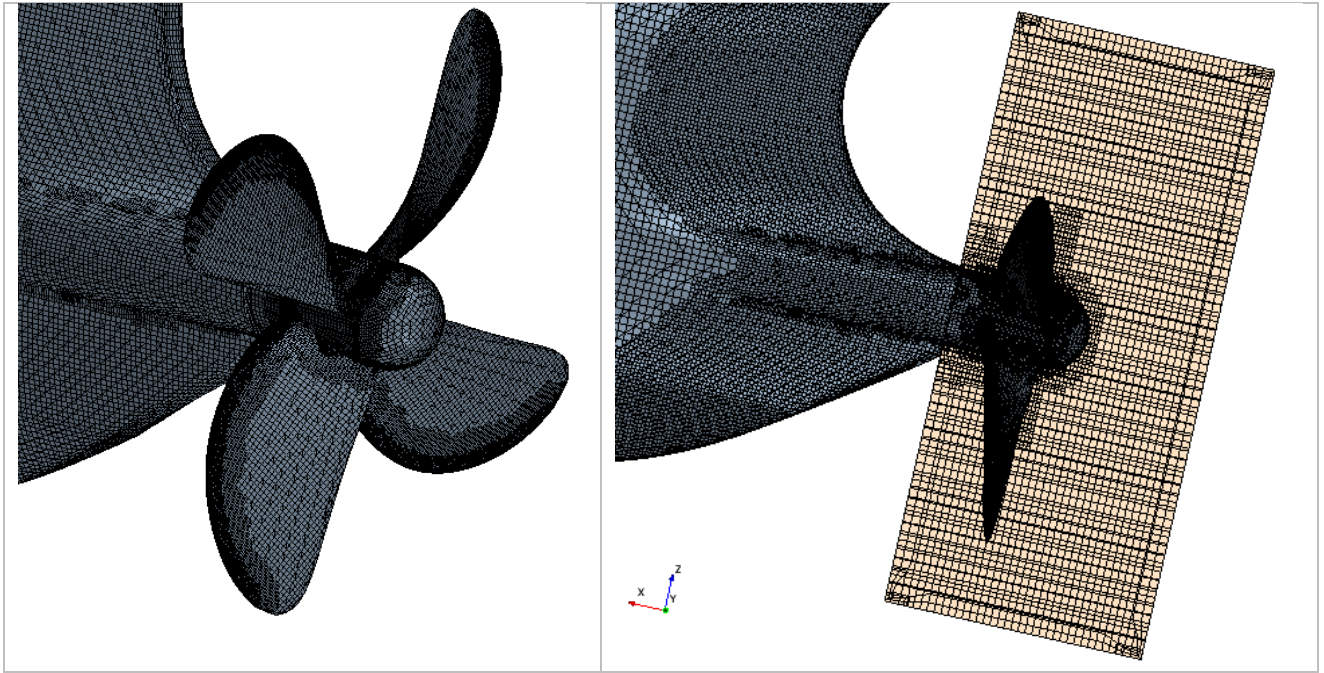


**Figure 3-5: 159,000 DWT tanker propeller mesh.**

A histogram of the wall  $y^+$  values for the propeller is shown in Figure 3-6. The  $y^+$  values show a wider spread than is ideal, with values exceeding 1200. This is due to the physical rotation of the propeller causing high relative velocities in the fluid near the wall. The bulk of the cells were in the 100 – 400 range which is acceptable for the All  $y^+$  wall function used.

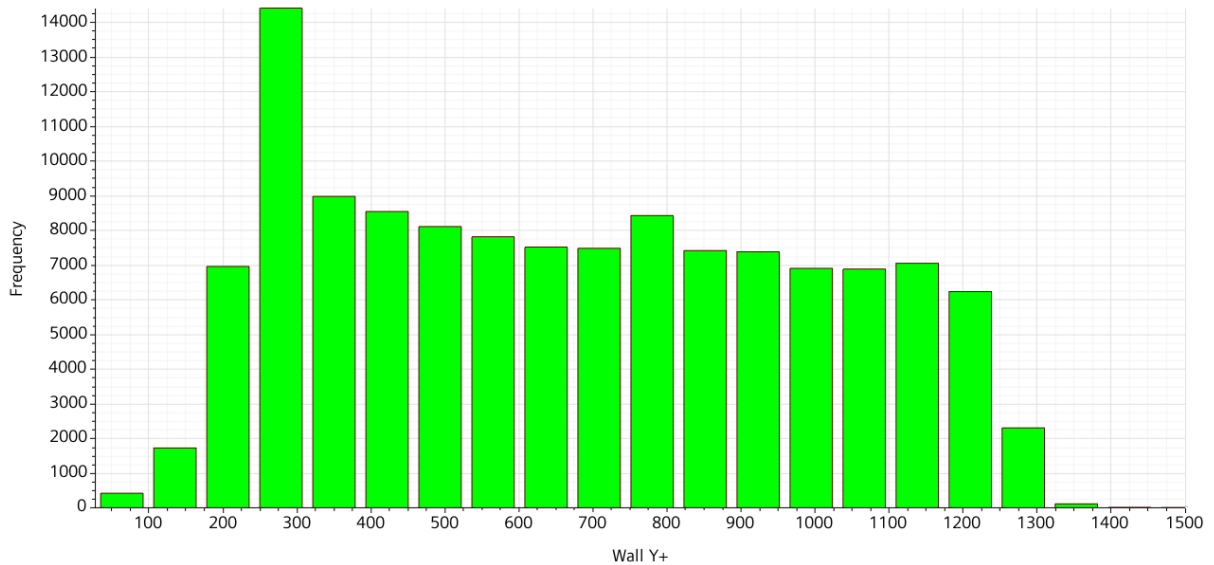


**Figure 3-6: 159,000 DWT tanker propeller wall  $Y^+$ .**

The simulation physical timestep was set to 2.5 ms which corresponded to a maximum propeller rotation of 2 degrees per timestep. The timestep is limited such that the interface cells did not translate more than one cell per timestep, ensuring good mapping, numerical stability, and minimal numerical diffusion due to the sliding mesh.

### 3.2.2. Ferry

For the ferry, the 100% Maximum Continuous Rating (MCR) condition at the operational draught was used. This corresponded to a draught of 5.5 m at the fore and 5.4 m at the aft perpendiculars with a propeller rotation rate of 195 RPM. The Holtrop-Mennen method predicted a forward speed of 10.6 m/s (20.7 knots) at these conditions (see Appendix B).

The ferry CFD domain was 1336 m in length, 1136 m wide, and 726 m tall and is shown in Figure 3-7. Velocity inlet boundary conditions were used for the inflow and top, symmetry for the bottom and sides, and pressure outlet for the outflow. The boundary conditions were slightly different than the tanker to ensure numerical stability. Functionally, the resulting behaviour should be identical due to the free-surface wave damping at the side, inflow, and outflow boundaries. The hull and propeller walls were no-slip and used Star-CCM+'s All  $y^+$  wall function, which switches between a low  $y^+$  and high  $y^+$  mode depending on the cell near wall spacing.

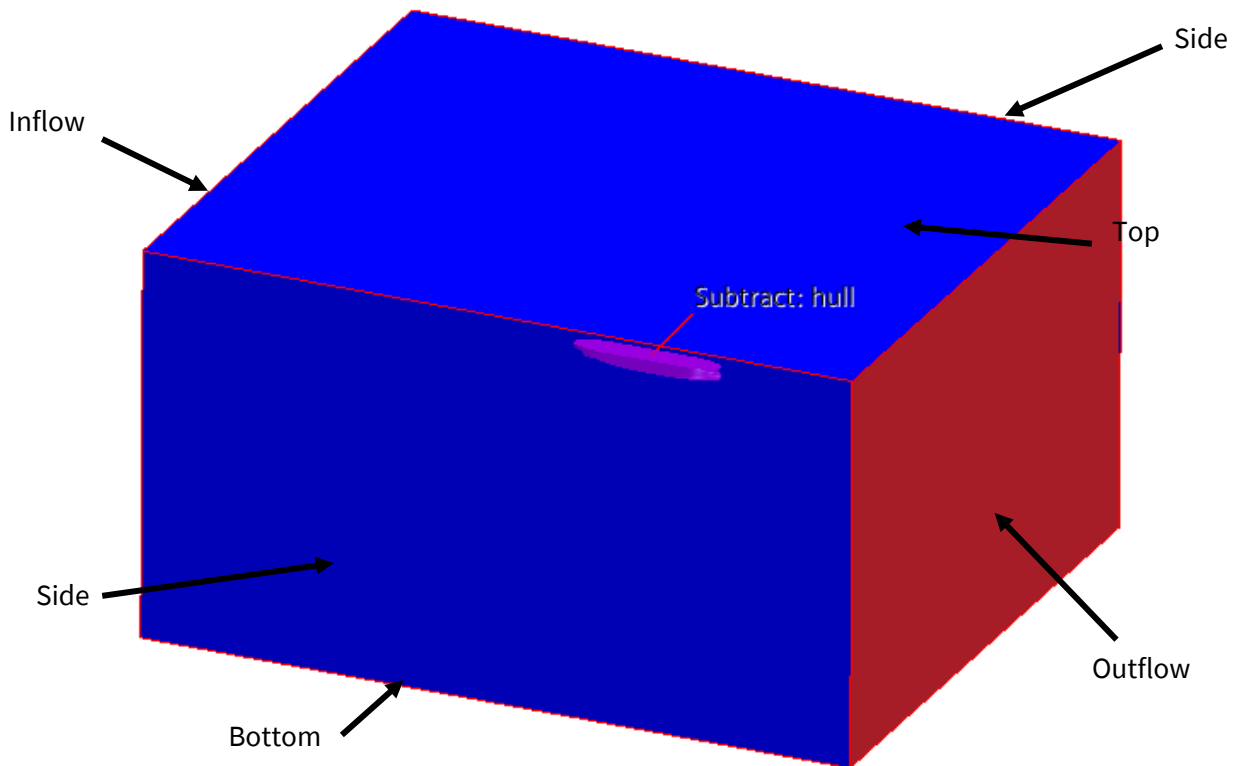


**Figure 3-7: Ferry CFD domain.**

The same hull and hub models from Section 2.5.2 were used. Star-CCM+'s trimmer style (hexahedral dominant) mesh was used for the overall domain mesh. Refinement regions were added around the hull and at the aft and stern. The free surface was also refined utilizing thin, flat cells to properly resolve the ship wake. The minimum cell dimension in the free surface was 0.127 m. A minimum cell dimension of 0.049 m was used around the hull. Prism layers around the hull were extruded from a first cell height of 0.007 m to an overall prism layer thickness of 0.65 m. A total of 7 prism layers were used. The overall domain consisted of a total of 3.5 million cells. Representative images of the mesh are shown in Figure 3-8.

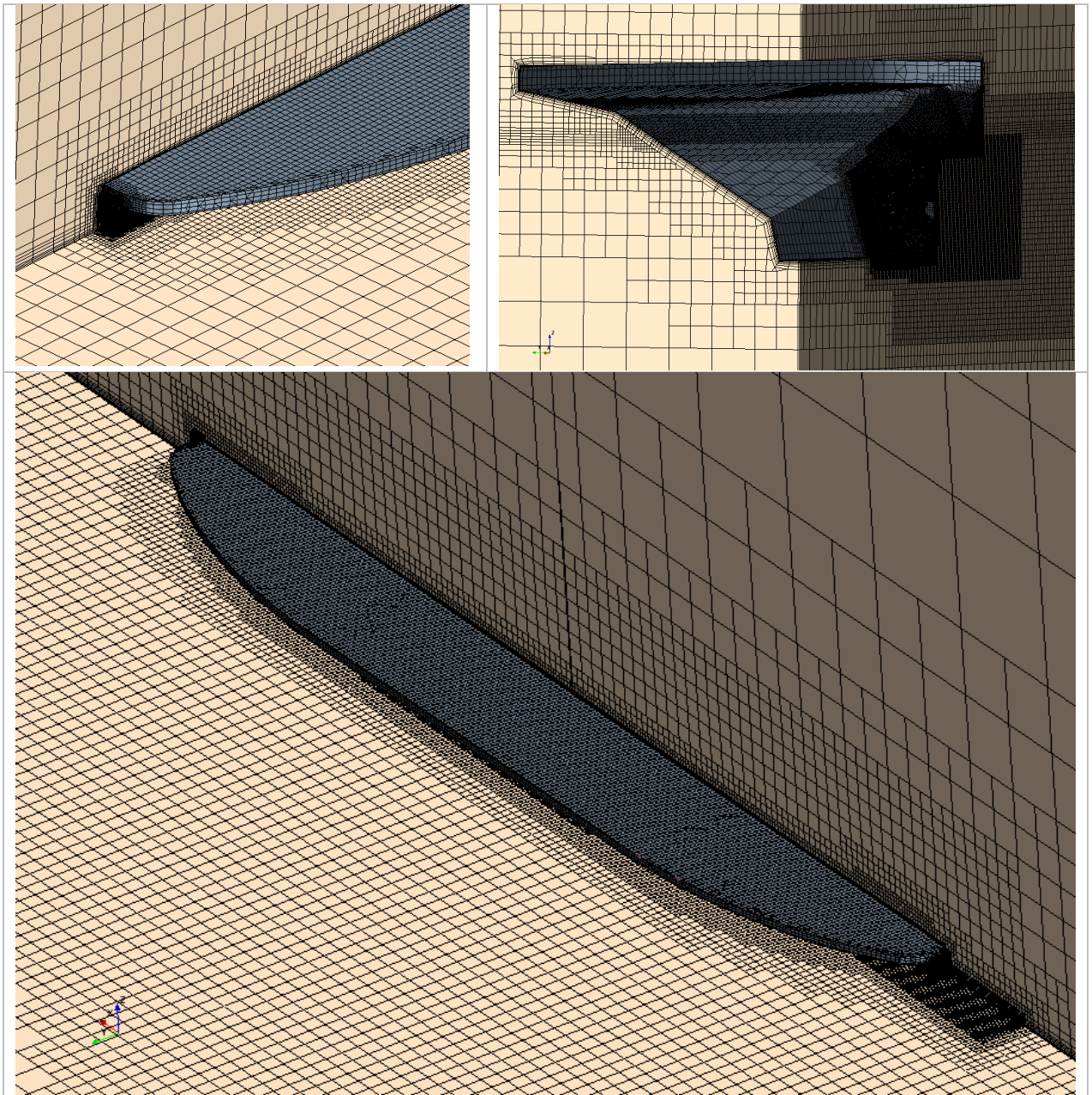


**Figure 3-8: Ferry Bay mesh.**

A histogram of the wall  $y^+$  values for the hull once the ship had reached a steady speed is shown in Figure 3-9. The bulk of the cells are around a  $Y^+$  of 100 – 800 and 1400 – 2200. The values were higher than ideal due to the higher ship speed, but should still reasonably resolve the hull drag using the All  $y^+$  wall function.

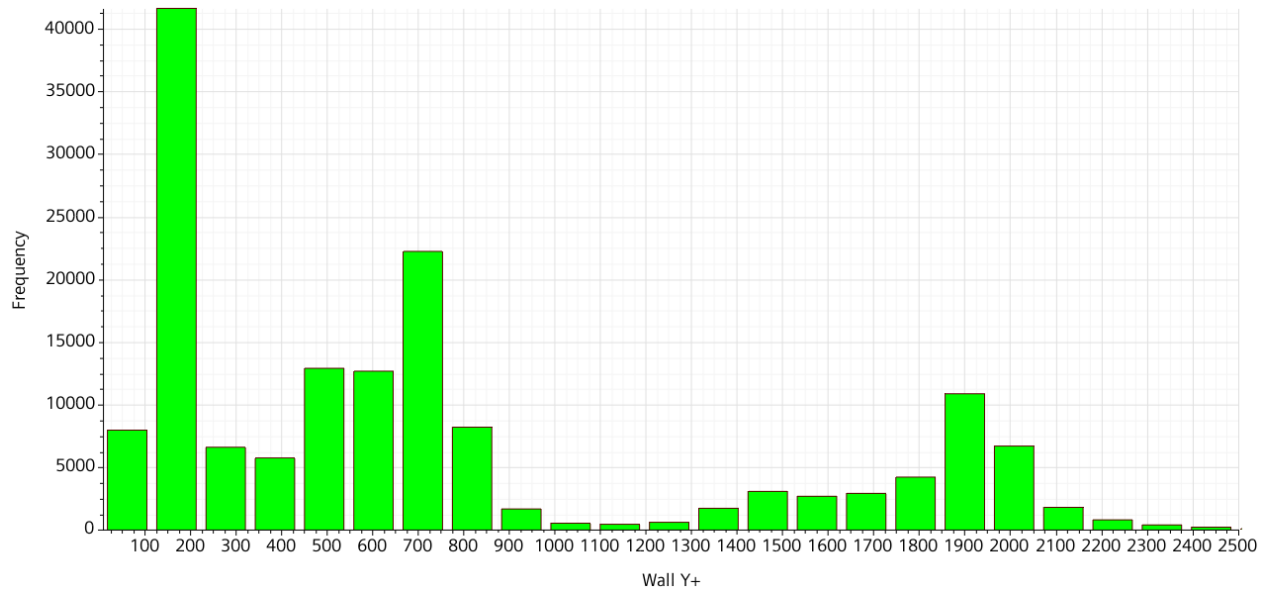


**Figure 3-9: Ferry hull wall Y+.**

The propeller geometry can be seen in Figure 3-10. The propeller domain was based on the propeller radius,  $R_{prop}$ , with a domain radius equal to  $1.1 R_{prop}$ . This is less than the ideal  $1.5 R_{prop}$  due to the proximity of the hull to the blade tips. The domain extended 0.65 m upstream of the propeller center and 1.75 m downstream.

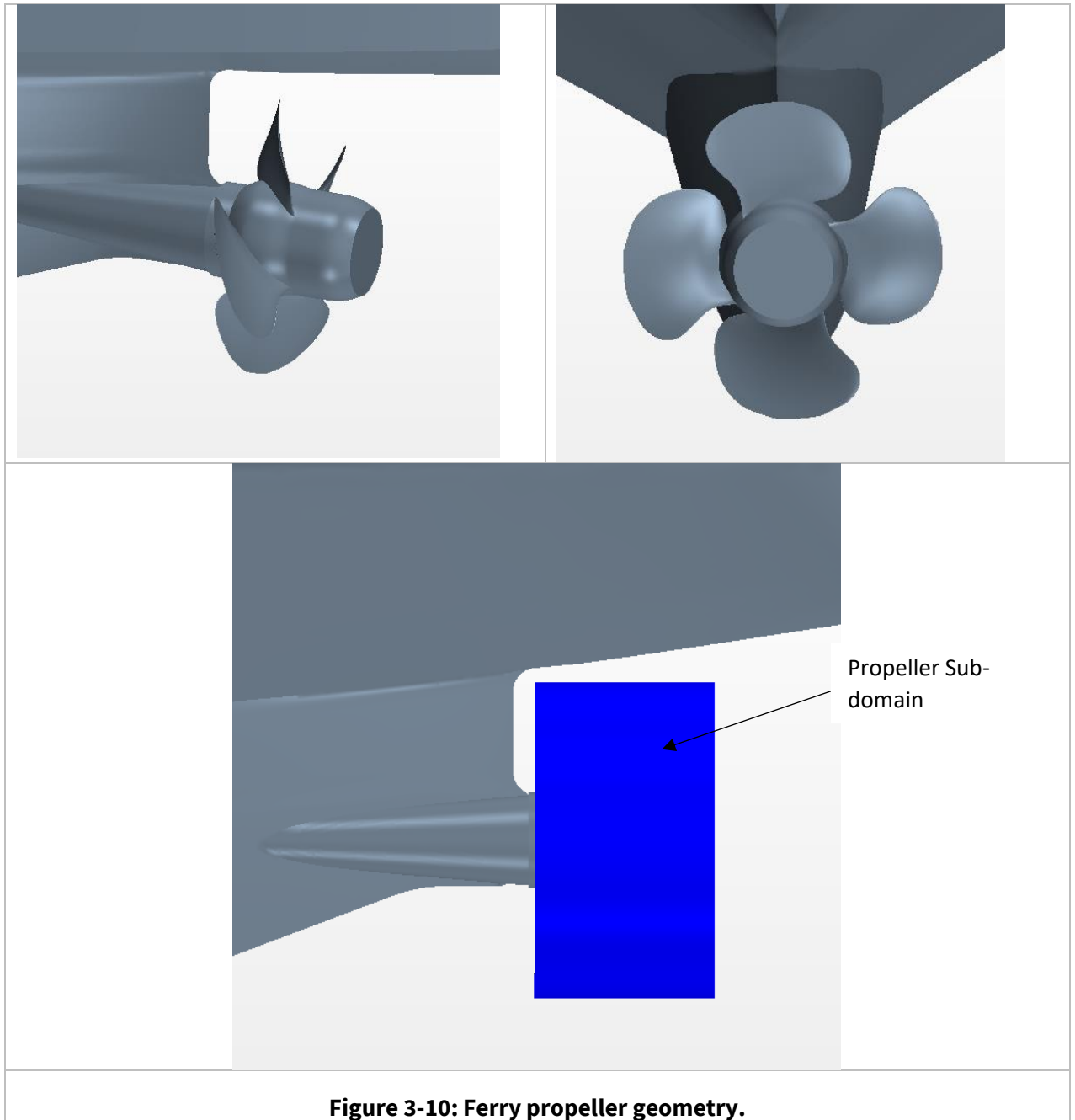


**Figure 3-10: Ferry propeller geometry.**

The propeller sub-domain mesh was generated using a trimmer style (hexahedral dominant) mesh. The propeller target cell dimension was 0.062 m with a minimum cell dimension of 0.005 m. In order to capture the boundary layer effects, prism layers were extruded with a first cell height of 0.001 m and a total thickness of 0.04 m. A total of 6 prism layers were utilized. Due to the complicated hub geometry, the same prism layer setting as the propeller were used. The minimum cell dimension around the interface was set to be 0.062 m in an attempt ensure a good transition between the overall domain and the rotating sub-domain. A total of 9 prism layers were used. The overall domain consisted of a total of 1.5 million cells. Representative images of the mesh are shown in Figure 3-11.

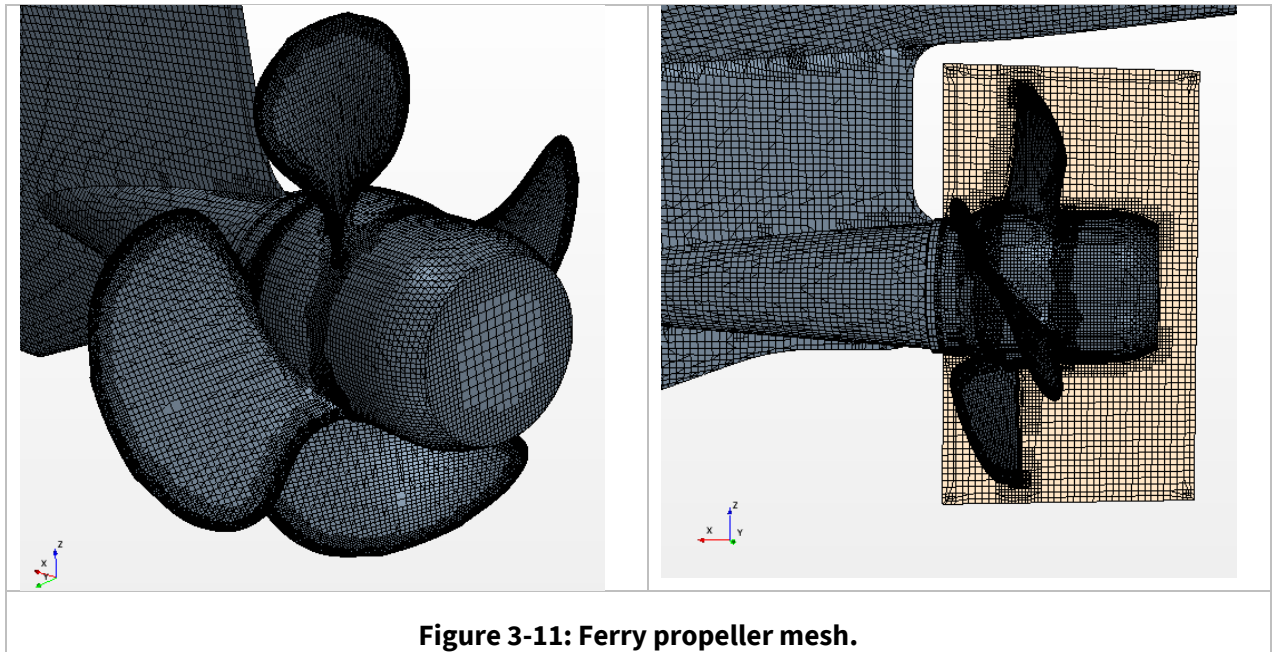


**Figure 3-11: Ferry propeller mesh.**

A histogram of the wall  $y^+$  values for the propeller is shown in Figure 3-12. The  $y^+$  values were in the 100 – 700 range, higher than ideal, but still acceptable for the All  $y^+$  wall function used.

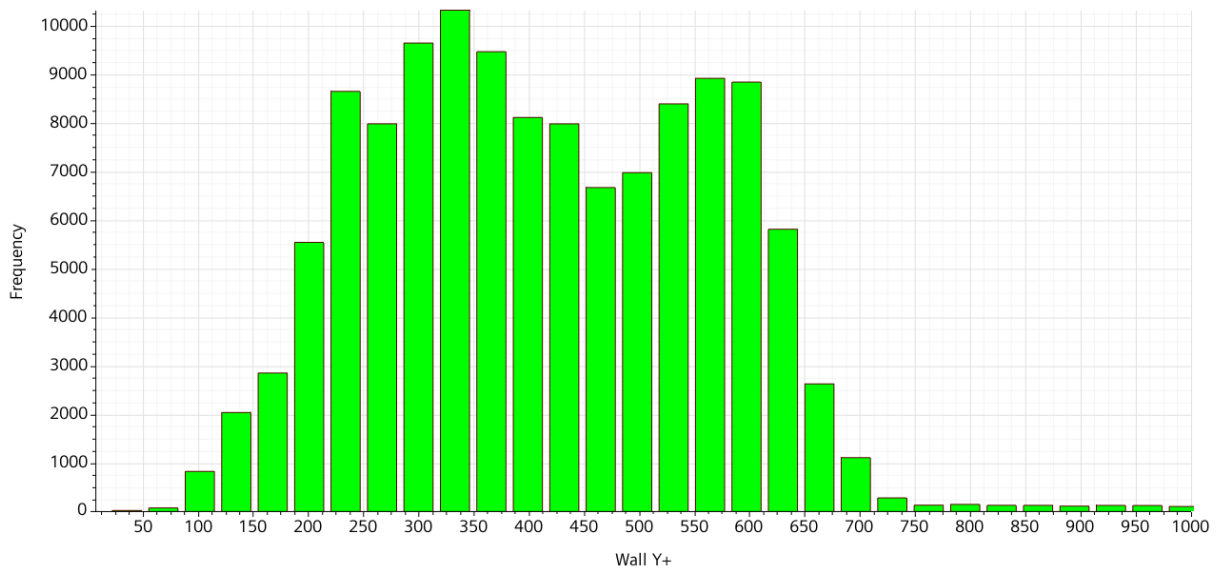


**Figure 3-12: Ferry propeller wall  $Y^+$ .**

The simulation physical timestep was set to 1.5 ms which corresponded to a maximum propeller rotation of 1.75 degrees per timestep. The timestep was limited such that the interface cells did not translate more than one cell per timestep, ensuring good mapping, numerical stability, and minimal numerical diffusion due to the sliding mesh.

### 3.3. Results

Results for the 159,000 DWT tanker and the ferry are presented in Sections 3.3.1 and 3.3.2 respectively.

Simulations for both ships were run on 168 cores for several days to achieve a steady state result. First the simulation was run to steady state using a rotating reference frame on the propeller region. The simulation was then stopped, and the sliding mesh methodology was enabled. The simulations were then re-run to a steady state speed.

### 3.3.1. 159,000 DWT Tanker

The 159,000 DWT Tanker reached a steady state velocity of 7.8 m/s (15.2 knots). The propeller shaft torque was 1314.4 kN-m. At 91 RPM this corresponds to a shaft power of 12525 kW. The propeller thrust was 1512 kN which corresponds to a propulsive power of 11795 kW. A summary and comparison of the CFD and speed power predictions is shown in Table 3-1. The two methods showed large discrepancies in the thrust and shaft power suggesting that simulation refinements such as a finer timestep may be necessary.

**Table 3-1: 159,000 DWT Tanker Comparisons**

Parameter	CFD	Speed Power	% Difference
Forward Speed (m/s)	7.8	7.97	-2.1
Thrust (kN)	1512	1765	-14.3
Shaft Power (kW)	12526	15659	-20.0

Images of the free surface and propeller axial velocity field are shown in Figure 3-13 and Figure 3-14 respectively.

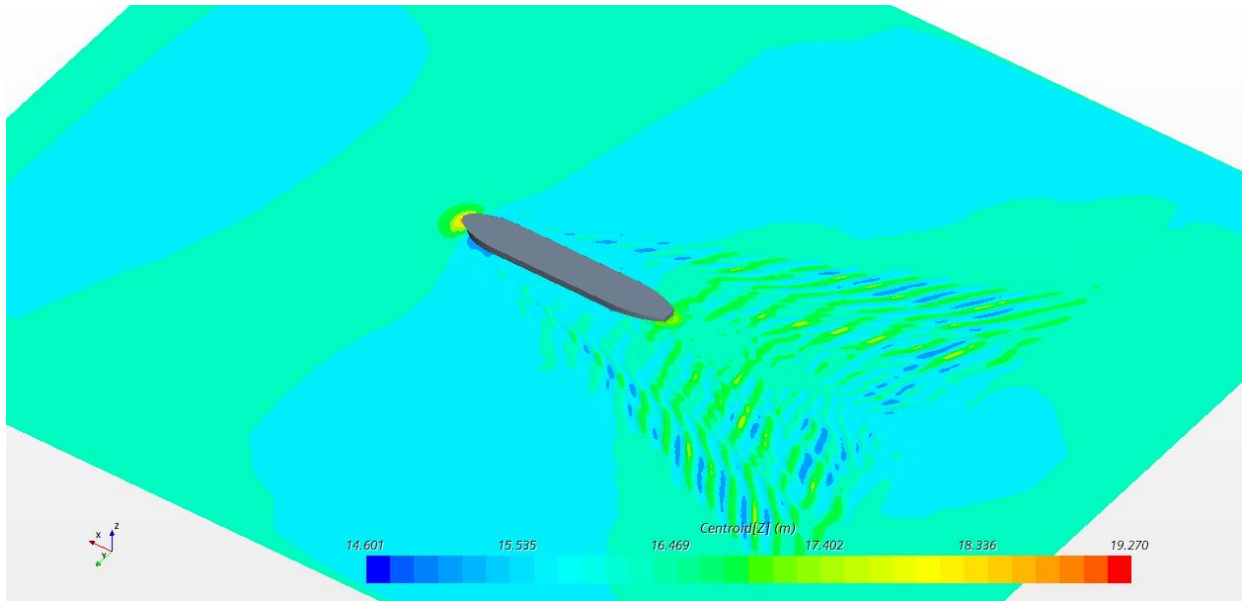


**Figure 3-13: 159,000 DWT tanker free surface**



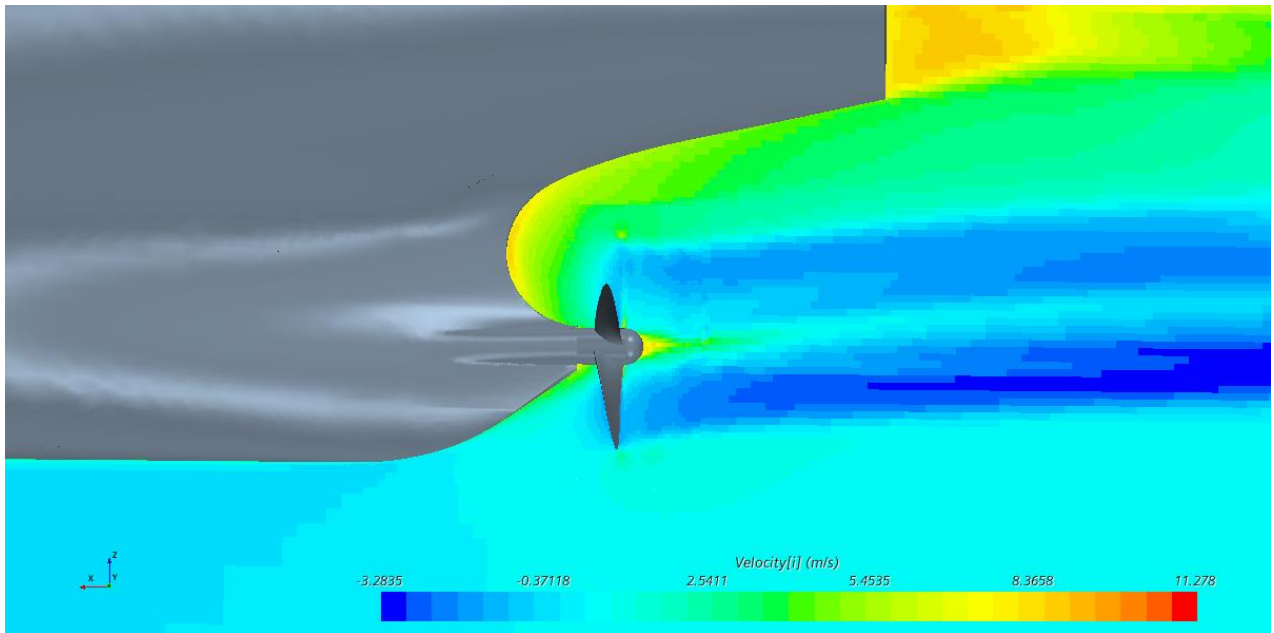


**Figure 3-14: 159,000 DWT tanker propeller axial velocity**

### 3.3.2. Ferry

The ferry reached a steady state velocity of 11.05 m/s (21.5 knots) compared to the speed-power predicted speed of 10.64 m/s. The propeller shaft torque was 381.8 kN-m. At 195 RPM this corresponds to a shaft power of 7796 kW. The propeller thrust was 534 kN which corresponds to a propulsive power of 5901 kW. A summary and comparison of the CFD and speed power predictions is shown in Table 3-2.

**Table 3-2: Ferry speed power comparisons**

Parameter	CFD	Speed-Power	% Difference
<b>Forward Speed (m/s)</b>	11.05	10.64	3.9
<b>Thrust kN</b>	534	581	-8.2
<b>Shaft Power kW</b>	7796	8502	-8.3

Images of the free surface and propeller axial velocity field are shown in Figure 3-15 and Figure 3-16 respectively. The ferry shows a cleaner free surface wake than the tanker with no oscillations.

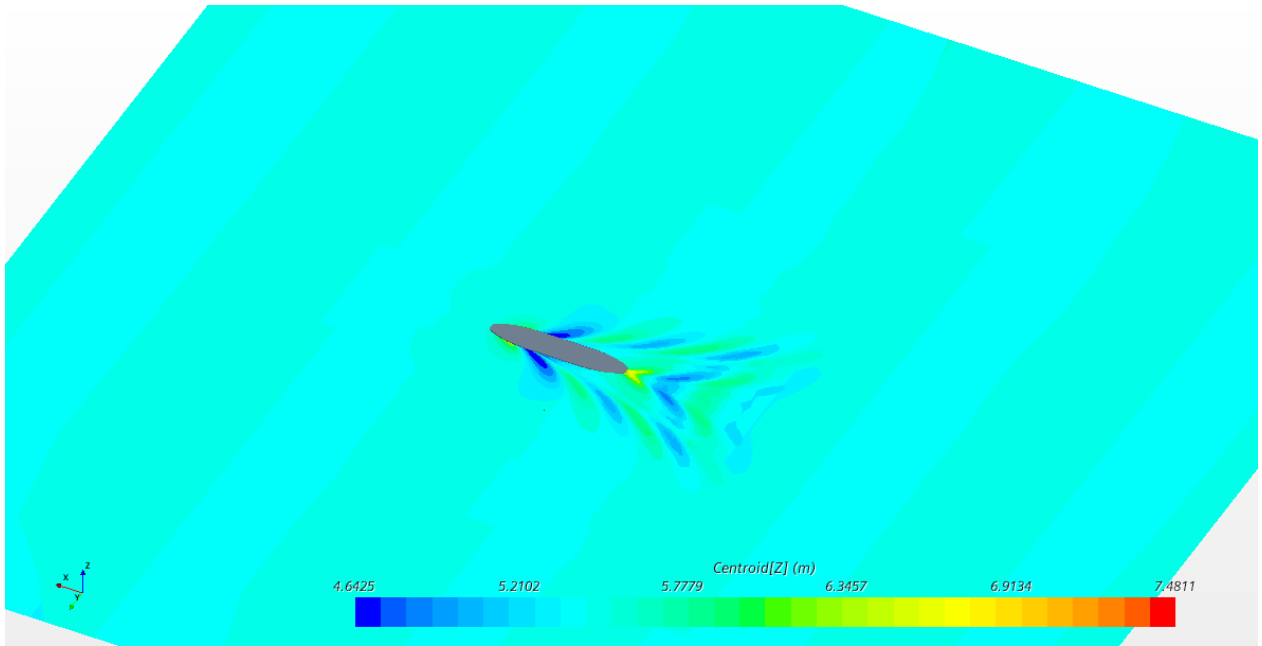


**Figure 3-15: Ferry free surface**

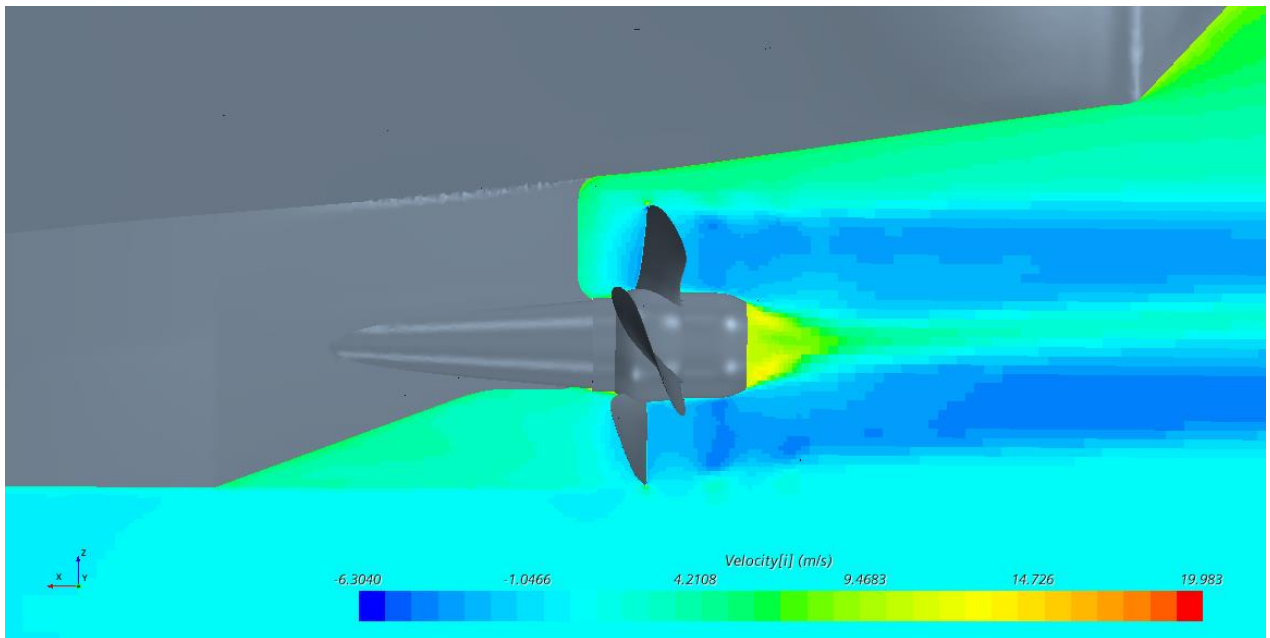


**Figure 3-16: Ferry propeller axial velocity**

## 4. Conclusion

Propeller optimization design studies for two typical commercial vessels, operating in the west coast of Canada, were performed to determine potential underwater radiated noise reduction benefits. Two vessels were selected:

- A 159,000 DWT tanker
- A ferry

To support the optimization and noise calculations, wake fields were simulated using a coupled Computational Fluid Dynamics (CFD) and potential flow approach. Results of the optimization study for both vessels are included in Appendix A and B for the 159,000 DWT tanker and ferry respectively.

Further CFD simulations of the vessels were performed using a sliding mesh methodology for the propeller. These simulation results were compared to speed power predictions. The ferry showed better agreement between the CFD and the speed power predictions, with a difference of 8% for the shaft power. The tanker showed a difference of 20% in the shaft power, suggesting that simulation setup refinements may be required to achieve better predictions.

## 5. References

- [1] Siemens PLM Software, *Simcenter Star-CCM+ - User Guide*, 2020.
- [2] “Cooperative Research Ships Report No. 28652-9-RD, User's guide PROCAL, version 2.4,” MARIN, Wageningen, The Netherlands, 2016.
- [3] F. R. Menter, “Two-Equation Eddy-Viscosity Turbulence Models for Engineering Applications,” *AIAA Journal*, vol. 32, no. 8, pp. 1598-1605, 1994.
- [4] Ship operator, *Bohai\_G1-100-006\_-\_LINES.pdf*.
- [5] Ship operator, *3d Hull.3dm*.
- [6] Ship operator, *A005253-ARRGMT OF SHAFTING.pdf*.

# **Appendix A 159,000 DWT Propeller Optimization Report**



**BETTER SHIPS, BLUE OCEANS**

## **159K DWT Oil tanker: study into the reduction of propeller cavitation noise**

Final report MS1

Report No. : 33418-1-POW  
Date : February 2022  
Version : 1.1  
Final report

# 159K DWT Oil tanker: study into the reduction of propeller cavitation noise

## Final report MS1

MARIN order No. : 33418  
MARIN Project Manager : Gert-Jan Zondervan

Classification : NDA  
Number of pages : 77

Ordered by : LR ATG (Martec Limited)  
237 Brownlow Ave  
Dartmouth, B3B 2C7, Canada

Order document : LR purchase order 1614012 February 17, 2021  
Reference : Teekay tanker  
Export licence No. : NL0074CDIU0148807

Reported by : Gert-Jan Zondervan, John Huisman, Mark Merkens  
Reviewed by : Arjan Lampe

Version	Date	Version description
1.1	February 2022	Updated after feedback from customer
1.0	April 2021	Final report

<b>CONTENTS</b>	<b>PAGE</b>
REVIEW OF REPORTS .....	IV
1 INTRODUCTION.....	1
2 OVERVIEW OF THE VESSEL DETAILS AND EMPLOYED DESIGN TOOLS.....	2
2.1 Main particulars .....	2
2.2 Design and analysis tools.....	2
3 SPEED-POWER PERFORMANCE CALCULATIONS.....	4
3.1 Design draught .....	4
3.1.1 Resistance.....	4
3.1.2 Propulsive performance .....	4
3.2 Ballast draught.....	5
3.2.1 Resistance.....	5
3.2.2 Propulsive performance .....	6
4 ANALYSIS OF INSTALLED PROPELLER.....	7
4.1 General design information .....	7
4.2 Wake field .....	8
4.3 Results.....	9
4.3.1 Open water efficiency.....	9
4.3.2 Cavitation predictions.....	9
4.3.2.1 Cavitation inception .....	10
4.3.2.2 Developed cavitation at 85% MCR power .....	10
4.3.2.3 Under water noise prediction.....	13
4.3.2.4 Propeller blade strength.....	15
5 DESIGN OF A 4-BLADE REPLACEMENT PROPELLER.....	17
5.1 Approach .....	17
5.1.1 Analysis of propeller variants .....	17
5.1.2 Goals and constraints .....	17
5.2 4-bladed propeller – constrained design .....	19
5.3 4-bladed propeller – unconstrained .....	21
5.4 Developed cavitation and URN predictions (85% MCR service condition at ballast draught) ..	23
6 THE EFFECT OF INCREASING THE NUMBER OF BLADES.....	26
6.1 5-bladed propeller.....	26
6.2 7-bladed propeller.....	28
6.3 Developed cavitation and URN predictions for selected 5 and 7 blade propellers .....	30
7 CONCLUSIONS AND RECOMMENDATIONS .....	33
REFERENCES .....	35





## REVIEW OF REPORTS

### Deliverables of the current project phase<sup>1</sup>

Deliverable	Item	Title	Date
MS1	Report No. 33418-1-POW	159K DWT Oil tanker: study into the reduction of propeller cavitation noise	February 2022

---

<sup>1</sup> At the moment of writing.

## 1 INTRODUCTION

Under an independent subcontractor agreement, the Maritime Research Institute Netherlands (MARIN) has been commissioned by Martec Limited (LR ATG) to carry out a series of propeller design studies. These studies aim to determine potential underwater radiated noise (URN) reduction benefits that can be achieved for typical commercial ships operating in the West Coast of Canada. The project is part of a broader programme of LR and DRDC Atlantic for Transport Canada.

The propeller design studies can be seen as a demonstration project for Transport Canada to show a general approach for silencing commercial shipping that is threatening underwater wildlife. The work covers the following tasks of the contract:

- Task 2: Numerical calculations of the existing propeller for a tanker operated by Teekay. These involve:
  - Analysis of provided information (drawings and performance data) and speed-power predictions using the Holtrop-Mennen method.
  - The numerical evaluation of the currently installed propeller using propeller analysis code PROCAL and the empirical tip vortex (ETV) prediction method developed by the Cooperative Research Ships (CRS) consortium. Besides the cavitation inception characteristics, the analysis also includes a prediction of the underwater noise levels with an upgraded version 3.0 of the ETV model that is combined with a semi-empirical model to compute the contribution of sheet cavitation.
- Task 3: Numerical calculations for the design of a new replacement propeller for the Teekay tanker. This involves:
  - Design optimisations using the PROPART propeller optimisation framework to investigate design trade-offs (e.g. efficiency and cavitation inception characteristics).
  - Propeller design keeping the mass and moment of inertia similar to the existing propeller.
  - Propeller design with no restrictions on mass and moment of inertia (MOI).
  - Provide load input for structural analysis of the propeller by LR.
- Task 4: Similar task items as Task 2 for a selected ferry.
- Task 5: Similar task items as Task 3 for the ferry.

This final report considers the reporting of Tasks 2 and 3. Chapter 2 provides details about the vessel and the employed propeller design tools. The results of the speed-power performance calculations are presented in Chapter 3. Chapter 4 presents the analysis of the installed propeller. The approach and results of the design optimisation study for a 4-bladed replacement propeller are described in Chapter 5. Results of a study into the possible advantages of increasing the number of propeller blades to 5 or even 7 are presented in Chapter 6. In Chapter 7 the conclusions and recommendations are listed. Throughout this report SI units are used unless indicated otherwise; a list of symbols is given in Appendix I.

## 2 OVERVIEW OF THE VESSEL DETAILS AND EMPLOYED DESIGN TOOLS

This chapter provides a concise overview of the particulars of the tanker and the tools employed in the propeller design optimisation exercise.

### 2.1 Main particulars

The main particulars of the ship are:

Description	Symbol	Design draught	Ballast draught	Unit
Length between perpendiculars	L <sub>PP</sub>	264.0	264.0	m
Length on waterline	L <sub>WL</sub>	269.0	259.6	m
Breadth moulded on WL	B	48.0	48.0	m
Draught moulded on FP	T <sub>F</sub>	16.0	5.6	m
Draught moulded on AP	T <sub>A</sub>	16.0	9.7	m
Displacement volume moulded	∇	165994	73068	m <sup>3</sup>
Displacement mass in seawater	Δ <sub>1</sub>	170310	13099	t
LCB position forward of ½ L <sub>PP</sub>	LCB	3.3	1.3	% <sup>*)</sup>
Block coefficient	C <sub>B</sub>	0.819	0.754	-
Midship section coefficient	C <sub>M</sub>	0.997	0.995	-
Prismatic coefficient	C <sub>P</sub>	0.821	0.763	-
Length-Breadth ratio	L <sub>PP</sub> /B	5.500	5.500	-
Breadth-Draught ratio	B/T	3.000	6.275	-

<sup>\*)</sup> LCF position indicated as a percentage of the L<sub>PP</sub>

Ballast values are assumed values based on comparable vessels.

Appendages:

- bilge keels
- 1 rudder

The table below indicates some relevant propulsion details of the ship:

Engine type	Diesel motor	-
Number and type of propulsors	1 fixed-pitch propeller	-
Available brake power at 100% MCR	16860	kW
Shaft line losses (estimated)	1	%

### 2.2 Design and analysis tools

In the design of the replacement propeller(s) extensive use was made of the PROPART propeller design tool. PROPART is a multi-objective optimisation method developed by MARIN within the Cooperative Research Ships (CRS) research consortium for carrying out propeller design studies. PROPART uses a parametric description of the propeller geometry and a coupling of propeller code PROCAL with an optimisation algorithm.

The numerical analysis has been carried out using propeller analysis code PROCAL. PROCAL is a boundary element method (BEM), developed within CRS, see the included software documentation sheet. PROCAL is able to predict the inception and extent of developed sheet cavitation, in order to

check for erosive types of sheet cavities. Tip vortices and tip vortex cavitation are not modelled in PROCAL. The inception of tip vortex cavitation is determined using the Empirical Tip Vortex (ETV) prediction method that was also developed within CRS.

PROCAL computations are performed for a large number of propeller geometries with varying radial distributions of the geometry parameters like the pitch, chord length and maximum thickness and camber. Also, the blade profile shape is optimised. After the PROCAL computations, often in multiple design conditions, the performance is evaluated in terms of cavitation behaviour, efficiency and constraining properties like the blade mass and inertia.

PROPART also features a cavitation inception analysis module which analyses the cavitation inception buckets for sheet-cavitation and tip-vortex cavitation for both pressure-side and suction-side cavitation. A range of propeller loading conditions are computed with PROCAL providing the pressure distributions on the propeller blade, while the ETV model provides an estimate of the cavitation inception of the tip vortices.

Besides the inception of cavitation, also predictions have been made of the underwater radiated noise levels using the ETV model for predicting tip vortex cavitation noise combined with a semi-empirical method for calculating the noise of sheet cavitation. It is emphasised that the latter is a very recent development that until now is validated only for pressure side cavitation measured during model scale cavitation tests in MARIN's Depressurised Wave Basin.

In the current propeller design study the possibilities of improving the propeller design and fulfilment of the design goals are shown in the form of Pareto front plots, see Figure 2-1. Each dot in the figure represents a candidate propeller design selected from the parametric design space of the propeller geometry. As the optimisation process advances, better propellers are created. This is shown in the figure as going from the earlier designs in blue to the latest ones in red. The Pareto front is given by the propellers represented by the deep red dots. Propellers on the Pareto front have the property that the margin against cavitation cannot be improved without compromising efficiency.

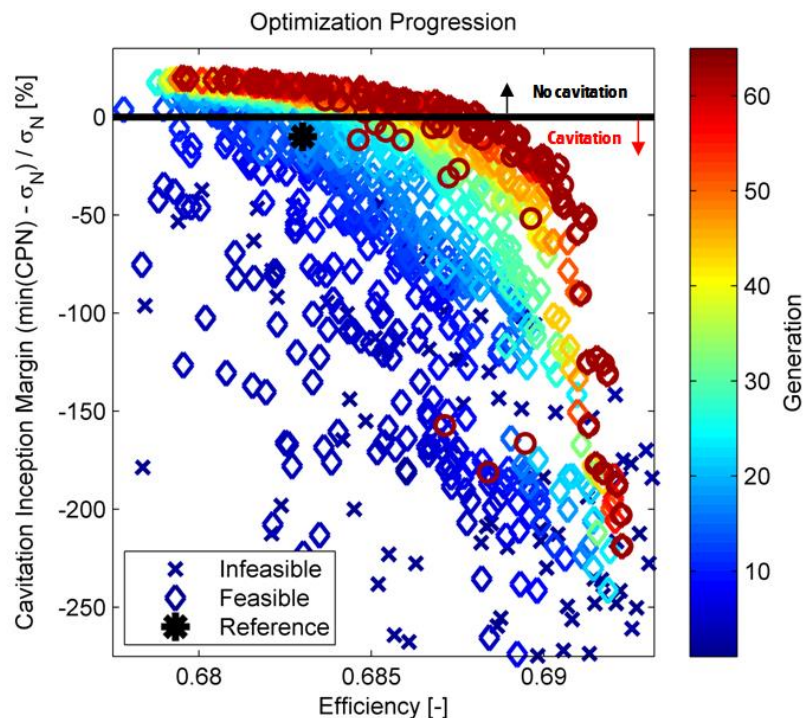


Figure 2-1: Example of optimisation case with final Pareto front in red. Both the margin against cavitation and efficiency were to be maximised.

### 3 SPEED-POWER PERFORMANCE CALCULATIONS

In absence of any information from sea trials or model tests calculations have been done to determine the necessary input for the propeller design. Speed-power predictions have been carried out with computer program DESP, see software documentation sheet. DESP is an implementation of the Holtrop-Mennen method for the prediction of the resistance and powering performance of ships. The predictions have been made based on correlation with similar tanker designs available in the database of MARIN. The predictions have been made for two assumed draughts of, the design draught of  $T_F/T_A = 16.0/16.0$  m and an assumed ballast draught of  $T_F/T_A = 5.6/9.7$  m. Particulars of the ship for these draughts are listed in the table on page T1.

In Sections 3.1 and 3.2 the results of the calculations are presented for the two draughts.

#### 3.1 Design draught

##### 3.1.1 Resistance

The following resistance variation with speed is found from the correlation with similar ships from the database of MARIN.

Table 3-1: Predicted resistance versus ship speed for design draught.

V [kn]	FN	R [KN]	P <sub>E</sub> [KW]
12.0	0.121	812	5013
13.0	0.131	930	6220
14.0	0.142	1103	7944
15.0	0.152	1253	9669
16.0	0.162	1445	11894
17.0	0.172	1728	15112

##### 3.1.2 Propulsive performance

The following table shows the predicted shaft power, rotation rate and propeller thrust versus the ship speed. Also shown are typical efficiency components assumed for the vessel.

Table 3-2: Propulsive performance for design draught (trial).

V [kn]	N [RPM]	P <sub>s</sub> [kW]	T-TOT [kN]	THDF	W	ETAH	ETAO	ETAR	ETAD
12	70.6	7289	1062.2	0.236	0.328	1.137	0.600	1.018	0.695
13	75.9	8995	1216.6	0.236	0.328	1.137	0.603	1.018	0.698
14	82.3	11546	1442.9	0.236	0.328	1.137	0.601	1.018	0.695
15	87.9	14020	1639.1	0.236	0.328	1.137	0.602	1.018	0.697
16	94.1	17298	1890.3	0.236	0.328	1.137	0.600	1.018	0.695
17	101.9	22266	2260.5	0.236	0.328	1.137	0.592	1.018	0.686

Based on the following propeller data a speed prediction is made for the 85% MCR condition.

Propeller diameter	8.200	[m]
Pitch / diameter	0.70	[-]
No. of propeller blades	4	
Blade area ratio	0.49	[-]
Rotation rate	88.5	[rpm]
Required shaft power	14331	[kW]
Thrust	1663.4	[kN]
Predicted speed	15.11	[kn]

The calculated results are for ideal trial conditions, implying unrestricted deep water of 15.0° C and a mass density of 1025.9 kg/m<sup>3</sup>, a clean hull and propeller blades and no effects of wind and waves.

Using a 15% sea margin on the shaft power the follow table shows the predicted service performance of the vessel:

Table 3-3: *Propulsive performance for design draught (service).*

V <sub>s</sub> [kn]	N [RPM]	P <sub>s</sub> [kW]	Thrust [kN]
12	73.3	8377	1189.7
13	78.8	10335	1362.6
14	85.4	13270	1616.1
15	91.2	16111	1835.8
16	97.7	19882	2117.1
17	105.9	25617	2531.8
<b>14.38</b>	<b>87.7</b>	<b>14331</b>	<b>1700.4</b>

On page F5 the variation of shaft power and propeller rotation rate is plotted against the ship speed.

### 3.2 Ballast draught

A similar resistance and speed-power prediction was made for the ballast draught.

#### 3.2.1 Resistance

Table 3-4: *Predicted resistance versus ship speed for ballast draught.*

V [kn]	FN	R [KN]	P <sub>E</sub> [KW]
12.00	0.121	651.0	4019
13.00	0.131	765.0	5116
14.00	0.142	928.0	6684
15.00	0.152	1089.2	8405
16.00	0.162	1315.3	10826
17.00	0.172	1658.9	14508

### 3.2.2 Propulsive performance

Table 3-5: Propulsive performance for ballast draught (trial).

V [kn]	N [RPM]	P <sub>s</sub> [kW]	T-TOT [kN]	THDF	W	ETAH	ETAO	ETAR	ETAD
12	62.7	5369	854.3	0.238	0.413	1.298	0.593	0.982	0.756
13	68.0	6838	1003.9	0.238	0.413	1.298	0.593	0.982	0.756
14	74.3	9026	1217.8	0.238	0.413	1.298	0.587	0.982	0.748
15	80.2	11411	1429.4	0.238	0.413	1.298	0.584	0.982	0.744
16	87.3	14913	1726.1	0.238	0.413	1.298	0.575	0.982	0.733
17	96.3	20557	2177.0	0.238	0.413	1.298	0.559	0.982	0.713

Based on the following propeller data a speed prediction is made for the 85% MCR condition at ballast draught.

Propeller diameter	8.2	[m]
Pitch / diameter	0.70	[-]
No. of propeller blades	4	
Blade area ratio	0.49	[-]
Rotation rate	86.2	[rpm]
Thrust	1677.9	[kN]
Required shaft power	14331	[kW]
Predicted speed	15.86	[kn]

The calculated results are for ideal trial conditions, implying unrestricted deep water of 15.0° C and a mass density of 1025.9 kg/m<sup>3</sup>, a clean hull and propeller blades and no effects of wind and waves.

#### Results with sea margin

Using a 15% sea margin on these results will give the following table:

Table 3-6: Propulsive performance for ballast draught (service).

V <sub>s</sub> [kn]	N [RPM]	P <sub>s</sub> [kW]	T [kN]
12	65.2	6179	956.9
13	70.7	7868	1124.4
14	77.3	10394	1364.0
15	83.5	13145	1600.9
16	90.9	17195	1933.2
17	100.4	23743	2438.3
<b>15.34</b>	<b>85.8</b>	<b>14331</b>	<b>1700.1</b>

On page F5 the variation of shaft power and propeller rotation rate is plotted against the ship speed.



## 4 ANALYSIS OF INSTALLED PROPELLER

In this chapter first the cavitation and performance predictions for a typical tanker propeller are presented.

### 4.1 General design information

Details of the ship and its engines have been obtained from LR and DRDC. The following lists the most important details of the design.

- The subject tanker is fitted with a right handed 4-bladed fixed-pitch propeller with a diameter of 8.2 metres. The propeller is driven directly by a MAN B&W 6S70 MC Diesel engine delivering an MCR power of 16860 kW at 91 RPM. The six-cylinder diesel engine can in principle be fitted with either a 4 or a 5-bladed propeller to prevent resonant vibration issues. The diameter of the installed propeller is near its optimum diameter based on a B-series diameter optimisation. Variation of the number of blades and diameter is considered in the propeller design study.
- Speed-power predictions have been determined for the vessel sailing at the given design draught of respectively 16.0/16.0 m (FWD/AFT) and the estimated ballast draught of 5.6/9.7 m (FWD/AFT), see Chapter 3. The 85% MCR design point in trial condition is taken to determine the pitch for the correct power/rpm relation. This is when the ship sails 15.11 kn at design draught. For the cavitation predictions the propeller is analysed in the 85% MCR trial and service conditions at both draughts.
- The main objective in the design of the replacement propeller is to reduce the underwater radiated noise (URN) in a relevant operational range of the vessel. In Trivyza et al. (2016) typical speed profiles are found for an Aframax tanker obtained from Banks et al. (2013), see Figure 4-1 and Figure 4-2. Assuming that the Teekay tanker sails at a similar speed profile it is estimated that these tankers typically spend most of the time operating in the 8 to 13 knot range for both design and ballast draughts. Since reducing the cavitation at the ballast draught is the most challenging one, the optimisation study focuses at maximising the cavitation inception speed of the vessel for that condition.

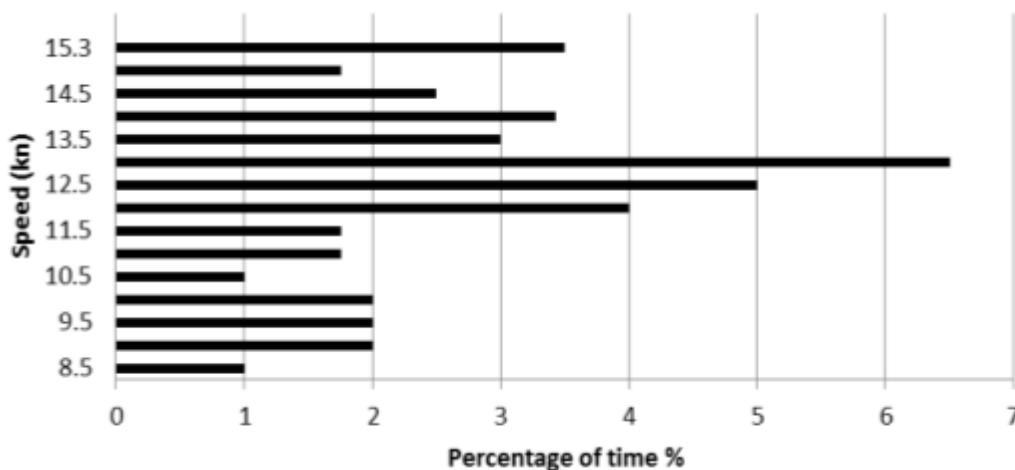


Figure 4-1: Typical speed profile for an Aframax tanker sailing on ballast conditions (Banks et al. 2013).

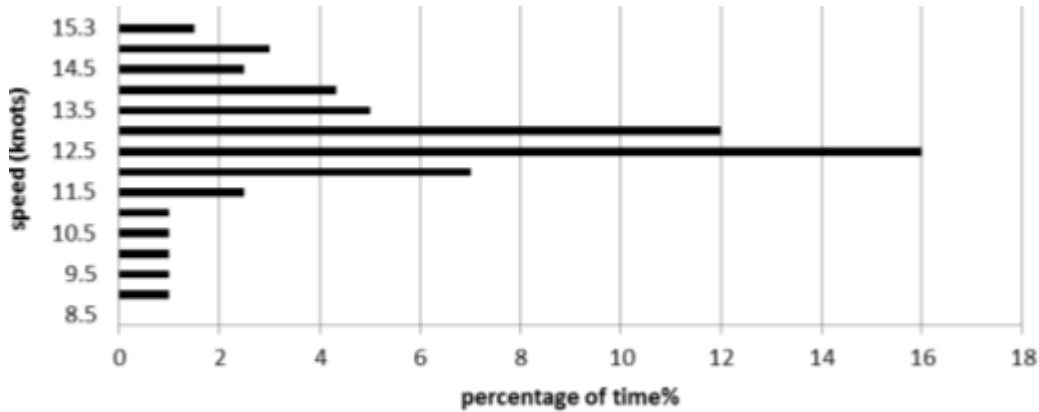


Figure 4-2: Typical speed profile for an Aframax tanker sailing at laden draught (Banks et al. 2013).

- To avoid the potential need for reanalysis and certification of the drive train of the vessel, it was requested to keep the mass and inertia of the replacement propeller within 2 per cent of the values of the currently installed propeller. In the next chapter the study continues with an investigation to determine the importance of this constraint on the delay of cavitation and noise reduction.
- The engines are able to provide a brake power at 100% MCR of 16860 kW. It is understood that the strength of the currently installed propeller has been designed for this power with a maximum thrust of 1961 kN at 91 RPM. No ice class strengthening is considered.
- The installed propeller has been designed following the classification rules of Lloyds Register. The propeller is made of Grade Cu3 NiAL Bronze and weighs 36370 kg. According to MARIN calculation the propeller blades weigh 26380 kg which leaves 9990 kg for the hub. The mass moment of inertia of the blades is 138695 kgm<sup>2</sup>. The contribution of the hub to the mass moment of inertia is 2723 kgm<sup>2</sup> giving a total estimated moment of inertia (wetted) of the propeller of 141418 kgm<sup>2</sup>.

## 4.2 Wake field

MARIN received effective wake fields computed by LR for the vessel sailing at design and ballast draughts. On pages F1 and F2 the axial and transverse velocity components of the wake field for the vessel at design draught is shown. On pages F3 and F4 the same is done for the ballast wake field.

Most notable properties of the provided wake field information is:

- The wake fields show the typical wake field of a full block hull with a deep wake peak (low axial velocities) at the 12 o'clock location. Clearly the ballast wake field has a wider wake peak but not much deeper.
- The wake is slightly asymmetric due to the action of the propeller. This agrees with Marin experience with RANS-BEM calculations.
- The average (integrated) wake fraction of the wake fields are 0.245 for the design wake field and 0.323 for the ballast wake field. In particular the wake fraction for the design draught deviates considerably from comparable ships in the Marin database.

### 4.3 Results

In Task 2 of the project, the performance of the propeller that is supposedly installed on the vessel has been investigated for the two operational draughts. Calculations have been carried out with BEM code PROCAL using the input of the speed-power characteristics of the vessel and the wake fields of the vessel computed by LR.

MARIN constructed a propeller geometry based on available drawings of the propeller design of the vessel and estimates made on remaining parameters that were not available. Notice therefore that the analysed propeller is an approximation of the installed propeller. In the remainder of the report this propeller is called the reference propeller. Details of the propeller geometry are provided in the plots in the next chapter.

#### 4.3.1 Open water efficiency

Open water calculations have been performed to determine the (full scale) open water efficiency of the propeller. Results of the calculations are plotted in the next figure and listed in the table on page T3.

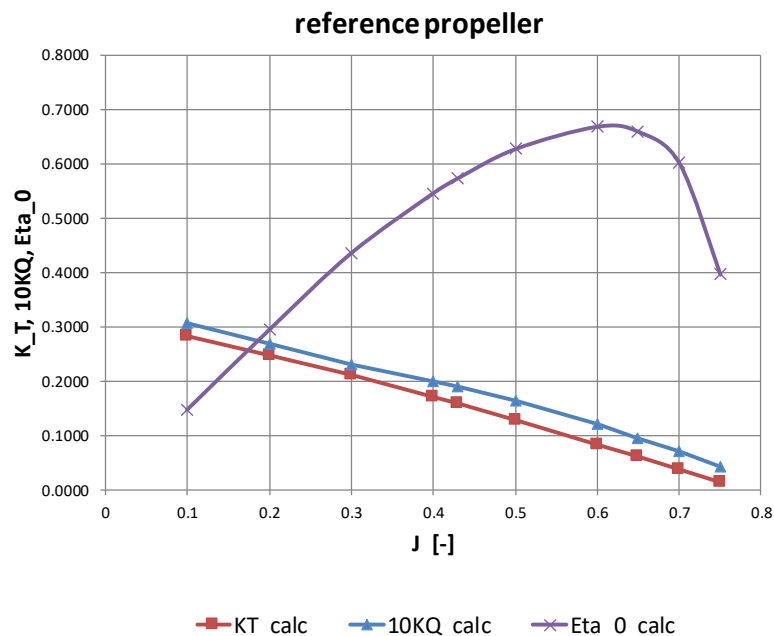


Figure 4-3: Computed open water characteristics of reference propeller (full scale).

At the design point of the propeller (around  $J = 0.43$ ) the open water efficiency is 0.573. Notice that by rule of thumb, very good propellers can have an efficiency value that is 0.565 (0.1515 lower than the ideal efficiency, which is around 0.72 for this propeller). This means that the open water efficiency of the generated propeller is at an expected level.

#### 4.3.2 Cavitation predictions

A series of PROCAL calculations have been performed to determine the cavitation inception characteristics and the extent of the cavitation at the intended operating conditions of the vessel (85% MCR in trial and service condition). In the following sections the results of these calculations are presented.

### 4.3.2.1 Cavitation inception

In the plots in Figure 4-4, the cavitation inception buckets are presented that have been computed for sheet and tip-vortex cavitation types. For each cavitation type, the plots show the variation with propeller loading (in terms of the thrust coefficient  $K_T$ ) of the cavitation inception at the suction side and the pressure side of the propeller blade. Also indicated in the plots are the operating curves for the ideal trial and 15 % sea margin service condition at ballast draught where the propeller is most sensitive to both cavitation occurring at the pressure side and the suction side of the blade.

From the plots and table T2 it can be concluded that the cavitation inception speed is at around 4 to 5 knots due to sharp suction peaks at the propeller in its design condition. It should be noted that some uncertainty exists with regard to the actual loading of the propeller tip because both the pitch at the tip as well as the camber of the profile section is unknown and had to be estimated from similar propeller designs. From the cavitation bucket for sheet cavitation it can be further observed that some pressure side cavitation is expected at the ballast draught trial condition when the propeller is most lightly loaded.

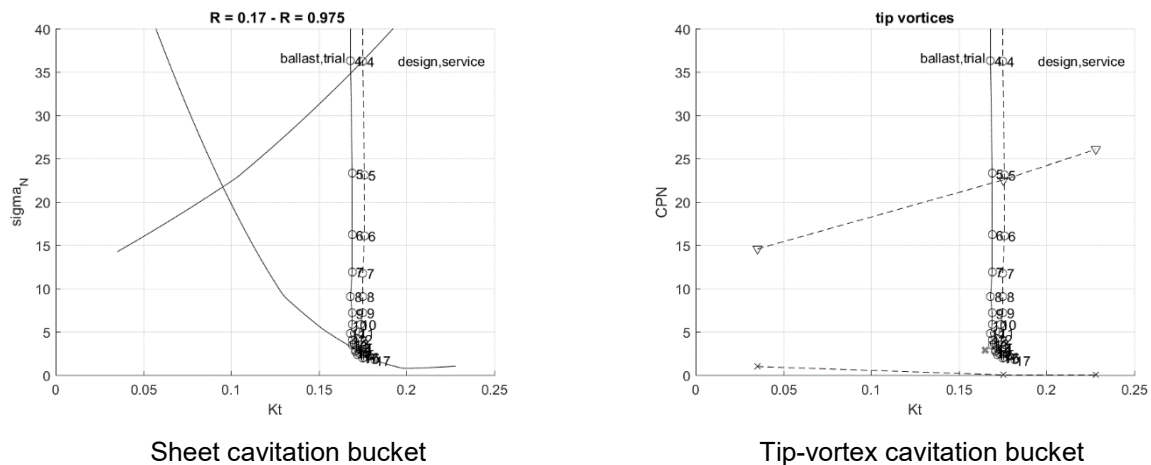


Figure 4-4: Computed cavitation inception buckets and operational curves for design, service and ballast trial conditions.

The cavitation characteristics of the propeller is further illustrated by the pressure distributions plotted on page F6. It can clearly be observed that a very sharp leading edge suction peak is present at the outer blade radii when the blade passes the wake peak of the hull. Indicated in the plots with the red horizontal line is the critical cavitation number at which cavitation is occurring in service (15% SM) at ballast draught. It can be observed that the upper half of the blade (from at least  $r/R = 0.7$  and above) the pressure at the leading edge of the suction side is well below vapour pressure, indicating a large cavity volume (or bubbles).

### 4.3.2.2 Developed cavitation at 85% MCR power

To illustrate the extent of the cavitation at the two draughts, predictions have been made with PROCAL to calculate the dynamic variation of the sheet cavitation

In Figure 4-5 to Figure 4-7 the computed sheet cavitation is shown as calculated for the trial and service condition with 15% sea margin for the propeller at design draught. In Figure 4-7 the sheet cavitation is predicted for the same service condition for the ship sailing at ballast draught. The plots show the sheet cavity developing at the suction side of the blade with the contours showing the pressure at the propeller blade. The pressure is non-dimensionalised by a factor  $ND$ , representing the propeller diameter  $D$  and the rotation rate  $N$ :

$$C_{PN} = \frac{P}{0.5 \rho N^2 D^2}$$

The plots for the design draught show that the sheet cavitation is concentrated at the propeller tip radii and has a large chordwise extent. The cavitation is shown to retreat towards the tip when the blade passes the wake peak around the 12 o'clock position. This behaviour is favourable with respect to the cavitation erosion damage risk.

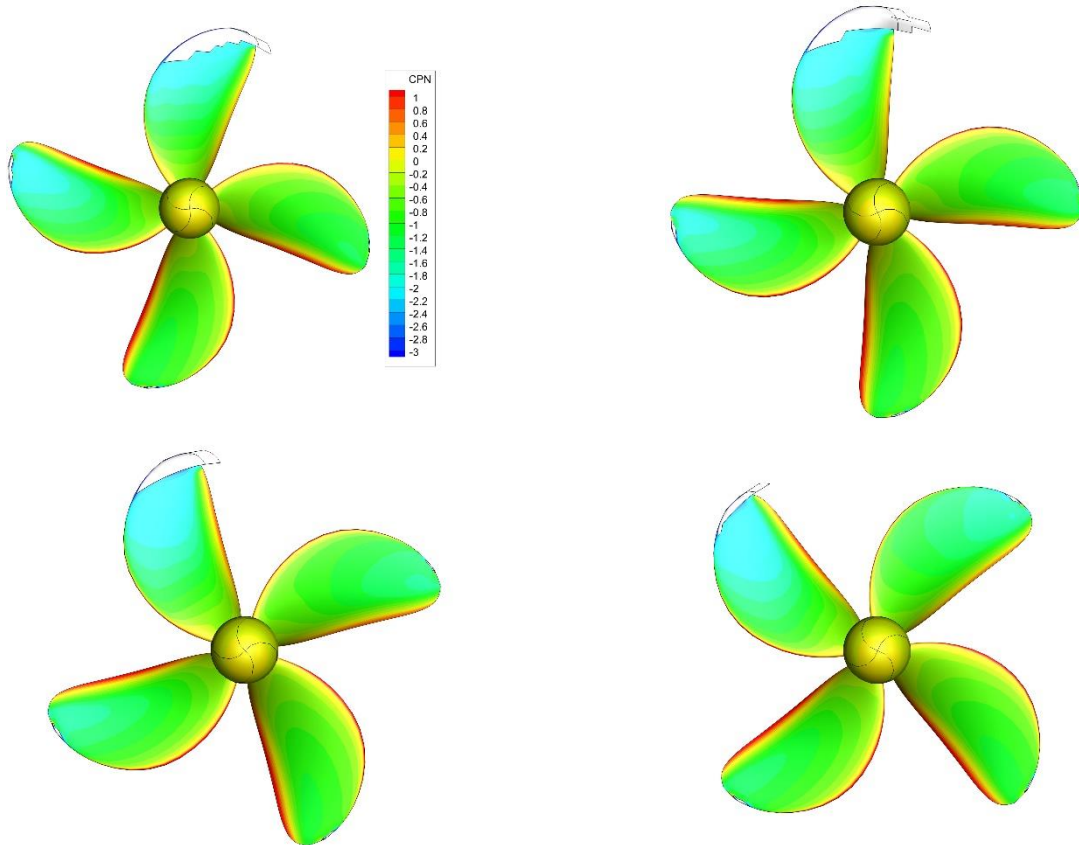


Figure 4-5: Illustration of predicted suction side sheet cavitation patterns and pressure distribution ( $C_{PN}$ ) (Design draught, trial, 85% MCR, 15.11 knots).

Comparison between Figure 4-5 and Figure 4-6 shows that there is not much difference in the extent of the cavitation between trial and service condition at design draught.

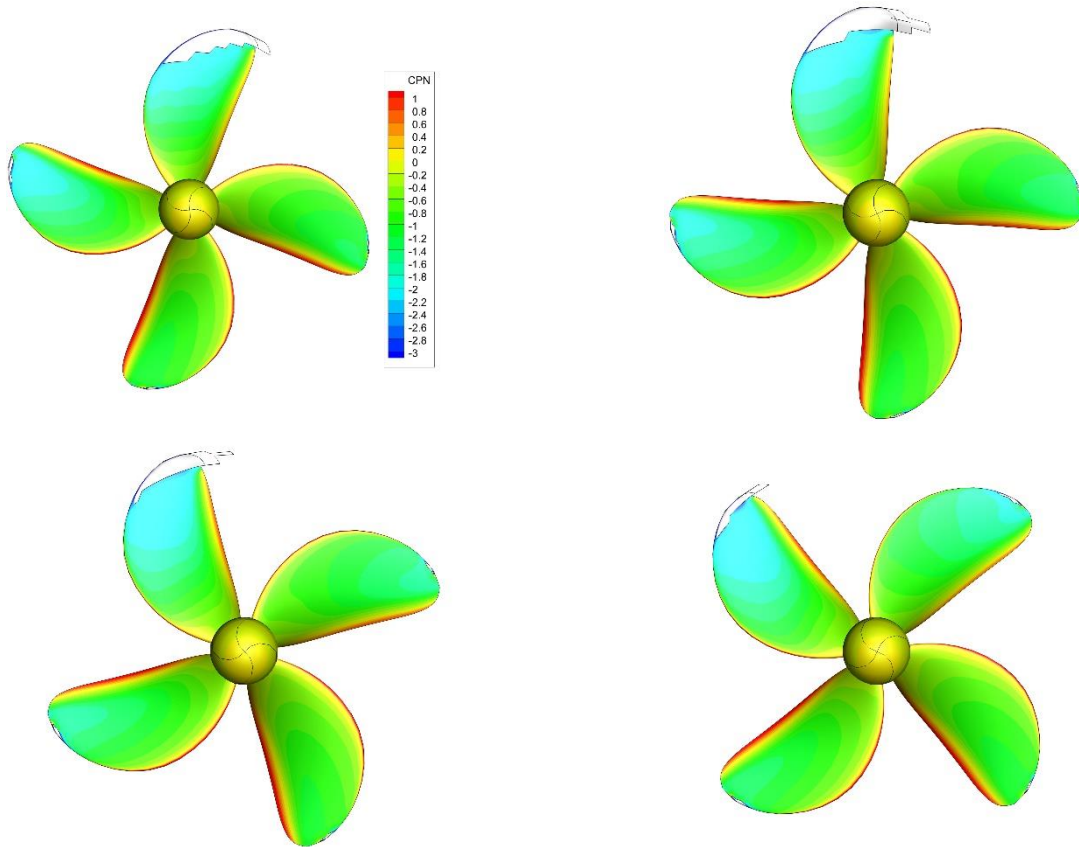


Figure 4-6: Illustration of predicted suction side sheet cavitation patterns and pressure distribution ( $C_{PN}$ ) (Design draught, Service 15% SM, 85% MCR, 14.38 knots).

On the other hand, in Figure 4-7 sheet cavitation development is plotted for the 15% sea margin service condition at ballast draught. A much larger extent of the sheet cavitation is seen with local sheet length exceeding the chord length. It is noted that these cavitation patterns are typically observed for propellers operating behind ship hulls with narrow and deep wake peaks such as seen for full hull form tankers and bulk carriers. Significant interaction of the sheet cavitation with the tip vortex is often seen. The tip vortex stabilises the sheet cavitation, which otherwise would shed collapsing cavities downstream instead of merging nicely with the tip vortex cavitation. A common technique to avoid cavitation erosion therefore is to keep the tip pitch rather high, resulting in a strong tip vortex. This leads to the early inception of tip vortex cavitation as seen in the previous section.

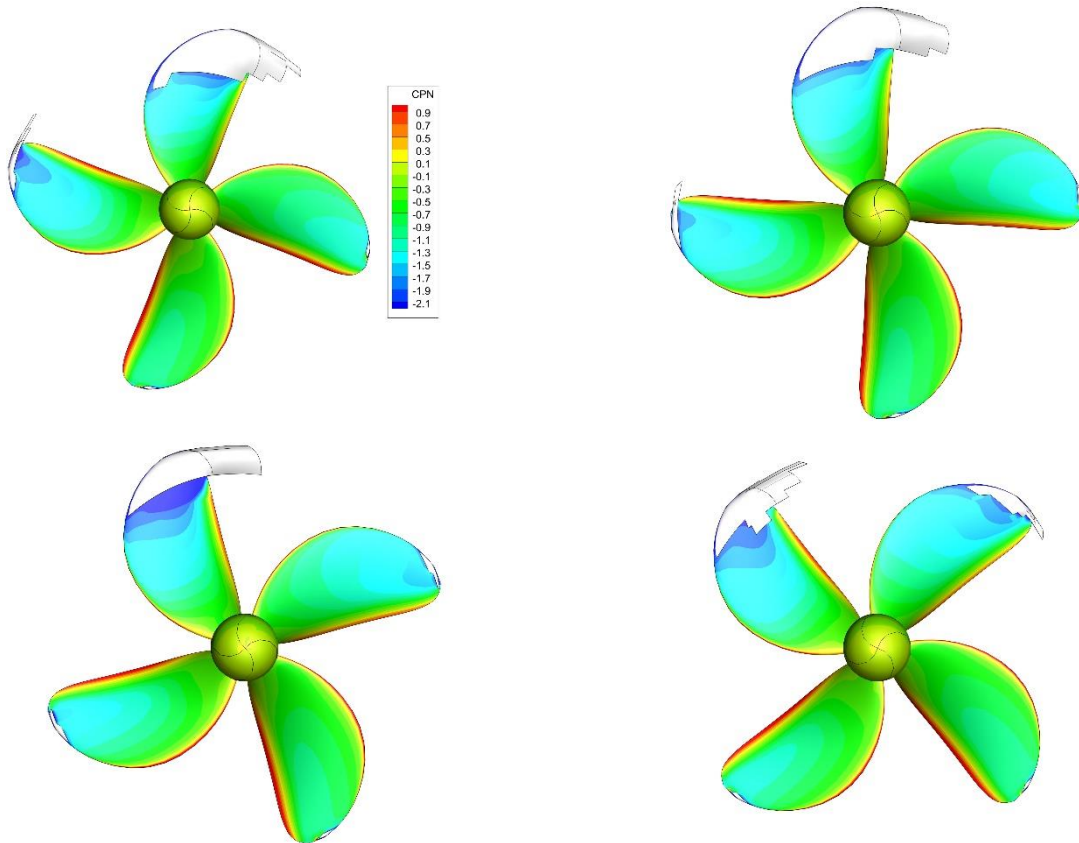


Figure 4-7: Illustration of predicted suction side sheet cavitation patterns and pressure distribution ( $C_{PN}$ ) (Ballast draught, Service 15% SM, 85% MCR, 15.34 knots).

#### 4.3.2.3 Under water noise prediction

Predictions of the underwater noise levels have been made using a recently upgraded version 3.0 of the ETV model to compute the contribution of tip-vortex cavitation, interacting with sheet cavitation at the tip, combined with a semi-empirical model to compute the contribution of isolated sheet cavitation. The latter model is based on the model published by Brown (2007) making use of the cavity areas computed by PROCAL. So far, the model has been validated and tuned using experimental data obtained in the DWB of propellers with isolated face side sheet cavitation, with validation studies for propellers with back-side sheet cavitation still to be performed.

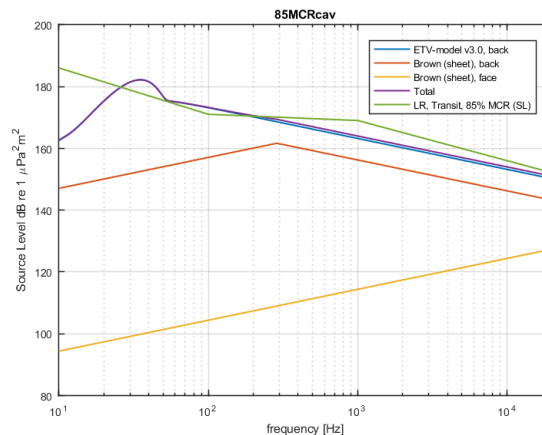


Figure 4-8: Under water noise level versus frequency for the vessel with reference propeller (trial condition at design draught).

In Figure 4-9 and Figure 4-10 the computed noise spectra of the four operational conditions are presented for the ship fitted with the reference propeller sailing in trial condition at design draught (85% MCR). Shown are the contributions of the different cavitation forms and the total source levels in terms of one-third-octave band levels in [dB, re  $1 \mu\text{Pa}^2\text{m}^2$ ]. The levels are compared with the URN limits presented by class society LR for a merchant ship sailing in transit at 85% MCR power. The levels by LR are used as limits and presented as source levels while other class societies present their limits as radiated noise levels, hence including the Lloyd-mirror effect which is a correction that accounts for the noise reflections of the water surface.

The noise plots show the contribution of some pressure side cavitation predicted by PROCAL for the trial condition for both design and ballast draughts and also for the 15% SM service condition at ballast draught. It should be realised that because the camber of the sectional profiles is not known the actual presence of pressure side cavitation on the propeller of the tanker is uncertain. The characteristics of the generated propeller anyway illustrate the noise contributions of the various types of cavitation. Most importantly the overview shows that the contribution of the tip vortex cavitation is the most significant of the cavitation types and its reduction will reduce the cavitation noise the most.

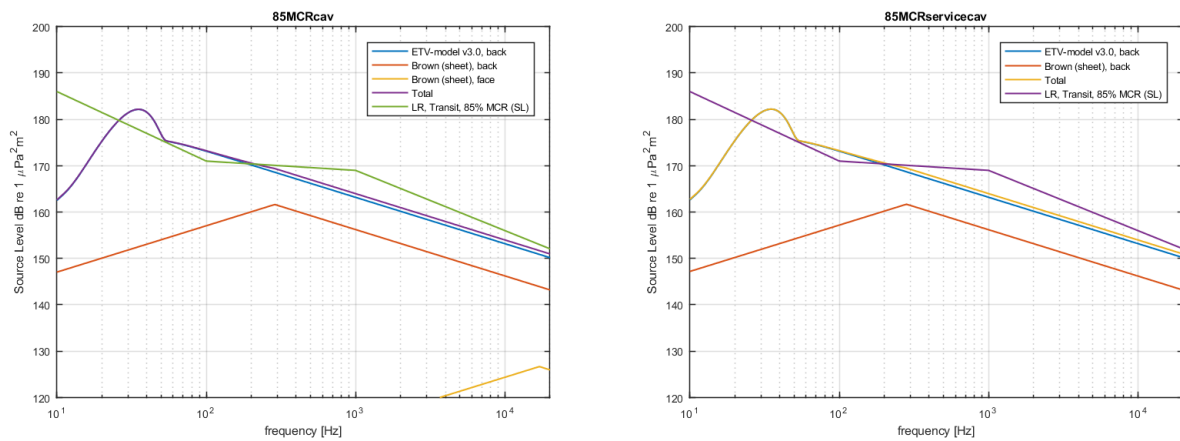


Figure 4-9: Under water noise level versus frequency for the vessel at design draught (left: trial, right: 15 SM service condition).

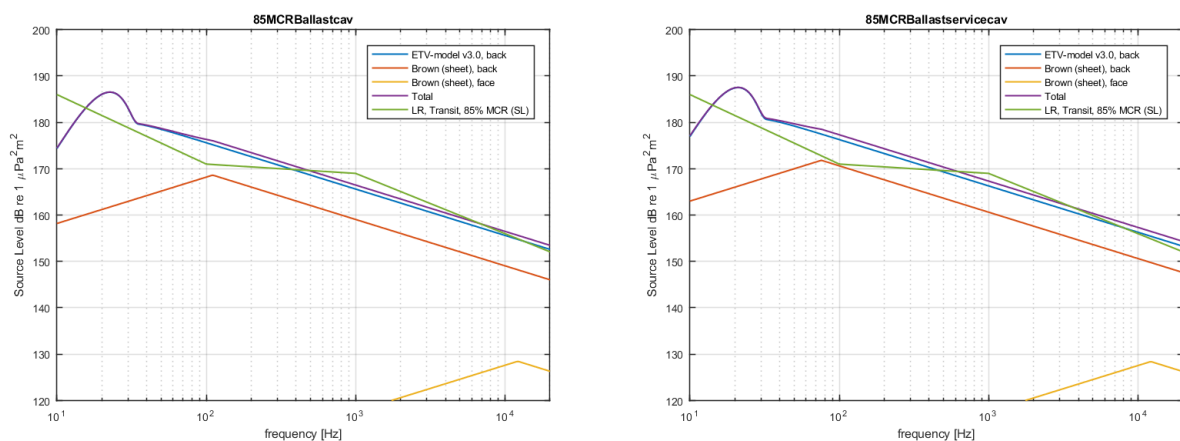


Figure 4-10: Under water noise level versus frequency for the vessel at ballast draught (left: trial, right: 15% SM service condition).



The computed noise levels are in acceptable agreement with the typical source levels for tankers as measured in e.g. the ECHO project, with results presented in Figure 4-11. Main conclusions of the noise calculations are that the calculated URN levels appear in line with levels typically seen for merchant ships and that tip vortex cavitation is the dominant source for propellers like this analysed tanker propeller.

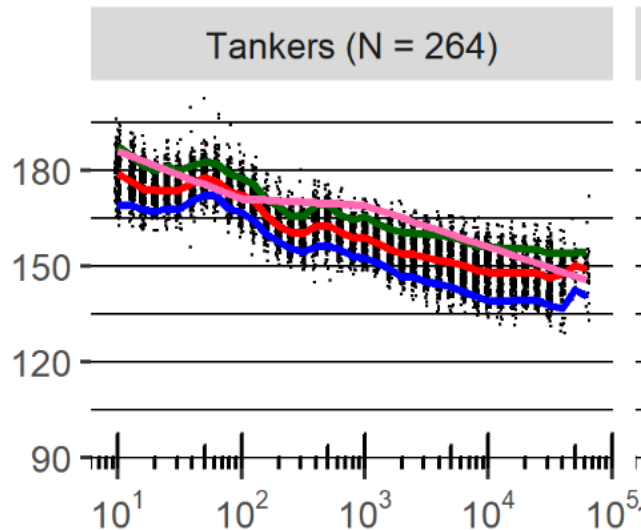


Figure 4-11: Monopole underwater noise source levels measured in the ECHO program, presented in dB re 1 uPa m as function of frequency in Hz. Results have been scaled to a tanker of 170 m, draught of 8.2 m, sailing at 7.5 m/s (14.6 knots), Hannay et al., (2019).

#### 4.3.2.4 Propeller blade strength

To check the strength of the propeller a series of stress calculations have been performed with the VAST FEM code of LR Martec on the basis of an unsteady PROCAL calculation without cavitation. In Figure 4-12 the stress distributions at the suction and pressure side of the blade are plotted for the computed 100% MCR condition. The two plots at the top show the stresses when the blade experiences the minimum blade load during a revolution. The two plots at the middle show the same stresses for an average blade load during the revolution. The plots at the bottom show the same information of a maximum blade load during a revolution.

The stresses are plotted for colour scales that represent the typically allowed stress levels to avoid metal fatigue problems based on MARIN experience. It is noted that these allowed levels are first estimates and depend of course on the quality of the cast bronze propeller as determined by the classification society involved. It can be concluded that for the minimum and average blade loads the stresses are well below the 65 MPa level. For the maximum blade load the blade load is also below the allowed maximum of 85 MPa. This unexpected result shows that there is considerable room for shifting some material (thickness) from the root towards the tip if this would be beneficial for reducing cavitation. It is noted that further FEM analysis of the various replacement propeller variants is further omitted. LR propeller strength rules, as opposed to FEM, are applied in PROPART. This leads to propeller design candidates that satisfy these rules, rather than a FEM computation.

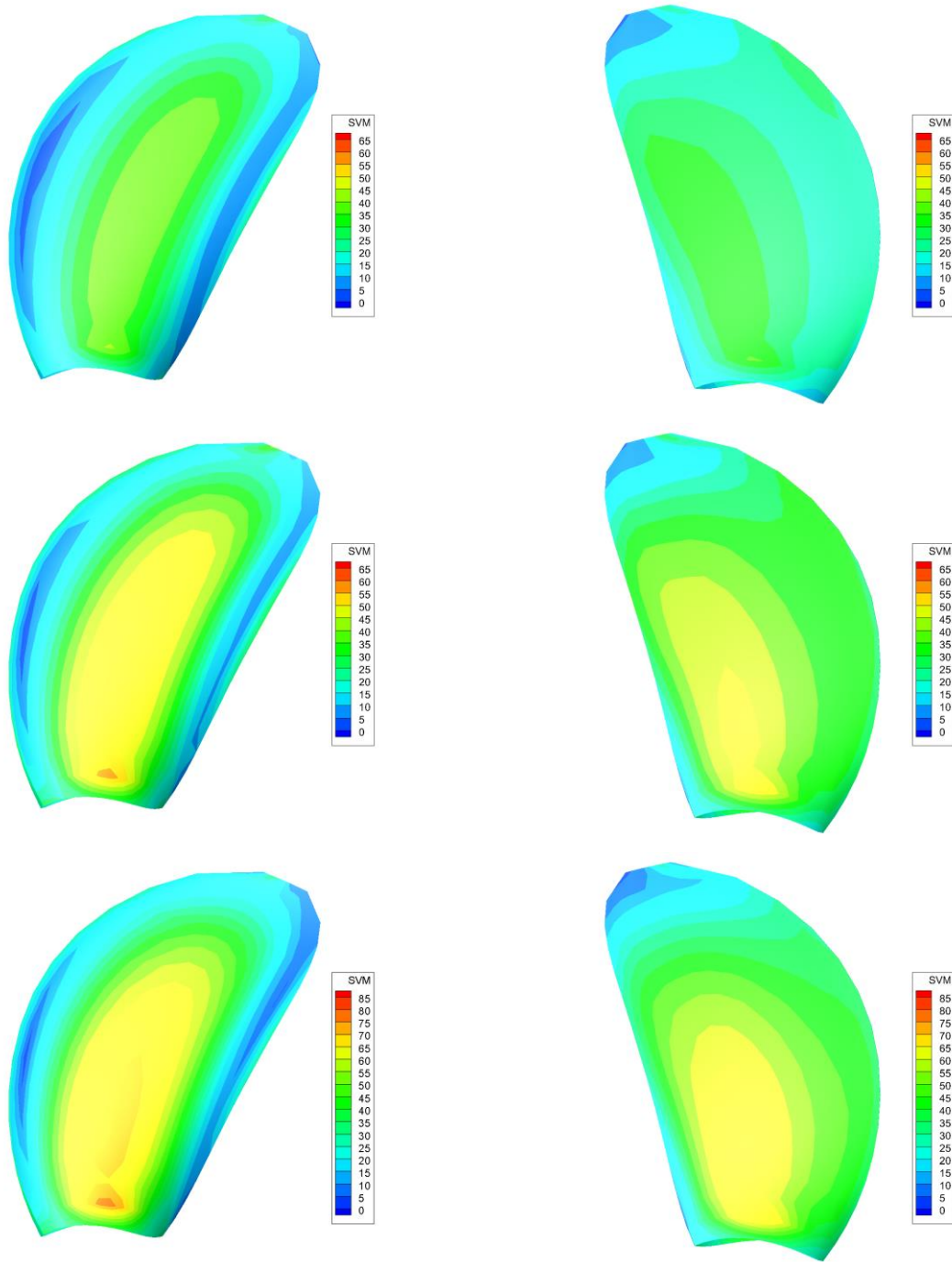


Figure 4-12: Von Mises stresses in the propeller blades (top: minimum blade load, mid: average blade load, bottom: maximum blade load, condition 100% MCR).

## 5 DESIGN OF A 4-BLADE REPLACEMENT PROPELLER

A propeller design optimisation was made with the PROPART tool described in Chapter 2. In the first part of the design study the focus has been the design of a replacement propeller with approximately the same mass and mass moment of inertia of the propeller blades. In an initial series of optimisation attempts the sensitivities of the design goals and constraints were tested. In this report only the results of the final optimisation runs are presented.

### 5.1 Approach

In this section, the details of the propeller optimisation study are first described. Then, in the remainder of the chapter, the design of a 4-blade replacement propeller is described.

#### 5.1.1 Analysis of propeller variants

A lot of possibilities exist in the design of a replacement propeller depending on the characteristics of the ship structure and engine. As a rule the number of blades should not coincide with the number of cylinders of the diesel engine. In this case the diesel engine has 6 cylinders, therefore allowing in principle a 4, 5 and perhaps also potentially the unusual choice of a 7-bladed propeller.

Initially a 4-bladed replacement propeller was studied, first with constraints for the mass and mass moment of inertia, secondly without these constraints. In this part of the study also the shape optimisation of the sectional profiles was considered. Thereafter a 5-bladed and also a 7-bladed propeller variant was optimised, again with both constraint options.

In the next table an overview is given of the propeller variants investigated.

# blades	Sectional profiles		Mass and MOI	
	Standard NACA	Optimised	Constrained	Unconstrained
4-bladed	√	√	√	√
5-bladed	-	√	√	√
7-bladed	-	√	√	√

#### 5.1.2 Goals and constraints

In the design optimisations of the above-described propeller variants the following design goals and optional constraints have been used:

- Maximisation of the in behind propeller efficiency at the 85% trial condition at ballast draught (goal).
- Maximisation of the minimum pressure on the surface of the propeller as well as the tip vortex core (goal).
- No pressure side cavitation at the maximum speed (constraint).
- Propeller blade mass moment of inertia  $I_x$  within 2 per cent of the value of the reference propeller  $138695 \text{ kgm}^2$  (constraint)
- Propeller blade mass within 2 per cent of the weight of the blades of the reference propeller 26380 kg (constraint).
- A further constraint has been posed on the envelope of the minimum pressure in radial direction. By requiring that the pressure decreases towards the tip, the extent of the cavitation will then increase towards the tip, which is required to prevent cavitation erosion.

During the optimisation process propeller design candidates are generated from the parametric design space. These propellers are analysed with respect to the imposed goals and constraints. Designs that violate the constraints are considered not feasible and are not considered in the genetic optimisation process (become extinct). The best performing candidates are selected that maximise or minimise the desired goal (e.g. efficiency). These candidates are used by the optimisation algorithm to converge towards the best possible candidates in the provided design space.

In the current optimisation a newly devised design goal was used combining the delay of both sheet as well as tip vortex cavitation. Notice that this goal is a new approach and is different than the one used for the ORCA patrol vessel where the inception tip vortex and sheet cavitation were treated separately.

In Figure 5-1 the Pareto fronts of optimum propeller designs resulting from the design optimisations for the different propeller design variants and design constraints are plotted in terms of the two specified design goals; the behind propeller efficiency and the minimum value of the cavitation inception margin as a percentage of the pressure coefficient CPN. Notice further that the variation of the efficiency is shown as a percentage of the efficiency of the reference propeller. The margin on CPN has a very large negative value, meaning there is always cavitation present. Also the difference of the mass of the blades of the design variants with the reference propeller is shown by colouring of the markings. The result clearly shows the trend of decreasing efficiency and improving cavitation margins with increasing blade mass.

From Figure 5-1 it can be observed that the propeller design variations with optimisation sectional profiles decisively outperform the variants with conventional NACA profiles, see run 5b compared to the others. The results of the optimisations for the NACA profiles are not further reported therefore. The best Pareto fronts for the 4-bladed propeller are obtained for run 6a for the mass and inertia constrained propeller design and run 8a for the unconstrained design. Results for 5 and 7 blades are reported in the next chapter.

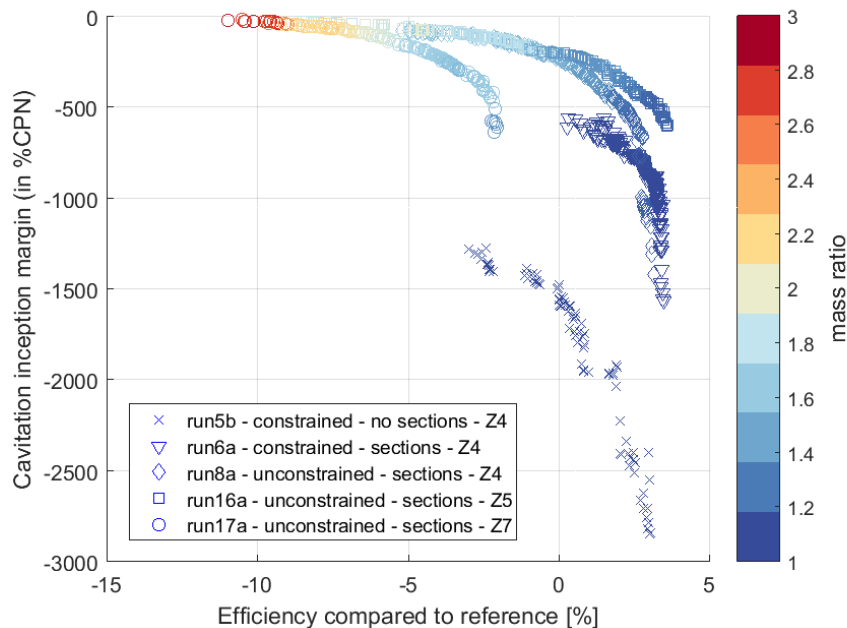


Figure 5-1: Pareto fronts for optimum designs for efficiency and cavitation inception margin.

## 5.2 4-bladed propeller – constrained design

The reported result involves the optimisation of a 4-bladed propeller design with mass and inertia constraints. In this optimisation the shape of the sectional profiles has been varied as well. The diameter was kept at the value of the installed propeller (8.2 m). From the Pareto front of optimum propellers two extremes (#157 and #173) were selected. The first with the highest efficiency and the second with the largest cavitation margin for similar efficiency, see Figure 5-2. A further reasonable choice could have been candidate #126 which could be seen as the best combination of both goals. Notice that in the Pareto plot also the values for the reference propeller are shown by a black marking at the bottom of the plot.

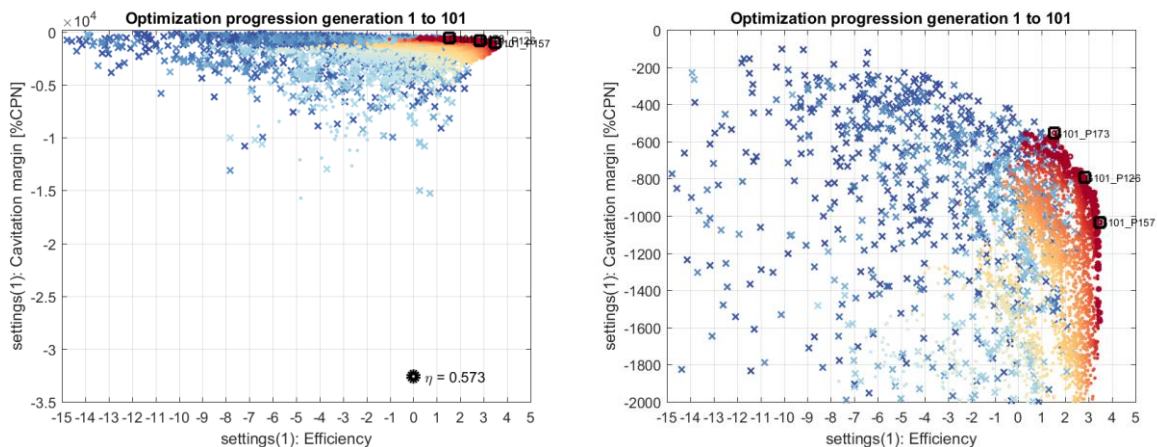


Figure 5-2: Constrained 4-bladed propeller: Pareto front plots showing percentage efficiency difference compared to the reference propeller and the cavitation margin (left: overall view, right: detail view).

In Figure 5-3 the radial variation of the minimum value of the pressure coefficient CPN on the blade sections is plotted (associated with sheet cavitation) and the minimum value at the tip (obtained from the ETV model associated with tip vortex cavitation). The latter is indicated by the bold symbol. Notice that for the optimum designs the sheet and tip vortex cavitation are delayed similarly, indicated by equal CPN values of the sheet and tip vortex points. As can be seen from the same plot, the pressure is favourably decreasing towards the tip, as intended in an effort to prevent the development of isolated sheet cavitation, which could lead to cavitation erosion.

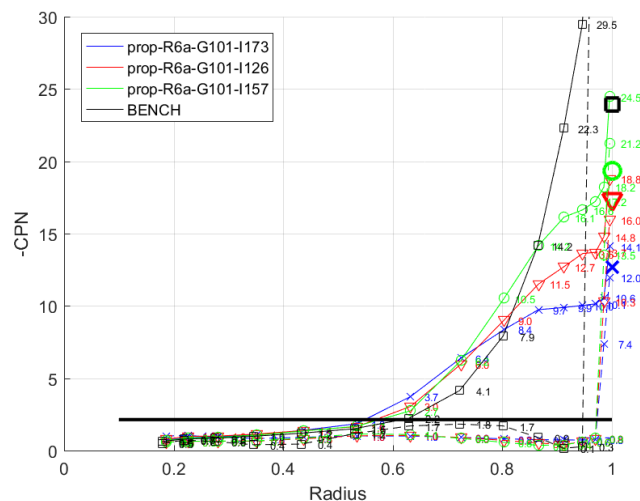


Figure 5-3: Constrained 4-bladed propeller: plot of minimum CPN over the radius  $r/R$ .

The minimum values of the CPN can be compared with the values of the cavitation number shown in the table on page T2. Notice that with a (still low) minimum value CPN of around -14 found for propeller #173, it can be observed from table T2 that for the ballast trial condition the cavitation inception speed can be expected to be between 6 and 7 knots. This is already a few knots higher compared to the reference propeller (estim. 4 – 5 knots). See also the cavitation inception diagrams in Appendix II.

Notice from Figure 5-3 that optimally, the value of the CPN for the tip vortex cavitation would be equal to that of sheet cavitation (i.e. the inception of both types occur at the same speed). This means that in case of propeller variant #173 the loading at the tip could have been slightly increased resulting in a slightly stronger tip vortex to arrive at the same CPN value. This option has not yet been considered in the goal definition of the current study but is certainly recommended to be considered for future optimisation studies. Alternatively one can optimise for cavitation noise directly.

In Figure 5-4 and on page F7 a comparison is shown between the geometries and geometry parameters of the selected candidate propellers with the reference propeller (Bench). Noticeable differences are:

- Allowed by the strength margin in the installed propeller some volume (thickness) is shifted towards the tip.
- A much reduced pitch and camber is obtained near the tip reducing the tip loading and delaying tip vortex cavitation.

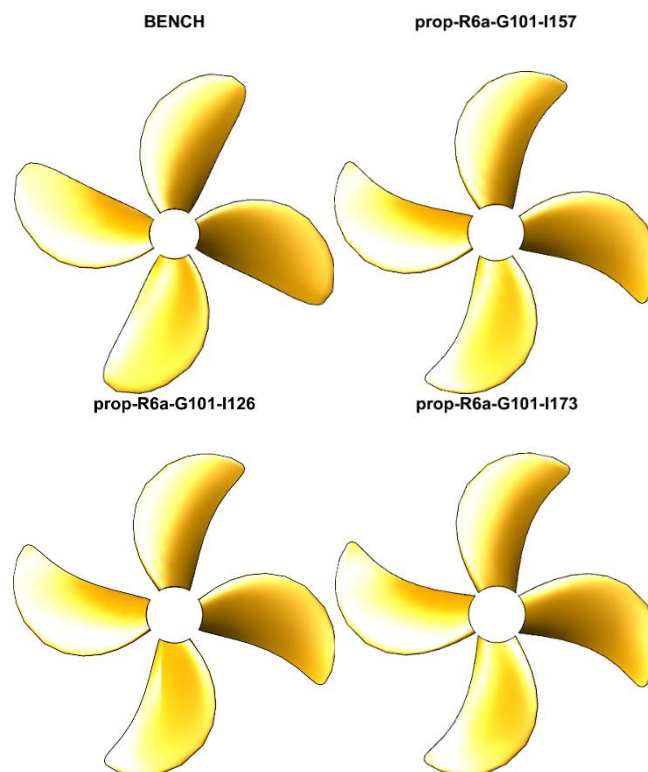


Figure 5-4: Constrained 4-bladed propeller: blade shape of reference propeller and three selected propellers from the Pareto front.

Further comparisons of the sectional profile shape of the selected propellers compared to the reference propeller are shown on pages F8 and F10.

For reference, values of the mass and mass moment of inertia of the propeller variants are listed in the table on page T4.

### 5.3 4-bladed propeller – unconstrained

The presented results involve the optimisation of a 4-bladed propeller design without mass and inertia constraints. Again the diameter was kept at 8.2 metres. From the obtained Pareto front of optimum propellers from this run two extremes (#42 and #176) were selected. The first with an efficiency that is almost 3 per cent higher than that of the reference propeller and the second one with the largest cavitation margin, see Figure 5-5. Notice that this choice is merely made to visualise the extremes of the optimum propellers along the Pareto front. Additional constraints on the efficiency level could easily lead to a different selection such as propeller #150 which has almost the same efficiency as the reference propeller. Notice further that again the reference propeller is shown in the left Pareto plot.

Similar as in Section 5.1.3 for the constrained propellers in Figure 5-6 the radial variation of the minimum value of the pressure coefficient CPN on the blade sections is plotted for the unconstrained 4-bladed propeller designs. As can be seen from the same plot, the pressure is favourably decreasing towards the tip, as intended in an effort to prevent the development of isolated sheet cavitation, which could lead to cavitation erosion.

Notice that with a minimum CPN of around -4.5 it can be observed from the cavitation numbers listed on page T2 for the ballast trial condition that cavitation inception for this propeller can be expected at around 11 knots, which is a very considerable improvement compared to the reference propeller (i.e. 4-5 knots). The efficiency penalty for this variant is about 5.5 per cent. With a minimum CPN of -7.6, variant #150 approaches a cavitation inception speed of 8 knots while its efficiency is more or less equal to that of the reference propeller. In other words, a 3 knot increase of the cavitation inception speed, from 8 to 11kn, has an efficiency penalty of about 5 per cent. See also the cavitation inception diagrams in Appendix II.

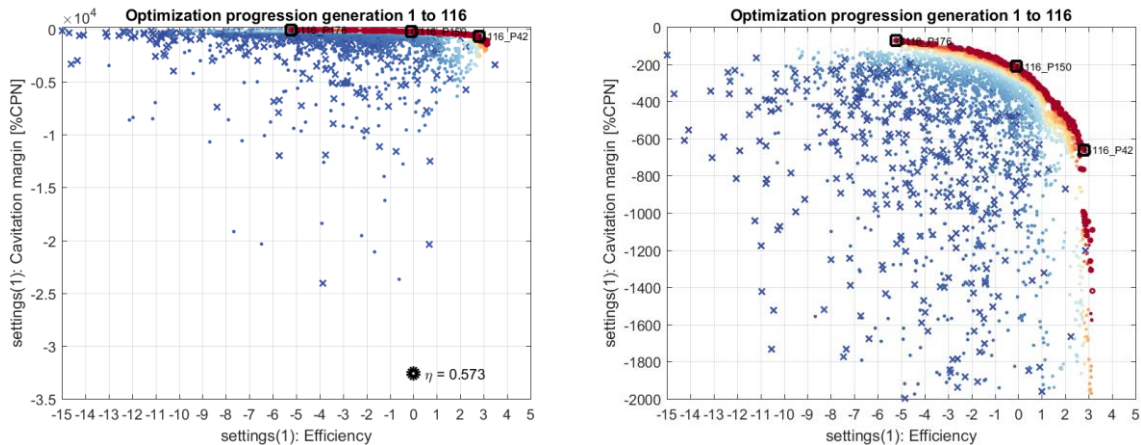


Figure 5-5: Unconstrained 4-bladed propeller: Pareto front plots showing percentage efficiency difference compared to the reference propeller and the cavitation margin (left: overall view, right: detail view).

The following provides details about the mass and mass moment of inertia of the blades and its percentage increase with respect to the blades of the reference propeller. An overview of all propeller design variants can be found on page T4.

- Propeller #42 has a blade mass of 29057 kg (+10.1%) and a mass moment of inertia  $I_x$  of 173220  $\text{kgm}^2$  (+24.9%).
- Propeller #150 has a blade mass of 39557 kg (+50%) and a mass moment of inertia  $I_x$  of 286630  $\text{kgm}^2$  (+106%).
- Propeller #176 has a blade mass of 43469 kg (+64%) and a mass moment of inertia  $I_x$  of 308710  $\text{kgm}^2$  (+ 122%).

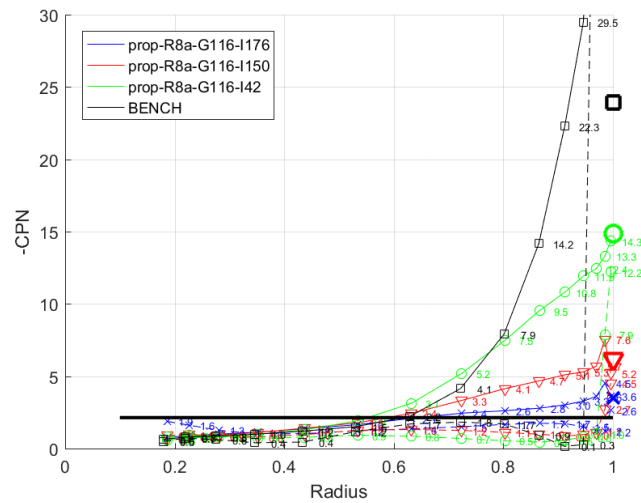


Figure 5-6: Unconstrained 4-bladed propeller: plot of minimum CPN over the radius  $r/R$  (right).

Again comparisons of the geometry parameters of the selected candidate propellers are made in Figure 5-7 and pages F8 and F9. Noticeable differences are:

- The thickness and chord length are considerably larger for variant #176 than for the reference propeller, in particular near the tip.
- Also a much reduced pitch and camber is seen for this variant reducing the tip loading and delaying tip vortex cavitation.

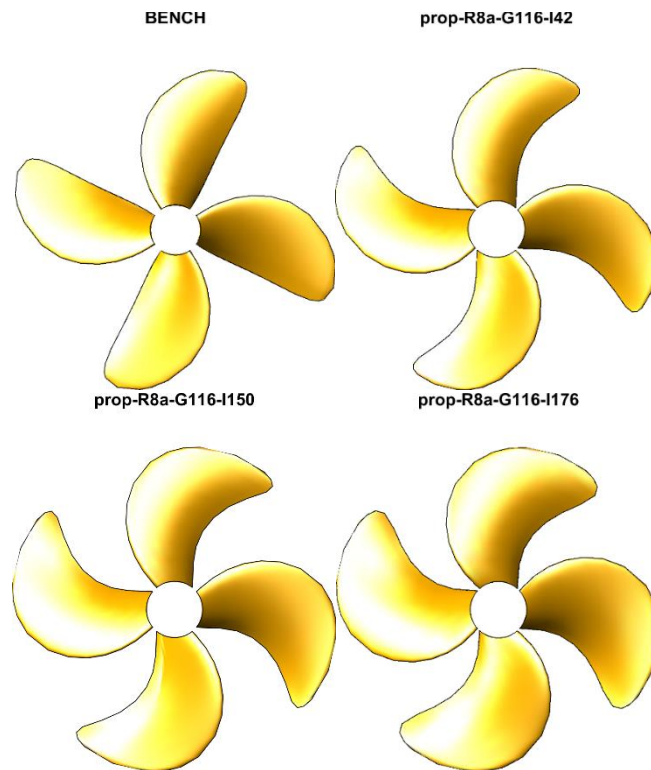


Figure 5-7: Unconstrained 4-bladed propeller: blade shape of reference propeller and three selected propellers from the Pareto front.



#### 5.4 Developed cavitation and URN predictions (85% MCR service condition at ballast draught)

A comparison is made of the cavitation patterns predicted for the selected constrained and unconstrained designs with the least amount of cavitation. The calculations have been made for the most critical condition (service at ballast draught) for constrained 4-bladed propeller #173 and unconstrained 4-bladed propeller #176. As can be observed from Figure 5-8 and Figure 5-9 there is a very large difference in the amount of sheet cavitation with only a limited amount of cavitation predicted for the unconstrained propeller.

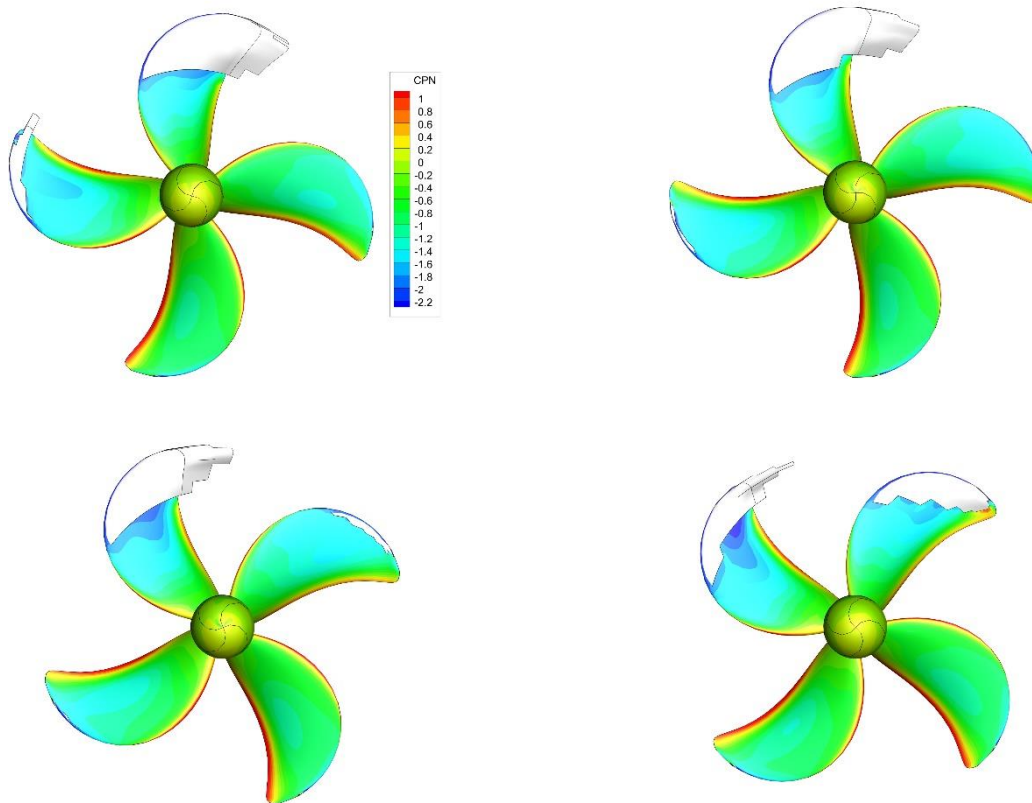


Figure 5-8: Predicted suction side sheet cavitation patterns and pressure distribution ( $C_{PN}$ ) (Constrained design variant #173, Ballast draught, Service 15% SM, 85% MCR).

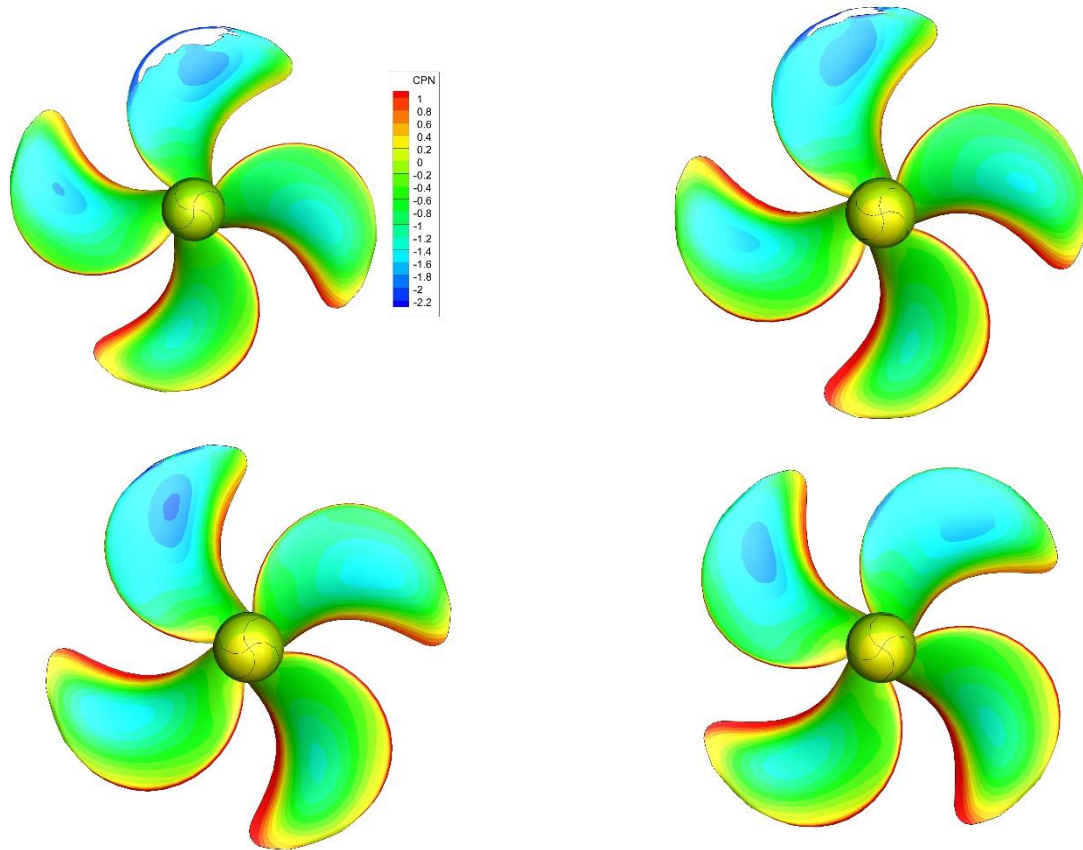


Figure 5-9: Predicted suction side sheet cavitation patterns and pressure distribution ( $C_{PN}$ ) (Unconstrained design variant #176, Ballast draught, Service 15% SM, 85% MCR).

Predictions of the underwater noise levels have been made for the same service condition at ballast draught based on the above presented sheet cavitation predictions and the tip vortex prediction of the ETV model. In Figure 5-10 the computed noise spectra of the constrained and unconstrained propeller variants are compared with the spectrum of the reference propeller. Shown are again the contributions of the different cavitation forms, the total source level and the reference source level of merchant ships sailing in transit at 85% power as determined by LR.

For the designed variants no pressure side sheet cavitation is contributing to the total noise levels. Constrained variant #173 generates a very similar noise level as the reference propeller, which is not unexpected given the modest reduction of the amount of cavitation. Unconstrained variant #176 shows a very large reduction of the underwater noise with peak levels dropping from about 187.5 dB at 10 Hz to 175.3 dB at 40 Hz corresponding to a reduction of the maximum noise level by 12 dB.

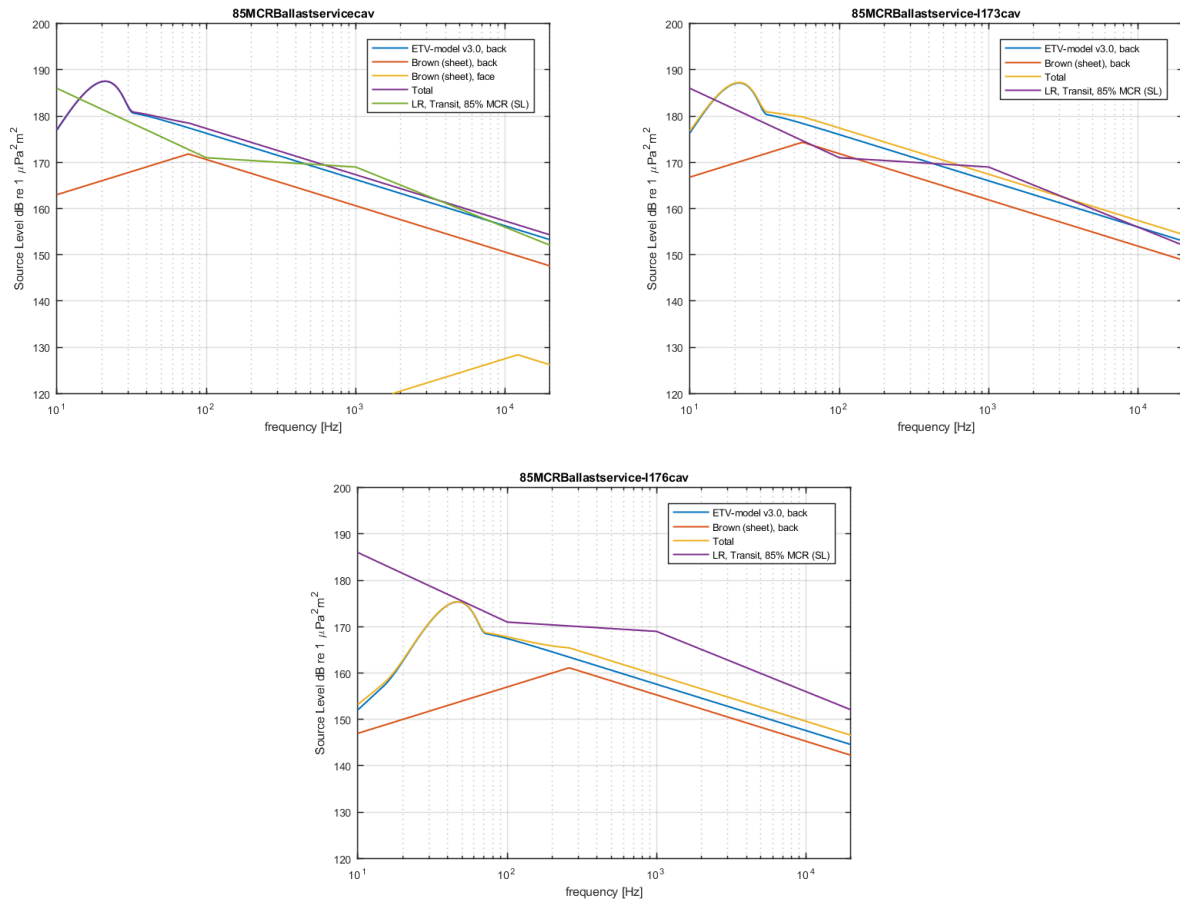


Figure 5-10: Under water noise level versus frequency for the vessel at ballast draught at 15% SM service condition (top left: reference propeller, top right: constrained variant #173, bottom: unconstrained variant #176).

## 6 THE EFFECT OF INCREASING THE NUMBER OF BLADES

Another possibility to reduce the underwater radiated noise of the tanker's propeller is the change to a 5 or even 7-bladed propeller. The idea behind this choice is that the loading of the (original) 4 blades is divided over an increased number of blades leading to a reduction of the circulation for each of the blades. This reduction and in particular the circulation near the tip will reduce the strength of the tip vortices and thereby could delay the inception of tip vortex cavitation or reduce its noise when cavitating.

Therefore an additional round of optimisation runs was performed for the same constraints and goals as for the 4-bladed propellers presented in Chapter 5 but now for a 5 and 7 bladed propeller. Notice that the diameter of a propeller that is optimum with regard to efficiency depends on the number of blades and therefore also the variation of the diameter was included in the parameter variation.

The Pareto fronts of a series of optimisation attempts are shown for constrained and unconstrained 5 and 7-bladed propeller are shown together with the results for the 4-bladed propellers in Figure 5-1. From the plot it can be concluded that there is a clear influence of the number of blades. Most promising appears to be the unconstrained 5-bladed propeller with regard to both cavitation margin as well as efficiency. The efficiency penalty of a 7-bladed propeller appears substantial, at least from this exercise. Also clearly the best results are obtained for the designs without mass and MOI restrictions.

### 6.1 5-bladed propeller

An optimisation calculation was done for a 5-bladed propeller design without mass and MOI constraints and including the variation of the sectional profiles. The diameter was varied between 7.3 and 8.2 metres. From the Pareto front of optimum propellers two extremes (#64 and #69) and the best of both (#155) with respect to the optimisation goals were selected. Propellers #64, #155 and #69 have slightly different diameters of respectively 8.07, 8.15 and 8.2 metres.

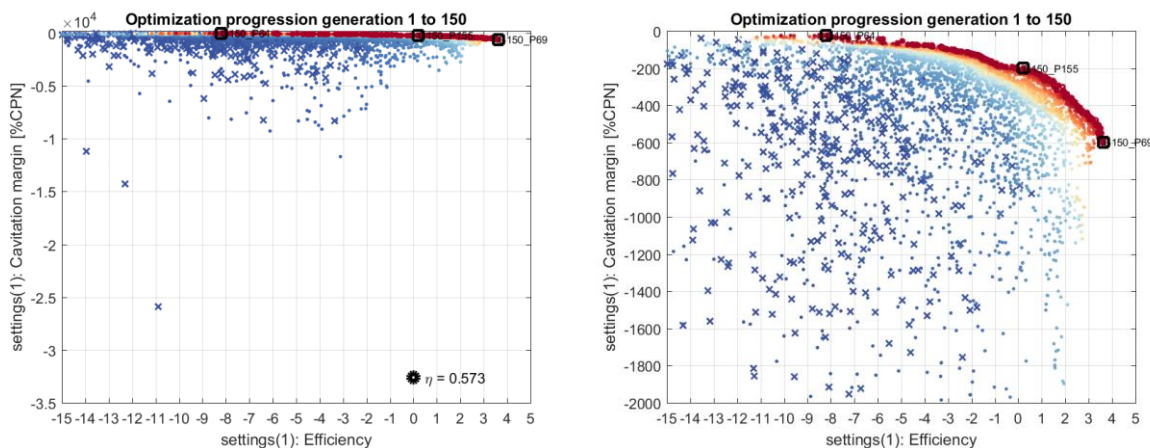


Figure 6-1: Unconstrained 5-bladed propeller: Pareto front plots showing percentage efficiency difference compared to the reference propeller and the cavitation margin (left: overall view, right: detail view).

In Figure 6-2 the radial variation of the minimum value of the pressure coefficient CPN on the blade sections is plotted for the three selected propellers. A lowest value of CPN of -3.1 is found for propeller #64. This corresponds with a cavitation inception speed in the ballast trial condition of about 14 knots, see the cavitation inception diagrams in Appendix II. This is at the expense of an approximate 8 per cent loss in efficiency which could be unacceptable. A choice for variant #155 with a similar efficiency as the reference propeller would lead to a CPN value of around -6.6 which allows a cavitation inception speed of around 9.5 knots. Notice that small diameter differences results in slightly different locations of the operating curves in the cavitation inception diagrams which is disregarded for the 5-bladed propellers.

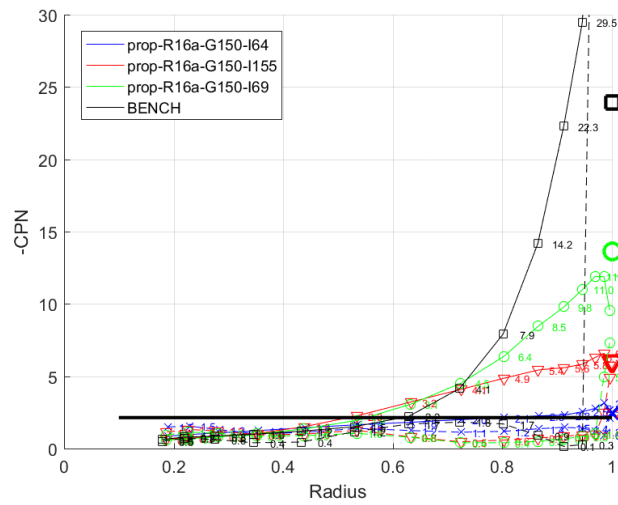


Figure 6-2: Unconstrained 5-bladed propellers: plot of minimum CPN over the radius  $r/R$  (right) for selected candidate designs compared to reference propeller (bench).

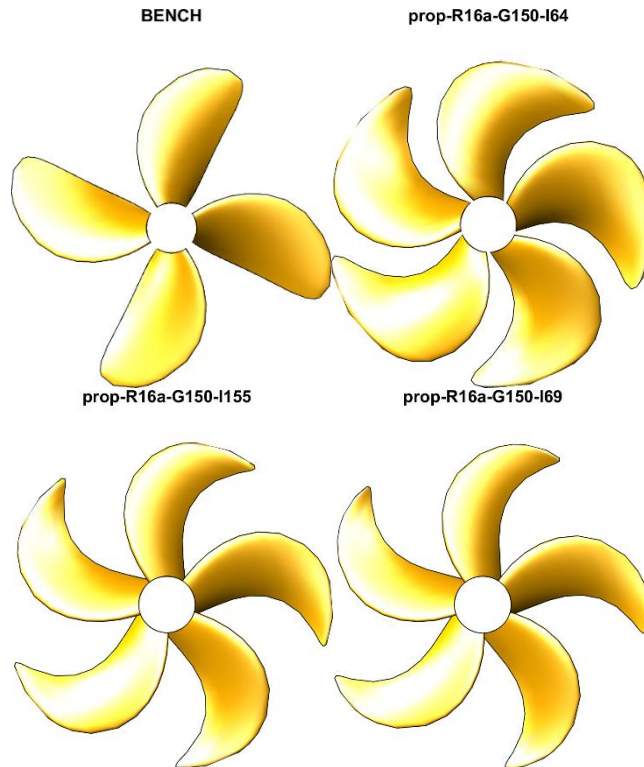


Figure 6-3: Unconstrained 5-bladed propeller: blade shapes of reference propeller and three selected propellers from the Pareto front.

In Figure 6-3 and on page F11 comparisons are shown of the geometries and geometry parameters of the selected candidate propellers with the reference propeller. Notice that similar trends are visible such as the shifting of volume (chord length and thickness) towards the tip.

Considering the similar efficiency of propeller variant #155 compared to the reference propeller the extent of the developed cavitation and the underwater noise of this propeller is further analysed in the next Section 6.3.

The following provides details about the mass and mass moment of the blades at its percentage increase with respect to the blades of the reference propeller. An overview of all propeller design variants can be found on page T4.

- Propeller #64 has a blade mass of 48030 kg (+82%) and a mass moment of inertia  $I_x$  of 372980  $\text{kgm}^2$  (+168%).
- Propeller #155 has a blade mass of 33766 kg (+28%) and a mass moment of inertia  $I_x$  of 226720  $\text{kgm}^2$  (+63.4%).
- Propeller #69 has a blade mass of 29438 kg (+12%) and a mass moment of inertia  $I_x$  of 166020  $\text{kgm}^2$  (+ 19.7%).

### 6.2 7-bladed propeller

A further optimisation was performed for a 7-bladed propeller variant without considering mass and MOI constraints and including the variation of the sectional profiles. The diameter was varied between 7.3 and 8.2 metres. From the Pareto front of optimum propellers two extremes (#89 and #100) and the best compromise of both (#50) with respect to the optimisation goals were selected. The diameters of propellers #50, #89 and #100 are respectively 7.82, 7.77 and 8.0 metres.

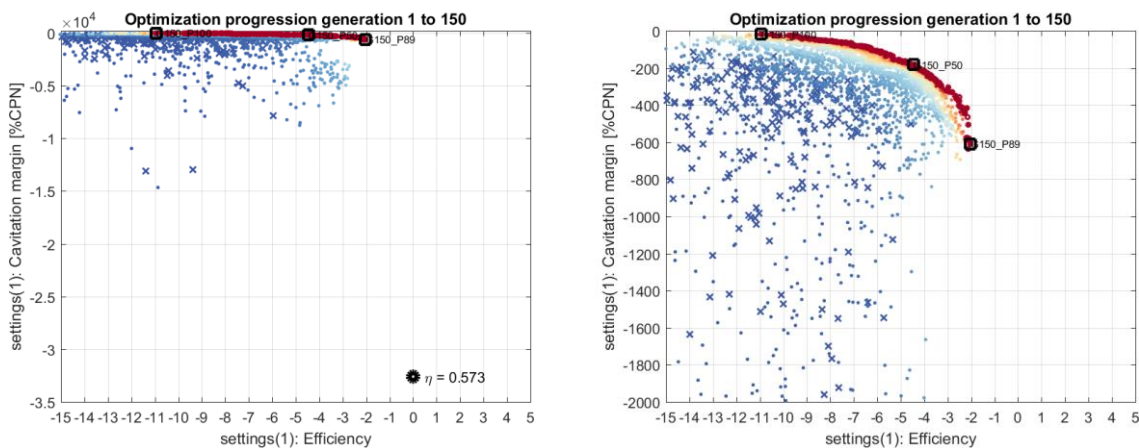


Figure 6-4 Unconstrained 7-bladed propeller: Pareto front plots showing percentage efficiency difference compared to the reference propeller and the cavitation margin (left: overall view, right: detail view).

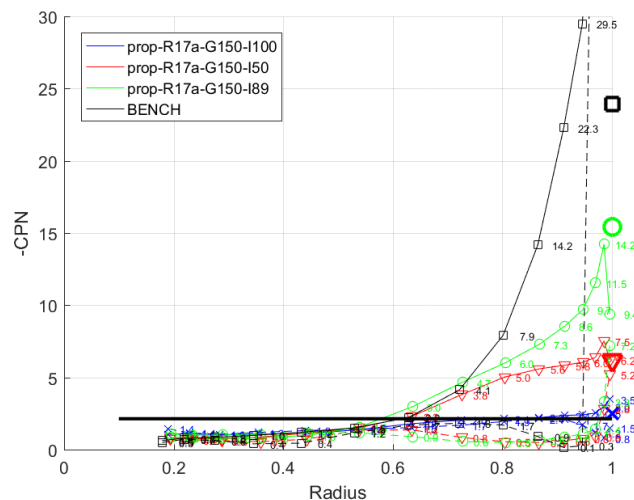


Figure 6-5: Unconstrained 7-bladed propellers: plot of minimum CPN over the radius  $r/R$  (right) for selected candidate designs compared to reference propeller (bench).

In Figure 6-5 the radial variation of the minimum value of the pressure coefficient  $CPN$  on the blade sections is plotted for the three selected propellers. A lowest value of  $CPN$  of  $-3.5$  is found for propeller #100, which is lower than 5-bladed propeller #64. This corresponds with a cavitation inception speed in the ballast trial condition of about 13 knots, see the table on page T2. A loss of efficiency of about 11 per cent compared to the reference propeller is even larger than that for the 5-bladed propeller. The compromise propeller #50 has a  $CPN$  value of  $-7.4$  corresponding to a cavitation inception speed of just below 9 knots and an efficiency loss of 4.5 per cent. See also the cavitation inception diagrams in Appendix II.

Comparisons of the geometry parameters of the selected candidate propellers are shown in

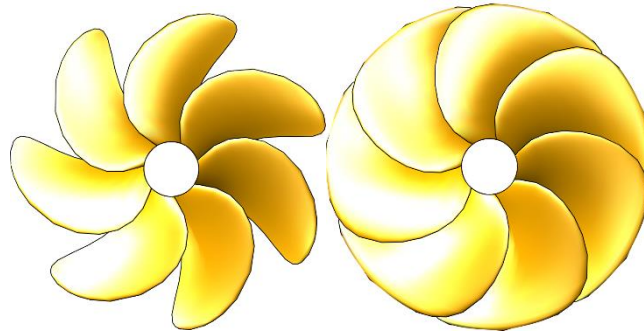


Figure 6-6 and page F12. From observation of the blade contours it becomes obvious that the very low efficiency of propeller #100 is caused by the large blade area of the propeller. The large area of the blades are apparently necessary for delaying inception of sheet cavitation.

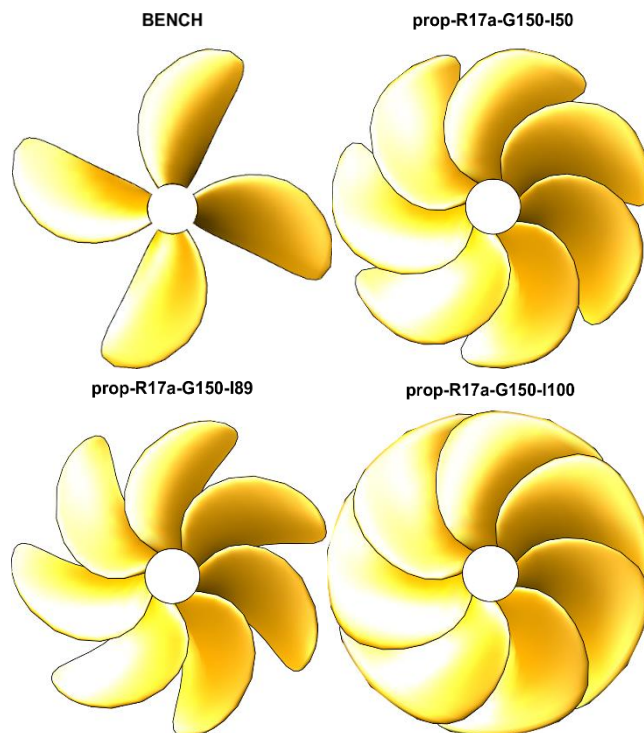


Figure 6-6: *Unconstrained 7-bladed propeller: blade shapes of reference propeller and three selected propellers from the Pareto front.*

Considering the limited loss of efficiency of 4.5 per cent of variant #50 compared to the reference propeller the extent of the developed cavitation and the underwater noise is further analysed for this propeller in the next section.

The following provides details about the mass and mass moment of the blades at its percentage increase with respect to the blades of the reference propeller. An overview of all propeller design variants can be found on page T4.

- Propeller #50 has a blade mass of 43504 kg (+82%) and a mass moment of inertia  $I_x$  of 328460  $\text{kgm}^2$  (+168%).
- Propeller #89 has a blade mass of 35608 kg (+28%) and a mass moment of inertia  $I_x$  of 22270  $\text{kgm}^2$  (+63.4%).
- Propeller #100 has a blade mass of 76375 kg (+64%) and a mass moment of inertia  $I_x$  of 632100  $\text{kgm}^2$  (+ 19.7%).

### 6.3 Developed cavitation and URN predictions for selected 5 and 7 blade propellers

A comparison is made of the cavitation patterns predicted for the selected unconstrained 5 and 7 blade propeller designs. The calculations have been again been made for the most critical condition (service at ballast draught) for unconstrained 5-bladed propeller #155 and unconstrained 7-bladed propeller #50. As can be observed from Figure 6-7 and Figure 6-8 there is a large difference in the amount of sheet cavitation with only a limited amount of cavitation predicted for the selected 7-bladed propeller variant. Notice also that because of the isolated character of the sheet cavitation on the 5-bladed propeller the propeller will not be acceptable from the point of risk of cavitation erosion.

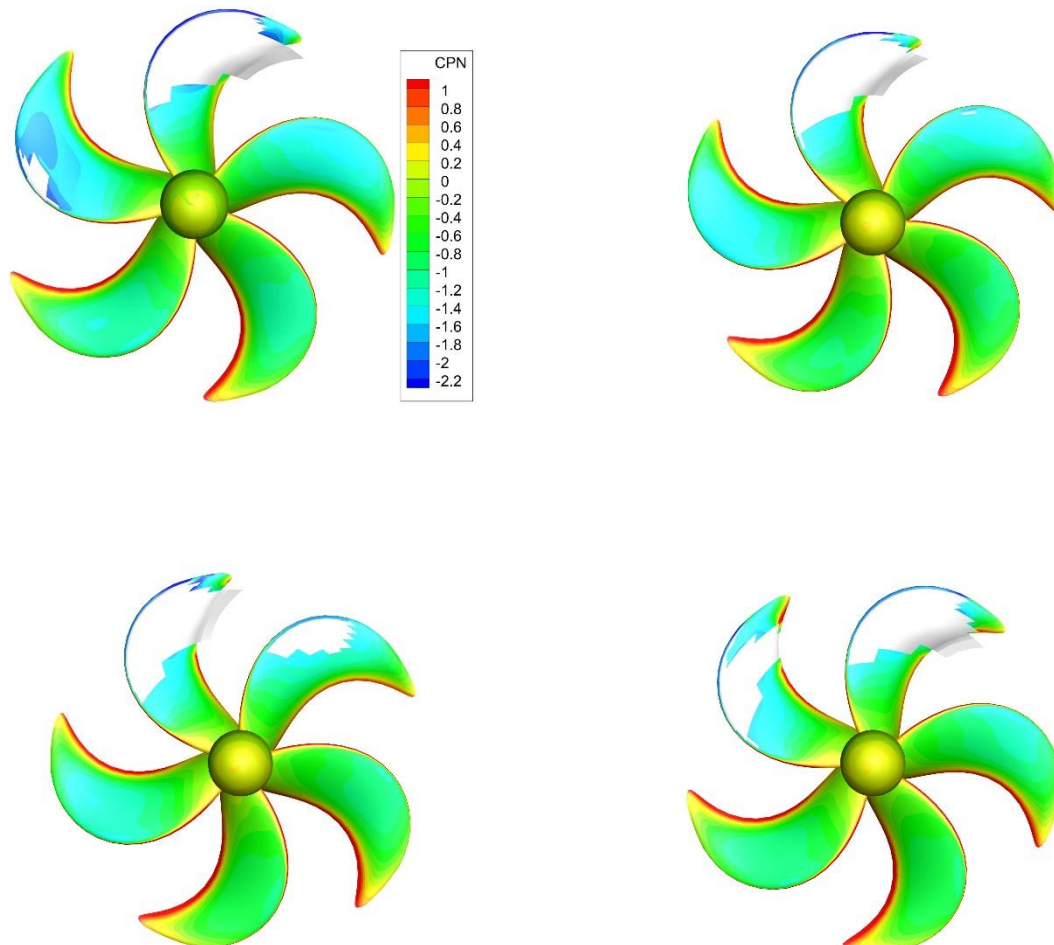




Figure 6-7: Predicted suction side sheet cavitation patterns and pressure distribution ( $C_{PN}$ ) (Constrained design variant #155, Ballast draught, Service 15% SM, 85% MCR).

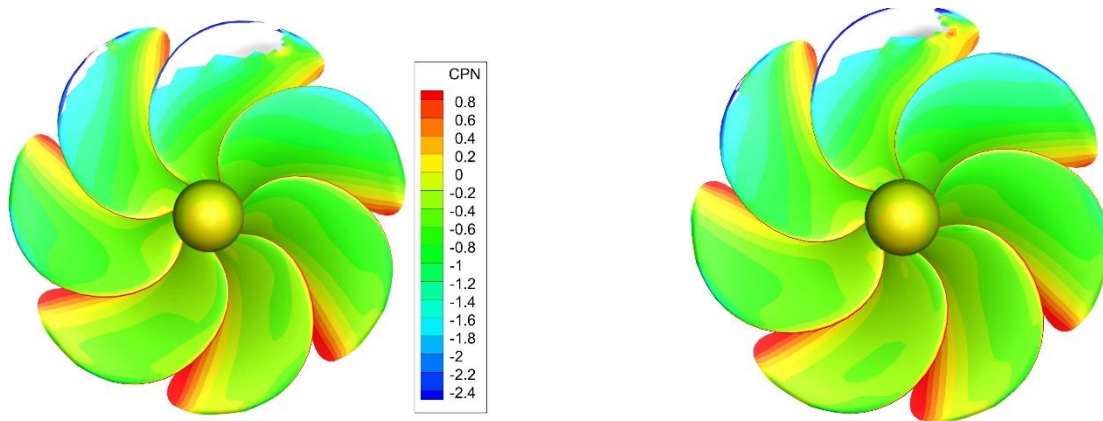


Figure 6-8: Predicted suction side sheet cavitation patterns and pressure distribution ( $C_{PN}$ ) (Unconstrained design variant #50, Ballast draught, Service 15% SM, 85% MCR).

Predictions of the underwater noise levels have been made for the same service condition at ballast draught based on the above presented sheet cavitation predictions and the tip vortex prediction of the ETV model. In Figure 6-9 the computed noise spectra of the selected unconstrained 5 and 7-bladed propeller variants are compared with the spectrum of the reference propeller. Shown are again the contributions of the different cavitation forms, the total source level and the limit source levels for merchant ships sailing in transit at 85% by LR.

From the plots it can be concluded that 5-bladed variant #155 shows a modest reduction of the underwater noise level, mostly due to the reduction of the noise of the tip vortex cavitation. The contribution of sheet cavitation is increasing as expected. In total however a reduction from a peak value of 7 dB from around 188 dB to about 181 dB is obtained. Unconstrained 7-bladed propeller variant #50 shows a similar reduction of the noise level. The largest reduction is now due to the reduction of the sheet cavitation noise.

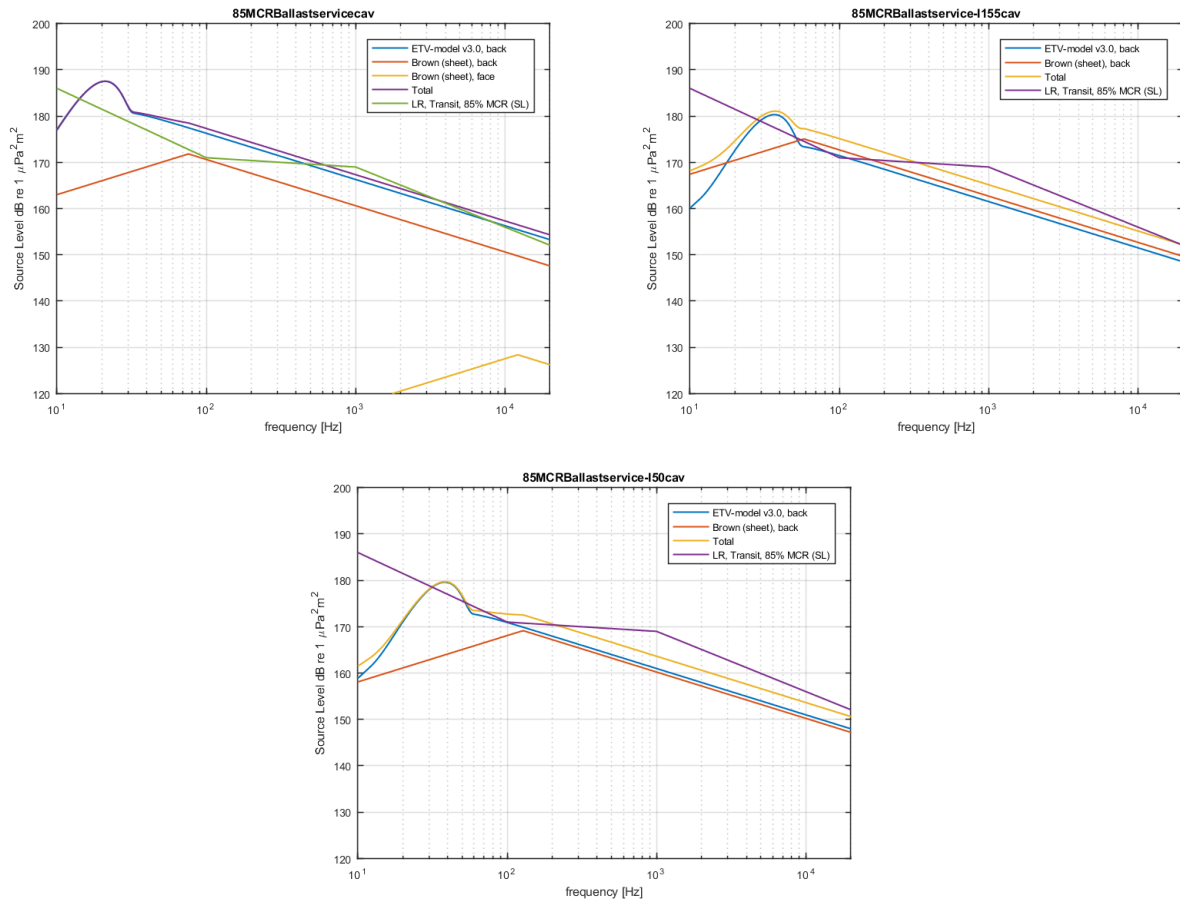


Figure 6-9: Under water noise level versus frequency for the vessel at ballast draught at 15% SM service condition (top left: reference propeller, top right: 5-bladed variant #155, bottom: 7-bladed variant #50).

## 7 CONCLUSIONS AND RECOMMENDATIONS

The following conclusions summarise the findings of the present project:

- The 150t tanker, fitted with the estimated geometry of a reference propeller, sailing at the design draught  $T_F/T_A = 16.0 / 16.0$  m is expected to reach a maximum ship speed of 15.11 knots in trial conditions, implying unrestricted deep water of 15.0° C and a mass density of 1025.9 kg/m<sup>3</sup>, a clean hull and propeller blades and no effects of wind and waves. In this condition the diesel engine of the vessel is operating at 85% MCR providing a shaft power of 14331 kW. The predicted rotation rate is 88.5 rpm.
- The tanker sailing at the same design draught in service conditions with a 15 per cent sea margin is predicted to achieve 14.38 knots for the same 85% MCR power while the reference propeller rotates at 87.7 RPM.
- The tanker sailing at an assumed ballast draught  $T_F/T_A = 5.6 / 9.7$  m is expected to reach a maximum ship speed of 15.86 knots in trial conditions for a shaft power of 1433 kW. The predicted rotation rate of the reference propeller is 86.2 RPM.
- The tanker sailing at the same ballast draught in service conditions with a 15 per cent sea margin is predicted to achieve 15.34 knots for the same 85% MCR power while the reference propeller rotates at 85.8 RPM.
- The vessel fitted with the reference propeller design has a low cavitation inception speed (CIS) of approximately 4 or 5 knots both in ideal trial as well as service conditions (15% sea margin). Both tip vortex and suction side sheet cavitation will develop at these low speeds for both operating draughts.
- For the 85% MCR sailing conditions at design and ballast draught the presence of sheet cavitation is predicted by PROCAL at the outer radii of the reference propeller. The extent of the sheet cavitation is particularly large for ballast condition. It should be realised that there is an interaction of the sheet cavitation with the tip vortex not modelled in PROCAL that is known to reduce the danger for cavitation erosion.
- Predictions have been made of the source levels of the underwater noise using a version of the Empirical Tip Vortex (ETV) model that includes the interaction with sheet cavity near the tip. In addition, a semi-empirical method was used for the calculation of the contribution of isolated sheet cavitation as predicted by PROCAL. The application of these models to single screw vessels requires further validation, but it was shown that the underwater noise levels predicted for the reference tanker propeller are in line with levels for tankers measured in the Echo project. The noise of the combined sheet cavity and cavitating tip vortex is the dominant noise source for propellers like the analysed tanker propeller.
- Propeller design optimisations carried out with the propeller optimisation toolbox PROPART show that there is a direct relation between the allowed increase of the blade mass and the reduction of propeller cavitation noise. It appears favourable to increase the chord length and thickness at the outer radii of the propeller blades. This results in a delay of the inception of sheet and tip vortex cavitation and also a reduction of the sheet cavitation volume at the higher sailing speeds.
- For a 4-bladed replacement propellers with constraints on the mass and MOI the possibilities of increasing the cavitation inception speed are limited. The cavitation inception speed (CIS) can be raised from about 4 to 5 knots as predicted for the reference propeller to about 6 to 7 knots. No reduction of the underwater noise level is obtained as the amount of cavitation at the analysed most critical condition at ballast draught remains large.

- Removing the constraints for the mass and MOI for the 4-bladed propeller results in an increase of the CIS to about 11 knots and an estimated reduction of the peak noise levels due to developed cavitation of 12 dB for the most critical service condition at ballast draught. However this propeller will have an efficiency penalty of about 5.5 per cent and a blade mass that is more than 60 per cent higher than that of the reference propeller. A propeller with roughly the same efficiency could be designed achieving a CIS of 8 knots. This propeller would still have a 50% higher blade mass.
- A limited exploration was made into the effect of increasing the number of blades of an (unconstrained) replacement propeller. The results show that a 5-bladed propeller can be designed with a very high CIS of 14 knots at the expense of an 8 per cent loss of efficiency and an 80% increased blade mass. An alternative 5-bladed propeller design can be designed with a similar efficiency and a CIS of 9.5 knots. The peak underwater noise levels drop with about 7 dB for the mentioned service condition. It is noted that the mass of the 5 propeller blades is 30 per cent higher than that of the 4-bladed reference propeller.
- A similar limited exploration of a 7-bladed unconstrained propeller shows worse results than the 5-bladed propellers. The efficiency losses of the 7-bladed propellers are higher, likely caused by the larger blade area. Delay of cavitation inception requires a larger chord length. When an efficiency loss of 4.5 per cent is accepted still only a CIS of 9 knots can be obtained. The peak underwater noise levels drop with about 7 dB for the mentioned service condition which is similar to the selected 5-bladed propeller. It is noted that the mass of the 7 propeller blades is 80 per cent higher than that of the 4-bladed reference propeller.

It should be clearly noted that the employed semi-empirical prediction method for the noise levels has not yet been validated for the kind of vessel studied here, but was developed using data of twin-screw vessels and model test data of propellers with face side sheet cavitation. It should also be realised that the potential of the 5 and 7-blade propellers has not been fully investigated in this study.

The following recommendations are made based on the findings of the study.

- A more direct optimisation of the cavitation noise could be performed by taking the total noise levels of tip vortex and sheet cavitation as an optimisation goal. Depending on criteria for noise level reductions a reduction of noise levels at certain frequencies could be pursued or it could be translated to an overall sound pressure level, which is not frequency dependent.
- Further limitations on the allowed efficiency penalties could focus the optimisation exercises in design spaces that provide more acceptable (bronze) replacement propellers. Alternative materials such as fibre reinforced composites could be evaluated as potential construction material for high volume propeller designs that could become prohibitively heavy when constructed from bronze.
- Another direction to reduce the cavitation noise is to improve the quality of the wake field of the ship. Solutions such as devices as fins or vortex generators should be mentioned as possible means to achieve this.

The above conclusions and suggestions do not supersede the statements made in the previous chapters and in the figures with results.

Wageningen, February 2022  
MARITIME RESEARCH INSTITUTE NETHERLANDS

Ir. G. Gaillarde  
Head Ships Business Unit

## REFERENCES

Brown, N.A. (2007). "Existing/future technology to address radiated noise by modifying vessel propulsion and operating parameters". NOAA Vessel Quieting Symposium.

Hannay, D., MacGillivray, A., Wladichuk, J., Pace, F., Frouin-Mouy, H., 2019, "Comparison of Class Society Quiet Notation maximum noise levels with ECHO program measurements". Transport Canada workshop on "Quieting ships to protect the marine environment", London, UK.

# **TABLES**

**PARTICULARS OF SHIP AND PROPELLERS**

Description	Symbol	Design draught	Ballast draught	Unit
Length between perpendiculars	L <sub>PP</sub>	264.0	264.0	m
Length on waterline	L <sub>WL</sub>	269.0	259.6	m
Breadth moulded on WL	B	48.0	48.0	m
Draught moulded on FP	T <sub>F</sub>	16.0	5.6	m
Draught moulded on AP	T <sub>A</sub>	16.0	9.7	m
Displacement volume moulded	∇	165994	73068	m <sup>3</sup>
Displacement mass in seawater	Δ <sub>1</sub>	170310	13099	t
LCB position forward of ½ L <sub>PP</sub>	LCB	3.3	1.3	%
Block coefficient	C <sub>B</sub>	0.819	0.754	-
Midship section coefficient	C <sub>M</sub>	0.997	0.995	-
Prismatic coefficient	C <sub>P</sub>	0.821	0.763	-
Length-Breadth ratio	L <sub>PP</sub> /B	5.500	5.500	-
Breadth-Draught ratio	B/T	3.000	6.275	-

Engine type	Diesel motor	-
Number and type of propulsors	1 fixed pitch propeller	-
Available brake power at 100% MCR	16860	kW
Shaft line losses (estimated)	1	%

Vs	Cavitation number $\sigma_N$ [-]			
	DT	BT	DS	BS
1	668.48	604.35	586.90	544.23
2	164.28	146.25	146.73	133.57
3	73.43	65.00	64.38	59.73
4	41.42	36.27	36.33	33.70
5	26.56	23.10	23.30	21.61
6	18.46	16.08	16.20	14.93
7	13.51	11.78	11.91	10.99
8	10.31	9.07	9.08	8.43
9	8.13	7.20	7.18	6.64
10	6.57	5.89	5.82	5.38
11	5.41	4.92	4.80	4.44
12	4.51	4.19	4.04	3.73
13	3.90	3.62	3.43	3.17
14	3.32	3.08	2.87	2.66
15	2.91	2.70	2.47	2.28
16	2.54	2.36	2.08	1.92
17	2.17	2.01	1.71	1.57

Variation of cavitation number with ship speed for design (D) and ballast (B) draught for trial (T) and service (S) conditions (4-bladed propeller with diameter of 8.2 meter)



## COMPUTED OPEN WATER RESULTS

BEM CODE PROCAL  
REFERENCE PROPELLER

$P0.7/D = 0.671$

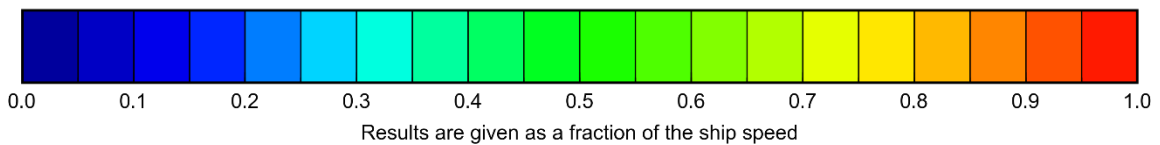
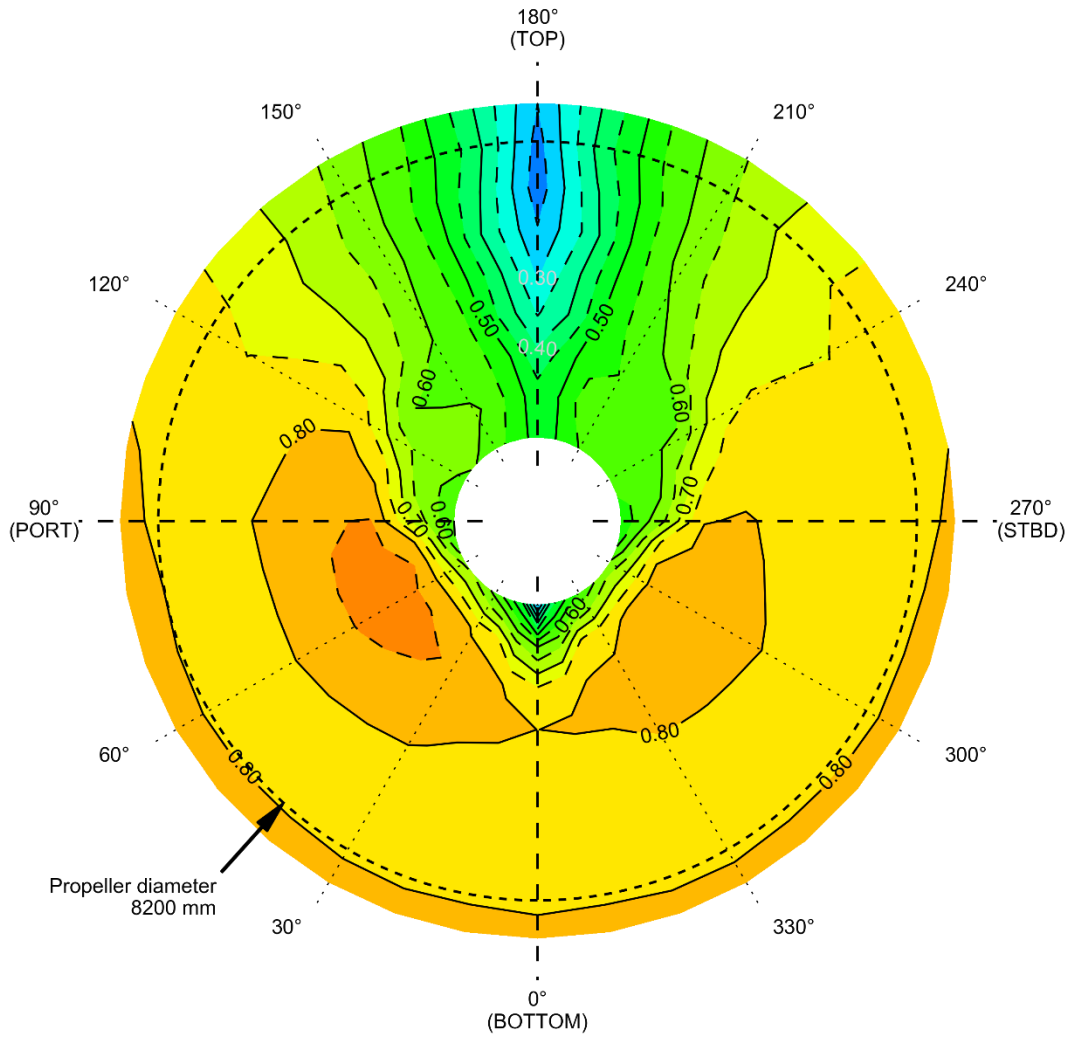
J	KT-O	KQ-O	ETA-O
.10	.2828	.03060	.147
.20	.2477	.02683	.294
.30	.2101	.02306	.435
.40	.1702	.01988	.545
.50	.1276	.01622	.626
.60	.0834	.01192	.667
.65	.0606	.00952	.658
.70	.0374	.00694	.600
.75	.0318	.00417	.395

4-bladed propellers (constrained)				Unit
Prop #	157	127	173	-
Mass	26261.0	26381.0	26261.0	Kg
%	-0.5	0.0	-0.5	-
MOI	138060.0	140420.0	138840.0	Kgm2
%	-0.5	1.2	0.1	-
4-bladed propellers (unconstrained)				
Prop #	42	150	176	-
mass	29057.0	39557.0	43469.0	Kg
%	10.1	50.0	64.8	-
MOI	173220.0	286630.0	308710.0	Kgm2
%	24.9	106.7	122.6	-
5-bladed propellers				
Prop #	64	155	69	-
mass	48030.0	33766.0	29438.0	Kg
%	82.1	28.0	11.6	-
MOI	372980.0	226720.0	166020.0	Kgm2
%	168.9	63.5	19.7	-
7-bladed propellers				
Prop #	50	89	100	
mass	43504.0	35608.0	76375.0	Kg
%	64.9	35.0	189.5	-
MOI	328460.0	22270.0	632100.0	Kgm2
%	136.8	-83.9	355.7	-

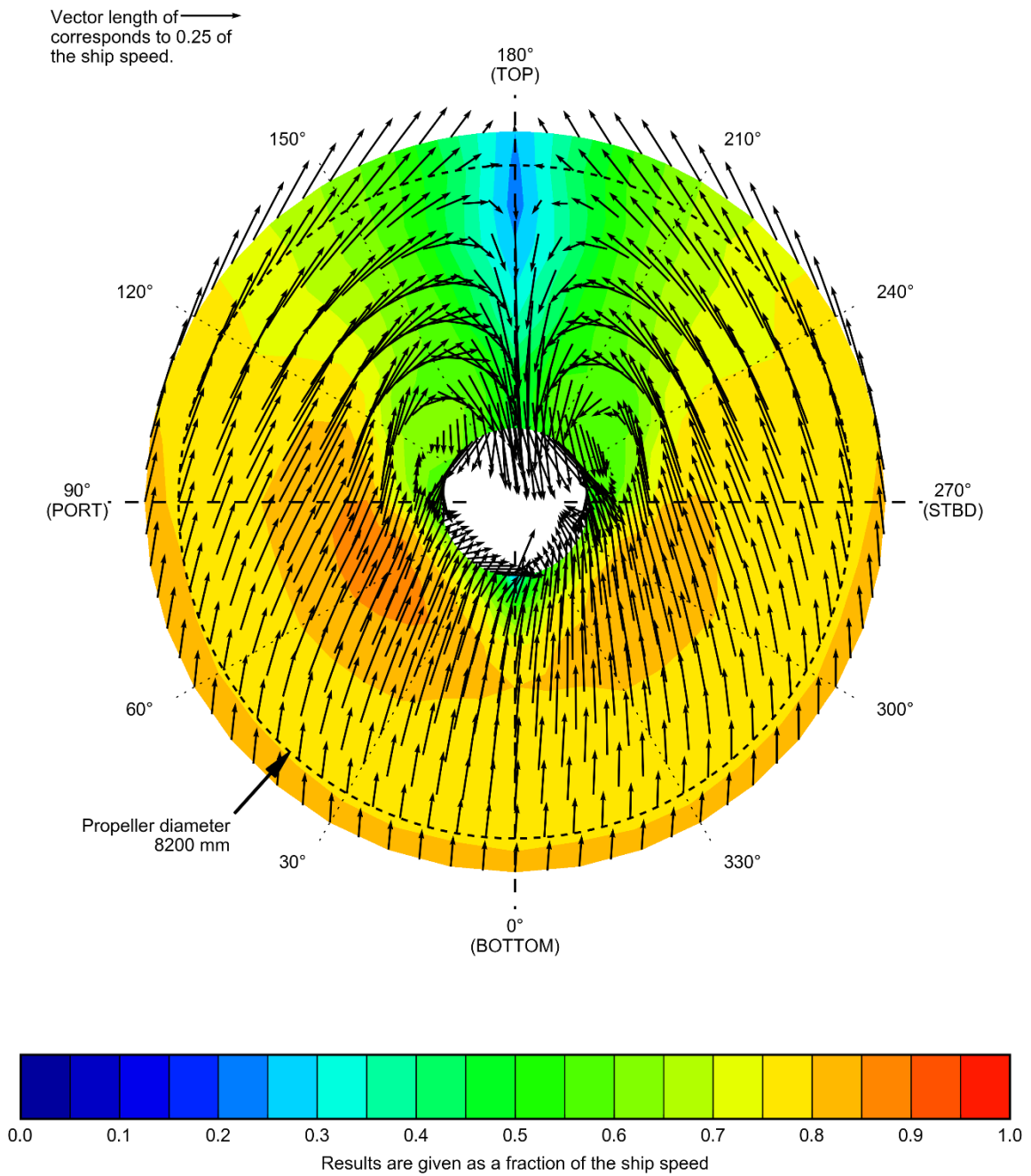
OVERVIEW OF PROPELLER MASS AND MASS MOMENT OF INERTIA FOR SELECTED PROPELLERS

# FIGURES

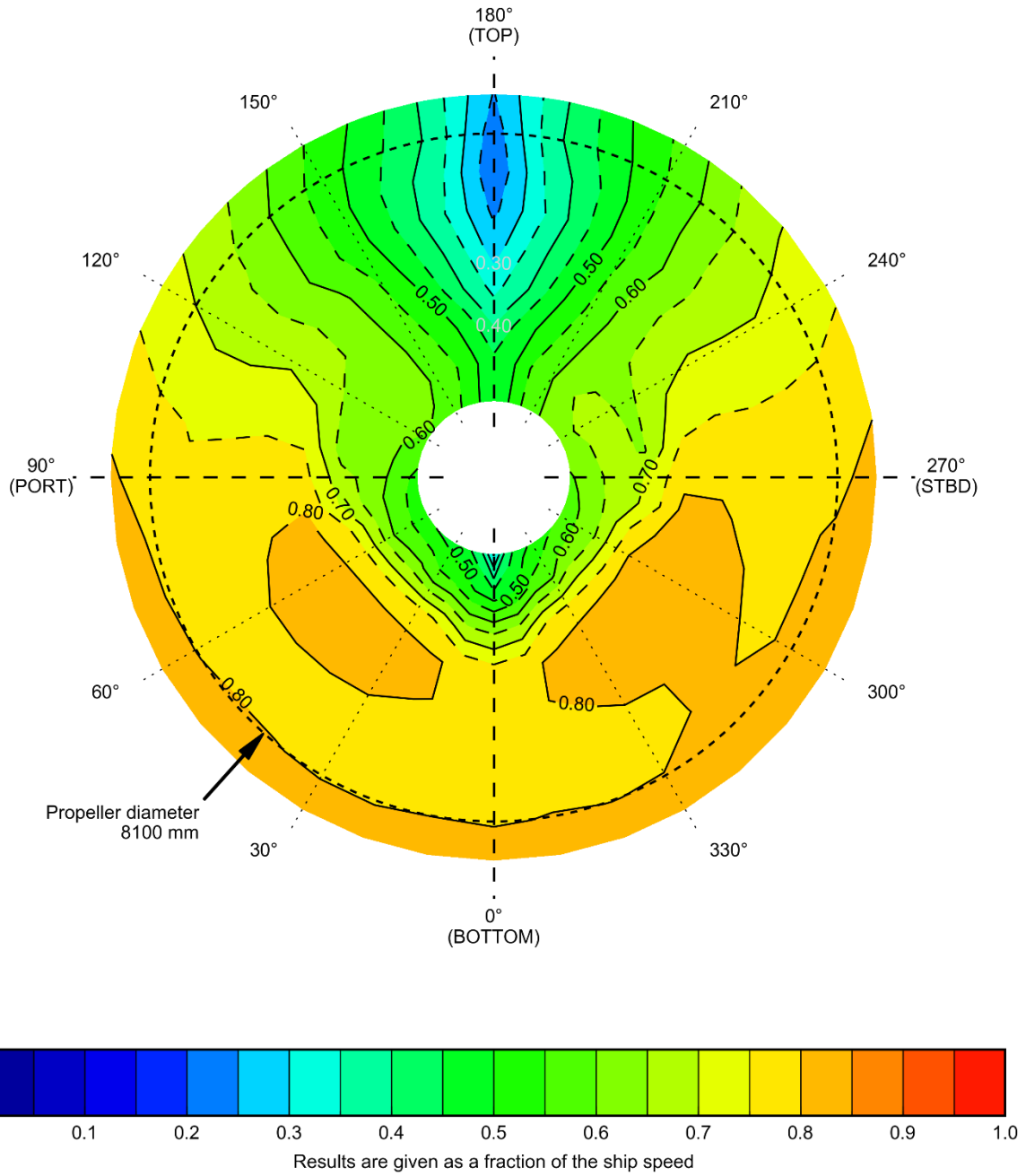
CALCULATION No.	: Lloyd Register	DRAUGHT FP	: 16.000	m	
WATER DEPTH	: inf	m	DRAUGHT AP	: 16.000	m
TURB. MODEL	: -	SHIP SPEED	: 12.00	kn	



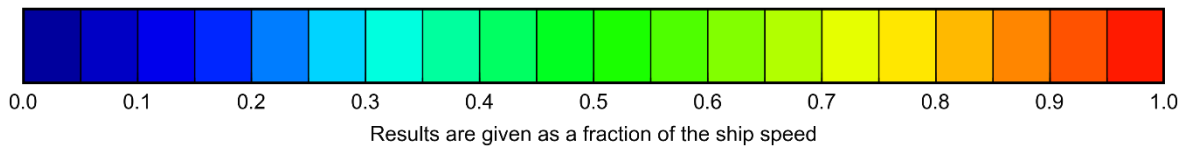
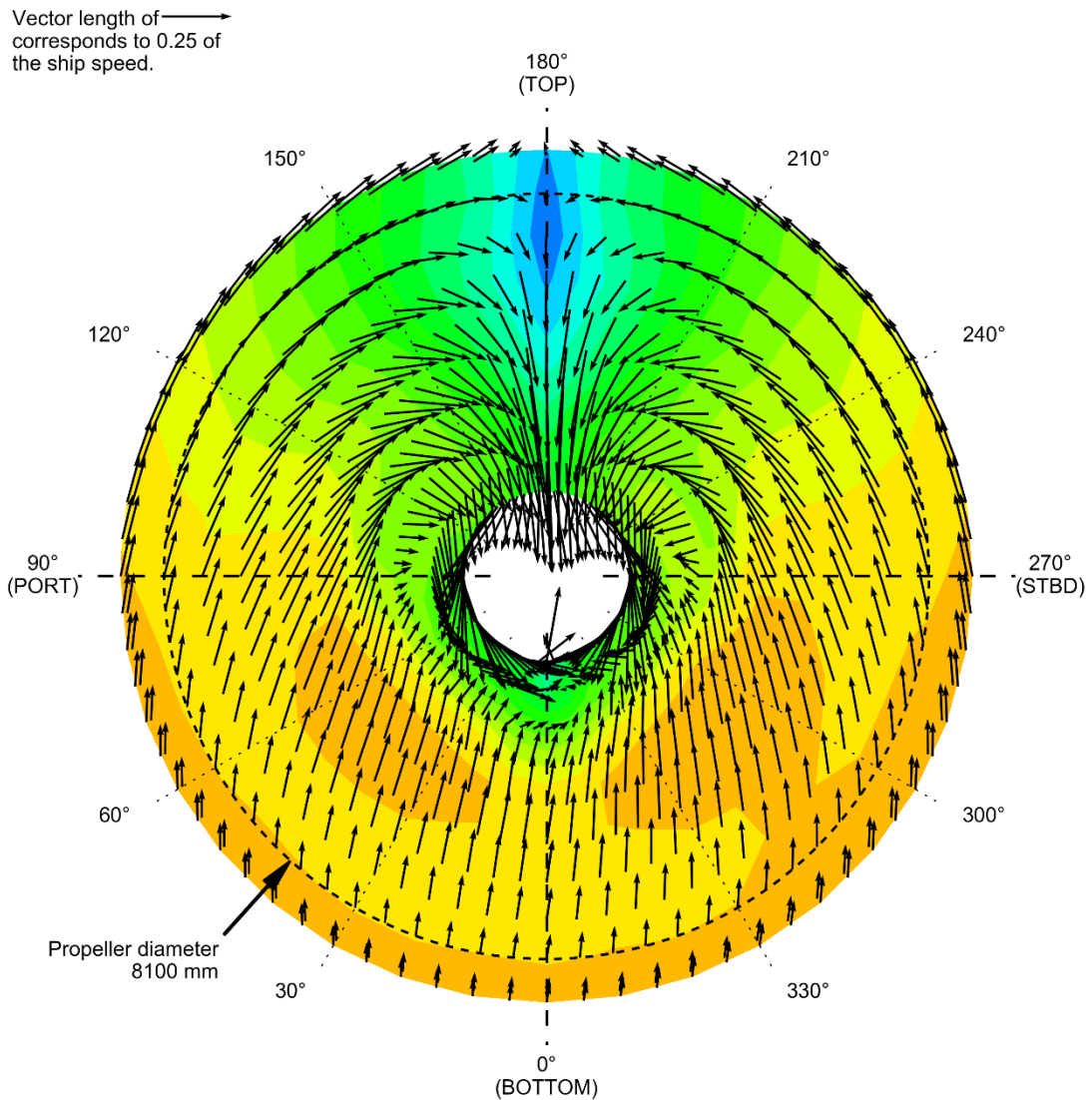
CONTOUR PLOT OF AXIAL VELOCITY COMPONENTS OF COMPUTED EFFECTIVE WAKE FIELD (DESIGN DRAUGHT)



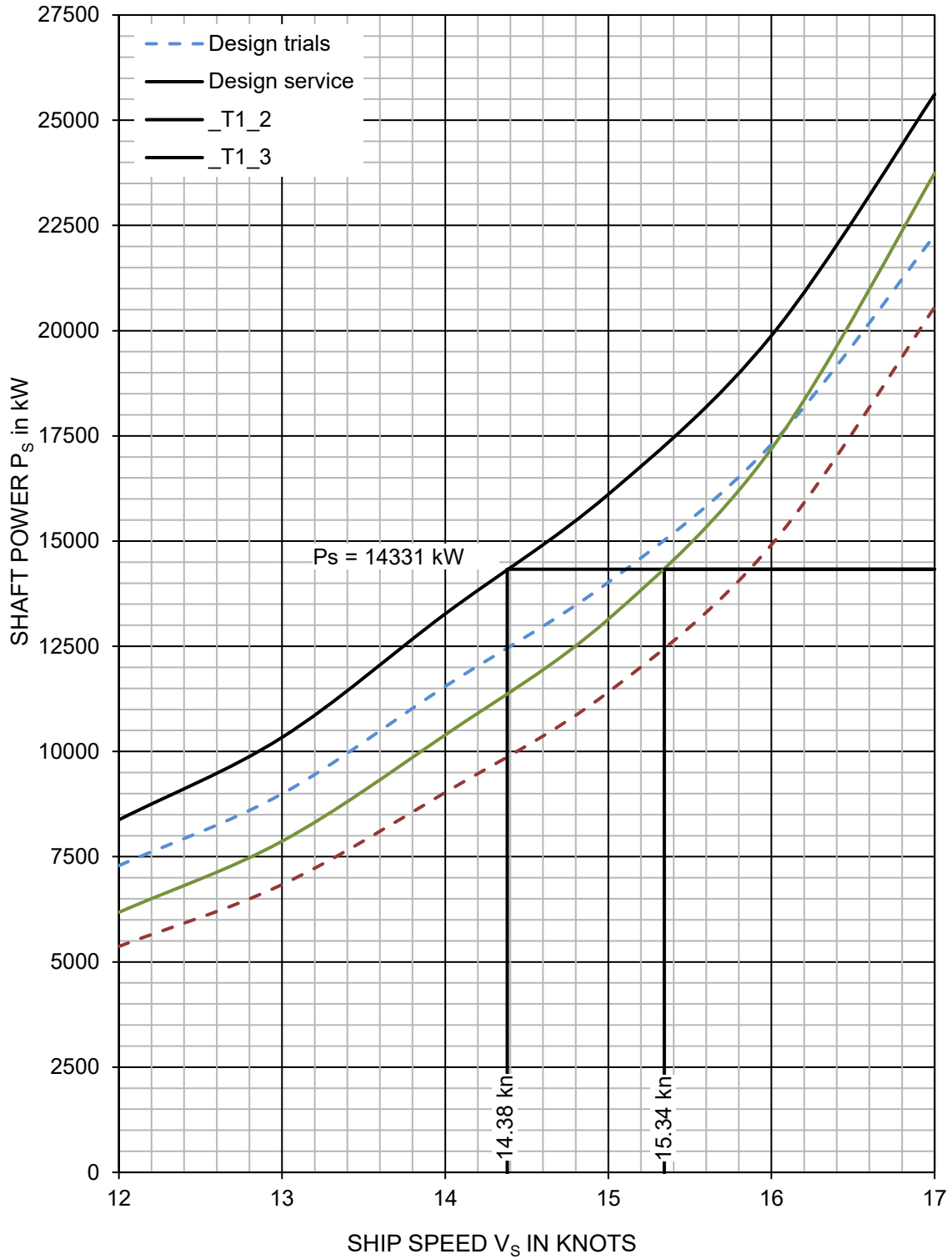
CONTOURS OF AXIAL- AND VECTORS OF TRANSVERSE VELOCITY COMPONENTS OF EFFECTIVE WAKE FIELD (DESIGN DRAUGHT)



CONTOUR PLOT OF AXIAL VELOCITY COMPONENTS OF COMPUTED EFFECTIVE WAKE FIELD (BALLAST DRAUGHT)

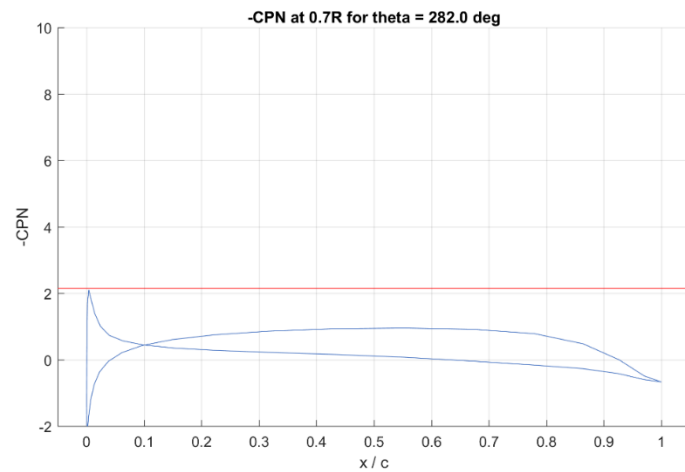
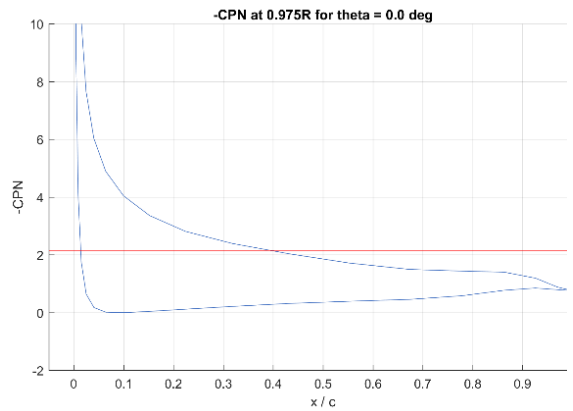
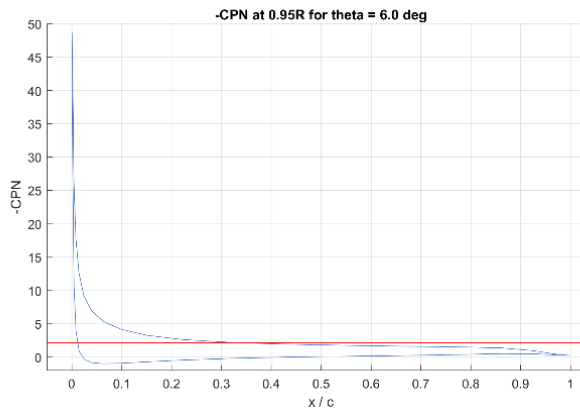
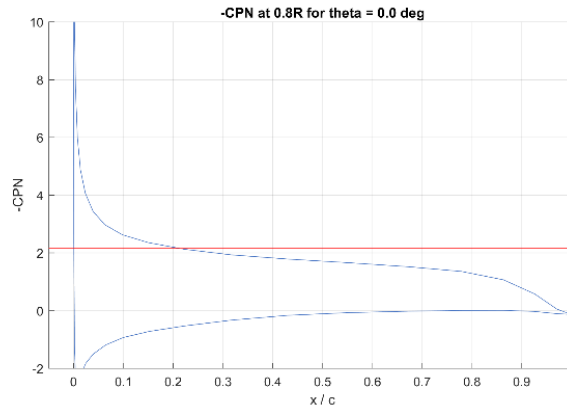
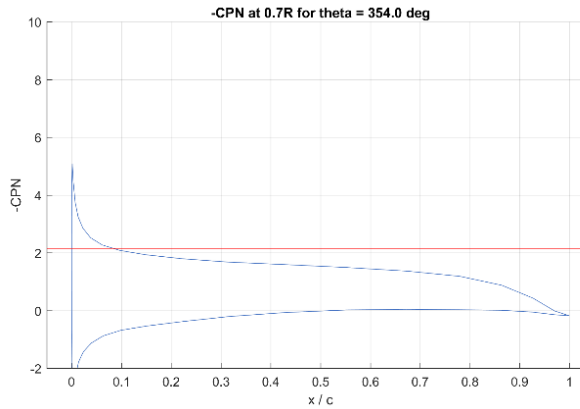
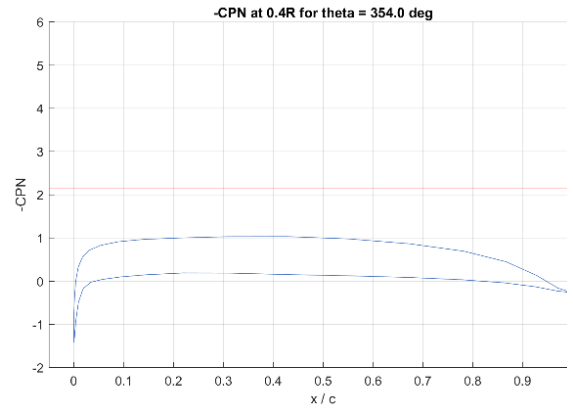
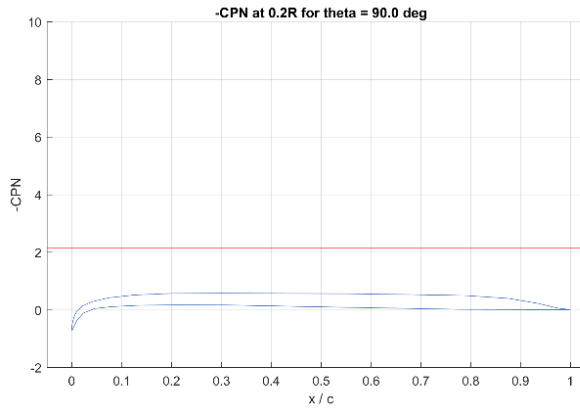


CONTOURS OF AXIAL- AND VECTORS OF TRANSVERSE VELOCITY COMPONENTS OF EFFECTIVE WAKE FIELD (BALLAST DRAUGHT)

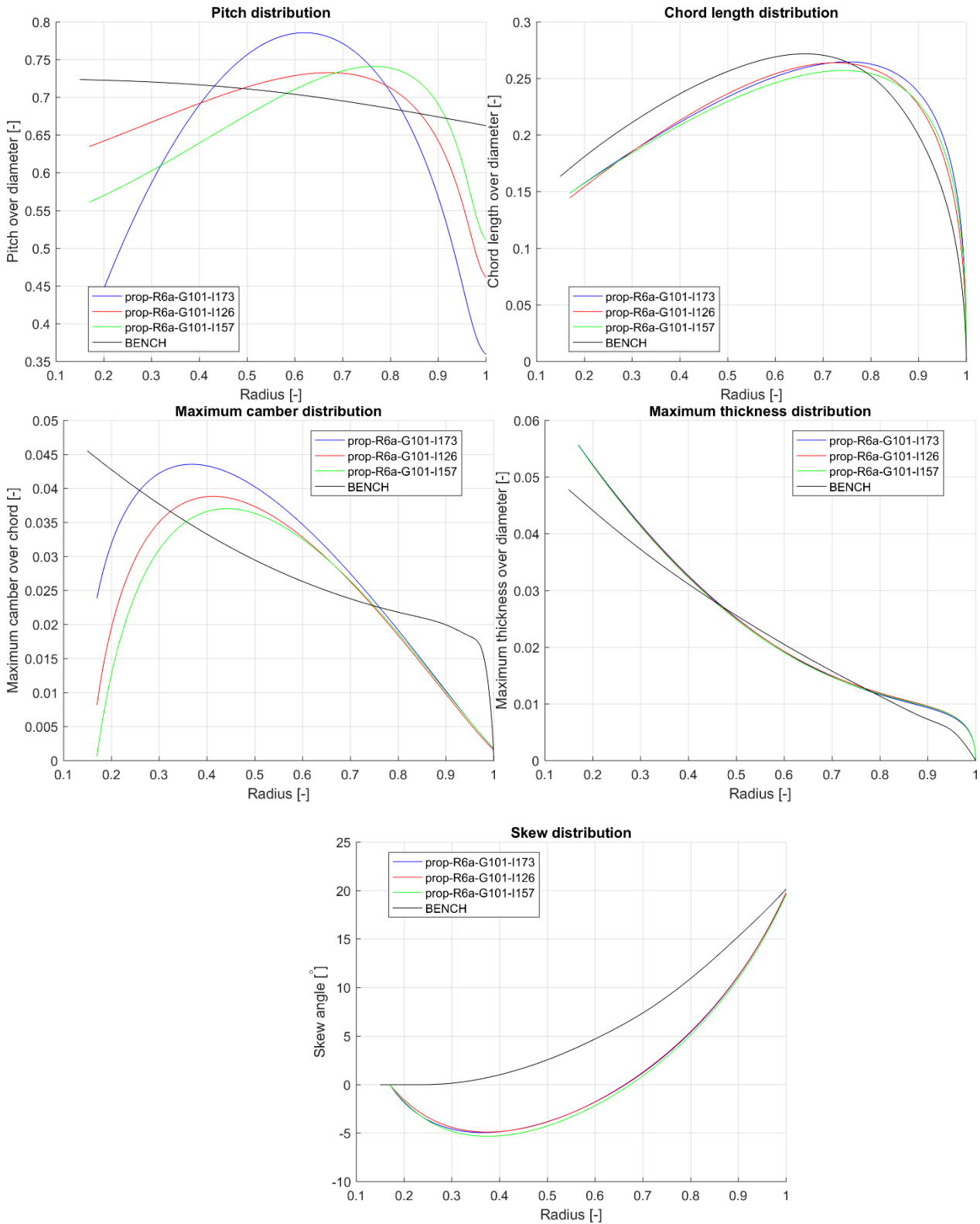


PREDICTED SHAFT POWER VERSUS SHIP SPEED FOR ESTIMATED DRAUGHTS

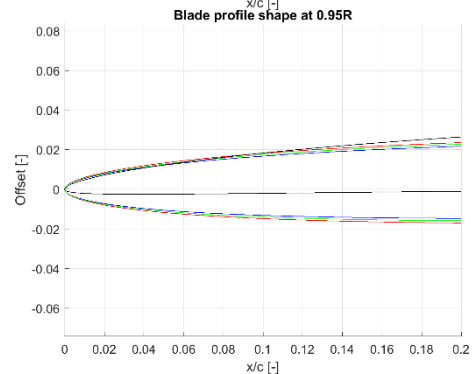
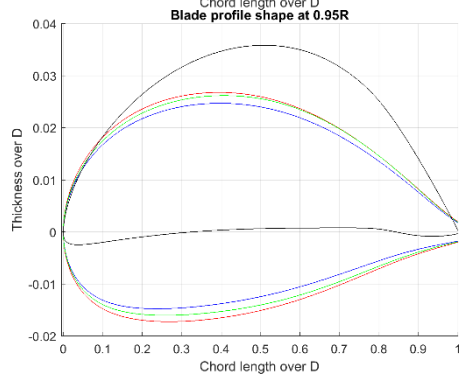
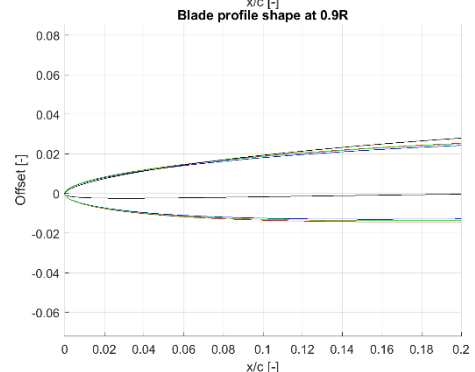
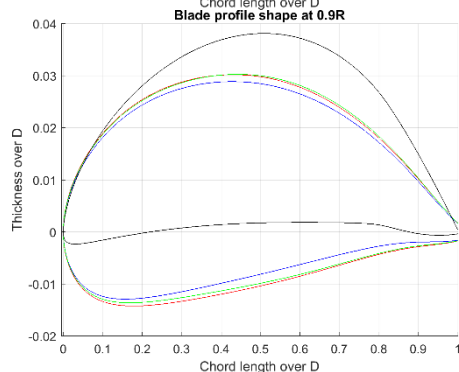
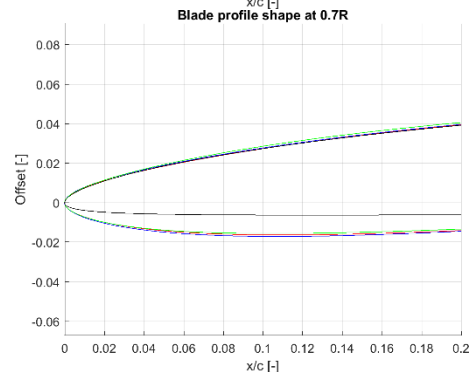
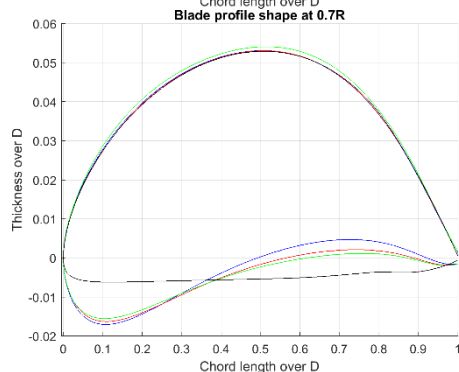
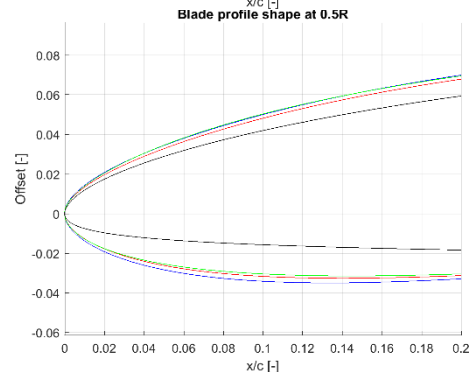
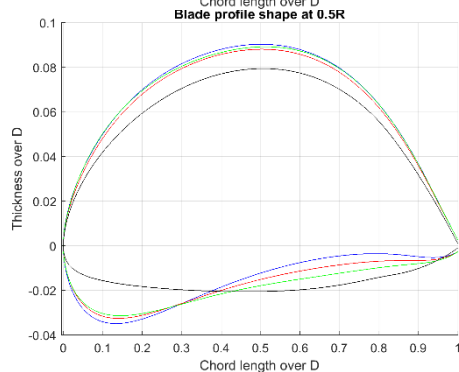
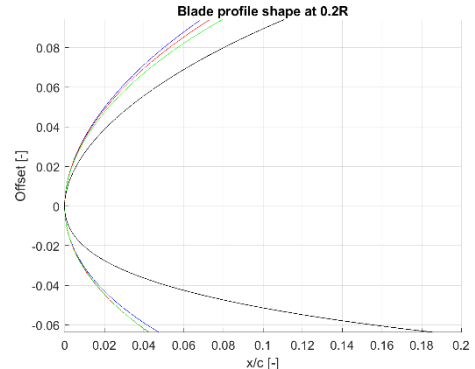
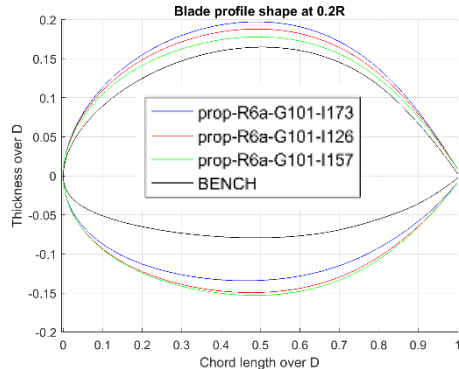




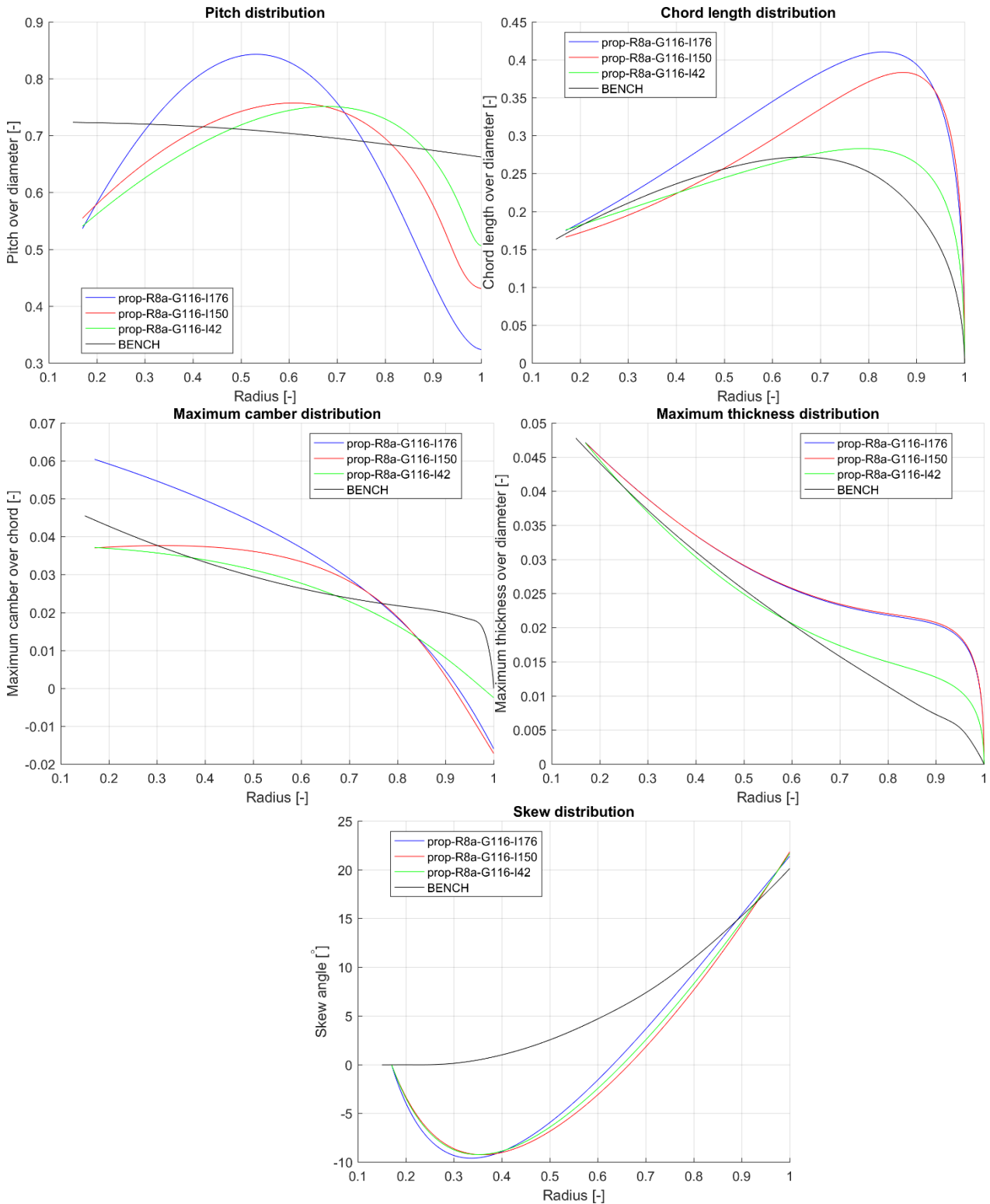
CHORDWISE VARIATION OF PRESSURE COEFFICIENT CPN FOR DIFFERENT BLADE RADII



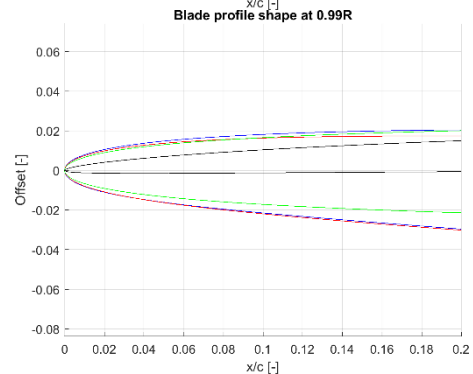
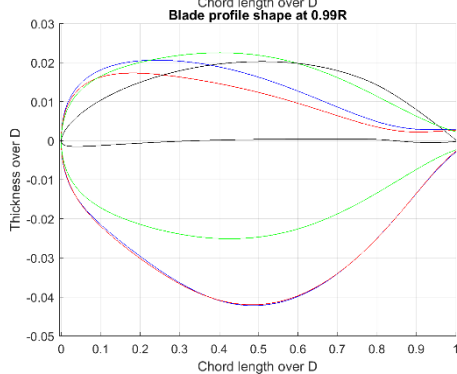
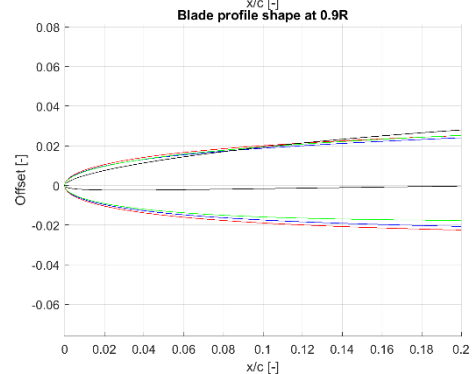
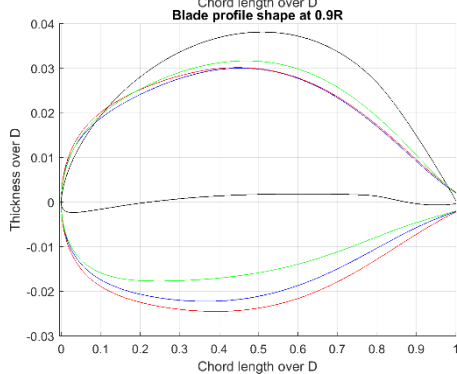
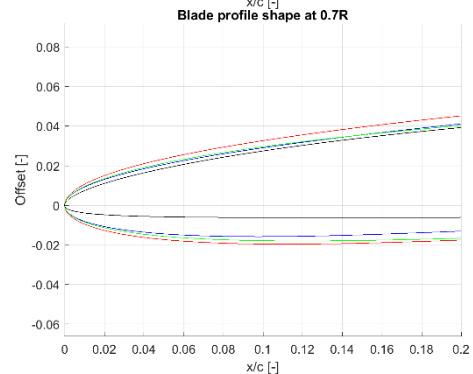
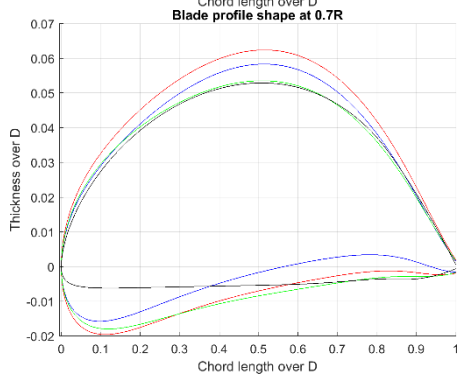
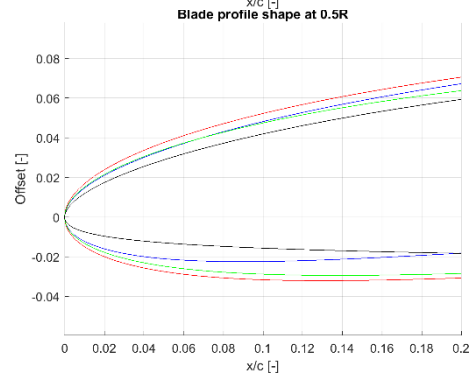
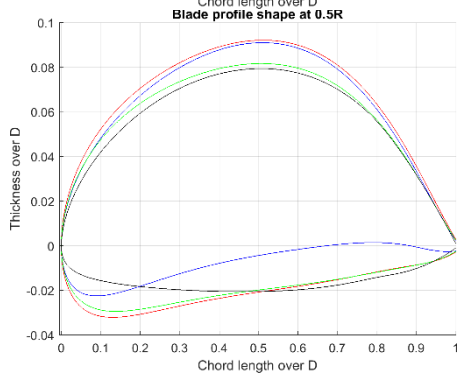
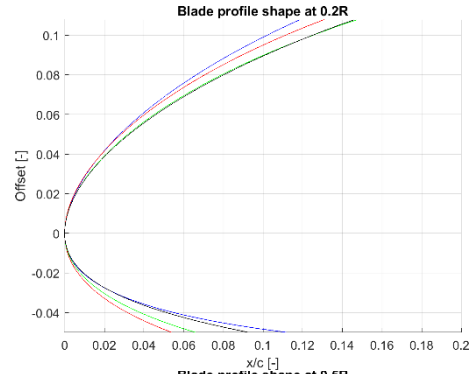
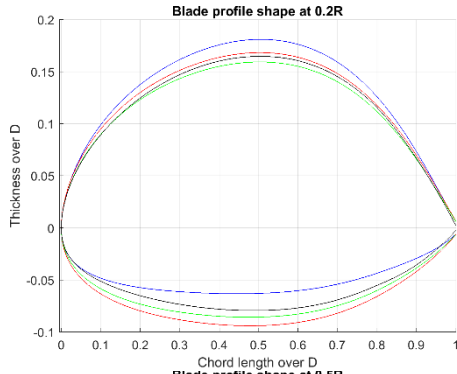
CONSTRAINED 4-BLADED PROPELLER: RADIAL GEOMETRY PARAMETER DISTRIBUTIONS OF SELECTED OPTIMUM PROPELLER VARIANTS COMPARED TO REFERENCE PROPELLER



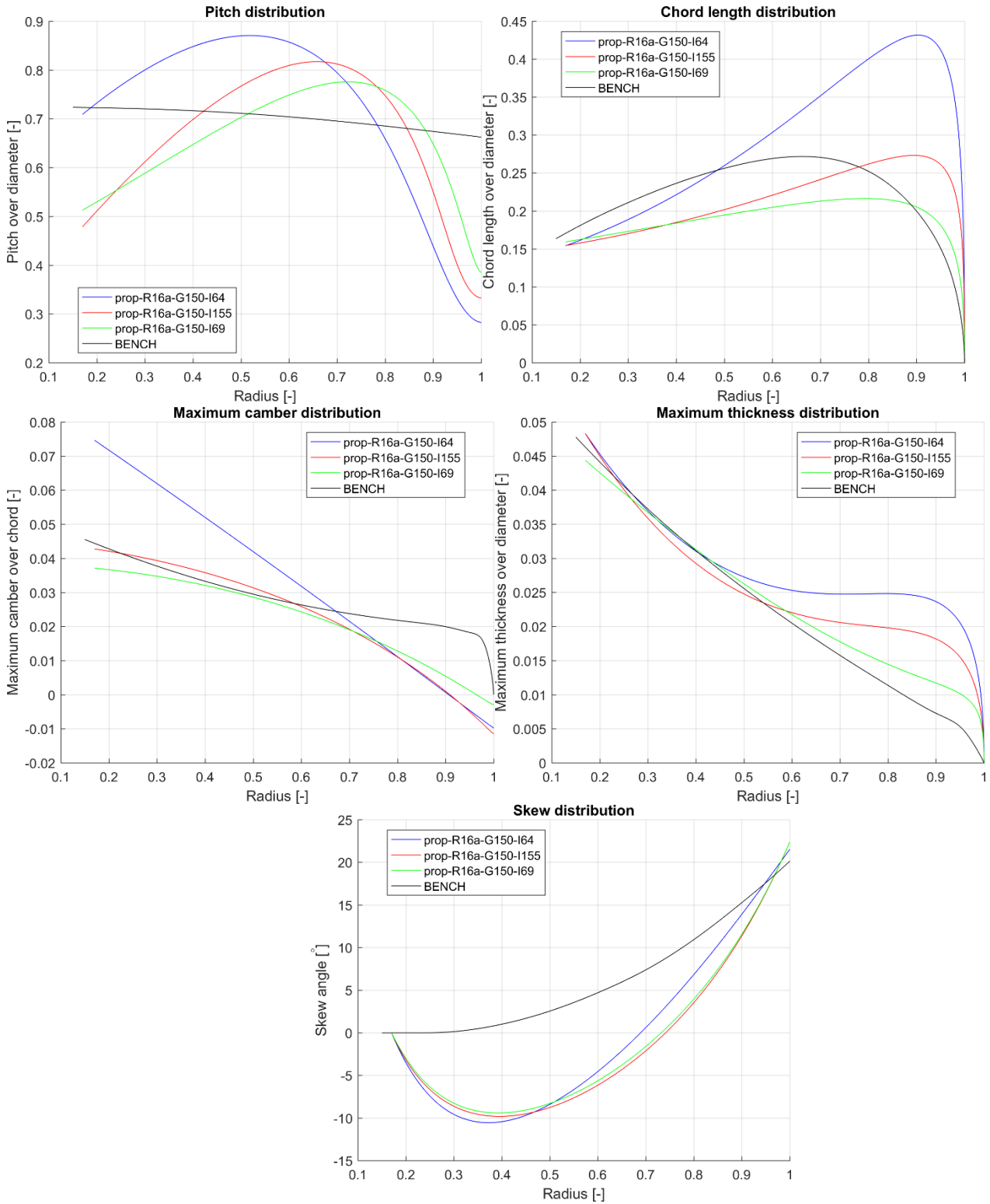
COMPARISON OF SHAPE OF SECTIONAL PROFILES (4-BLADED PROPELLER, CONSTRAINED)



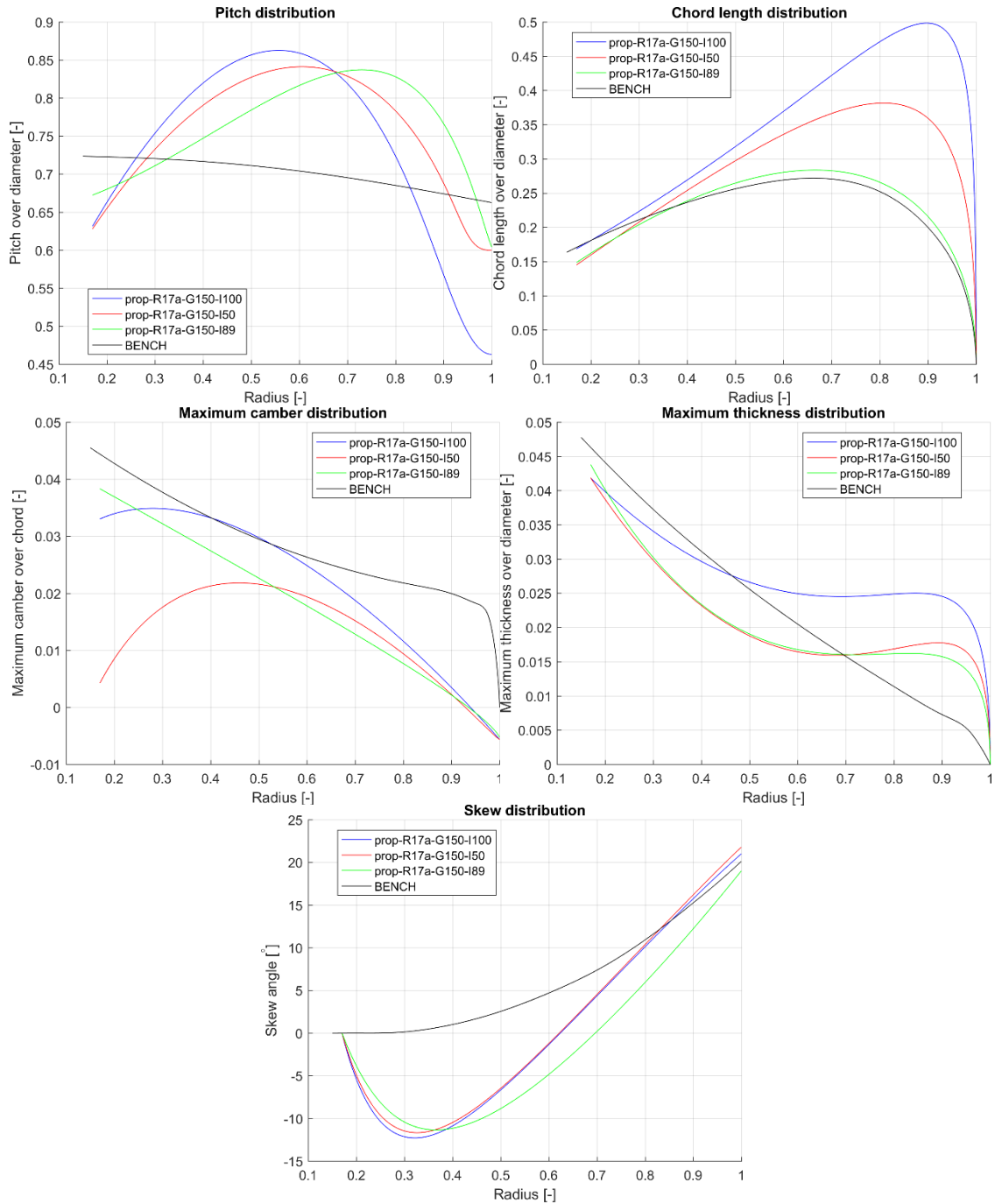
UNCONSTRAINED 4-BLADED PROPELLER: RADIAL GEOMETRY PARAMETER DISTRIBUTIONS OF SELECTED OPTIMUM PROPELLER VARIANTS COMPARED WITH REFERENCE PROPELLER.



COMPARISON OF SECTIONAL PROFILES (4-BLADED PROPELLER, UNCONSTRAINED)



UNCONSTRAINED 5-BLADED PROPELLER: RADIAL GEOMETRY PARAMETER DISTRIBUTIONS OF SELECTED OPTIMUM PROPELLER VARIANTS COMPARED WITH REFERENCE PROPELLER.



UNCONSTRAINED 7-BLADED PROPELLER: RADIAL GEOMETRY PARAMETER DISTRIBUTIONS OF SELECTED OPTIMUM PROPELLER VARIANTS COMPARED WITH REFERENCE PROPELLER.

# APPENDICES



## APPENDIX I

### LIST OF SYMBOLS

Symbol	Symbol in computer print	Title
<b>GEOMETRY OF SHIP AND PROPELLER</b>		
$A_{BT}$		Transverse cross-section area of bulbous bow
$A_E$		Expanded propeller blade area
$A_E/A_O$		Expanded propeller blade area ratio
$A_M$		Midship sectional area below still waterline
$A_O$		Propeller disc area
$A_T$		Transom area below still waterline
$A_T/A_M$		Transom area ratio
$A_W$		Waterplane area
$A_X$		Maximum transverse sectional area below still waterline
$A_V$	AV	Area of portion of ship above waterline projected normally to the direction of relative wind
B		Maximum breadth moulded at or below still waterline
$B_M$		Maximum breadth moulded at midship
$B_{WL}$		Maximum breadth moulded at still waterline
c		Chord length of propeller blade section
c/D		Chord length-diameter ratio
$c_{REF}$		Chord length between reference line and leading edge
$c_t$		Chord length between maximum thickness point and leading edge
$C_B$		Block coefficient
$C_M$		Midship section coefficient
$C_P$		Longitudinal prismatic coefficient
$C_{WP}$		Waterplane area coefficient
d		Hub diameter
d/D		Hub-diameter ratio
D		Propeller diameter
FB		Position of centre of buoyancy aft of FP
f		Camber of propeller blade section
$h_o$		Submergence of propeller shaft axis measured from still water-plane
$h_B$		Height of centroid of $A_{BT}$ above keel
$i_E$		Half angle of entrance
LOA		Length overall
LOS		Length overall submerged
LPP		Length between perpendiculars
LWL		Length on still waterline
LCB		Longitudinal position of centre of buoyancy

Symbol	Symbol in computer print	Title
P		Propeller pitch
P/D		Pitch-diameter ratio
r		Radius of propeller blade section
R		Radius of propeller
S,S <sub>HULL</sub>		Projected wetted surface bare hull
S <sub>APP</sub>		Wetted surface area appendages
S <sub>1</sub> ,S <sub>TOT</sub>		Total wetted surface area
t		Maximum thickness of propeller blade section
t/c		Maximum thickness-chord length ratio
T		Mean draught moulded
T <sub>A</sub>		Moulded draught at aft perpendicular
T <sub>F</sub>		Moulded draught at forward perpendicular
dTA	dTA	Dynamic draught change at aft perpendicular
dTF	dTF	Dynamic draught change at forward perpendicular
Z		Number of blades
λ		Scale ratio
Φ		Pitch angle of propeller section
∇	DISV	Displacement volume moulded
-m	-M	Subscript for model
-s	-S	Subscript for ship

Symbol	Symbol in computer print	Title
<b>RESISTANCE, OPEN WATER AND PROPULSION</b>		
$AC_{Res}$		Ship resistance admiralty coefficient
$AC_{Prop}$		Ship propulsive power admiralty coefficient
$C_A$	CA	Total Incremental resistance coefficient for model-ship correlation
$C_{A0}$	CA_0	$C_A$ basic
$C_{Arough}$	Crough	$C_A$ roughness
$C_{Aas}$	Caas	$C_A$ air resistance
$C_{Abk}$	Cbk	$C_A$ bilge keels
$C_{Aballast}$	Cballast	$C_A$ small draught
$C_{AD}$	CAD	Admiralty coefficient for propulsion
$C_D$		Drag coefficient
$C_{D\bar{V}}$		Power-displacement coefficient
$C_E$	CE	Admiralty coefficient for resistance
$C_F$	CF	Specific frictional resistance coefficient
$\Delta C_F$		Roughness allowance coefficient
$C_L$	CL	Lift coefficient
$C_P$		Power loading coefficient
$C_Q$	CQ	Propeller torque coefficient
$C_{QBL}$	CQBL	Propeller blade spindle torque coefficient
$C_R$	CRES	Specific residual resistance coefficient
$C_T$	CT	Specific total resistance coefficient
$C_{Th}$		Thrust loading coefficient
$C_{TP}$	CTP	Propeller thrust coefficient
$C_{TD}$	CTD	Duct thrust coefficient
$C_V$	CV	Specific total viscous resistance coefficient
$C_W$	CW	Specific wavemaking resistance coefficient
$C_X$	CX	Specific air resistance coefficient
Ⓒ	CIRCC	R.E. Froude's resistance coefficient
F	F	Towing force in propulsion test
$F_D$	FD	Viscous scale effect on resistance
$F_n$	FN	Froude number
$F_P$	PULL	Pull of ship
$F_{PO}$	PULL	Pull of ship in bollard condition
Ⓕ	CIRCF	R.E. Froude's frictional resistance coefficient
g		Acceleration due to gravity
J	J	Advance coefficient
$J_V$	JV	Apparent advance coefficient
1+k	1+K	Three-dimensional form factor on flat plate friction

Symbol	Symbol in computer print	Title
$K_p$		Equivalent sandroughness of propeller blade surface
$K_s$		Roughness height of hull surface
$K_{siP}$	$K_{siP}$	Dependency of propulsive efficiency with resistance increase
$K_{siN}$	$K_{siN}$	Dependency of propeller shaft speed with power increase
$K_{siV}$	$K_{siV}$	Dependency of propeller shaft speed with speed change
$K_Q$	$K_Q$	Torque coefficient
$K_T$	$K_T$	Thrust coefficient
$K_{TD}$	$K_{T-D}$	Duct thrust coefficient
$K_{TP}$	$K_{T-P}$	Propeller thrust coefficient
$K_{TS}$	$K_{T-S}$	Stator thrust coefficient
$\textcircled{K}$	CIRCK	R.E. Froude's speed-displacement coefficient
MCR		Maximum continuous rating
SMCR		Specified maximum continuous rating
NCR		Normal continuous rating
$n$	$N$	Rate of revolutions
$P_B$		Brake power
$P_D$	$PD$	Power delivered to the propeller(s)
$P_E$	$PE$	Effective power
$P_I$		Indicated power
$P_S$	$PS$	Shaft power
$Q$	$Q$	Torque
$R$	$R$	Resistance in general
$R_n$	$RN$	Reynolds number
$R_A$		Model-ship correlation resistance
$R_F$	$RF$	Frictional resistance
$R_V$	$RV$	Total viscous resistance
$R_W$	$RW$	Wavemaking resistance
$s_A$		Apparent slip ratio
$s_R$		Real slip ratio
$t$	$THDF$	Thrust deduction fraction
$t^*$		Thrust deduction fraction from load variation test
$T$	$TH$	Thrust
$T_D$	$TH-D$	Duct thrust
$T_P$	$TH-P$	Propeller thrust
$T_S$	$TH-S$	Stator thrust
$T_U$	$TH-U$	Azimuthing thruster unit thrust
$t_v$	$TV$	Running trim

Symbol	Symbol in computer print	Title
$V$	$V$	Speed of ship or ship model
$V_r$	$V_r$	Radial flow velocity component in the direction of the z-axis of the Pitot tube, and is positive if directed down for strut orientation tests or outward in a wake survey
$V_t$	$V_t$	Tangential flow velocity component in the direction of the y-axis of the Pitot tube, and is positive if directed to port for strut orientation tests or in clockwise direction in a wake survey
$V_x$	$V_x$	Longitudinal flow velocity component in the direction of the x-axis of the Pitot tube, and is positive if directed aft
$V_A$	$V_A$	Advance speed of propeller relative to water flow
$w_T$	$W_T$	Effective wake fraction on thrust identity
$w_Q$	$W_Q$	Effective wake fraction on torque identity
$\beta$		Advance angle of propeller blade section
$\beta_h$		Angle of the flow in the x-y plane of the Pitot tube co-ordinate system, and is positive if the flow is directed to port for strut orientation tests
$\beta_v$		Angle of the flow in the x-z plane of the Pitot tube co-ordinate system, and is positive if the flow is directed to the hub for strut orientation tests
$\eta_B$		Propeller efficiency behind ship
$\eta_D$	ETA-D	Propulsive efficiency
$\eta_\varepsilon$	ETA- $\varepsilon$	Merit coefficient
$\eta_G$		Gearing efficiency
$\eta_H$	ETA-H	Hull efficiency
$\eta_M$		Mechanical efficiency
$\eta_o$	ETA-O	Propeller efficiency in open water
$\eta_R$	ETA-R	Relative-rotative efficiency on thrust or torque identity
$\eta_S$		Shafting efficiency

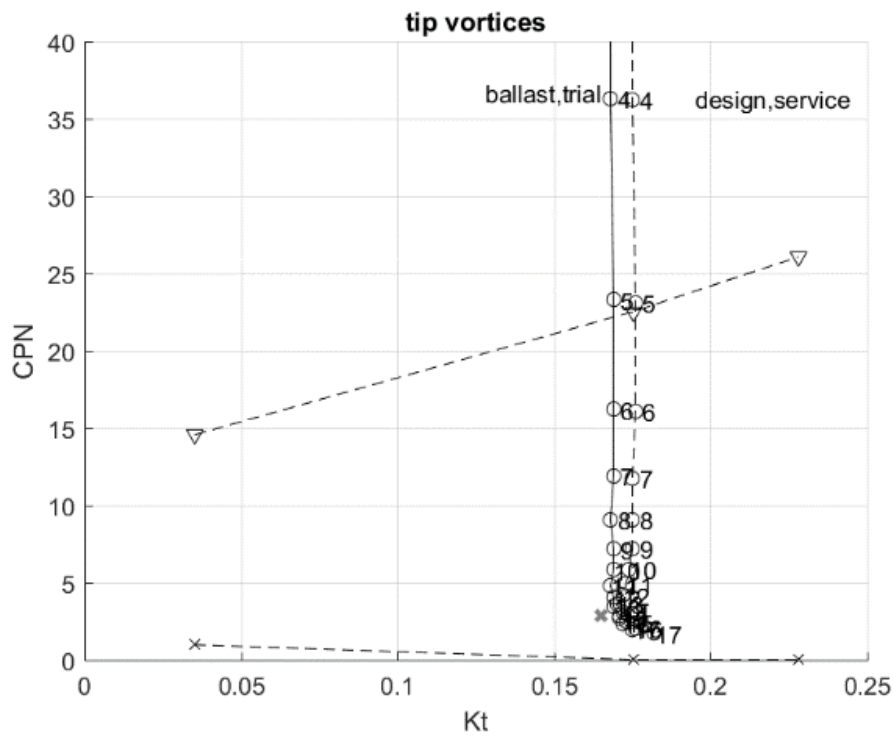
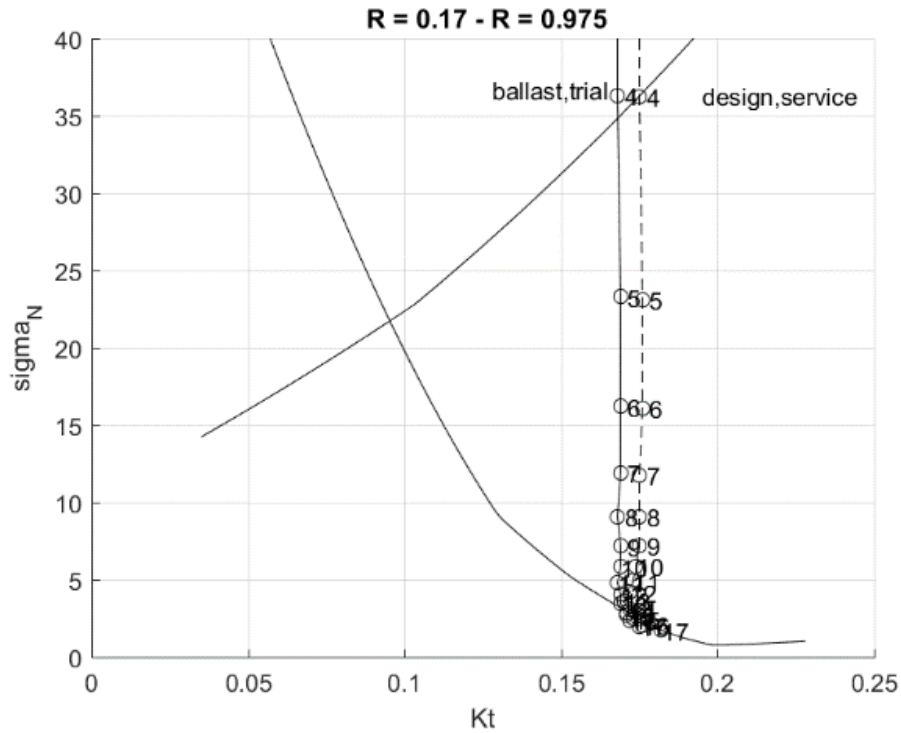
Symbol	Symbol in computer print	Title
<b>CAVITATION, HULL PRESSURES, SHAFT FORCES AND NOISE</b>		
$a_{x0.8}$		Longitudinal clearance from propeller clearance curve to stern frame at a height of 0.8 R above propeller shaft axis
$a_z$		Vertical clearance of propeller tip in top position to the hull
$A_i$		Single amplitude of i-th harmonic component of periodic pressure signal
$B_s$		Waterline beam at station at most forward point of screw aperture
$c$		Speed of sound
$C$		Empirical constant
$C_p$		Pressure coefficient
$D_M$		Depth moulded
$E_{H,V}$		Thrust eccentricity
$f$		Frequency in general
$f_1$		Blade passage frequency
$f(\Theta)$		Function of mean periodic pressure signal
$F_{H,V}$		Propeller-induced dynamic force acting on the shaft
$F_{x,y,z}$	FX,FY,FZ	Propeller-induced dynamic force acting on the hull
$F_{z\ eq}$		Equivalent vertical excitation force
$g$		Acceleration due to gravity
$h$		Immersion in general
$J$	J	Advance coefficient
$M_{H,V}$		Propeller-induced dynamic moment acting on the shaft
$M_{x,y,z}$	MX,MY,MZ	Propeller-induced dynamic moment acting on the hull
$n$	N	Rate of revolutions
$p$		Sound pressure
$p_o$		Ambient pressure
$p_v$		Vapour pressure of water
$r$		Distance to cavitating propeller
$R_n$	RN	Reynolds number
$V$	V	Speed of ship or model
$V_A$	VA	Advance speed of propeller relative to water flow
$\alpha_i$		Phase angle of i-th component in harmonic function
$\Theta$		Angular propeller blade position
$\rho$		Mass density of water

Symbol	Symbol in computer print	Title
$\sigma_f$		Non-dimensional parameter for frequency
$\sigma_n$		Cavitation number related to rotation rate
$\sigma_p$		Non-dimensional parameter for sound pressure
$\sigma_v$		Cavitation number related to flow velocity

-H	-H	Subscript for horizontal
-m	-M	Subscript for model
-s	-S	Subscript for ship
-v	-V	Subscript for vertical

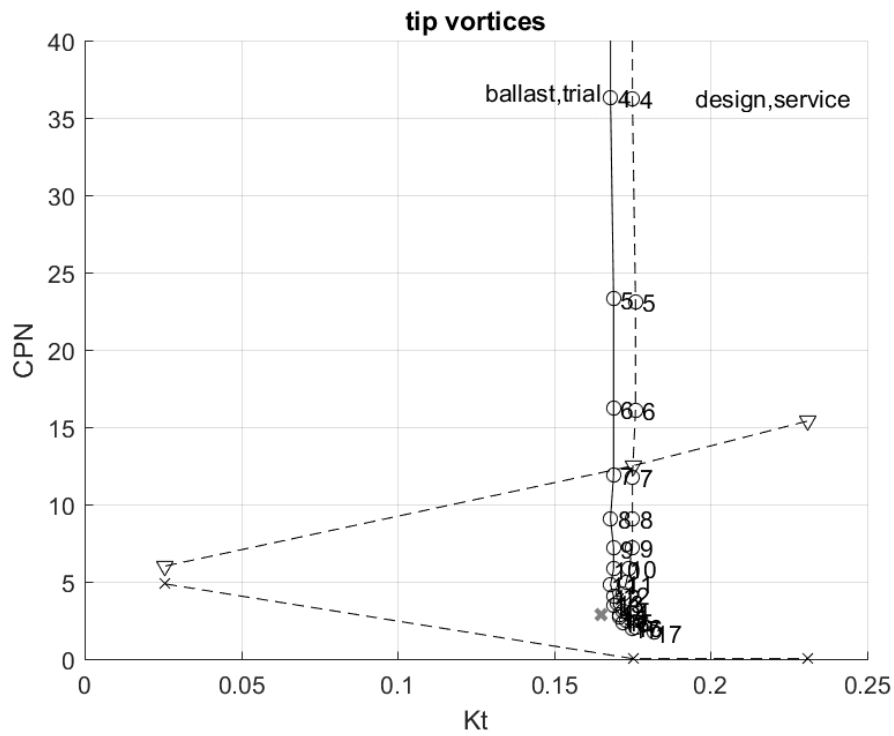
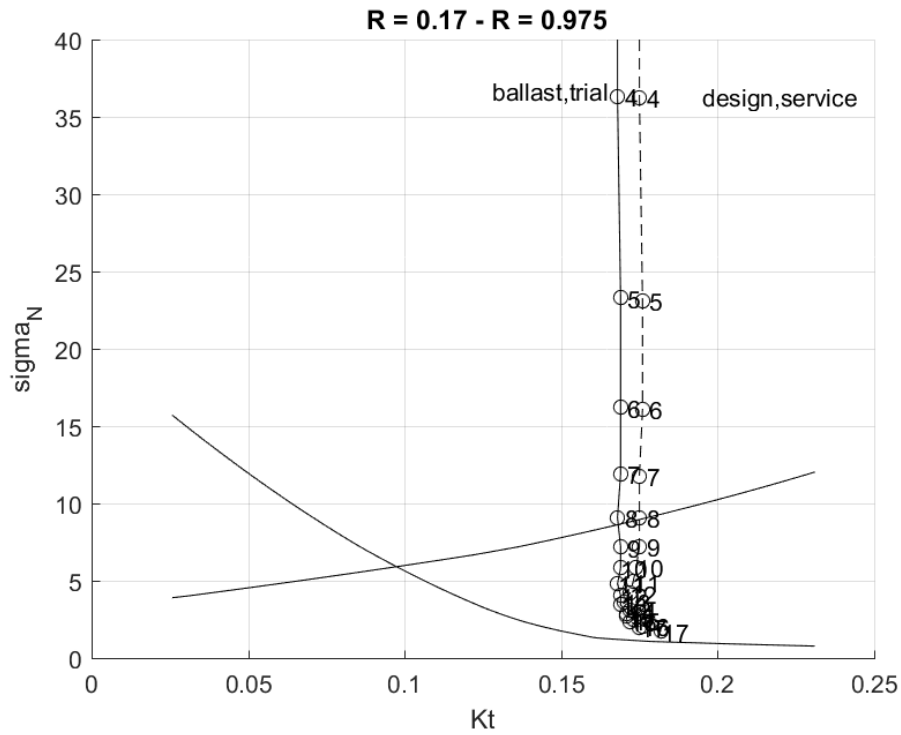
**APPENDIX II**

**CAVITATION INCEPTION DIAGRAMS**

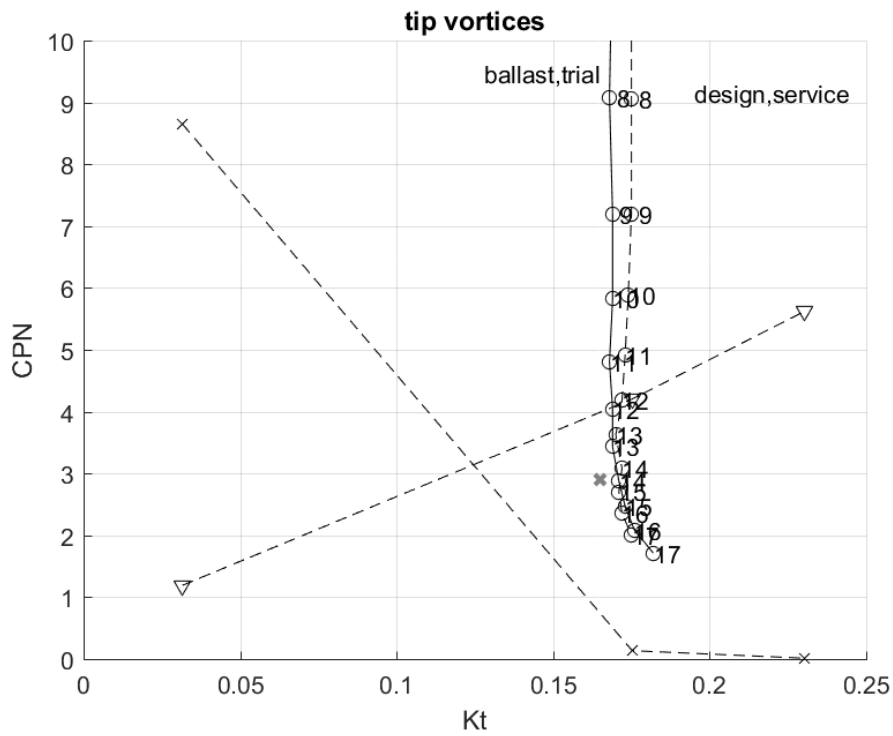
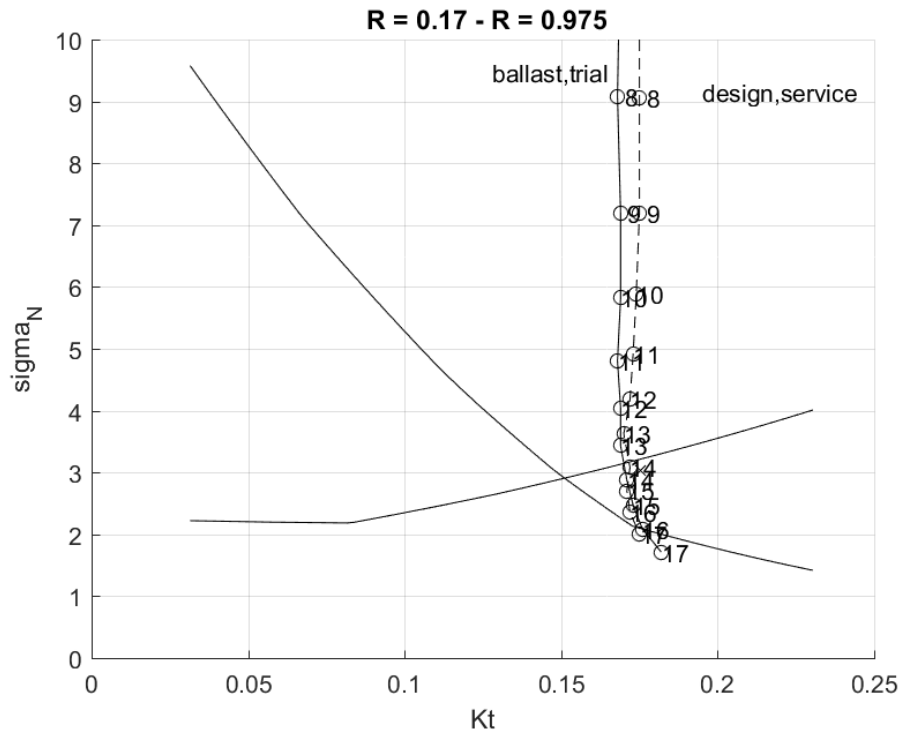


CAVITATION INCEPTION BUCKETS FOR REFERENCE PROPELLER

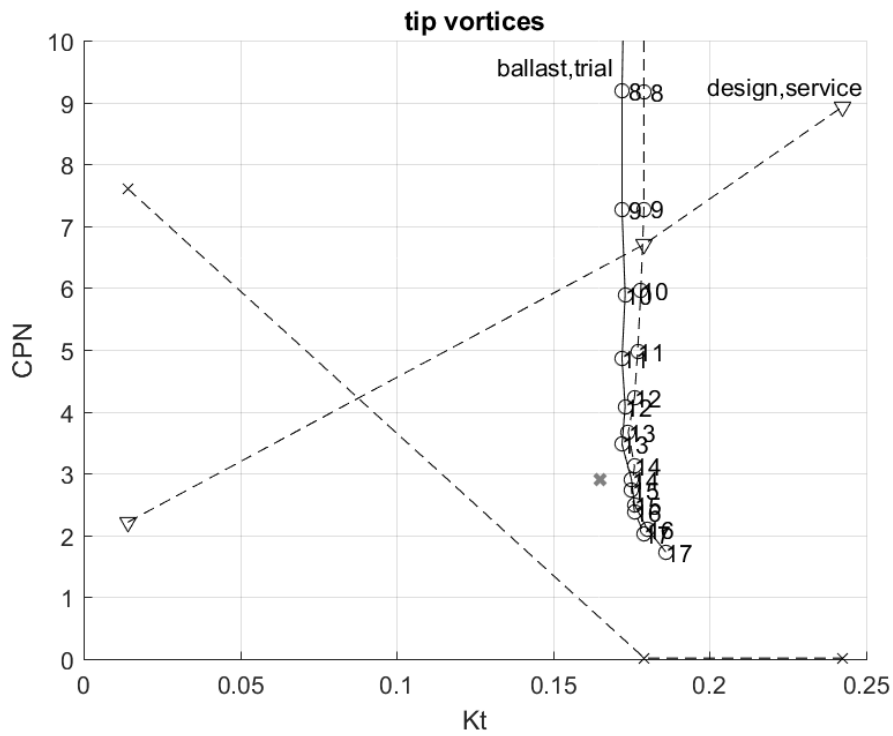
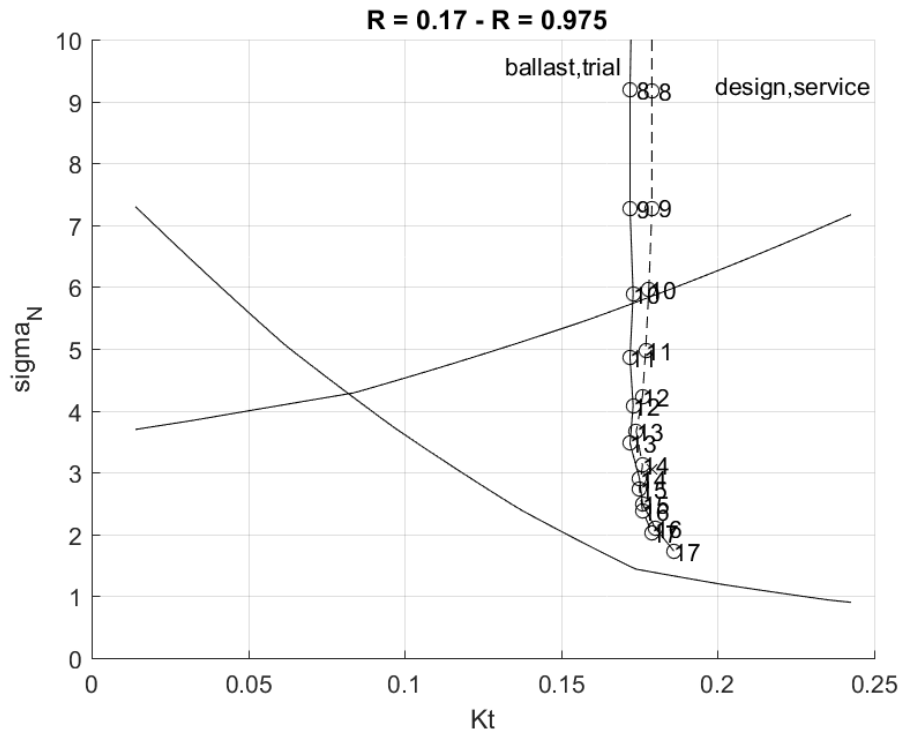




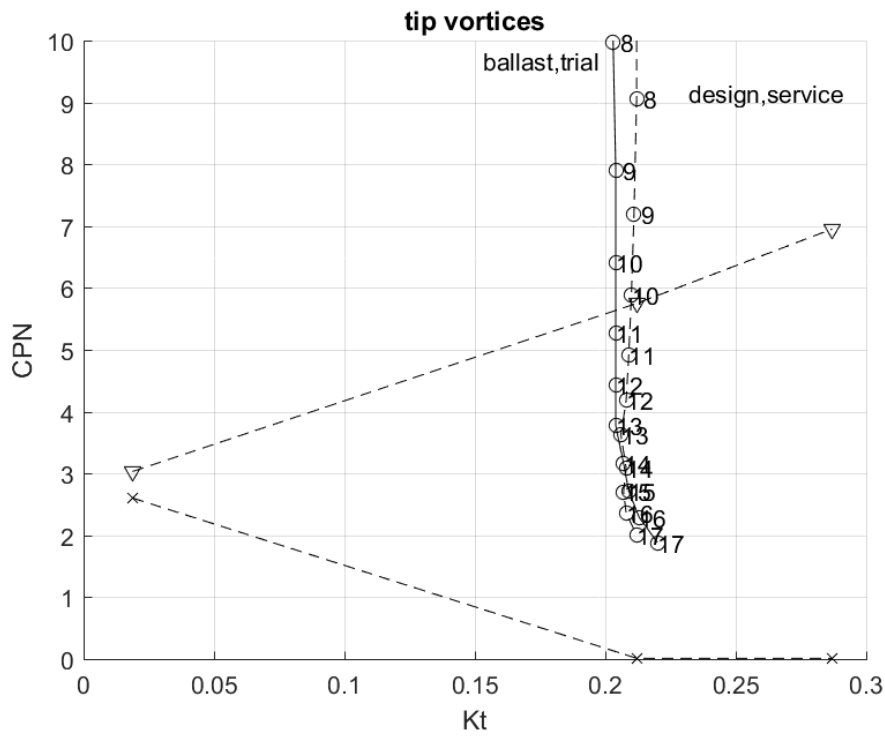
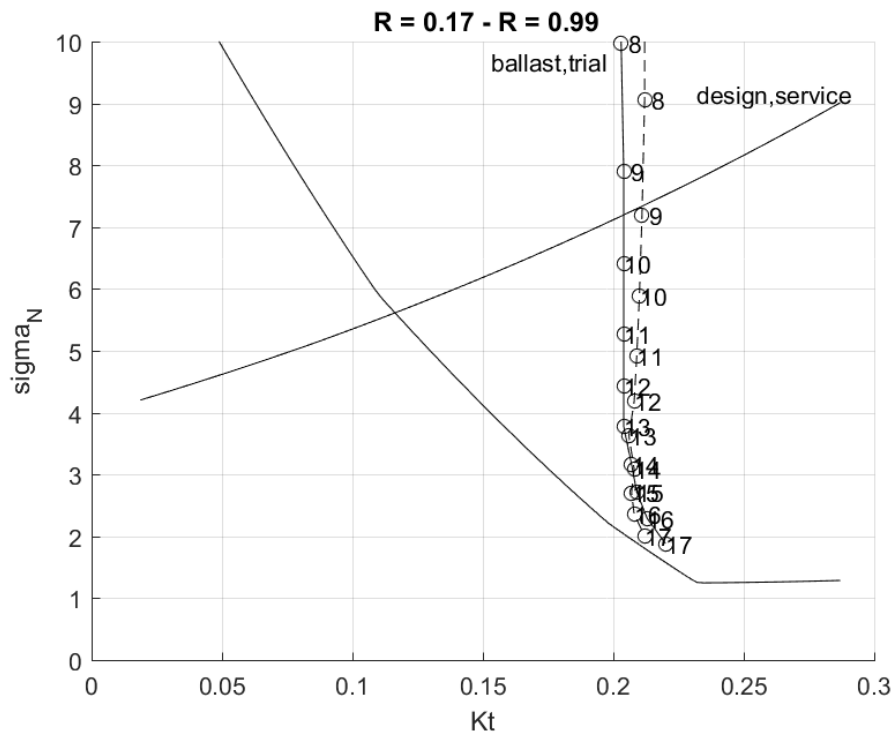
CAVITATION INCEPTION BUCKETS FOR 4-BLADED CONSTRAINED PROPELLER #173



CAVITATION INCEPTION BUCKETS FOR 4-BLADED UNCONSTRAINED PROPELLER #176



CAVITATION INCEPTION BUCKETS FOR 5-BLADED UNCONSTRAINED PROPELLER #155



CAVITATION INCEPTION BUCKETS FOR 7-BLADED UNCONSTRAINED PROPELLER #50



# **DOCUMENTATION SHEETS**



# DESP

## Prediction of propulsive performance

The computer program DESP predicts the resistance and propulsion characteristics of displacement ships. The predictions are based on formulas obtained from a regression analysis on results of model experiments and sea trials.

### References

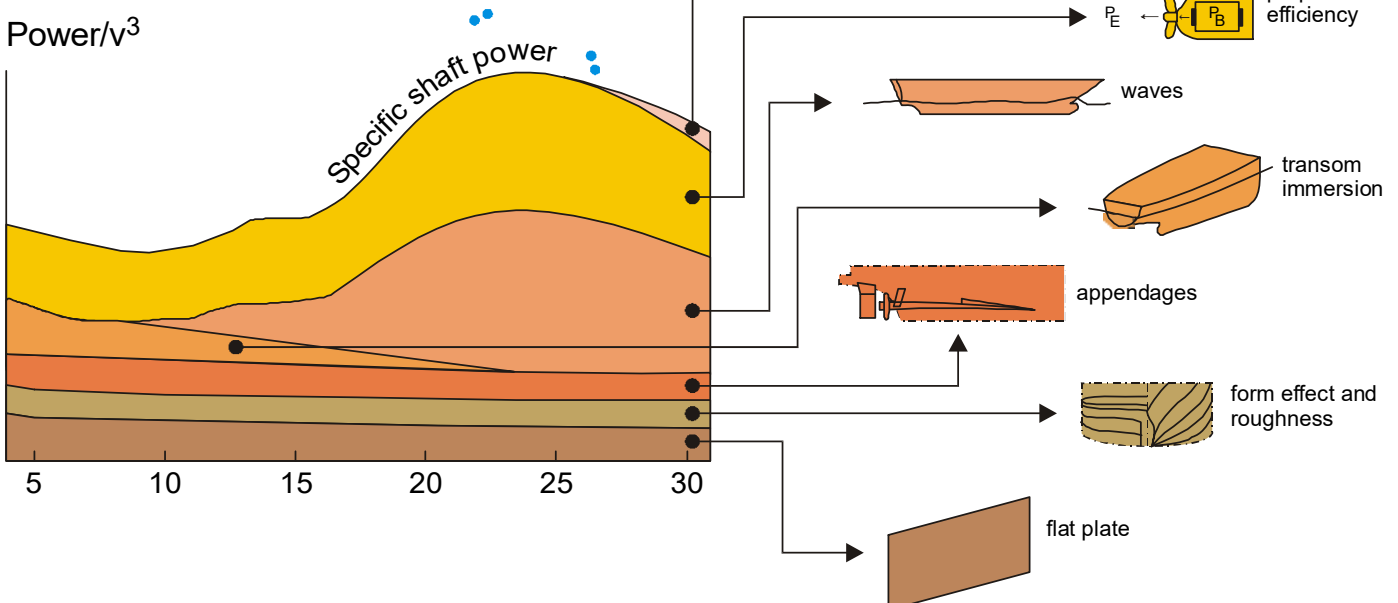
- Holtrop, J.; "A Statistical Resistance Prediction Method with a Speed Dependent Form Factor", SMSSH 88, Varna, October 1988.
- Holtrop, J.; "A Statistical Re-analysis of Resistance and Propulsion Data", International Shipbuilding Progress 31, November 1984.

### Applications

DESP can be used to estimate the speed and power in the early design stage. The level of confidence in the results can be improved by correlation with test or trial data of similar ships. These data can be used to derive an addition to the Correlation Allowance to be applied as input for the new design.

Example of statistical power prediction

- Full-scale trials



For more information contact MARIN:  
SOSC  
T + 31 317 49 32 37  
E [sosc@marin.nl](mailto:sosc@marin.nl)

## Input

The input of DESP consists of the main dimensions of the ship, the displacement volume, the form coefficients CM, CWP LCB, the bulb particulars, the immersed transom area when at rest and various parameters related to the propeller arrangement. For the calculation of the drag of stream-lined, flow oriented appendages either the equivalent appendage drag factor and wetted surface area or a detailed description of the various appendages can be provided.

## Output

The output consists of the resistance and efficiency components for the design speed or the design power, a review of the resistance, the thrust and the propulsive power as a function of the speed and tables of the pulling performance at both constant torque and at constant power.

## Accuracy

As to the accuracy of DESP it is noted that both systematic and random deviations occur. The latter are about 8 per cent of the delivered power for large comparatively slow ships ( $F_n < 0.25$ ) and tend to be larger in the steep, pre-hump range around  $F_n = 0.3$ .

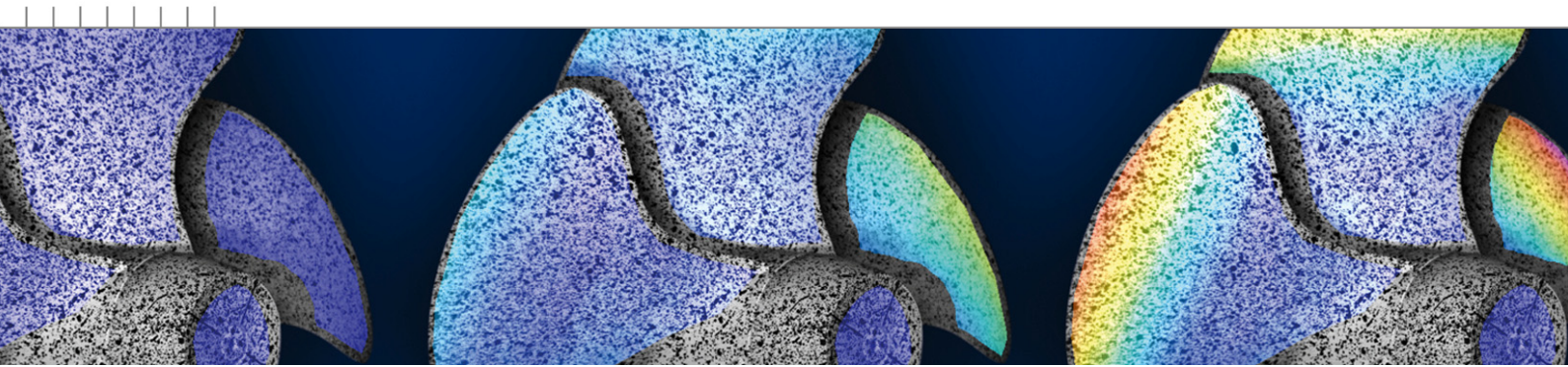
The accuracy in the post hump range is comparable with the accuracy at low speeds. Only when DESP is correlated with relevant model test data, an accuracy similar to model tests can be achieved.

Regarding the systematic deviations it is noted that DESP represents 'the average ship'. Optimised hull forms can perform 5-10 percent better than predicted by DESP. For special hull forms such as dredgers and barges DESP can be used only when checked first against results of similar ships. DESP cannot be used for planing craft.

## Computational approach

DESP applies a simple hydrodynamic model for the resistance components according to the form factor method. As to the propeller-hull interaction statistical formulas were derived for the wake fraction, the thrust deduction factor and the relative-rotative efficiency. A propeller is preliminary designed by using the Wageningen B-series or Ka-series polynomials. The propeller can be designed either for a fixed speed or for a fixed power.

In addition, either the diameter or the rotation rate can be optimised within given constraints. Effects of cavitation on the propulsion, if any, are approximated. Applying DESP for optimising hull forms or hull form details is advised against since the performance effects of various parameters are modelled with limited accuracy.

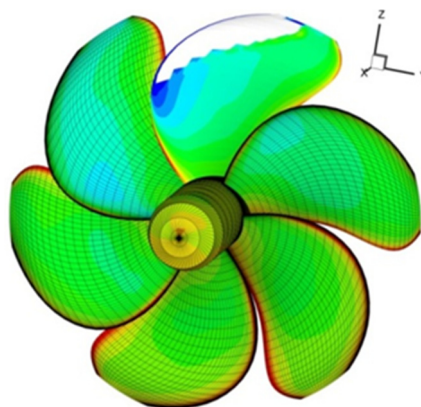


# PROCAL

## Calculating propeller performance in potential flow

MARIN internal use only

The computer program PROCAL calculates the unsteady inviscid flow including sheet cavitation around a propeller geometry using a boundary element method. It is used for the analysis of the propeller performance operating in open water or in a wake field of a ship hull. For the analysis of the hull pressure fluctuations of the non-cavitating and cavitating propeller, a coupling is made with the boundary element method EXCALIBUR, which solves the acoustic wave equation and takes the diffraction of the ship hull and the free surface into account. PROCAL has been developed in the period 2003-2008 within the Cooperative Research Ships organisation (CRS). Extensive use has been made of MARIN's experience in the implementation and application of boundary element methods for propeller analysis.



### Applications

The PROCAL code has been applied to a wide variety of propeller geometries to analyse:

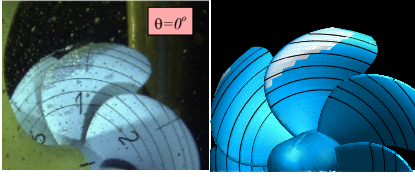
- Open water performance (shaft thrust and torque)
- Behind-hull performance (blade and shaft forces and moments)
- Sheet cavitation inception, extent and volume
- Field velocities and propeller-induced pressure fluctuations

The code is capable of analysing multi-component propulsors and its application for podded propellers, propeller-rudder combinations and ducted propellers is currently being investigated. The code has also been applied for the analysis of wings at varying angles of attack.

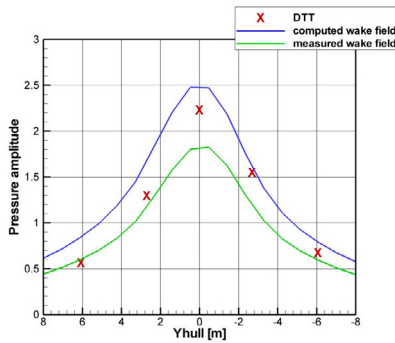
### Accuracy

The code has been validated for a large number of different propeller geometries and it gives, in general, good results. The accuracy depends somewhat on the propeller geometry and the operating point, but PROCAL results are very consistent making it a reliable propeller analysis tool for a wide range of propeller geometries. The sheet cavitation model shows very realistic patterns and good correlation with model scale and full-scale observations while predicting only a small phase lead in the growth of the cavity compared to experiments. An acceptable prediction of the pressure pulses on the hull for the first blade passage frequency is obtained.





Comparison between cavitation extents observed during experiments in the Depressurised Towing Tank (DTT) and computed by PROCAL.



Variation of pressure fluctuations on the hull in the propeller plane. PROCAL results are shown using a measured wake field and a PARNASSOS computed ship wake and compared with model scale measurements in the DTT.

## References

- Vaz, G. and Bosschers, J.; “Modelling Three-dimensional Sheet Cavitation on Marine Propellers Using a Boundary Element Method”, Sixth international symposium on Cavitation, CAV2006, Wageningen, 2006.
- Bosschers, J., Vaz, G., Starke, A.R., Wijngaarden, E. van; “Computational Analysis of Propeller Sheet Cavitation and Propeller-ship interaction”, RINA conference MARINE CFD2008, Southampton, 2008.

For more information contact MARIN:  
SOSC  
T +31 317 49 32 37  
E [sosc@marin.nl](mailto:sosc@marin.nl)

## Input

The graphical user interface PROVICE, developed by DRDC Atlantic within the CRS, helps to generate and visualise the panel distribution for the propeller and the hub, to generate the other input files and to analyse the results. The propeller geometry needs to be described by a propeller description file using tabular offset data for the foil sections and radial distribution data of pitch, chord, skew and rake. A hub geometry of arbitrary shape can be generated in PROVICE. The propeller inflow velocity field, representing the effective wake field of the hull, is specified in a ship wake file. Finally, the coordinates where field point velocities and pressures are to be calculated need to be selected. The wake field of the ship hull can be obtained from model tests or from computations using MARIN's RANS solvers PARNASSOS and REFRESCO. These computations can be made for model scale and full-scale conditions. Several methods are available for obtaining effective wake fields from nominal or total wake fields.

## Output

A large variety of output files are generated, showing pressure, cavity thickness and velocity distributions on the propeller and hub geometry, pressure and velocities in field points and hull points, radial distribution of loading, cavity length and volume on the propeller blade, and the integrated forces and moments for each blade and as transmitted to the propeller shaft. All results can easily be visualised using PROVICE.

## Computational approach

PROCAL uses the Morino formulation to solve for the velocity potential. The geometry of the propeller wake is modelled by either an empirical formulation or by an iterative approach computing the wake pitch and tip vortex roll-up. An iterative procedure is applied to satisfy the pressure Kutta condition at the propeller blade trailing edge. The cavitation model iteratively solves the non-linear boundary conditions assuming that the cavity thickness remains small. The analysis of the propeller in a wake field is performed in the time domain for a number of shaft revolutions until the change in propeller wake strength and blade loading between subsequent revolutions is sufficiently small.

## Restrictions

As the code is based on inviscid flow theory, the influence of boundary layers, flow separation and vortex formation is not included. These effects may become important for the analysis of high skew propellers and propellers operating in off-design conditions. The cavitation model is restricted to sheet cavitation and therefore does not include vortex cavitation and cloud cavitation that can be generated from the aft end of the sheet.

MARIN  
P.O. Box 28

6700 AA Wageningen  
The Netherlands

T +31 317 49 39 11  
E [info@marin.nl](mailto:info@marin.nl)

I [www.marin.nl](http://www.marin.nl)  
   

## **Appendix B Ferry Propeller Optimization Report**



**BETTER SHIPS, BLUE OCEANS**

## **Double-ended Ferry: study into the reduction of propeller cavitation noise**

Final report MS3

Report No. : 33418-2-POW  
Date : February 2022  
Version : 1.2  
Final report

# Double-ended Ferry: study into the reduction of propeller cavitation noise

## Final report MS3

MARIN order No. : 33418  
MARIN Project Manager : Gert-Jan Zondervan

Classification : NDA  
Number of pages : 58

Ordered by : LR ATG (Martec Limited)  
237 Brownlow Ave  
Dartmouth, B3B 2C7, Canada

Order document : LR purchase order 1614012 February 17, 2021  
Reference : -  
Export licence No. : NL0074CDIU0148807

Reported by : Gert-Jan Zondervan, Daniel Weeteling  
Reviewed by : Jesse Slot

Version	Date	Version description
1.2	February 2022	Updated after feedback from customer
1.1	October 2021	Final report
1.0	July 2021	Preliminary report

<b>CONTENTS</b>	<b>PAGE</b>
REVIEW OF REPORTS .....	III
1 INTRODUCTION.....	1
2 OVERVIEW OF THE VESSEL DETAILS AND EMPLOYED DESIGN TOOLS.....	3
2.1 Main particulars .....	3
2.2 Design and analysis tools.....	3
3 ANALYSIS OF SPEED-POWER PERFORMANCE.....	5
3.1 Speed-power predictions.....	5
3.1.1 Predicted resistance.....	5
3.1.2 Predicted propulsive performance .....	5
3.1.3 Analysis of operational data .....	6
4 CURRENTLY INSTALLED PROPELLER .....	10
4.1 General propeller design information .....	10
4.2 Wake field .....	11
4.3 Results.....	11
4.3.1 Cavitation inception prediction .....	12
4.3.2 Developed cavitation.....	13
4.3.3 Under water noise source level predictions .....	15
5 DESIGN OF A REPLACEMENT PROPELLER.....	18
5.1 Approach .....	18
5.1.1 Goals and constraints .....	18
5.2 Unconstrained propeller design.....	19
5.3 Constrained design.....	21
5.4 Developed cavitation and noise source level predictions.....	22
5.4.1 Developed cavitation.....	22
5.4.2 Comparison of underwater noise source levels .....	25
6 CONCLUSIONS AND RECOMMENDATIONS .....	27
REFERENCES .....	29
Figure pages .....	F1 – F10
APPENDIX I : List of symbols.....	A1.1 – A1.7

Software documentation sheets:      DESP  
  PROCAL

## REVIEW OF REPORTS

### Deliverables of the current project phase<sup>1</sup>

Task	Item	Title	Date
2, 3 and 5	Report No. 33418-1-POW	159m DWT Oil Tanker; study into the reduction of propeller cavitation noise	February 2022
4 and 5	Report No. 33418-2-POW	Double-ended Ferry: study into the reduction of propeller cavitation noise	February 2022

---

<sup>1</sup> At the moment of writing.

## 1 INTRODUCTION

Under an independent subcontractor agreement, the Maritime Research Institute Netherlands (MARIN) has been commissioned by Martec Limited (LR ATG) to carry out a propeller design study. The reported study is the second of two studies aiming at demonstrating the potential improvements that can be made to propeller designs of commercial ships in reducing the underwater radiated noise (URN) due to propeller cavitation.

This report provides a description of a propeller design study on the controllable pitch propeller of the double-ended C-class ferries, see Figure 1-1. The project is sponsored by Transport Canada in a programme aimed at investigating the potential for silencing commercial shipping that is threatening underwater wildlife.

This report covers the reporting (task 5) of the propeller design study for the second ship type (task 4) of the contract. The work consists of the following:

- Evaluation of the currently installed propeller involving:
  - Analysis of provided information (drawings and performance data) and speed-power predictions using the Holtrop-Mennen method.
  - The numerical evaluation of the currently installed propeller using propeller analysis code PROCAL and the empirical tip vortex (ETV) prediction method developed by the Cooperative Research Ships (CRS) consortium, see Bosschers (2009). Besides the cavitation inception characteristics, the analysis also includes a prediction of the underwater noise levels with an upgraded version 3.0 of the ETV model that is combined with a semi-empirical model to compute the contribution of sheet cavitation.
- Numerical calculations for the design of a new replacement propeller for the ferry. This involves:
  - Design optimisations using the PROPART propeller optimisation framework to investigate design trade-offs (e.g. efficiency and cavitation inception characteristics).
  - Propeller design keeping the mass and moment of inertia similar to the existing propeller.
  - Propeller design with no restrictions on mass and moment of inertia.
  - Provide load input for structural analysis of the propeller by LR.



Figure 1-1: C-class ferry and its currently installed CP propellers.



The contents of this report is as follows. Chapter 2 provides details about the vessel and the employed propeller design tools. The results of the speed-power performance calculations, comparison with sea trial data and the definition of the conditions to be analysed are presented in Chapter 3. Chapter 4 presents the analysis of the installed propeller. The approach and results of the design optimisation study for the replacement propeller are described in Chapter 5. In Chapter 6 the conclusions and recommendations are listed. Throughout this report SI units are used unless indicated otherwise; a list of symbols is given in Appendix I.

## 2 OVERVIEW OF THE VESSEL DETAILS AND EMPLOYED DESIGN TOOLS

This chapter provides a concise overview of the particulars of the ferry and the tools employed in the optimisation exercise for the propeller design.

### 2.1 Main particulars

The main particulars of the ship are:

Description	Symbol	Design draught	Unit
Length between perpendiculars	$L_{PP}$	127.2	m
Length on waterline	$L_{WL}$	133.1	m
Breadth moulded on WL	B	21.98	m
Draught moulded on FP	$T_F$	5.5	m
Draught moulded on AP	$T_A$	5.4	m
Displacement volume moulded	$\nabla$	5586.4	m <sup>3</sup>
Displacement mass in seawater	$\Delta_1$	5731.1	t
LCB position forward of $\frac{1}{2} L_{PP}$	LCB	0.00	%
Block coefficient	$C_B$	0.350	-
Midship section coefficient	$C_M$	0.640	-
Prismatic coefficient	$C_P$	0.547	-
Length-Breadth ratio	$L_{PP}/B$	5.787	-
Breadth-Draught ratio	$B/T$	4.033	-

The ferry is a double-ended ferry fitted with a single 4-blade controllable pitch propeller at each end of the ship. The table below indicates some relevant propulsion details of the ship and propellers:

Engine type	Diesel motor	-
Number and type of propulsors	2 controllable pitch propellers (bow side prop in feathering pitch setting)	-
Available brake power at 100% MCR	8723	kW
Shaft losses (estimated)	2.5	%

### 2.2 Design and analysis tools

In the design of the replacement propeller(s) extensive use was made of the PROPART tool for propeller design. PROPART is a multi-objective optimisation method developed by MARIN within the Cooperative Research Ships (CRS) research consortium for carrying out propeller design studies. PROPART uses a parametric description of the propeller geometry and a coupling of propeller code PROCAL with an optimisation algorithm.

The numerical analysis has been carried out using propeller analysis code PROCAL. PROCAL is a boundary element method (BEM), developed within CRS, see the included software documentation sheet at the end of the report. PROCAL is able to predict the inception and extent of developed sheet cavitation, in order to check for erosive types of sheet cavities. Tip vortices and tip vortex cavitation are not modelled in PROCAL. The inception of tip vortex cavitation is determined using the Empirical Tip Vortex (ETV) prediction method that was also developed within CRS.

PROCAL computations are performed for a large number of propeller geometries with varying radial distributions of the geometry parameters like the pitch, chord length, maximum thickness and maximum camber. Also, the blade profile shape is optimised. After the PROCAL computations, often in multiple design conditions, the performance is evaluated in terms of cavitation behaviour, efficiency and constrained properties like the blade mass and inertia.

PROPART also features a cavitation inception analysis module which analyses the cavitation inception buckets for sheet-cavitation and tip-vortex cavitation for both pressure-side and suction-side cavitation. A range of propeller loading conditions are computed with PROCAL providing the pressure distributions on the propeller blade, while the ETV model provides an estimate of the cavitation inception of the tip vortices.

Besides the inception of cavitation, also predictions have been made of the underwater radiated noise levels using the ETV model for predicting tip vortex cavitation noise combined with a semi-empirical method for calculating the noise of sheet cavitation. It is emphasised that the latter is a very recent development that until now is validated only for pressure side cavitation measured during model scale cavitation tests in MARIN's Depressurised Wave Basin.

In the current propeller design study the possibilities of improving the propeller design and fulfilment of the design goals are shown in the form of Pareto front plots, see Figure 2-1 for an example. Each dot in the figure represents a candidate propeller design selected from the parametric design space of the propeller geometry. As the optimisation process advances, better propellers are created. This is shown in the figure as going from the earlier designs in blue to the latest ones in red. The Pareto front is given by the propellers represented by the deep red circles. Propellers on the Pareto front have the property that the margin against cavitation cannot be improved without compromising efficiency.

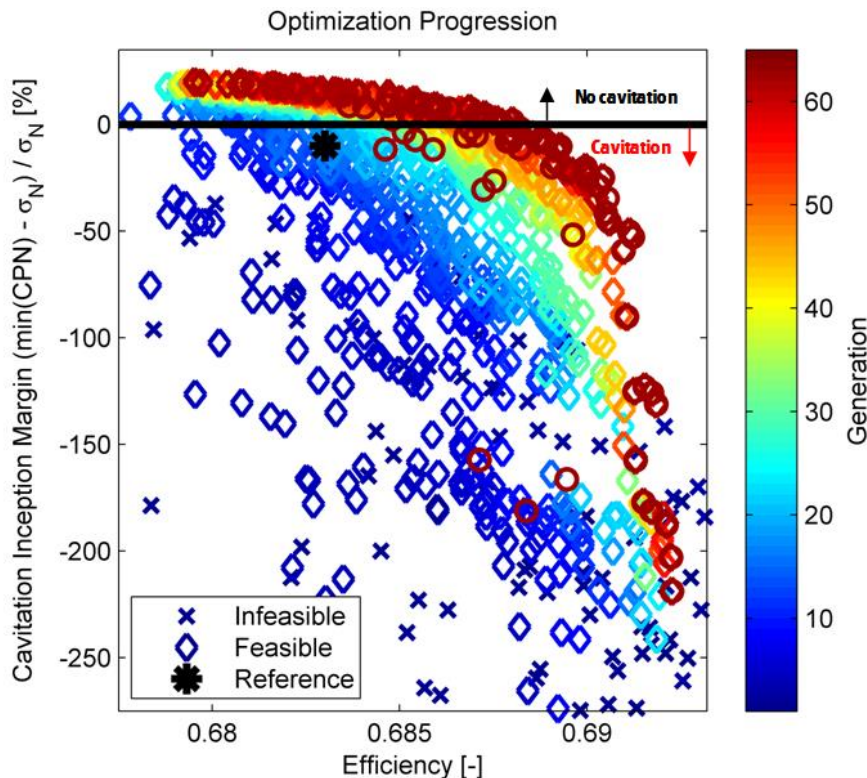


Figure 2-1: Example of optimisation case with final Pareto front in red. Both the margin against cavitation and efficiency were to be maximised.

### 3 ANALYSIS OF SPEED-POWER PERFORMANCE

Speed-power predictions have been carried out for generating the required input for the propeller design calculations. The results of these predictions have been compared with operational data that was received from LR providing valuable information about the speed profile and how the pitch of the controllable propellers of the vessel is operated. Based on this analysis the design points for the propeller design operation have been determined.

The speed-power calculations have been carried out with computer program DESP, see the software documentation sheet at the end of this report. DESP is an implementation of the Holtrop-Mennen method for the prediction of the resistance and powering performance of ships. The predictions are based on correlation with similar double-ended ferry designs available in the database of MARIN. The predictions have been made for an operational draught of  $T_F/T_A = 5.5/5.4$  m at which the vessel was sailing during the onboard measurements. In the following sections the results of the speed-power predictions are presented and compared with the provided operational data.

#### 3.1 Speed-power predictions

##### 3.1.1 Predicted resistance

The following resistance variation with speed is found from DESP. The resistance includes the contribution of the inactive bow propeller set in feathering pitch setting.

Table 3-1: Predicted resistance versus ship speed for operational draught.

V [kn]	FN	R [KN]	P <sub>E</sub> [KW]
15.0	0.214	226.3	1746
16.0	0.228	262.8	2163
17.0	0.242	304.3	2661
18.0	0.256	350.8	3248
19.0	0.271	402.3	3933
20.0	0.285	459.7	4729
21.0	0.299	522.1	5641

##### 3.1.2 Predicted propulsive performance

Predictions have been made of the propulsive performance of the vessel operating in ideal trial conditions as well as an assumed service condition with 15% sea margin. The calculations with the Holtrop-Mennen method were made for a CPP propeller set at constant pitch thus it is used as a fixed pitch propeller. This approach is commonly used for controllable pitch propellers to determine the maximum speed of the vessel. This assumption is valid because it was determined that the efficiency drop becomes only notable at the lower ship speeds below 18 knots (2.5 per cent reduction in efficiency in constant RPM mode compared to the constant pitch mode). The provided combinator diagram suggests that the propeller is used both with varying pitch and propeller rotation rate. Therefore it was assumed that the fixed pitch assumption would be sufficient.

In the speed-power predictions the polynomials of MARIN's C-series propellers are used which represent the performance of contemporary controllable pitch propellers. In the following tables the predicted shaft power, rotation rate and propeller thrust are presented versus the ship speed. Also shown are typical efficiency components assumed for the vessel. The calculations are made for the characteristics of the currently installed propeller. This 4-blade propeller has a diameter of 3.81 metres and a blade area ratio of about 0.7.

In Table 3-2 the speed-power data for the ideal trial condition is shown. Indicated in red is the prediction for the condition where the propeller is absorbing 100% of the MCR power. The calculated results are for ideal trial conditions, implying unrestricted deep water of 15.0° C and a mass density of 1025.9 kg/m<sup>3</sup>, a clean hull and propeller blades and no effects of wind and waves. In Table 3-3 the prediction is presented for the selected service condition with 15% sea margin. Indicated in red again is the speed prediction for the 100% MCR power condition.

Table 3-2: Propulsive performance for operational draught (trial, fixed pitch mode).

V [kt]	N [RPM]	P <sub>s</sub> [kW]	T-TOT [kN]	THDF	W	ETAH	ETAO	ETAR	ETAD
15	134.1	2710	264.1	0.143	0.139	0.996	0.676	0.966	0.651
16	143.9	3367	306.3	0.142	0.139	0.996	0.673	0.968	0.649
17	154.0	4158	354.3	0.141	0.138	0.997	0.671	0.967	0.647
18	164.3	5096	407.9	0.140	0.138	0.997	0.667	0.968	0.644
19	174.9	6198	467.3	0.139	0.137	0.998	0.664	0.967	0.641
20	185.7	7490	533.2	0.138	0.136	0.998	0.660	0.968	0.638
20.68	195	8501.9	581.4	0.137	0.136	0.999	0.656	0.967	0.634
21	199.4	9058	604.8	0.137	0.136	0.999	0.651	0.967	0.629

Table 3-3: Propulsive performance for operational draught (15% SM service condition, fixed pitch mode).

V [kt]	N [RPM]	P <sub>s</sub> [kW]	T-TOT [kN]	THDF	W	ETAH	ETAO	ETAR	ETAD
15	139.9	3128	299.6	0.138	0.146	1.010	0.658	0.967	0.643
16	150.0	3877	346.7	0.137	0.146	1.010	0.656	0.968	0.642
17	160.4	4773	399.9	0.136	0.145	1.010	0.653	0.968	0.639
18	171.1	5831	459.0	0.136	0.145	1.011	0.651	0.966	0.636
19	182.0	7068	524.2	0.135	0.144	1.011	0.647	0.969	0.634
19.96	194.8	8501.5	593.4	0.134	0.144	1.011	0.640	0.969	0.634
20	195.4	8567	596.2	0.134	0.143	1.011	0.640	0.969	0.627

### 3.1.3 Analysis of operational data

Operational data has been analysed that was measured on board of the subject ferry during a series of crossings in its operating area in Canada. The measured data consists of power and thrust readings obtained from shaft sensors on both bow end and stern end propellers. Further data consists of the GPS speed of the vessel (heading, wind speed and angle and water depth. The data taken at 1 minute intervals covered several consecutive crossings providing a good overview of typical operations of the ship including transit as well as departures, arrivals and other events.

In Figure 3-4 the measured shaft power for both propellers (the stern propeller in operation and the bow propeller set in feathering condition), denoted A and B, is shown compared to the predicted shaft power curves according to Section 3.1.2. In the plot the scatter of the measured shaft data is shown for each of the propellers. Notice that when the propeller is feathering the shaft load becomes close to zero. The orange and green curves respectively represent the speed-power prediction made for the fixed pitch propeller equivalent for trial and 15% SM service conditions. At the higher ship speeds the measurement points are clustering around the prediction curves while at the lower speeds the points show the behaviour of the propellers manoeuvring and stopped conditions.

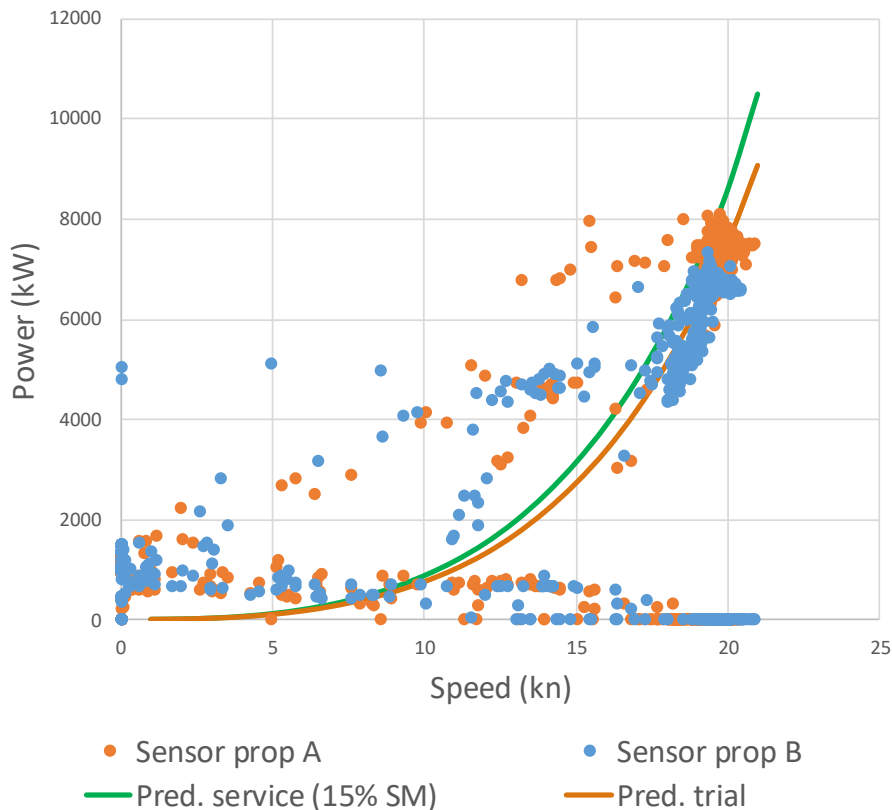


Figure 3-4: Measured shaft power for bow and stern propellers compared to predictions.

Figure 3-5 shows the same information in more detail. From the sea trial data for eight crossings, two crossings were taken for which the recorded wind speed seems to be moderate. The measured data of these crossings are highlighted by the dark blue and brown points in the plot. It is noted that the faint dots in the plot indicate the data points from the crossings that were not selected. From the data it was determined that during one of the two consecutive crossings one propeller is operating at around 80% (6985 kW) of the maximum available engine power (8500 kW) while during the other crossing the (other) propeller is operating at 70% MCR (5990 kW). The different wind direction could be a cause for this notable difference. From these two conditions the more severe 80% MCR condition was selected for the propeller analysis.

Further to this condition a point was taken from the dataset in which the propeller momentarily absorbs 60% of the MCR power. This condition is a typical condition where CP propeller are designed to operate free of pressure side cavitation. Furthermore, a maximum (100%) MCR power condition can be taken from the fixed pitch trial curve which better represents the measured data. These three conditions, shown by red dots in Figure 3-5, will be used for the analysis of the installed propeller.

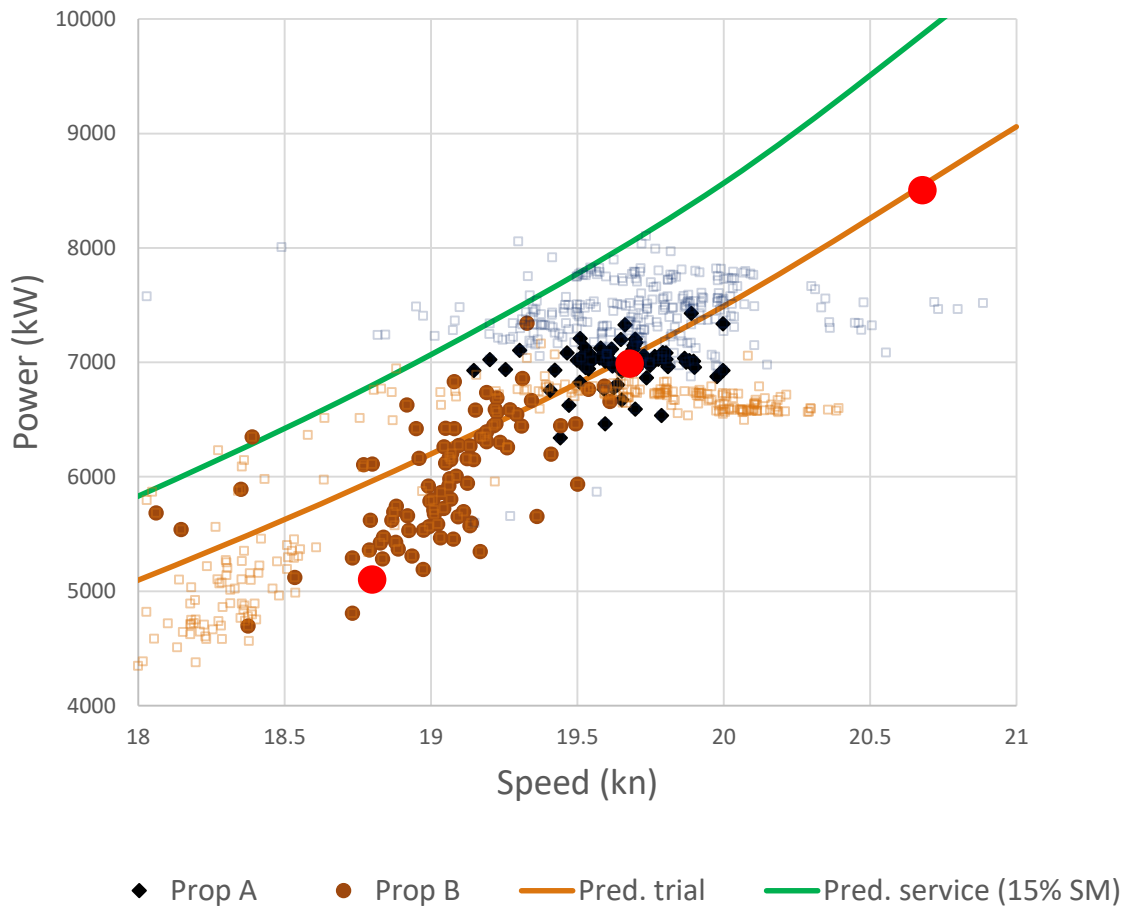


Figure 3-5: Measured shaft power for bow and stern propellers compared to predictions. Red points indicate selected conditions for analysis and design.

Zooming further into the speed range between 18 and 20 knots a selection of measurements is shown in Figure 3-6. In the plots the measured propeller power, thrust and propeller rotation rate are shown compared with the presented predictions. The plots show the variation of the ship speed and rotation rate of the propellers with the resulting variations of the shaft power and propeller thrust. As a result of the variations of the thrust and the rotation rate also the parameters that are relevant for the cavitation inception characteristics are varying; the non-dimensional thrust coefficient  $K_T$  and the cavitation number  $\sigma_n$ . In the bottom right plot of Figure 3-6 the green points show the variation of the parameters in the selected speed range. The orange points show the variations outside of the selected range, mostly representing conditions where the ship is manoeuvring. The plot shows the area of interest where an elimination or reduction of the cavitation will result in under water noise reduction during the transit phase of the crossings.

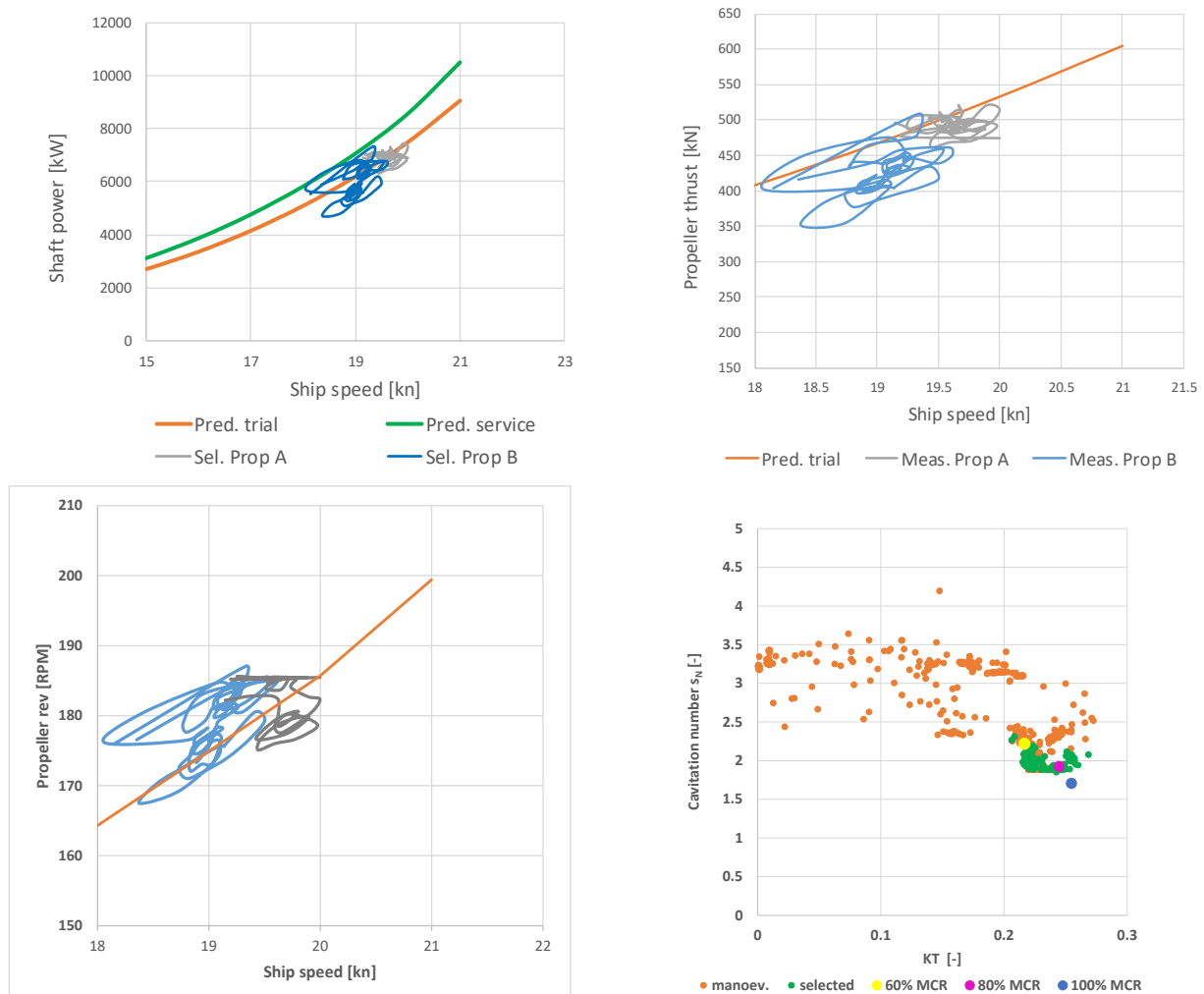


Figure 3-6: Power, thrust and propeller revolution rates from trial data versus prediction line. Right bottom: Operational range of the propeller from the operational data.

From the analysis the main conclusions are the following:

- The provided full scale operational data matches best with the prediction made for the ship sailing in trial condition. Therefore the analysis of the currently installed propeller and the design of the replacement propeller was performed for the ship operating in this condition.
- Three conditions were selected for the analysis. These are the high speed sailing conditions where the propeller absorbs 80% and 100% of the available MCR power and the lower speed 60% MCR condition which is selected as a typical lower speed condition where the propeller is probably designed to be free of pressure side cavitation.

In the next chapter the predictions of the cavitation inception characteristics, developed cavitation and cavitation noise are presented.



## 4 CURRENTLY INSTALLED PROPELLER

In this chapter the cavitation and under water noise predictions are presented that have been performed for the installed propeller.

### 4.1 General propeller design information

The following lists the most important details of the ferry and its propellers.

- The ferry is a double-ended ferry fitted with a single 4-blade controllable pitch propeller at each end of the ship. It appears that at one side a right-handed propeller is installed while at the other end a left-handed propeller is fitted. The propellers are each driven by two MAK 12M441AK diesel engines. According to the provided propeller drawing, each propeller is designed for a maximum combined engine output of 8723 kW at 195 RPM.
- The diameter of the installed propeller is 3.81 metres. Based on a B-series diameter optimisation it follows that the diameter is close to its optimum diameter.
- The propeller combinator plot, see the left plot of Figure 4-1, containing the programmed pitch control versus the handle position was provided. This plot presents the relation between the propeller rotation rate and the propeller pitch angle. Using the measured operational data the relation between pitch setting and rotation rate with the ship speed has been deduced, see the right plot of Figure 4-1. From this relation the selected propeller pitch angle could be approximated for the design points for the analysis and design optimisations.

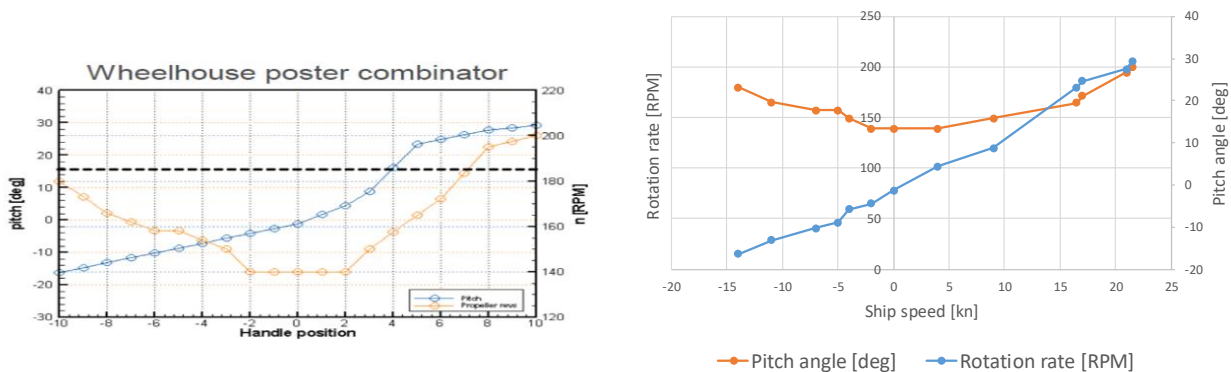


Figure 4-1: Combinator plot and deduced propeller pitch and revolution rate versus ship speed (trials).

- From this data the pitch deflections for the calculated conditions are determined. The design pitch of the propeller is  $P_{0.7}/D = 1.23$ . For the 100% MCR trial condition the propeller is supposed to be rotating at 195 RPM leading to a pitch ratio  $P_{0.7}/D = 1.15$ . For the 80% MCR trial condition the pitch control setting is near position 8 and the pitch reduction is calculated to be 3.12 degrees, leading to a pitch setting of around  $P_{0.7}/D = 1.09$ . For the 60% MCR condition the pitch ratio is  $P_{0.7}/D = 1.03$ .
- An important conclusion from the combinator plot is that the pitch reduction in the astern condition is limited to about 16 degrees. It was determined that this means the blades do not need to pass each other as is normally seen with CP propellers.
- The main objective in the design of the replacement propeller is to reduce the underwater radiated noise (URN) in a relevant operational range of the vessel by reducing the source level (SL) noise produced by the propeller. The first focus was the reduction of the amount of cavitation during cruise speeds (green area in Figure 3-6).
- The installed propeller has been designed following the classification rules of Lloyds Register. The propellers are designed with ice strengthening according Lloyds Register ice class 2. It is assumed that this old ice class corresponds with modern LR ice class 1D. This ice class incorporates an

addition of 8 per cent to the maximum thickness of the profile sections of the blade. The ice rules also includes requirements for the thickness measured near the leading edge of the blades.

- According to the propeller drawing the currently installed propellers are made of stainless steel with a minimum tensile strength of 638 N/mm<sup>2</sup>. According to MARIN calculation the four blades weigh 3072 kg excluding the weight of the blade foot disc and root fillets assuming a material density of 7750 kgm<sup>3</sup>. The total mass moment of inertia of the four blades is 7374 kgm<sup>2</sup> including an estimated contribution of the entrained water of 2886 kgm<sup>2</sup>. For the strength rules an allowable stress of 41.0 N/mm<sup>2</sup> is used.
- To avoid the potential need for reanalysis and certification of the drive train of the vessel, it was requested to keep the mass and inertia of the replacement propeller within 2 per cent of the values of the currently installed propeller. Also a limited variation was allowed of the spindle torque moment generated by the hydrodynamic loading of the propeller and centrifugal mass forces. In the next chapter the study continues with an investigation to determine the importance of this constraint on the delay of cavitation and noise reduction.

## 4.2 Wake field

MARIN received an effective wake field computed by LR for the vessel sailing at an operational draught of FWD/AFT = 5.9/5.9 m. On pages F1 and F2 the axial and transverse velocity components of the wake field for the vessel at design draught are shown.

Most notable properties of the provided effective wake field information is:

- The plot of the axial wake field velocity distribution shows a pronounced wake peak near the 12 o'clock position. Noteworthy is that the wake peak stretches out over the entire radius of the propeller blades in the effective wake field which is not the case in the nominal wake field (not reported).
- Also at the 6 o'clock position an axial wake deficit is visible presumably from the wake of the skeg.
- The transverse velocity vector field shown on page F2 shows quite large radial velocities at the upper half of the propeller disc and at the inner blade radii for the entire wake field.

## 4.3 Results

As part of Task 4 of the project, the performance of the currently installed CP propeller has been investigated. Calculations have been carried out with BEM code PROCAL using the input of the speed-power characteristics of the vessel, the effective wake field of the vessel computed by LR and the pitch settings determined from the provided combinator plot.

MARIN constructed a propeller geometry based on the provided drawing of the propeller design of the vessel (document A011296 C.P.PROPELLER FOR DOUBLE ENDED FERRY RD MAR-80.PDF). It is noted that all information of the propeller design was provided in this drawing and that therefore the analysed propeller geometry is closely resembling the installed propeller. In the remainder of the report this propeller is called the reference propeller.

It is noted the ferry is fitted with one right handed and one left handed propeller. In the calculations due to the symmetry of the wake field the performance of the right handed propeller is presented.

### 4.3.1 Cavitation inception prediction

Figure 4-2, shows the computed cavitation inception characteristics of the sheet and tip-vortex cavitation types for the propeller set at the pitch setting for the 80% MCR trial condition ( $P_{0.7}/D = 1.09$ ). In the figure the green points again show the operational points selected from the data points measured during the trials. Also the three conditions (60%, 80% and 100% MCR trial condition) in which the propeller is analysed are shown. For each cavitation type, the plots show the variation with propeller loading (in terms of the thrust coefficient  $K_T$ ) of the cavitation inception at the suction side and the pressure side of the propeller blade. The black curves show the sheet cavitation inception curves while the red curve represents the inception of tip vortex cavitation. Enclosure of the green points by the cavitation bucket curves would indicate that the propeller is free of cavitation.

When considering the entire propeller blade the sheet cavitation bucket curve for the total blade is located at high values of the cavitation number indicating that propeller cavitation is occurring on the propeller and large negative margins against cavitation inception are present. From the results it was found that the most sensitive area is the tip region where large suction pressure peaks are developing at the leading edges of the propeller blades. Further insight into the cavitation sensitivity can be obtained by omitting the outer blade radii from the results. The dashed curves show the resulting sheet cavitation inception buckets when omitting the radii outward of  $0.8R$  and  $0.6R$ , respectively. It is shown that clearly the most critical area is the tip region. The diagram further shows that also tip vortex cavitation is predicted.

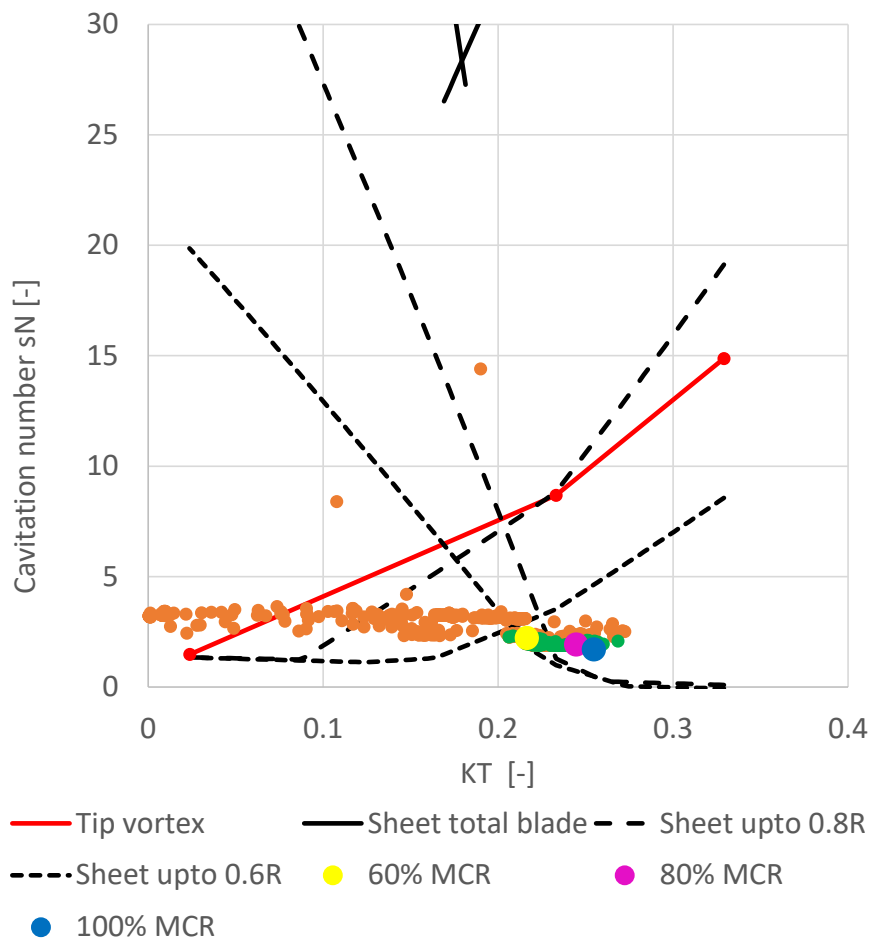


Figure 4-2: Computed cavitation inception buckets for the propeller at pitch setting  $P_{0.7}/D = 1.09$ .

Notice that of course the presented cavitation inception diagram only illustrates the large negative margins against inception of cavitation for the 80% MCR trial condition.

### 4.3.2 Developed cavitation

To illustrate the extent of the cavitation developing on the currently installed propeller predictions have been made with PROCAL for the three operational conditions

In Figure 4-3 the computed sheet cavitation is shown as calculated for the 80% trial condition when the ship is sailing at the operational draught of 5.5/5.4 m FWD/AFT. The plot shows the sheet cavity developing at the suction side of the blade with the contours showing the pressure at the propeller blade. The pressure is non-dimensionalised by a factor ND, representing the propeller diameter D and the rotation rate N:

$$C_{PN} = \frac{P - P_{shaft}}{0.5 \rho N^2 D^2}$$

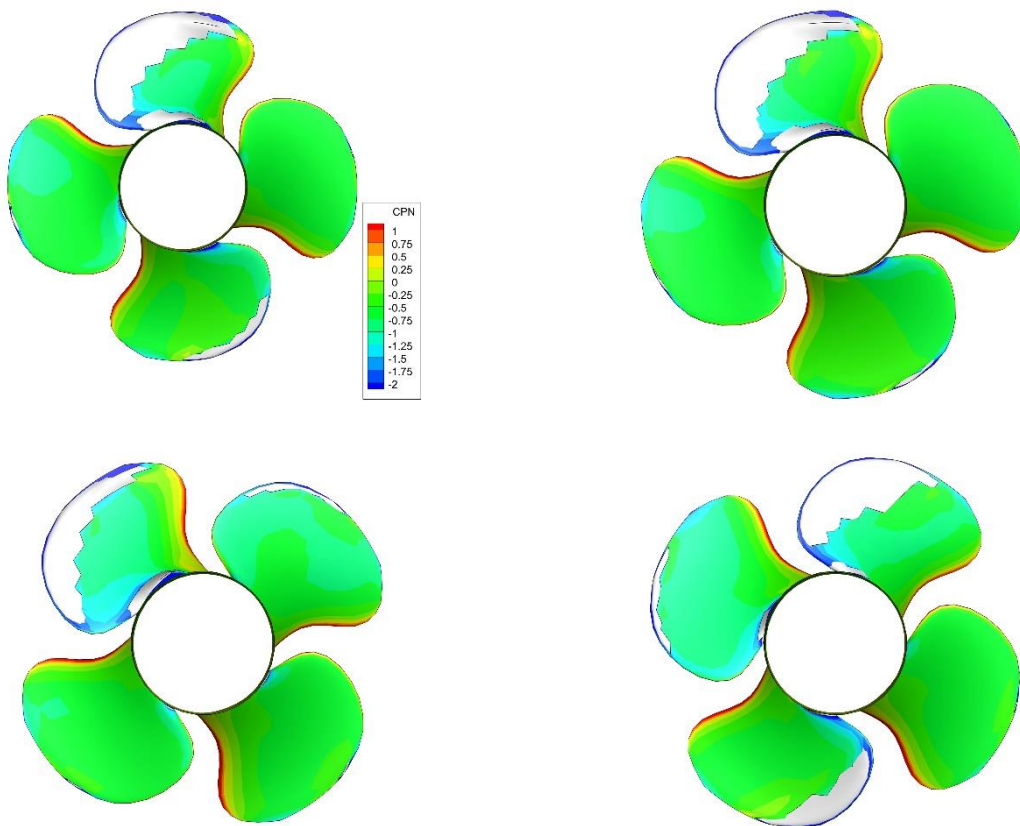


Figure 4-3: Illustration of predicted suction side sheet cavitation patterns and pressure distribution ( $C_{PN}$ ) (Trial, 80% MCR, 19.68 knots,  $N = 183.6$  RPM,  $P_{0.7}/D = 1.09$ ).

As Figure 4-3 shows the propeller blade is covered by a large sheet cavity that is extending over most of the blade radius. At the lower radius an interruption of the sheet cavitation is seen while at the blade root the propeller blade is again quite extended. After passing the wake peak at the tip the sheet cavity retreats favourably towards the tip where it will merge with the tip vortex. Note that tip vortices and tip vortex cavitation are not modelled in PROCAL and are therefore not seen in the cavitation plots. The extent and dynamic behaviour of the sheet cavities result in a low risk of cavitation erosion damage.

In Figure 4-4 the cavitation patterns predicted for the 100% MCR trial condition are shown. A somewhat larger extent of the sheet cavitation is seen with local sheet length exceeding the chord length. Notice that again the sheet cavitation will merge with the well-developed tip vortex cavitation near the tip. Because the extent of the cavitation and the noise levels generated by the cavitation (see section 4.3.3) are quite similar to that for the 80% MCR condition, the 100% MCR condition is not considered further in the design of the replacement propeller (see Chapter 5).

Finally the cavitation patterns computed for the 60% trial condition are shown in Figure 4-5. It can be observed that only a small trace of sheet cavitation is found at the higher blade radii. None of the analysed conditions predict cavitation on the pressure side of the blade. This observation could be a conscious choice by the propeller designer. As is known to MARIN, propellers that are used at near constant RPM mode of operation are designed with sufficiently large margins against pressure side cavitation to prevent potential cavitation erosion problems or raised noise levels when the propeller is operated at reduced pitch.

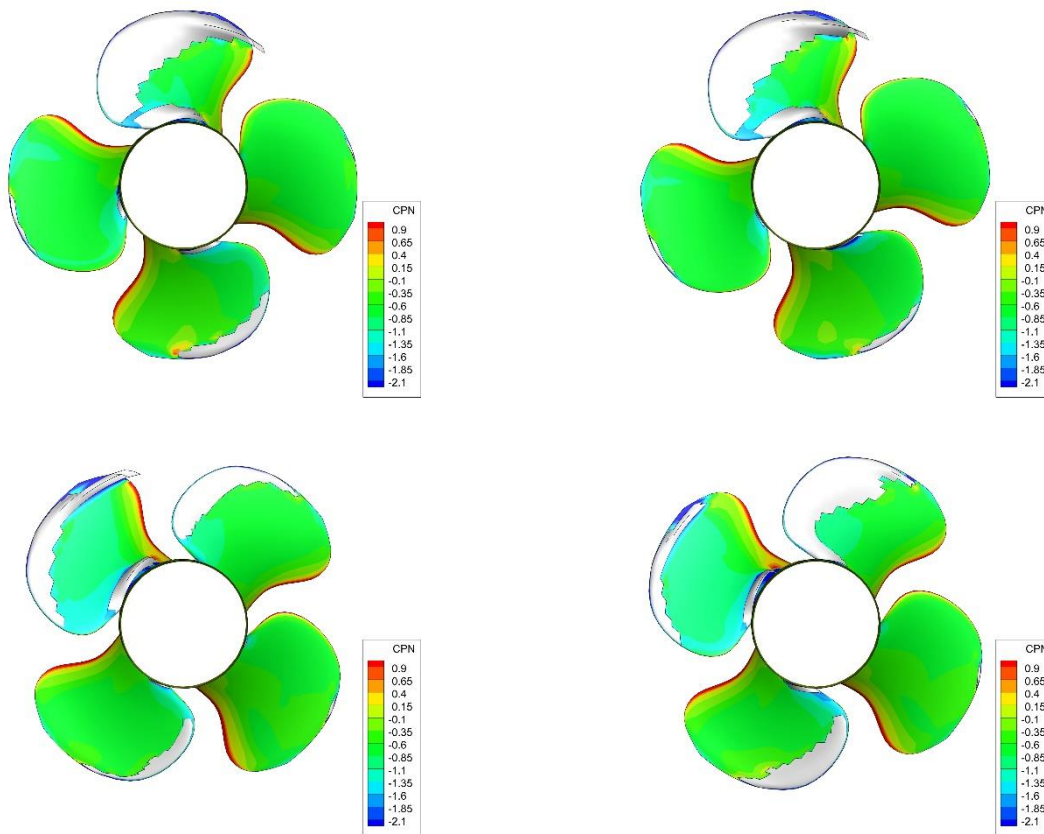


Figure 4-4: Illustration of predicted suction side sheet cavitation patterns and pressure distribution ( $C_{PN}$ ) (Trial, 100% MCR, 20.68 knots,  $N = 195.0$  RPM,  $P_{0.7}/D = 1.15$ ).

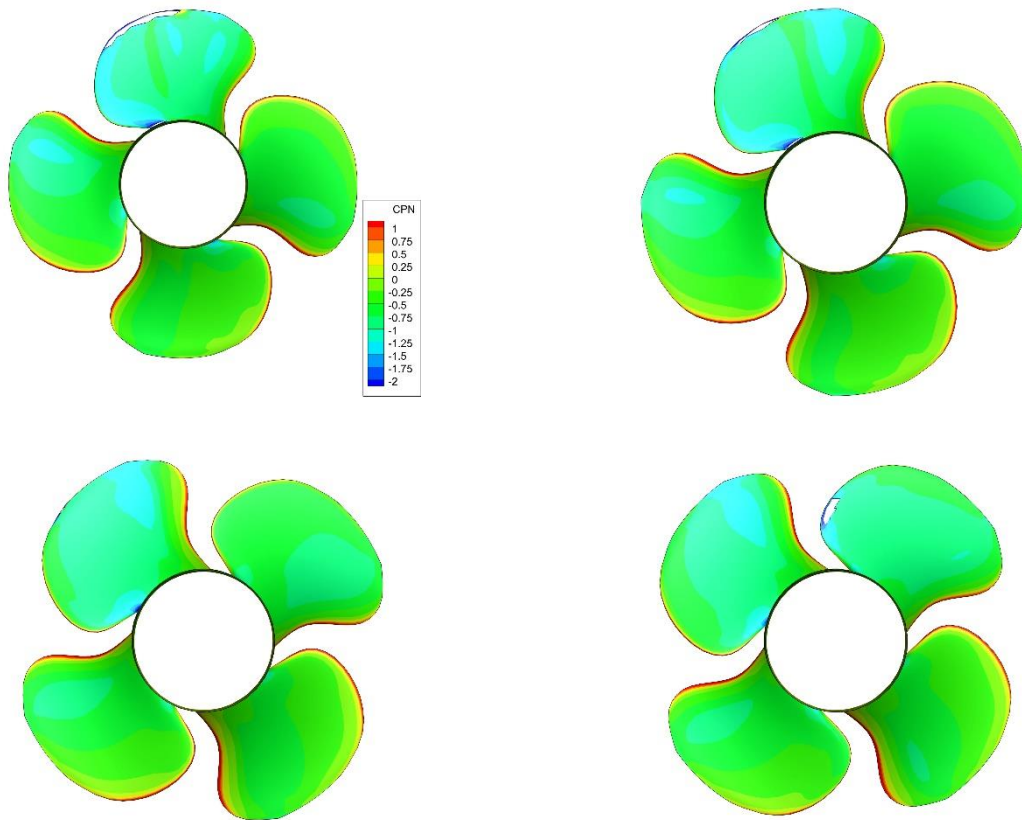


Figure 4-5: Illustration of predicted suction side sheet cavitation patterns and pressure distribution ( $C_{PN}$ ) (Trial, 60% MCR, 18.8 knots,  $N = 171.0$  RPM,  $P_{0.7}/D = 1.03$ ).

### 4.3.3 Under water noise source level predictions

Predictions of the underwater noise levels have been made using a recently upgraded version 3.0 of the ETV model. It computes the contribution of tip-vortex cavitation that is interacting with sheet cavitation at the tip. The ETV results are combined with a semi-empirical model to compute the contribution of isolated sheet cavitation. The latter model has similarity with the model published by Brown (2007) making use of the cavity areas computed by PROCAL. So far, the model has been validated and tuned using experimental data obtained in the DWB of propellers with isolated face side sheet cavitation, with validation studies for propellers with back-side sheet cavitation still to be performed.

In Figure 4-6 to Figure 4-8 the computed noise spectra for the three selected operational conditions are presented for the ship fitted with currently installed propeller sailing in trial condition. Shown are the contributions of the different cavitation forms and the total source levels in terms of one-third-octave band levels in [dB, re  $1 \mu\text{Pa}^2\text{m}^2$ ]. The levels are compared with the source level limits presented by class society LR for merchant ships in transit at 85% MCR power. This criterion is taken because of the significant amount of cavitation on the controllable pitch propeller of this ferry. The levels by LR are used as limits and presented as source levels while other class societies present their limits as radiated noise levels, hence including the Lloyd-mirror effect which is a correction that accounts for the noise reflections of the water surface.

The noise plots show that for the 80% and 100% MCR conditions tip vortex cavitation is the dominant noise source. Without it the contribution of the suction side sheet the noise level would be below the LR transit criterion although the amount of sheet cavitation is substantial. On the basis of the PROCAL calculation for the 60% MCR a small contribution of pressure side sheet cavitation is predicted, see Figure 4-8. Notice again that the 100% MCR condition is not considered further in Chapter 5.

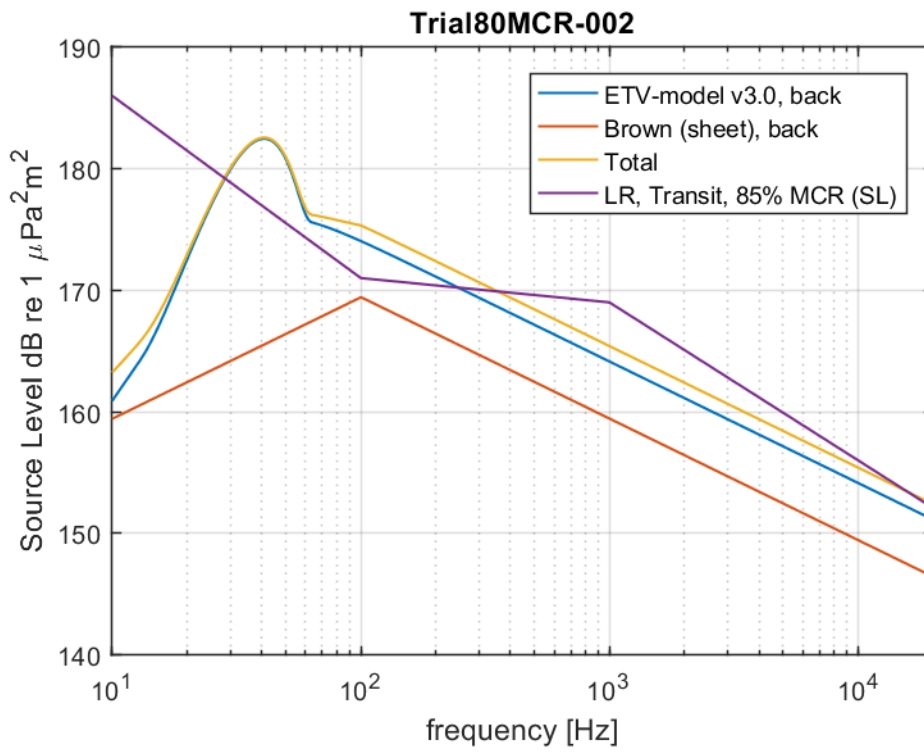


Figure 4-6: Under water noise level versus frequency (Trial, 80% MCR, 19.68 knots,  $N = 183.6$  RPM,  $P_{0.7}/D = 1.09$ ).

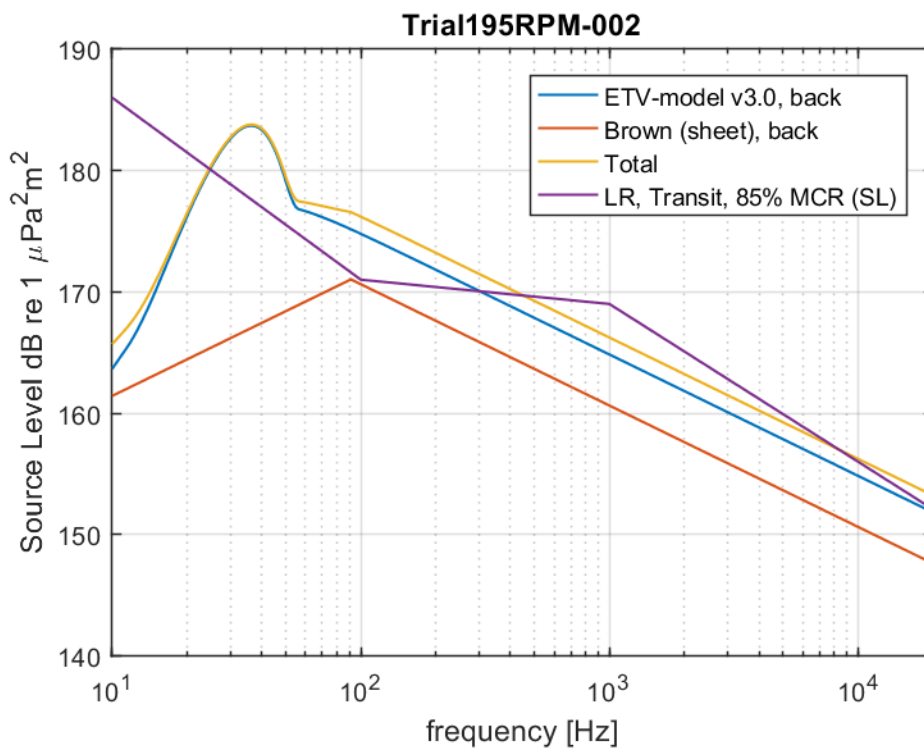


Figure 4-7: Under water noise level versus (trial, 100% MCR, 20.68 knots,  $N = 195.0$  RPM,  $P_{0.7}/D = 1.15$ ).

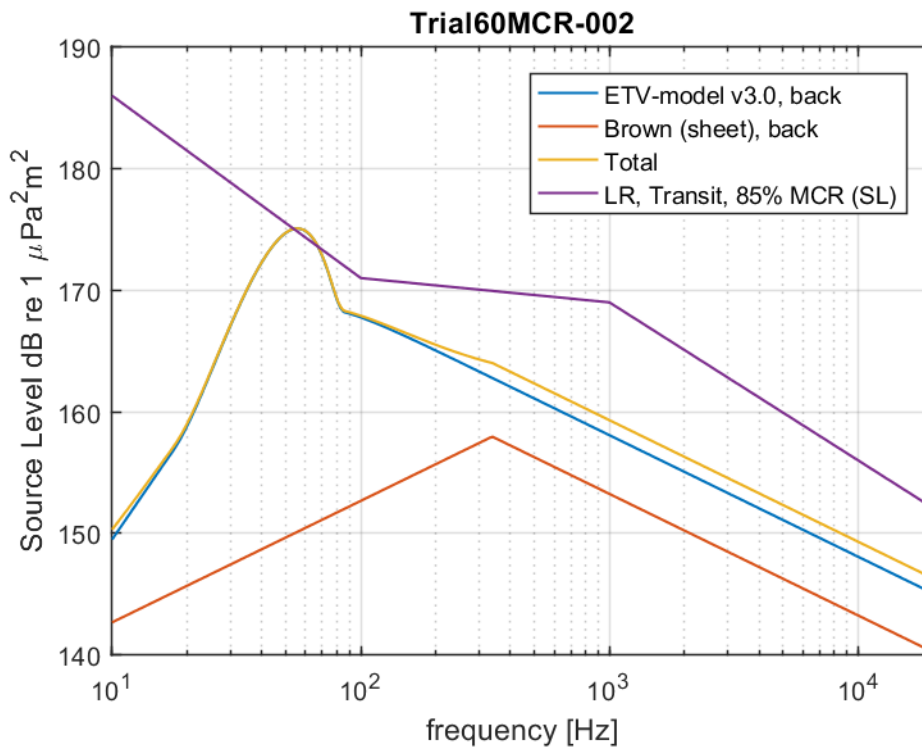


Figure 4-8: Under water noise level versus (trial, 60% MCR, 18.8 knots,  $N = 171.0$  RPM,  $P_{0.7}/D = 1.03$ ).

Main conclusions of the noise calculations are that the calculated underwater noise source levels exceed the LR limits for 80% MCR in the frequency range from about 15 to 400 Hz and that tip vortex cavitation is the dominant source for propellers like this analysed ferry propeller.



## 5 DESIGN OF A REPLACEMENT PROPELLER

A propeller design optimisation was made with the PROPART tool described in Chapter 2. In the first part of the design study the focus has been the possibility of designing a propeller with approximately the same mass, mass moment of inertia and blade spindle torque as the currently installed propeller. It is assumed that this propeller could replace the currently installed propeller in combination with the existing drive train and pitch control mechanism. In the second part of the study the limitations to these requirements are dropped to see if this could provide additional noise reduction. Such a propeller would need to be made of alternatives to conventional stainless steel or bronze to fulfil the original requirements.

In the study a series of optimisation attempts were made to explore the sensitivities of the imposed constraints and design goals on the solution. In this report only the results of the final optimisation runs are presented.

### 5.1 Approach

#### 5.1.1 Goals and constraints

In the design optimisations the following design goals and constraint options are used for the 80% MCR trial condition at operational draught of  $T_F/T_A = 5.5/5.4$  m:

- Maximisation of the in behind propeller efficiency (goal).
- Maximisation of the noise margin with the LR criterion (goal). This objective implies a (positive) distance of the peak noise level at the critical frequency with the criterion.
- Maximisation of the margin against all cavitation types (goal). This means that if the results will show a negative margin that will indicate that some type of cavitation is occurring on the propeller blade.
- Limitation of the volume of the suction side sheet cavitation (constraint). This design goal helps to prevent obtaining propellers with very large amounts of sheet cavitation which is less noisy as tip vortex cavitation.
- Compliance with the cavity planform criterion to prevent potentially erosive types of cavitation (constraint). This constraint is imposed on both the 60% MCR and the 80% MCR conditions, which were also analysed by means of a cavitation prediction by PROCAL during the optimisation runs.
- Propeller blade mass moment of inertia  $I_x$  within 2 per cent of the value of the reference propeller, being  $7374 \text{ kgm}^2$  (constraint).
- Propeller blade mass within 2 per cent of the weight of the blades of the reference propeller, being 3072 kg (constraint).
- Compliance with the LR ice class rules 1D (assumed light ice class 2 according to the propeller drawing). These rules include requirements for the maximum profile thickness (8% addition to the thickness without ice strengthening) and a requirement for the blade edge thickness (thickness at 1.25t from the leading edge not less than 50% of the tip thickness). As a side note it is remarked that according to MARIN calculation and the assumed properties of the construction material the currently installed propeller does not meet the 1D ice class requirements. For example the required maximum profile thickness at section 0.6R is 76.1 mm while the actual thickness is 74.4 mm.
- The torque around the spindle axis of the blades should be similar to the value computed for the installed propeller. Notice that the spindle torque is an important property that determines if the blade design is suitable for the pitch control system of the ship.

During the optimisation process propeller design candidates are generated from the parametric design space. The results for these propellers are analysed with respect to the imposed goals and constraints.

Designs that violate the constraints are considered not feasible and are not considered in the genetic optimisation process and become extinct. The best performing candidates are selected that maximise or minimise the desired goal (e.g. efficiency). These candidates are used by the optimisation algorithm to converge towards the best possible candidates in the provided design space.

## 5.2 Unconstrained propeller design

In this section the results are presented of the optimisation study for the propeller in which the most important constraints regarding similarity with the currently installed propeller are dropped. These are:

- The mass and mass moment of inertia is allowed to deviate significantly from the blades of the installed propeller. This means that the thickness of the blade can be much larger if this is advantageous for the reduction of cavitation noise.
- More variation is allowed at the blade foot connection, meaning that the design of the profile sections near the blade root can be designed with much more variation of the profile shape (thickness and camber) and the pitch at which the blade root is intersecting the blade foot disc.

In Figure 5-1 two plots show the three optimisation goals; efficiency, noise margin and the margin against cavitation inception, being for all types of cavitation. Together with the individuals up to the final 150<sup>th</sup> generation also the values for the installed propeller are shown indicated by the red arrows. Notice that for this reference propeller the efficiency (behind ship) is 0.693 while the noise margin is close to -5.5 dB indicating that the noise level exceeds the LR criterion. Notice also that the computed cavitation margin is around -500% in terms of CPN. It is noted that these large negative margins could be due to very large suction peaks calculated by PROCAL at the leading edge of the blade which could be less realistic. Both plots show contours of a Pareto front of optimum designs. It is noted that a reduction of the noise level is mainly caused by the reduction of tip vortex cavitation and the unloading of the blade tip. This has also an efficiency penalty as is confirmed by the left plot. The same is more or less the case for the (total) margin against cavitation which also includes the suction side tip vortex. The margin is always negative indicating that it is not possible to get a cavitation-free propeller.

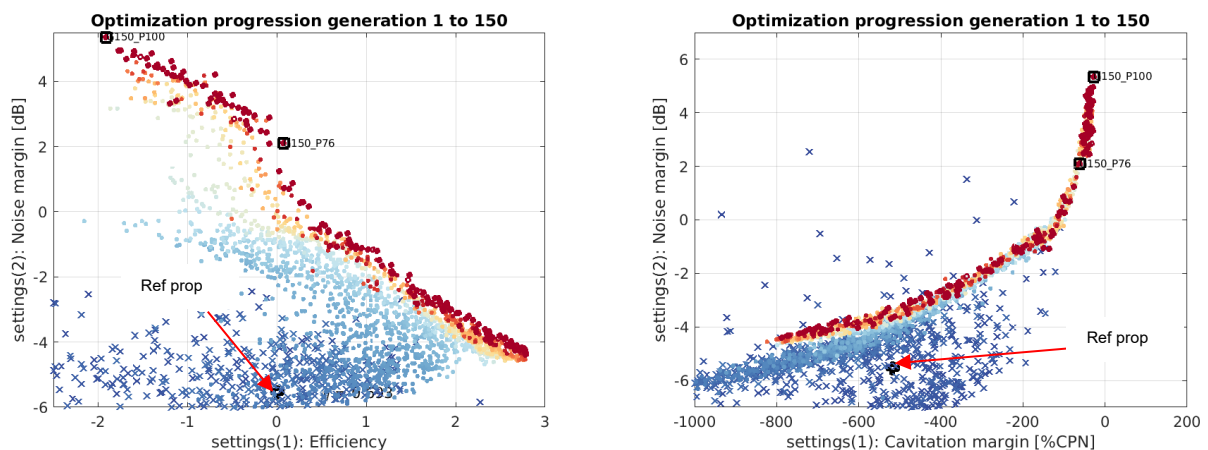


Figure 5-1: Unconstrained design: Pareto front plots showing the optimum range of propeller with regard to the optimisation goals in comparison with the reference propeller (80% MCR).

From the obtained last generation (#150) two candidate propellers (#76 and #100) have been selected from the Pareto fronts. Propeller #76 has the same efficiency as the reference propeller but has a positive noise margin implying that the propeller meets the LR noise source level criterion for this sailing condition. The noise margin with the LR criterion is about 2 dB hence an improvement by 7dB. Depending on the allowed efficiency penalty a further reduction of the peak noise level is possible. Propeller #100 shows the largest gain in the peak noise level with a noise margin of about 5 dB. This

improvement comes at the expense of a 2 per cent reduction of the propeller efficiency. Note that in Section 5.4.2 the noise spectra are further compared with that of the reference propeller.

The right plot of Figure 5-1 shows that a reduction of the peak noise level correlates to a reduction of the cavitation margin but an asymptotic behaviour is seen near propeller #100. As was expected, it is apparently not possible to arrive at a cavitation free propeller.

The following provides details about the mass and mass moment of the blades and its percentage increase with respect to the blades of the reference propeller:

- Propeller #76 has a blade mass of approximately 3581.9 kg (+16.6%) and a mass moment of inertia  $I_x$  of 8752.8  $\text{kgm}^2$  (+18.7%), including the contribution of the entrained water.
- Propeller #100 has a blade mass of 4073.5 kg (+30.8%) and a mass moment of inertia  $I_x$  of 9645.1  $\text{kgm}^2$  (+30.8%).

Comparisons of the geometry parameters of the selected candidate propellers are made in Figure 5-2 and pages F3 and F4. Noticeable differences are:

- The width of the blade is considerably larger for the selected design variants than for the reference propeller as seen by the significant increase of the chord length.
- The thickness of the blades of the selected propellers has increased compared to the reference propeller.
- The pitch distribution of the selected candidate designs shows a significant reduction of the pitch near the tip. Together with a reduced camber this reduces the tip load strength of the tip vortex.
- While the total skew angle is not high (around 25 degrees for both propellers) in comparison with 15 degrees skew for the reference propeller, the leading edge of the selected propellers has much more skew due to the larger variation of the chord length in radial direction. The high leading edge skew causes a more gradual variation of the load and pressure peaks when the blades pass the wake peak of the ship. Given the dominance of tip vortex cavitation on the noise level it is thought that the circulation distribution near the tip is also positively influenced by this feature.

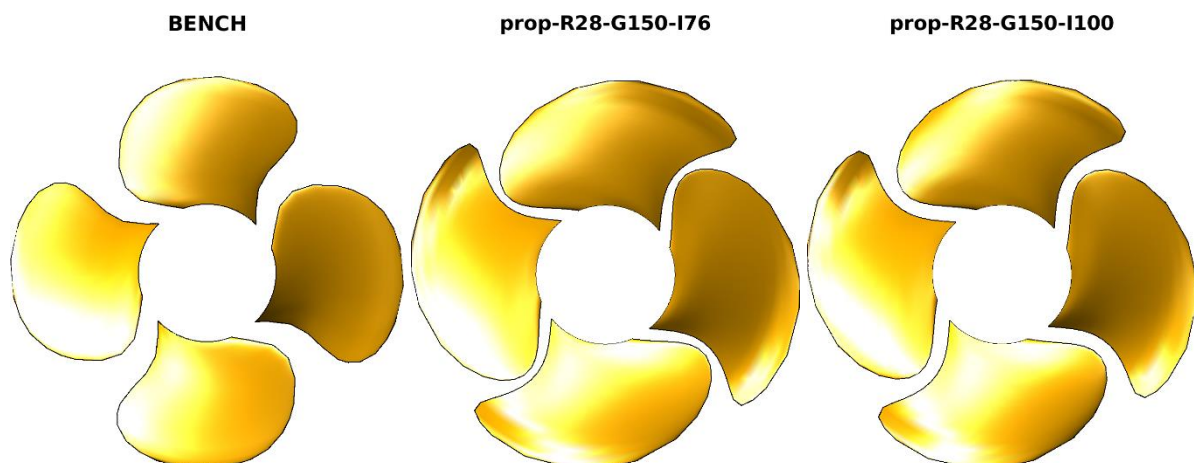


Figure 5-2: Unconstrained propeller: blade shape of reference propeller and selected propellers #76 and #100.

### 5.3 Constrained design

In this section the design is presented of a replacement propeller with mass and inertia properties similar to the currently installed propeller. In the PROPART optimisation the variation of the values of these properties are restricted to a range of 2% around the values of the installed propeller. The other goals and constraints have been taken identical to the unconstrained case.

In Figure 5-3 the Pareto fronts are shown that have been obtained after 150 generations of the optimisation algorithm. The plots show the relation between the three optimisation goals; efficiency, noise margin and the margin against cavitation inception. Three design candidates (#115, #174 and #188) from the final 150<sup>th</sup> generation are shown illustrating the choices that can be made regarding the desired propeller characteristics. Propeller # 188 has an efficiency that is equal to that of the reference propeller (also indicated in the plots), but still with a negative noise margin of about 1.5 dB. This propeller therefore does not satisfy the LR noise criterion. Candidate #115 is the best performing propeller that was found during the optimisation with a noise margin that is just positive. The penalty to efficiency for reaching the approximate 1.5 dB noise margin increase, needed to satisfy the LR noise criterion is, 1.5%. A further candidate (#174) is included to illustrate that both efficiency as well as noise can be improved as can be concluded from the Pareto front. Note again that in Section 5.4.2 the noise source level spectra are further compared with that of the reference propeller.

It is noted again that the reduction of the noise level is mainly caused by the reduction of tip vortex cavitation and the unloading of the blade tip mostly at the expense of efficiency. The same is more or less the case for the margin against cavitation which also includes the suction side tip vortex.

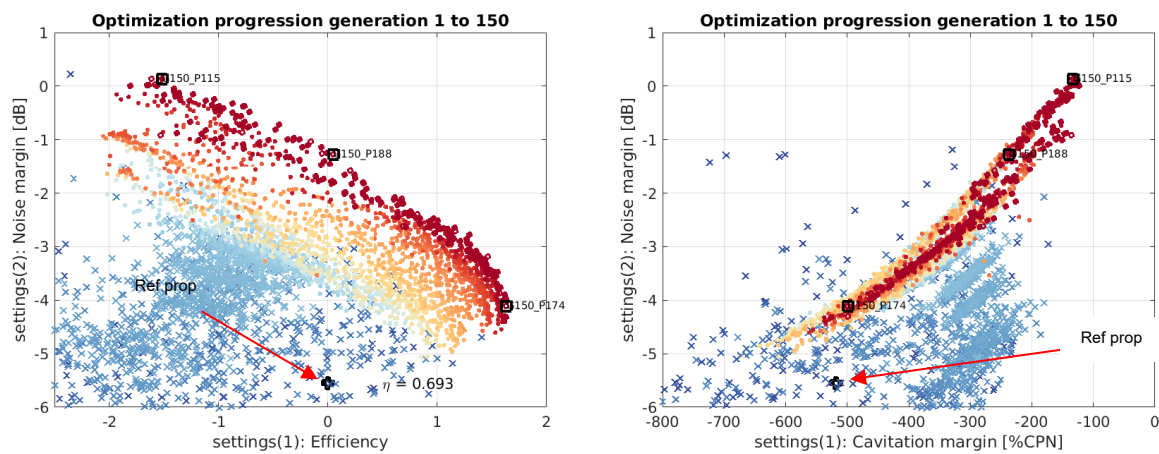


Figure 5-3: Constrained design: Pareto front plots showing the optimum range of propeller with regard to the optimisation goals in comparison with the reference propeller (80% MCR).

Comparisons of the geometry parameters between the selected candidate propellers are made in Figure 5-4 and pages F5 and F6. Noticeable differences are:

- The radial distribution of the pitch and the maximum camber of the selected candidate designs is significantly different than that of the reference propeller. The trends are similar to that of the unconstrained design with a significant reduction of the pitch near the tip. Together with a reduced camber this reduces the tip load strength of the tip vortex.
- Chord length distribution and skew are very comparable with the reference propeller. The skew of the leading edge in the tip region is also quite similar to that of the reference propeller.
- The thickness distribution is also quite similar due to the mass constraint and it is not very particular.

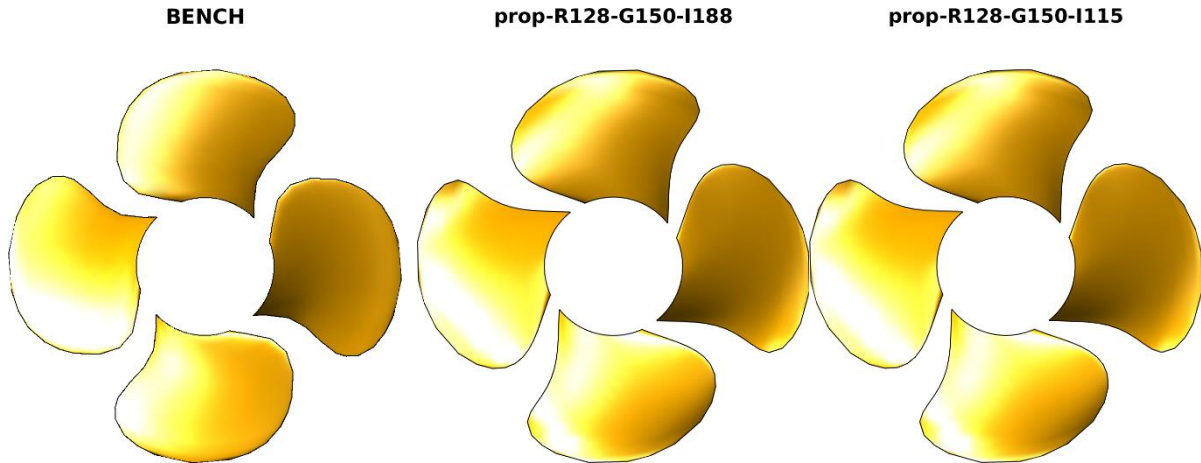


Figure 5-4: Unconstrained propeller: blade shape of reference propeller and selected propellers #115 and #188.

#### 5.4 Developed cavitation and noise source level predictions

In the next sections a comparison is made of the cavitation patterns and noise levels predicted for the selected constrained and unconstrained candidate designs. The results are presented for the most relevant 80% and 60% MCR trial conditions.

##### 5.4.1 Developed cavitation

In Figure 5-5 and Figure 5-6 the suction side cavitation patterns computed for the 80% MCR trial condition are presented for unconstrained propeller designs #76 and #100. It can be observed that for variant #76 near the tip, sheet cavitation is present for the entire revolution of the propeller. Design candidate #100 has much less sheet cavitation. For both propellers some traces of cavitation is seen in the blade root area, which appears hard to avoid for this propeller.

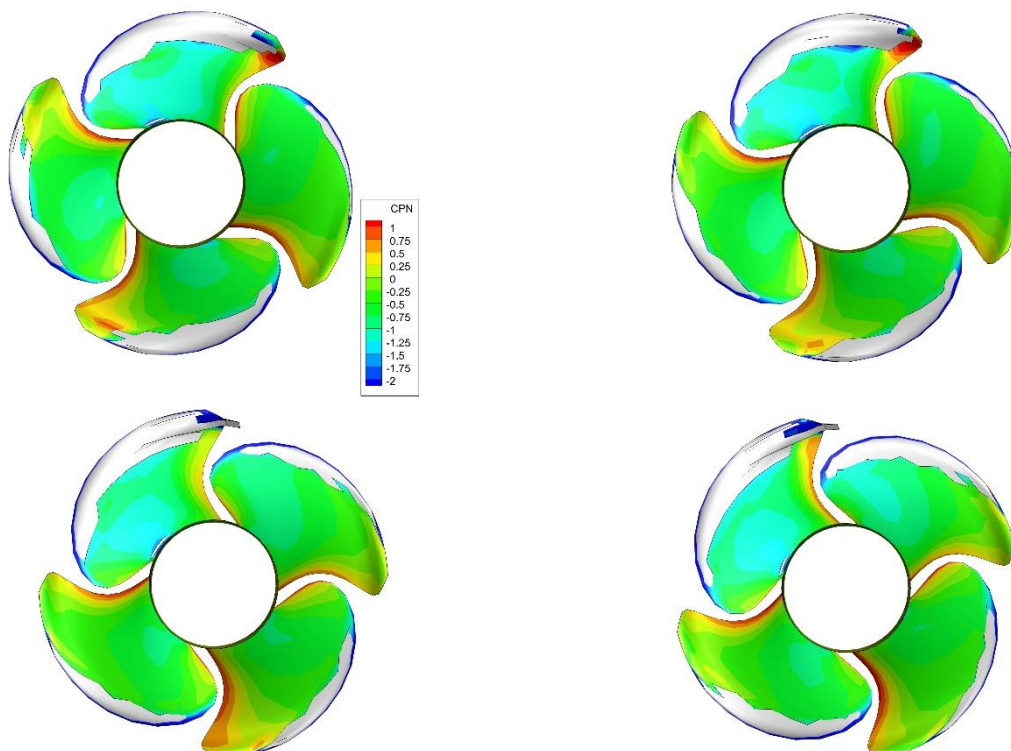


Figure 5-5: Predicted suction side sheet cavitation patterns and pressure distribution ( $C_{PN}$ ) (Unconstrained design variant #76, 80% MCR).

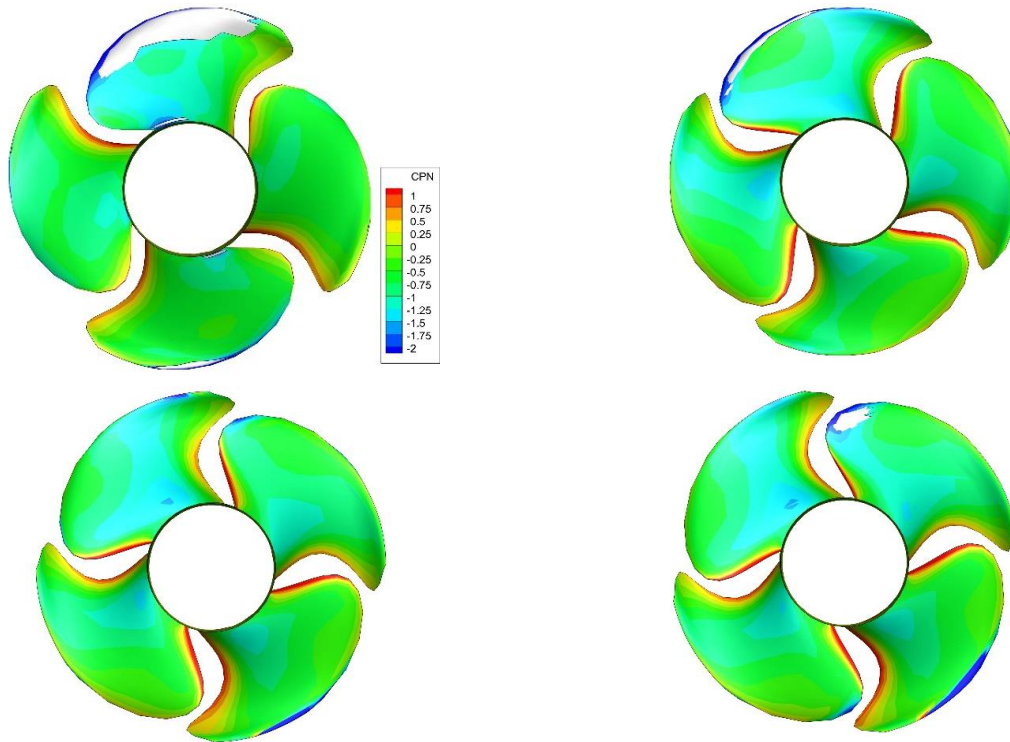


Figure 5-6: Predicted suction side sheet cavitation patterns and pressure distribution ( $C_{PN}$ ) (Unconstrained design variant 100, 80% MCR).

For the constrained propeller case the same results are shown in Figure 5-9 and Figure 5-7 for propeller design candidates #115 (largest peak noise reduction) and #188 (largest peak noise reduction for the same efficiency as the reference propeller). It can be observed that both design candidates show a fair amount of sheet cavitation at the suction side of the blade with slightly less cavitation seen for candidate #115. Also again some traces of cavitation is seen in the blade root area.

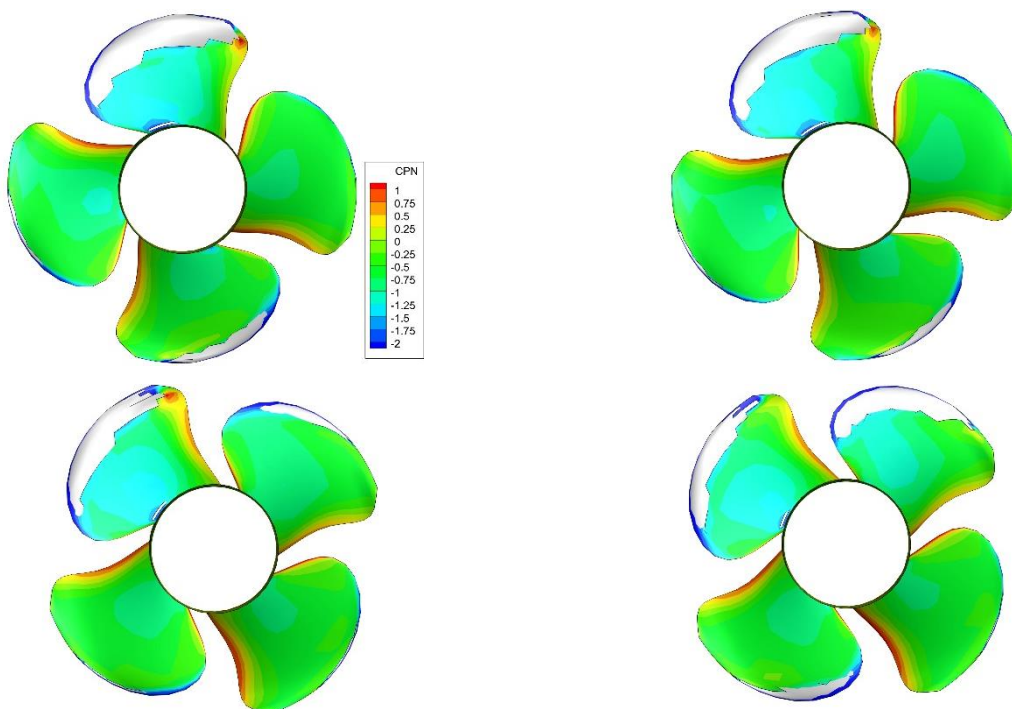


Figure 5-7: Predicted suction side sheet cavitation patterns and pressure distribution ( $C_{PN}$ ) (Constrained design variant #188, 80% MCR).

In Figure 5-8 the pressure side cavitation predictions for the 60% MCR trial condition is shown for both design candidates. Some pressure side sheet cavitation is predicted. The sheet cavitation and the dynamics are considered acceptable with regard to cavitation erosion.

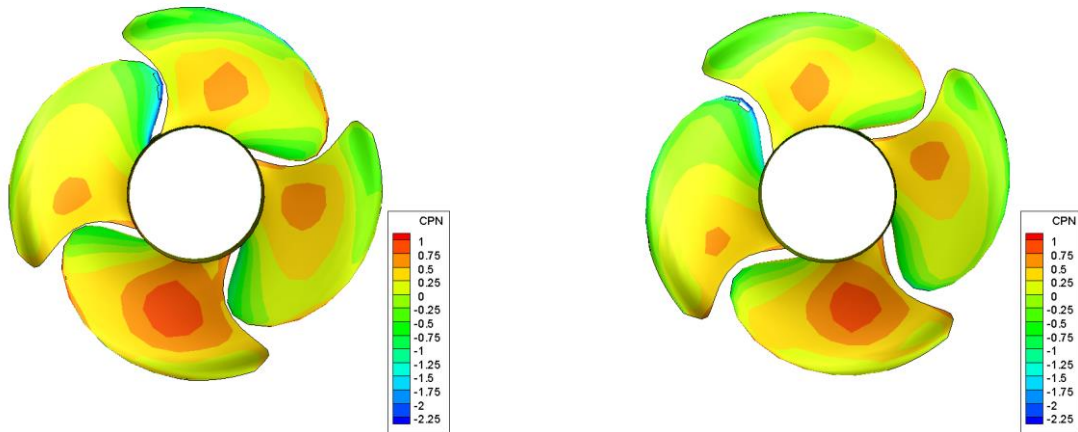


Figure 5-8: Comparison of pressure side sheet cavitation patterns and pressure distribution ( $C_{PN}$ ) for unconstrained design variants #76 (left) and 100 (right), 60% MCR).

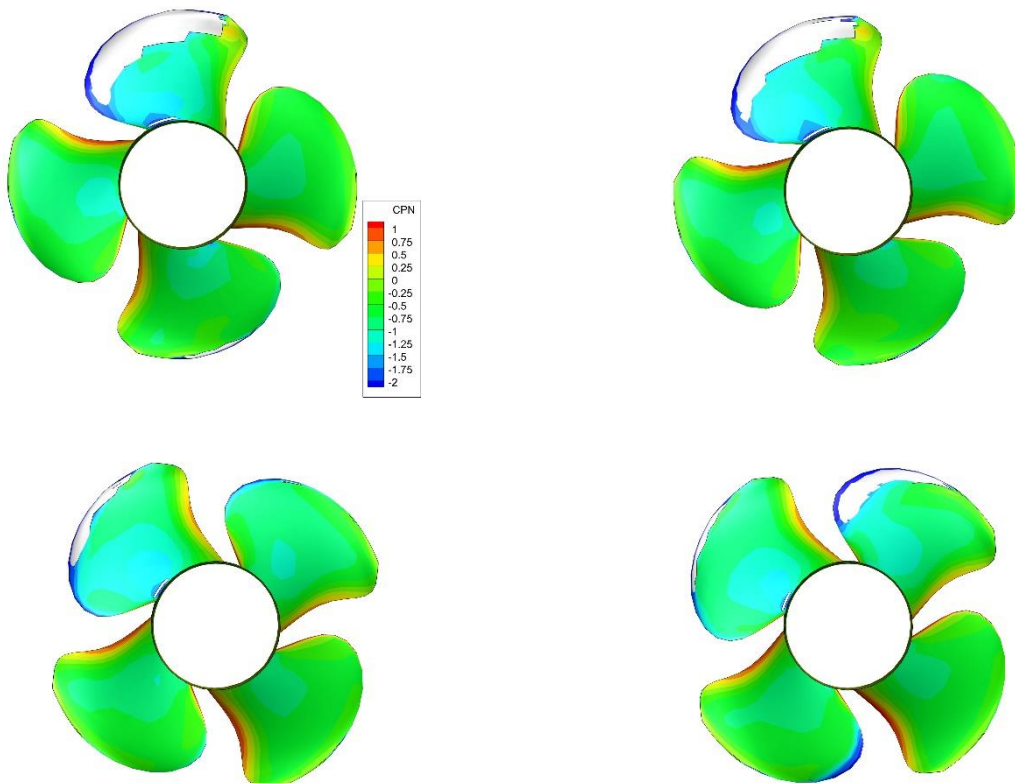


Figure 5-9: Predicted suction side sheet cavitation patterns and pressure distribution ( $C_{PN}$ ) (Constrained design variant #115, 80% MCR).

In Figure 5-10 the pressure side cavitation predictions for the 60% MCR trial condition is shown for both design candidates. Again some pressure side sheet cavitation is predicted. Also for the constrained design the sheet cavitation patterns and their dynamics are considered acceptable with regard to cavitation erosion.

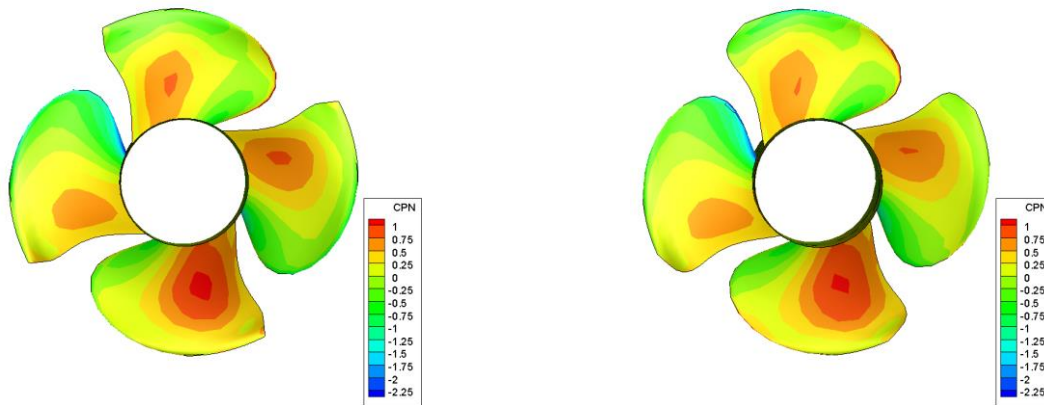


Figure 5-10: Comparison of pressure side sheet cavitation patterns and pressure distribution ( $C_{pN}$ ) for Constrained design variants #115 (left) and #188 (right), 60% MCR).

#### 5.4.2 Comparison of underwater noise source levels

Predictions of the underwater noise levels have been made for the three operational conditions based on the above presented sheet cavitation predictions and the tip vortex prediction of the ETV model. On pages F7 through F10 the computed noise source level spectra of the selected propeller design candidates are compared with the spectrum of the reference propeller. The best performing propellers are compared with the reference propeller in Figure 5-11 and Figure 5-12. Shown are the contributions of the different cavitation forms, the total source level and the reference source level of merchant ships sailing in transit at 85% power as determined by LR.

From the plots it can be concluded that:

- Unconstrained propeller design candidates #76 and #100 are able to meet the LR SL criterion in all computed conditions with variant #100 slightly better than variant #76. For propeller variant #100 peak levels are dropping from about 182.6 dB at 41 Hz for the reference propeller to 165.2 dB at 162 Hz corresponding to a very large reduction of the maximum noise level by 17.5 dB. The main remaining contributor for this variant is the suction side sheet cavitation.
- Unconstrained variant #76, which has an efficiency equal to the reference propeller, shows the peak noise level dropping to 168.8 dB at 114 Hz (-13.8 dB compared to the reference propeller) with a larger contribution of the tip vortex to the underwater noise source level than propeller #100.
- For both unconstrained designs the applied noise model predicts a reduction of the noise source levels with respect to the reference propeller.
- For the constrained propeller designs smaller noise reductions are predicted with a reduction of 11.6 dB (to a peak value of 171 dB at 93 Hz) for propeller #115 and 7.6 dB for propeller #188 (to a peak value of 175 dB at 65 Hz). Propeller candidate # 115 just meets the LR criterion with this reduction while # 188 does not.
- The noise levels for the 60% MCR condition are also reduced for both constrained variants.
- The comparisons show that the additional volume of the unconstrained propeller design leads to the ability to reduce the peak noise levels with another 6 dB over the already 11.6 dB reduction of the constrained design. With a value of 0.5%, the difference in the efficiency between the best performing unconstrained and constrained propeller is rather small.



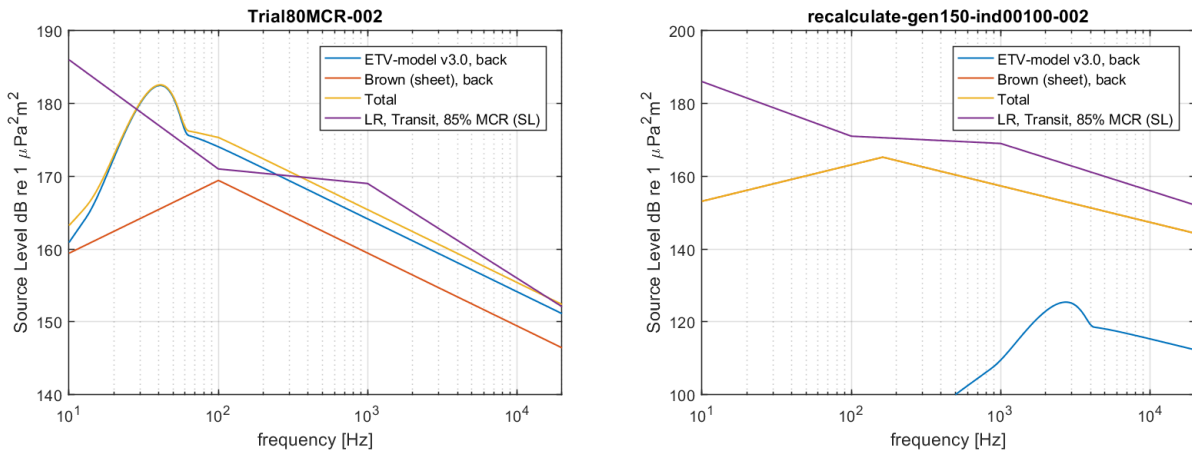


Figure 5-11: Comparison of underwater noise level spectrum for the reference propeller (left) and the best performing unconstrained propeller variant #100 (right) at 80% MCR trial condition.

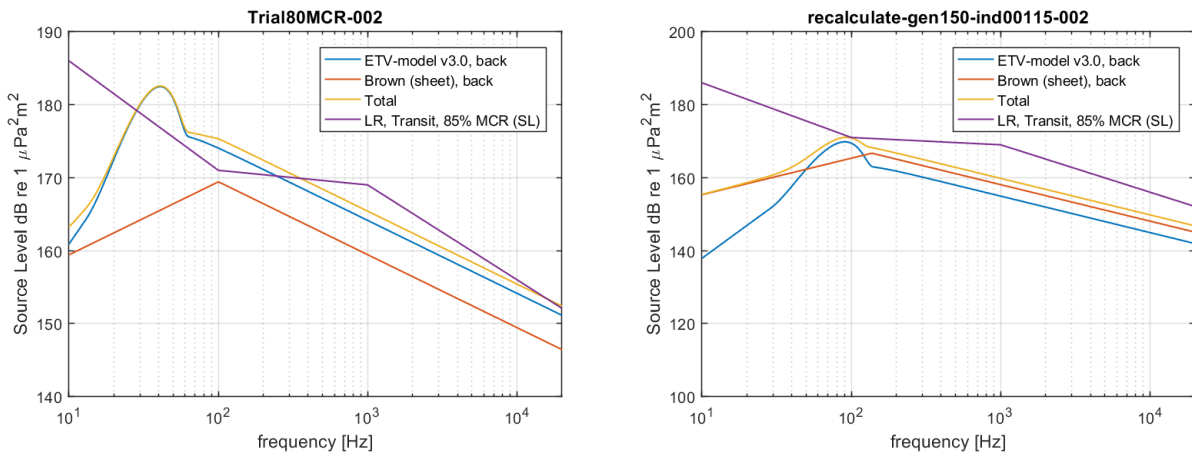


Figure 5-12: Comparison of underwater noise level spectrum for the reference propeller (left) and the best performing constrained propeller variant #115 (right) at 80% MCR trial condition.

## 6 CONCLUSIONS AND RECOMMENDATIONS

The following conclusions summarise the findings of the present project:

- Results from onboard speed-power measurements on a double-ended ferry have been compared with speed-power predictions made with the Holtrop-Mennen method. The results show that the measurements compare best with the predictions made for the ship for the same operational draught of  $T_F/T_A = 5.5 / 5.4$  m sailing in ideal trial conditions implying unrestricted deep water of  $15.0^\circ$  C and a mass density of  $1025.9 \text{ kg/m}^3$ , a clean hull and propeller blades and no effects of wind and waves.
- Based on the predictions and trial data three conditions were selected for the propeller design study for the controllable pitch propellers of the ferry class. These are the conditions where the propeller absorbs 60%, 80% and 100% of the available MCR engine power. In these conditions the ship is sailing at respectively 18.8, 19.7 and 20.7 kn while the propeller rotation rates are 171, 183.6 and 195 RPM. For each of these conditions the propeller is assumed to be set at the pitch settings following from the provided propeller combinator curves.
- From the analysis of the cavitation inception characteristics of the installed propeller it is concluded that that this propeller cavitates and the cavitation-free range is absent. The cavitation inception bucket is very narrow caused by the deep wake peak of the wake field of the ship. The provided operational data and the combinator diagram also show that the pitch of the controllable pitch propeller is reduced considerably causing the propeller blades to operate outside the cavitation-free range. Designing a replacement propeller that is free of cavitation was therefore determined infeasible. The focus in the propeller design study therefore shifted to the reduction of underwater noise due to propeller cavitation.
- Cavitation predictions have been made with propeller analysis code PROCAL showing that for the 80% and 100% MCR operating conditions a fair amount of sheet cavitation is present on the reference propeller blades. The Empirical Tip Vortex (ETV) model also predicts the presence of a cavitating tip vortex at the suction side of the blades in these conditions.
- Calculations for the 60% MCR operating condition show a small amount of sheet cavitation and the absence of pressure side cavitation as well as pressure side tip vortex cavitation on the reference propeller.
- Predictions have been made of the underwater noise levels using the sheet cavitation predictions made by PROCAL and the tip vortex cavitation predictions made by the ETV model. The calculations for the currently installed propeller show that for the 80% and 100% MCR operating conditions the underwater noise levels exceed the levels of the LR criterion for underwater radiated noise levels for merchant ships sailing in transit at 85% MCR. At the 60% MCR operating condition the maximum noise level is close to this criterion. In all cases the contribution of suction side tip vortex cavitation appears to give the largest contribution to the underwater noise.
- Propeller design optimisations have been carried out for two design cases. In one case constraints were put on the mass and mass moment of inertia of the propeller blades and in a second these constraints were lifted. The results for both cases show that it is quite feasible to substantially reduce the underwater noise source levels at the higher speed range of the ferry without sacrificing efficiency.
- For the constrained propeller optimisation the results show that it is just possible to meet the LR SL criterion for merchant ships. For a selected propeller design candidate a reduction of 11.6 dB of the peak underwater noise source level is predicted compared to the peak value of the currently installed propeller. This improvement goes at the expense of a 1.5% reduction of the (in behind) efficiency of the propeller.

- For the unconstrained propeller optimisation the results show that an even larger reduction of the peak underwater noise source levels is possible with a maximum of 17.5 dB for a selected propeller design candidate. This goes at the expense of a 2% efficiency loss compared to that of the currently installed propeller.
- The reduction of the cavitation noise is mainly obtained by reducing the amount of tip vortex cavitation. This is achieved by increasing the chord length in the tip area and by reducing the loading of the tip. The analysis for the 60% MCR condition suggests that some minor traces of pressure side sheet cavitation are present but the contribution to the total noise level is low.
- The releasing of the constraint for blade mass and inertia leads to much heavier blades when constructed from bronze or stainless steel. The mass and moment of inertia of the propeller blades are shown to increase by 30% for the propeller design candidate with the largest reduction of the cavitation noise. Increasing the chord length at the tip of the blades helps delaying the inception of tip vortex cavitation while the increased thickness is necessary to maintain appropriate volume, shape and dynamic behaviour of the sheet cavitation to prevent large contribution to the noise or possible erosive cavitation.

It should be clearly noted that the employed semi-empirical prediction method for the noise levels has not yet been validated for the kind of vessel studied here, but was developed using data of twin-screw vessels and model test data of propellers with face side sheet cavitation.

The following recommendations are made based on the findings of the study.

- Further limitations on the allowed efficiency penalties could focus the optimisation exercises in design spaces that provide more acceptable (bronze) replacement propellers. Alternative materials such as fibre reinforced composites could be evaluated as potential construction material for high volume propeller designs that could become prohibitively heavy when constructed from bronze.
- Another direction to reduce the cavitation noise is to improve the quality wake field of the ship. Solutions such as devices as fins or vortex generators should be mentioned as possible means to achieve this.

The above conclusions and suggestions do not supersede the statements made in the previous chapters and in the figures with results.

Wageningen, February 2022  
MARITIME RESEARCH INSTITUTE NETHERLANDS

Ir. G. Gaillarde  
Head Ships Business Unit

## REFERENCES

Brown, N.A. (2007). "Existing/future technology to address radiated noise by modifying vessel propulsion and operating parameters". NOAA Vessel Quieting Symposium.

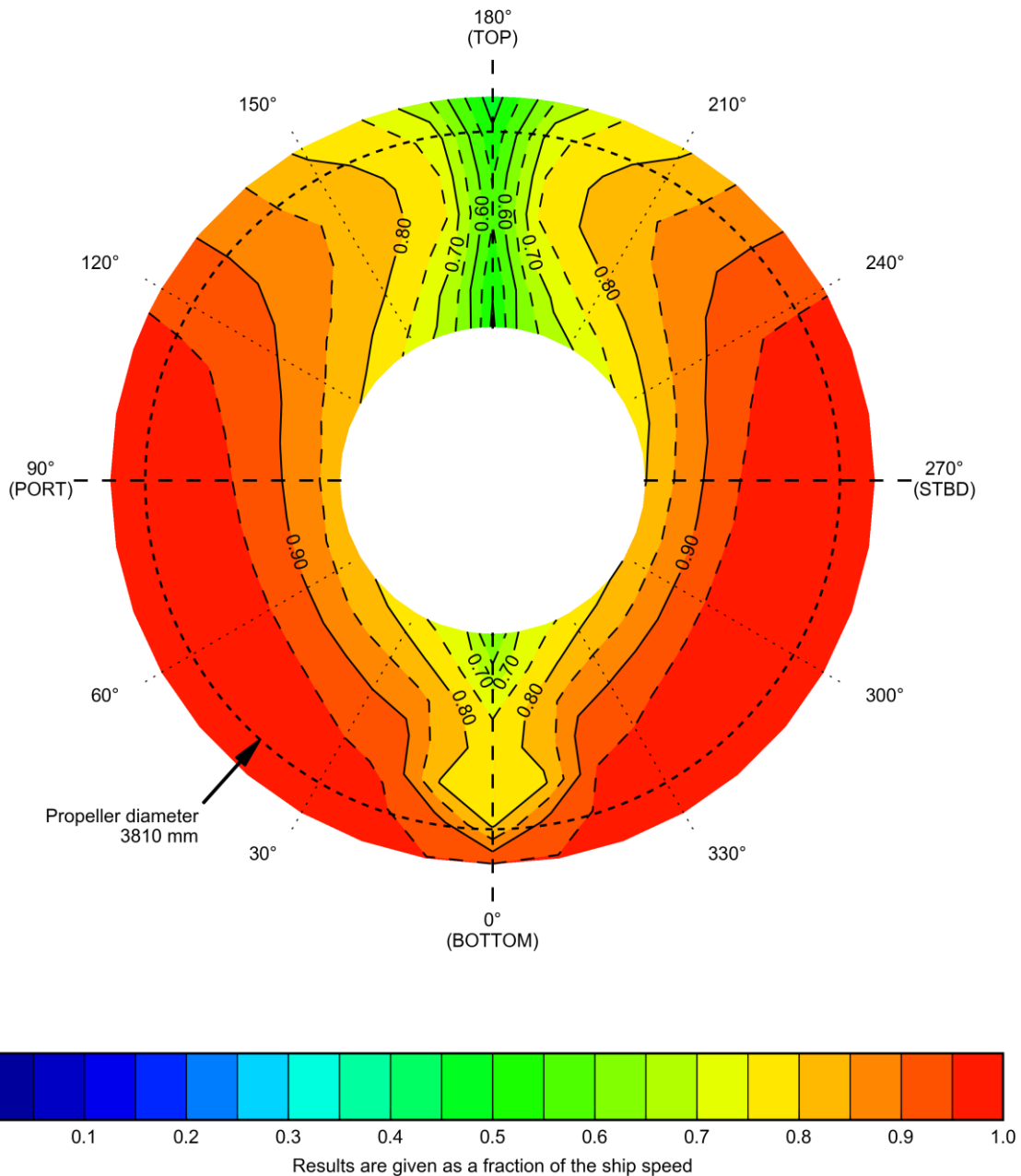
J. Bosschers (2018), "A semi-empirical prediction method for broadband hull pressure fluctuations and underwater radiated noise by propeller tip vortex cavitation", *Journal of Marine Science and Engineering* 6, 49

Hannay, D., MacGillivray, A., Wladichuk, J., Pace, F., Frouin-Mouy, H., (2019), "Comparison of Class Society Quiet Notation maximum noise levels with ECHO program measurements". Transport Canada workshop on "Quieting ships to protect the marine environment", London, UK.

# FIGURES

CALCULATION BY : Lloyd Register  
WATER DEPTH : inf m  
TURB. MODEL : -

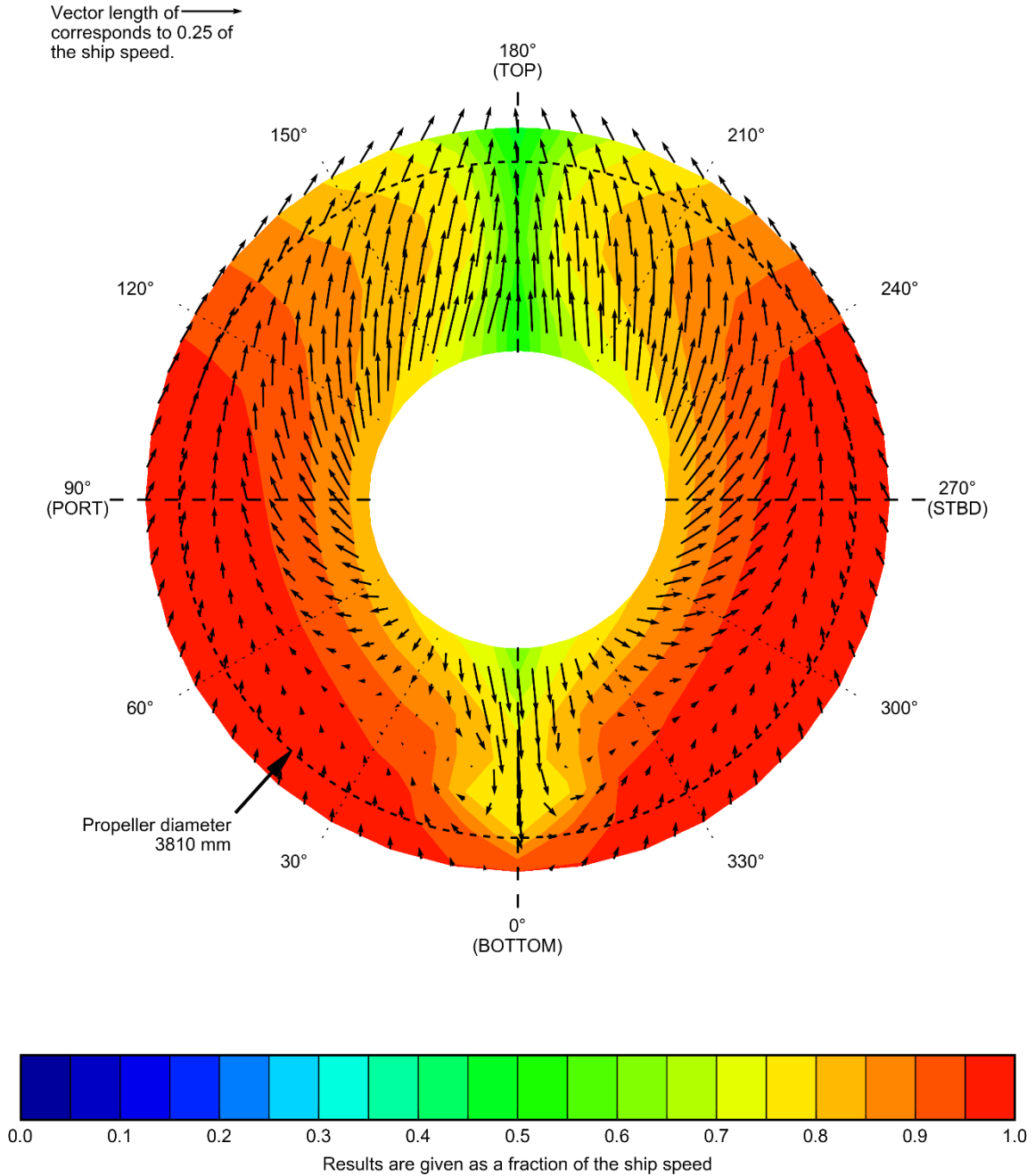
DRAUGHT FP : 5.900 m  
DRAUGHT AP : 5.900 m



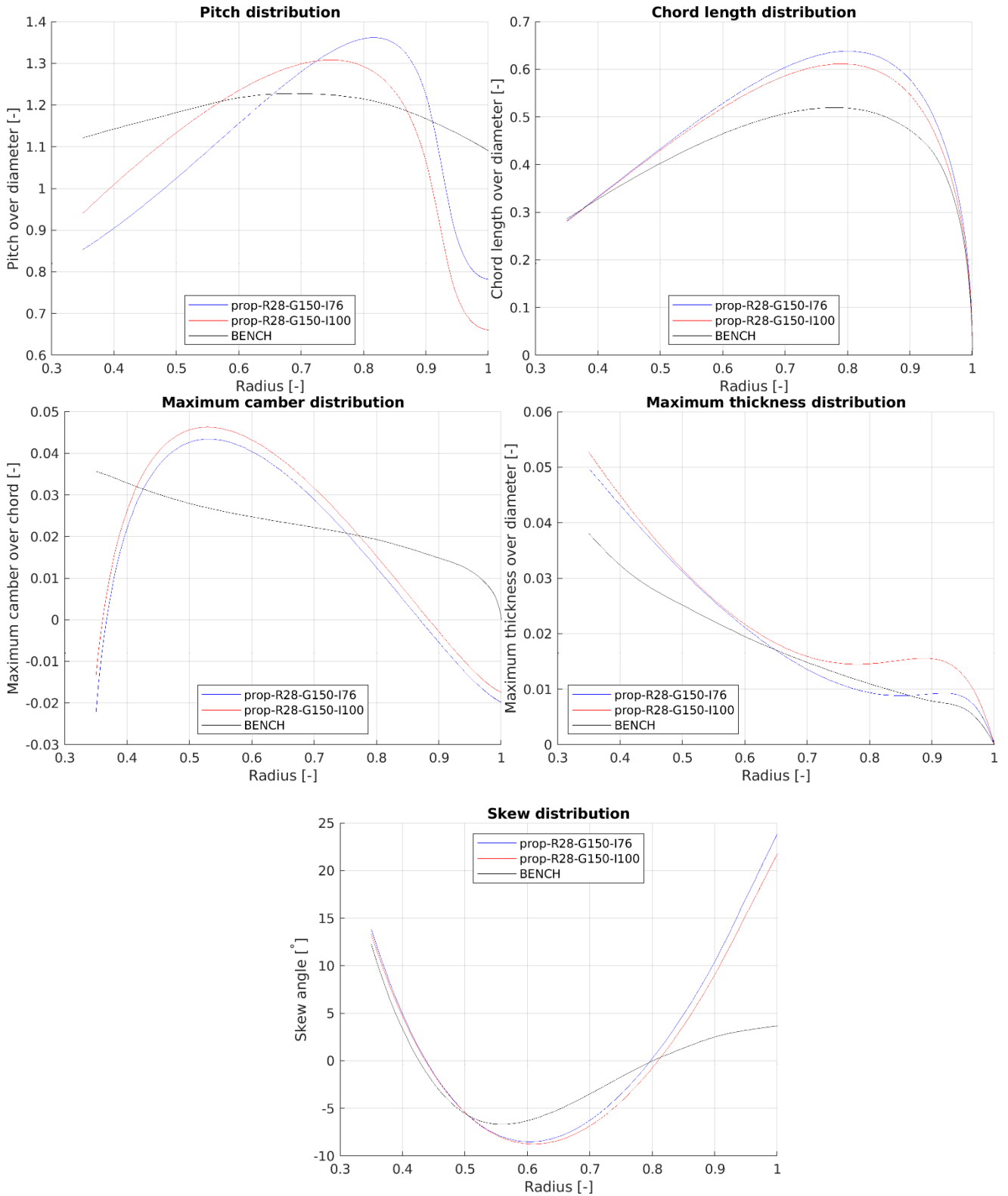
CONTOUR PLOT OF AXIAL VELOCITY COMPONENTS OF COMPUTED EFFECTIVE WAKE FIELD

CALCULATION BY : Lloyd Register  
WATER DEPTH : inf m  
TURB. MODEL : -

DRAUGHT FP : 5.900 m  
DRAUGHT AP : 5.900 m

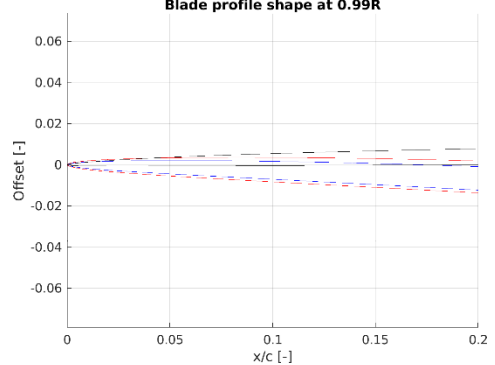
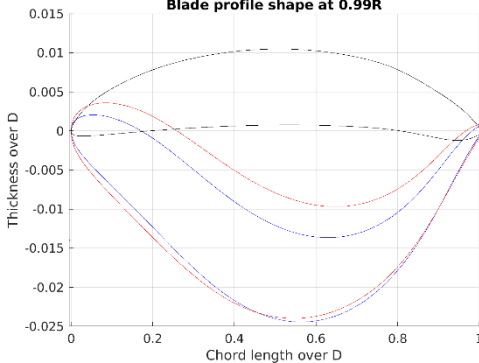
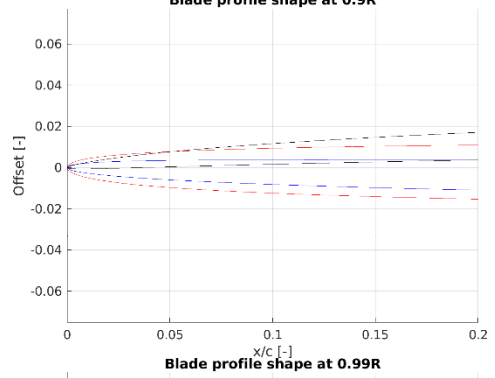
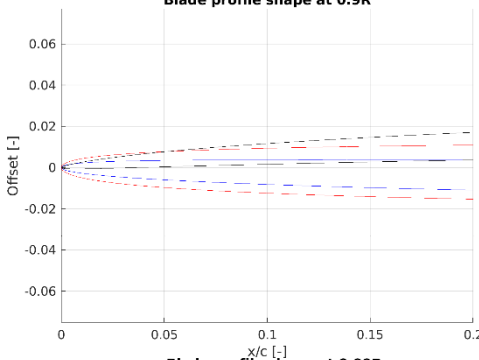
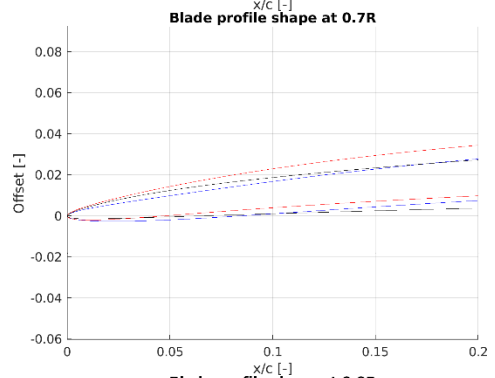
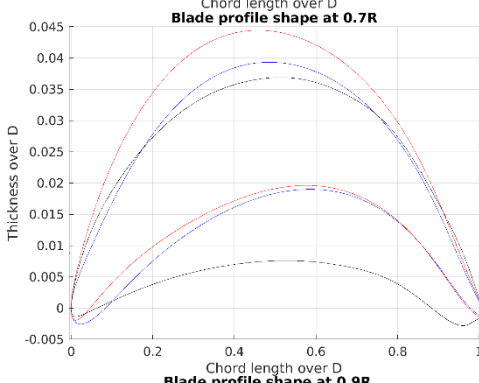
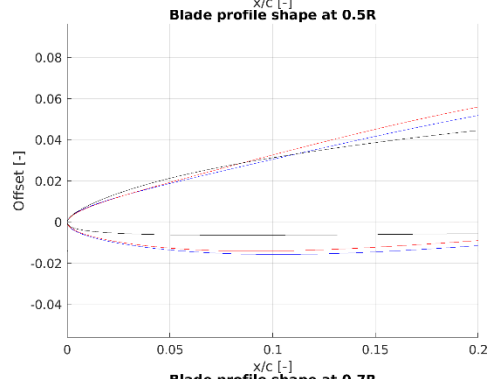
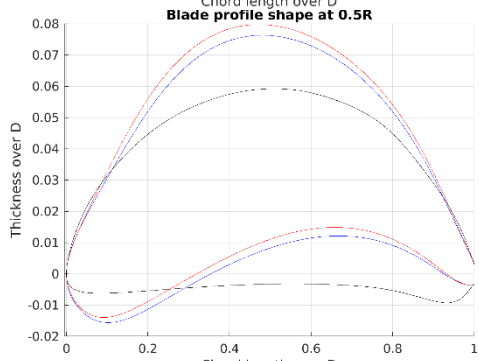
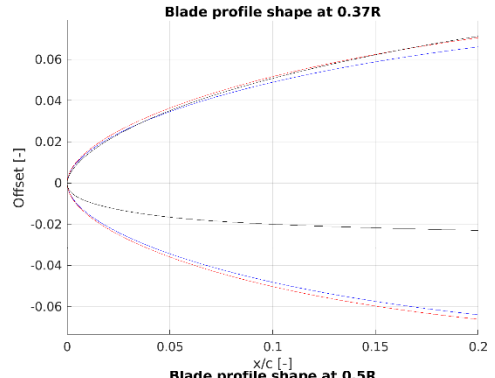
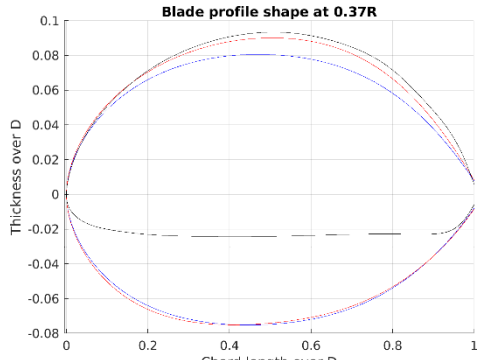


CONTOUR PLOT OF AXIAL VELOCITY COMPONENTS OF COMPUTED EFFECTIVE WAKE FIELD

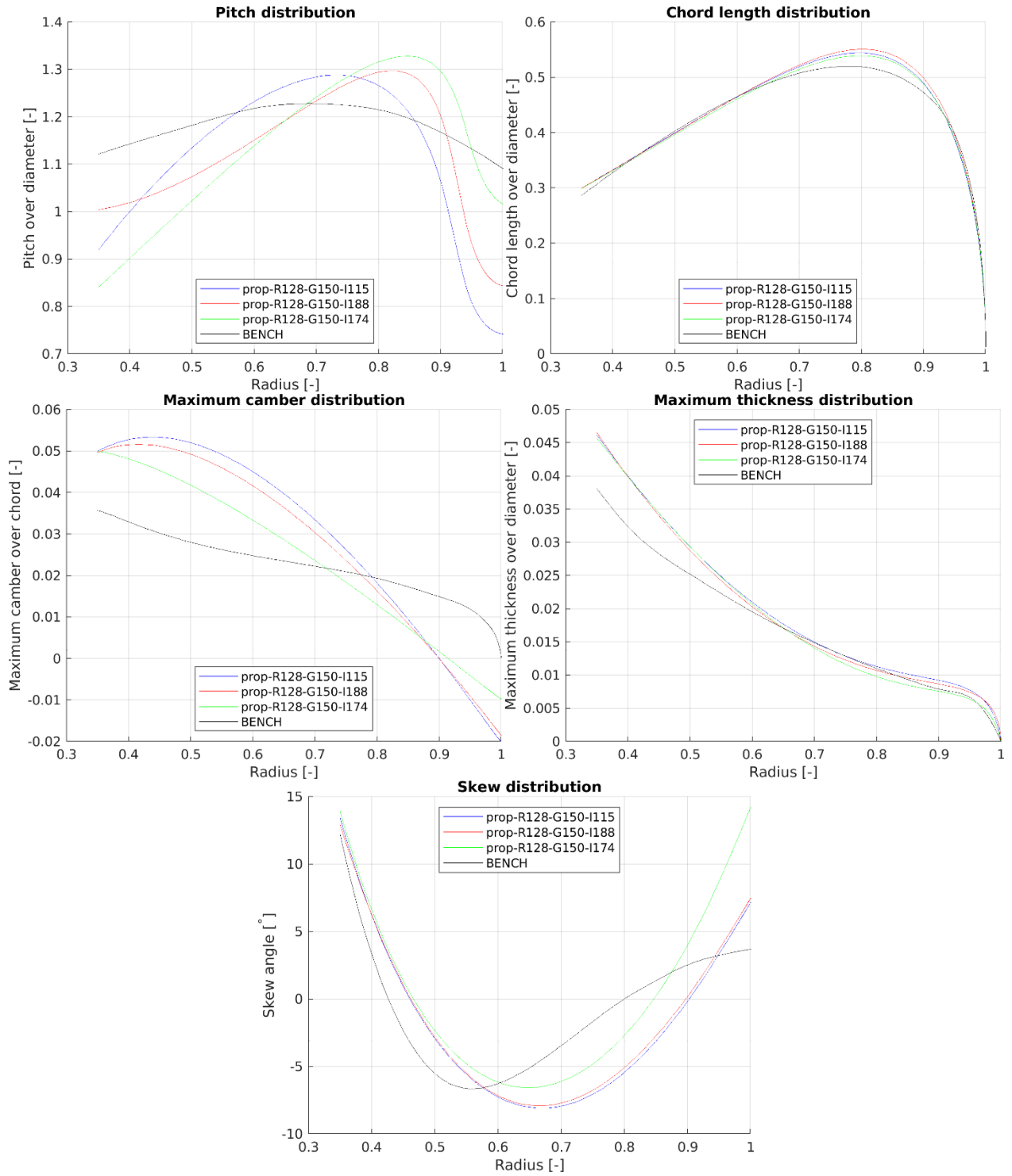


UNCONSTRAINED PROPELLER: RADIAL GEOMETRY PARAMETER DISTRIBUTIONS OF SELECTED OPTIMUM PROPELLER VARIANTS COMPARED TO REFERENCE PROPELLER

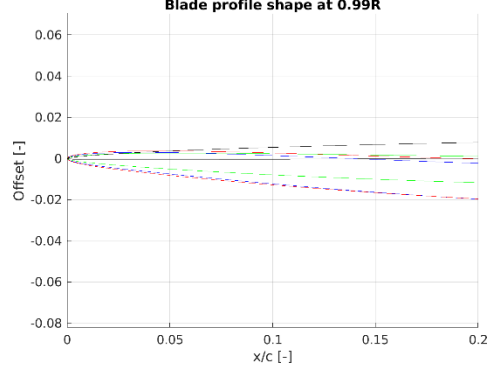
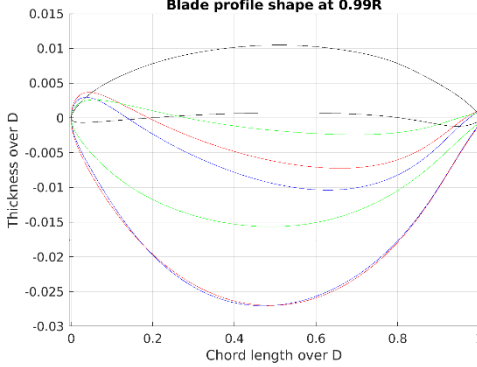
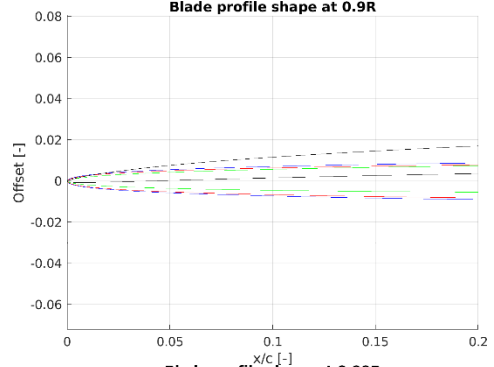
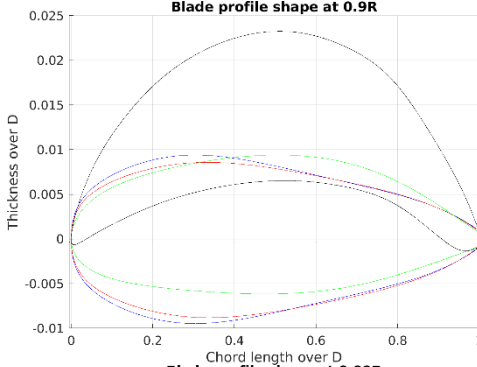
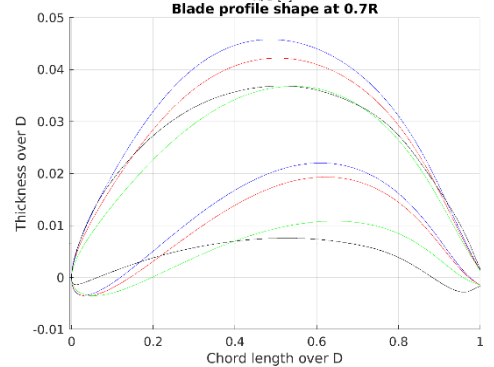
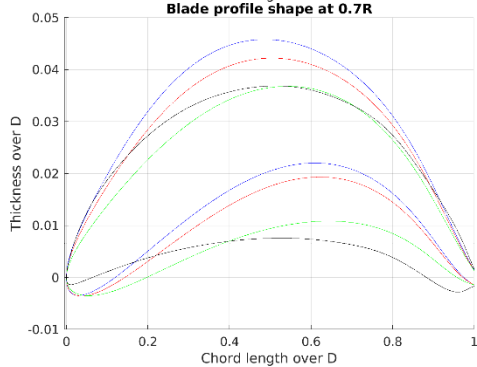
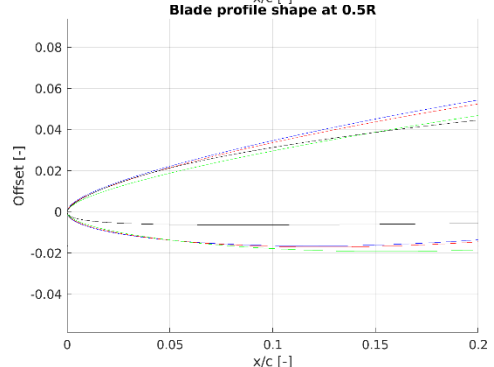
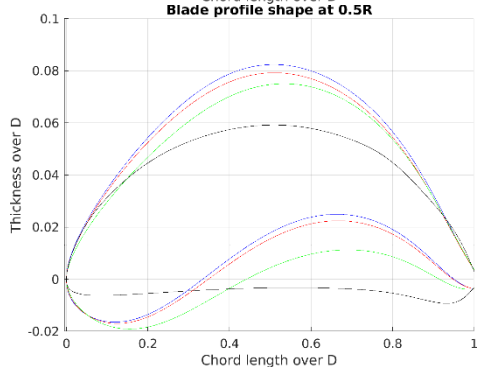
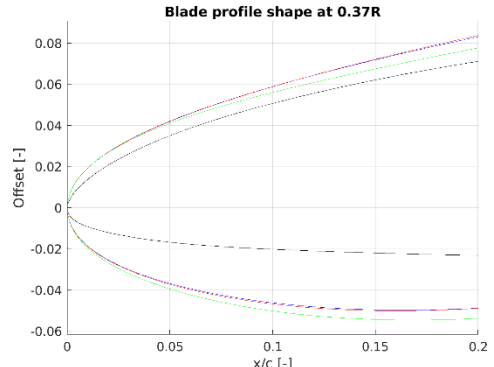
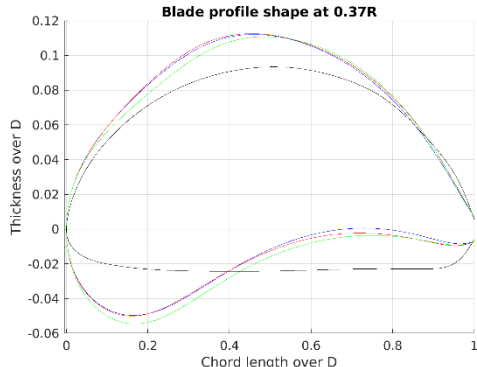




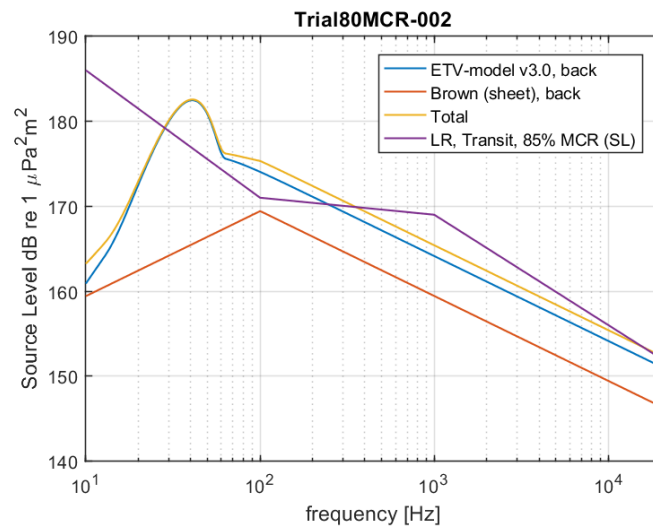
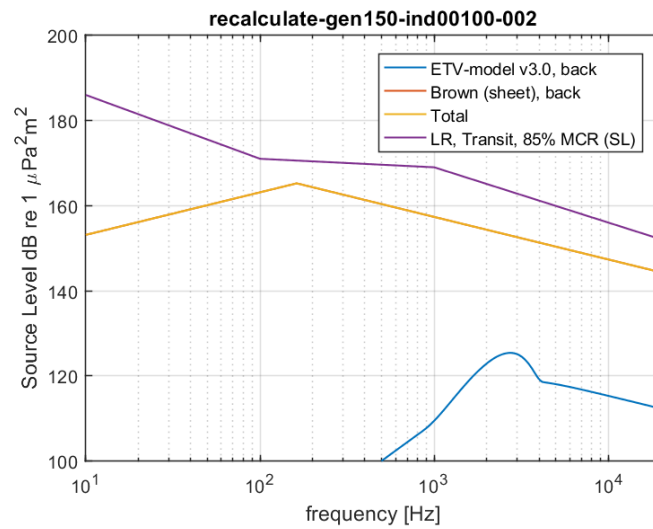
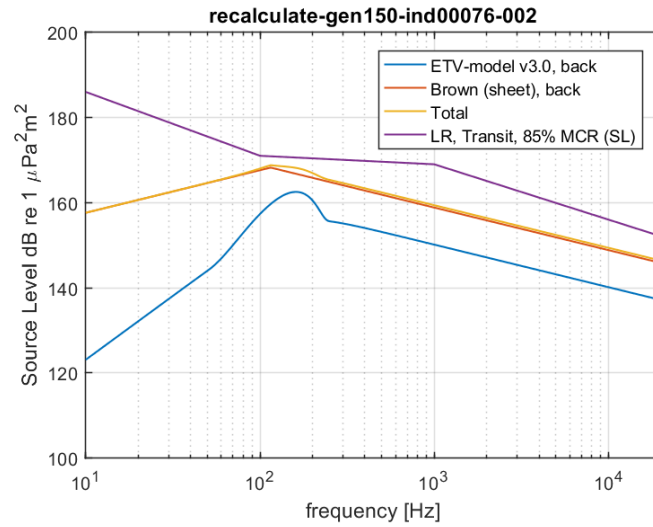
COMPARISON OF SECTIONAL PROFILES (UNCONSTRAINED)



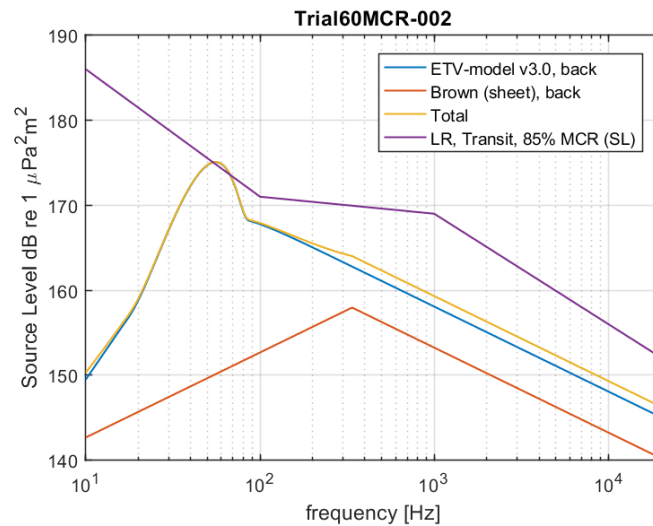
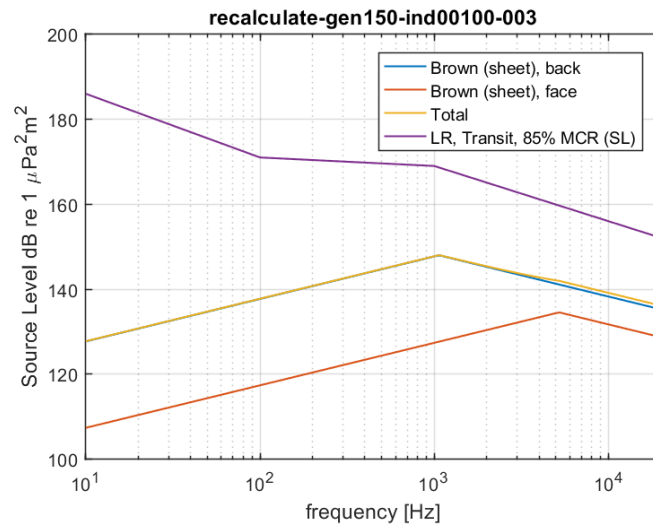
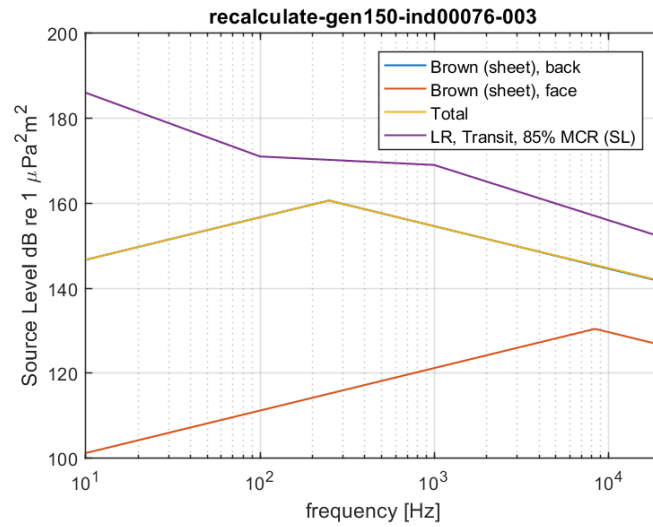
CONSTRAINED PROPELLER: RADIAL GEOMETRY PARAMETER DISTRIBUTIONS OF SELECTED OPTIMUM PROPELLER VARIANTS COMPARED TO REFERENCE PROPELLER



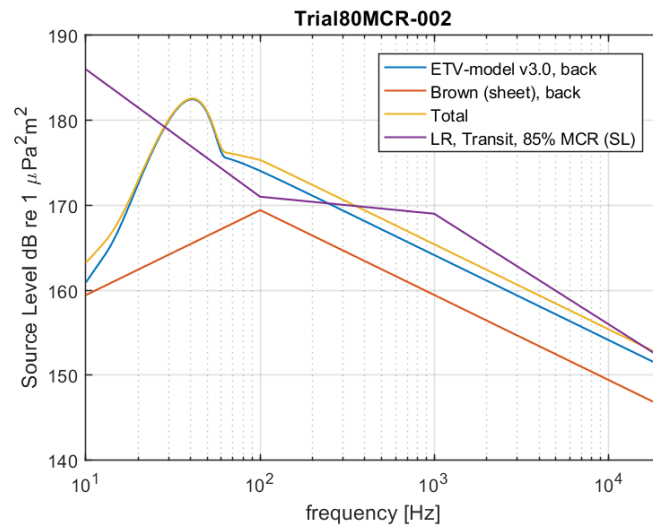
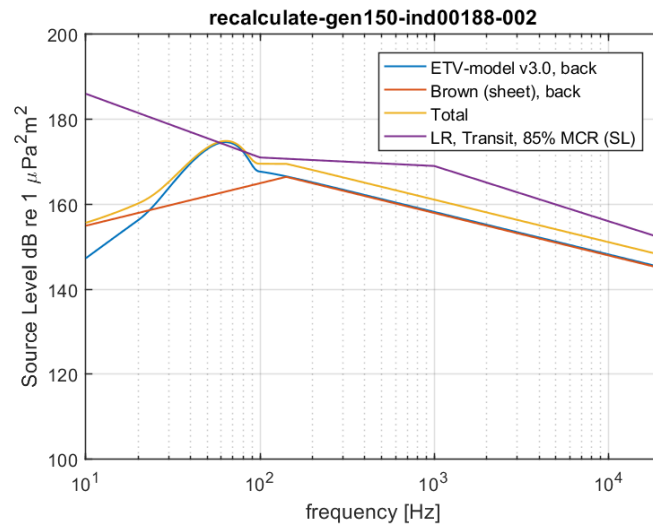
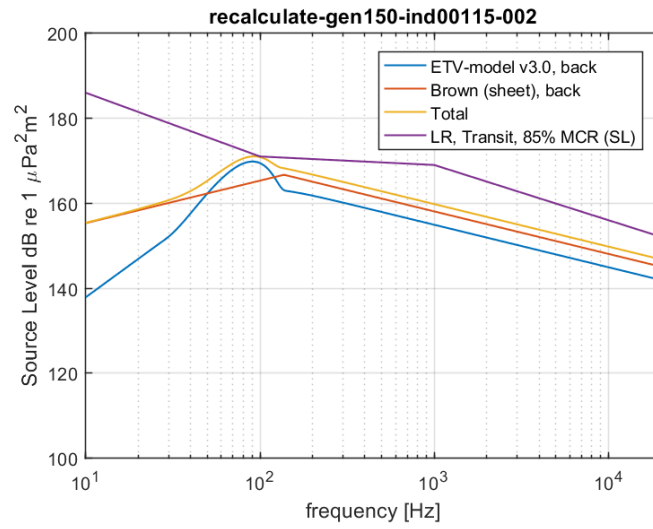
COMPARISON OF SECTIONAL PROFILES (CONSTRAINED)



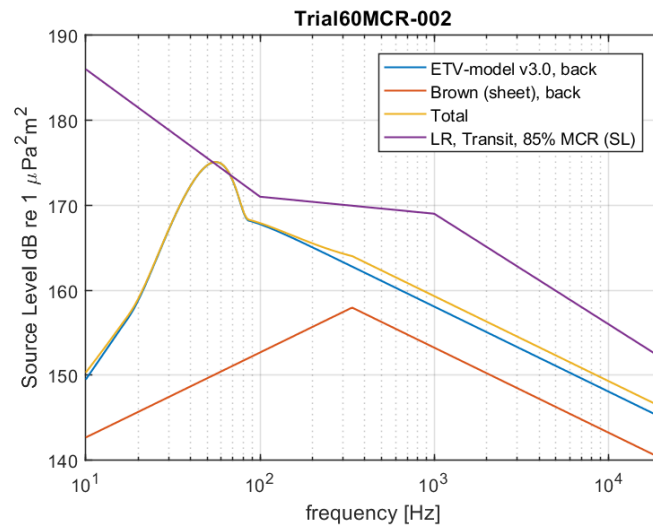
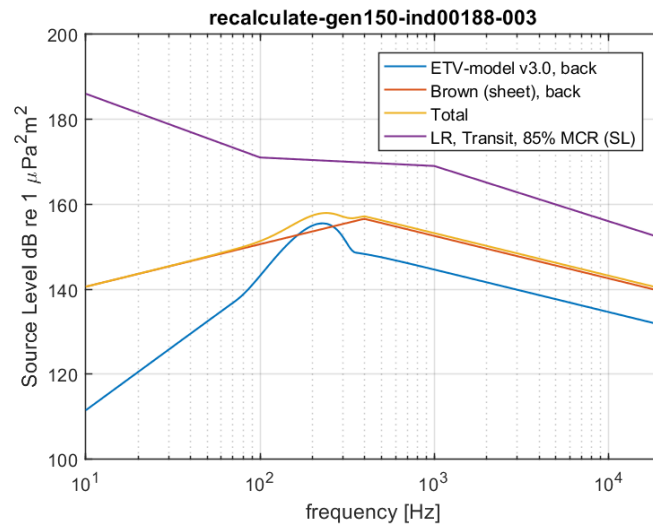
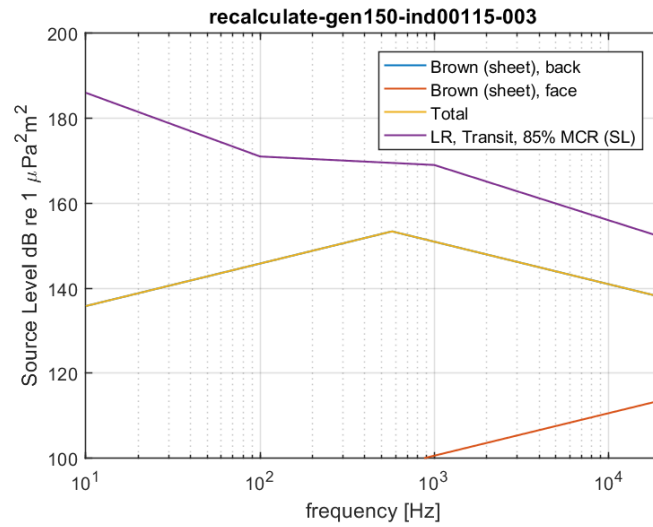
UNDER WATER NOISE LEVEL VERSUS FREQUENCY FOR THE VESSEL IN OPERATIONAL CONDITION AT 80% MCR (TOP : UNCONSTRAINED PROPELLER #76, MIDDLE: UNCONSTRAINED VARIANT #100, BOTTOM: REFERENCE PROPELLER).



UNDER WATER NOISE LEVEL VERSUS FREQUENCY FOR THE VESSEL IN OPERATIONAL CONDITION AT 60% MCR (TOP: UNCONSTRAINED PROPELLER #76, MIDDLE: UNCONSTRAINED VARIANT #100, BOTTOM: REFERENCE PROPELLER).



UNDER WATER NOISE LEVEL VERSUS FREQUENCY FOR THE VESSEL IN OPERATIONAL CONDITION AT 80% MCR (TOP: CONSTRAINED PROPELLER #115, MIDDLE: CONSTRAINED VARIANT #188, BOTTOM: REFERENCE PROPELLER).



UNDER WATER NOISE LEVEL VERSUS FREQUENCY FOR THE VESSEL IN OPERATIONAL CONDITION AT 60% MCR (TOP: CONSTRAINED PROPELLER #100, MIDDLE: CONSTRAINED VARIANT #188, BOTTOM: REFERENCE PROPELLER).

# **APPENDICES**



## APPENDIX I

### LIST OF SYMBOLS

Symbol	Symbol in computer print	Title
<b>GEOMETRY OF SHIP AND PROPELLER</b>		
$A_{BT}$		Transverse cross-section area of bulbous bow
$A_E$		Expanded propeller blade area
$A_E/A_O$		Expanded propeller blade area ratio
$A_M$		Midship sectional area below still waterline
$A_O$		Propeller disc area
$A_T$		Transom area below still waterline
$A_T/A_M$		Transom area ratio
$A_W$		Waterplane area
$A_X$		Maximum transverse sectional area below still waterline
$A_V$	AV	Area of portion of ship above waterline projected normally to the direction of relative wind
B		Maximum breadth moulded at or below still waterline
$B_M$		Maximum breadth moulded at midship
$B_{WL}$		Maximum breadth moulded at still waterline
c		Chord length of propeller blade section
c/D		Chord length-diameter ratio
$C_{REF}$		Chord length between reference line and leading edge
$C_t$		Chord length between maximum thickness point and leading edge
$C_B$		Block coefficient
$C_M$		Midship section coefficient
$C_P$		Longitudinal prismatic coefficient
$C_{WP}$		Waterplane area coefficient
d		Hub diameter
d/D		Hub-diameter ratio
D		Propeller diameter
FB		Position of centre of buoyancy aft of FP
f		Camber of propeller blade section
$h_o$		Submergence of propeller shaft axis measured from still water-plane
$h_B$		Height of centroid of $A_{BT}$ above keel
$i_E$		Half angle of entrance
$L_{OA}$		Length overall
$L_{OS}$		Length overall submerged
$L_{PP}$		Length between perpendiculars
$L_{WL}$		Length on still waterline
LCB		Longitudinal position of centre of buoyancy

Symbol	Symbol in computer print	Title
P		Propeller pitch
P/D		Pitch-diameter ratio
r		Radius of propeller blade section
R		Radius of propeller
S,S <sub>HULL</sub>		Projected wetted surface bare hull
S <sub>APP</sub>		Wetted surface area appendages
S <sub>1</sub> ,S <sub>TOT</sub>		Total wetted surface area
t		Maximum thickness of propeller blade section
t/c		Maximum thickness-chord length ratio
T		Mean draught moulded
T <sub>A</sub>		Moulded draught at aft perpendicular
T <sub>F</sub>		Moulded draught at forward perpendicular
dTA	dTA	Dynamic draught change at aft perpendicular
dTF	dTF	Dynamic draught change at forward perpendicular
Z		Number of blades
$\lambda$		Scale ratio
$\Phi$		Pitch angle of propeller section
$\nabla$	DISV	Displacement volume moulded
-m	-M	Subscript for model
-s	-S	Subscript for ship

Symbol	Symbol in computer print	Title
<b>RESISTANCE, OPEN WATER AND PROPULSION</b>		
$AC_{Res}$		Ship resistance admiralty coefficient
$AC_{Prop}$		Ship propulsive power admiralty coefficient
$C_A$	CA	Total Incremental resistance coefficient for model-ship correlation
$C_{A0}$	CA_0	$C_A$ basic
$C_{Arough}$	Crough	$C_A$ roughness
$C_{Aas}$	Caas	$C_A$ air resistance
$C_{Abk}$	Cbk	$C_A$ bilge keels
$C_{Aballast}$	Cballast	$C_A$ small draught
$C_{AD}$	CAD	Admiralty coefficient for propulsion
$C_D$		Drag coefficient
$C_{D\bar{V}}$		Power-displacement coefficient
$C_E$	CE	Admiralty coefficient for resistance
$C_F$	CF	Specific frictional resistance coefficient
$\Delta C_F$		Roughness allowance coefficient
$C_L$	CL	Lift coefficient
$C_P$		Power loading coefficient
$C_Q$	CQ	Propeller torque coefficient
$C_{QBL}$	CQBL	Propeller blade spindle torque coefficient
$C_R$	CRES	Specific residual resistance coefficient
$C_T$	CT	Specific total resistance coefficient
$C_{Th}$		Thrust loading coefficient
$C_{TP}$	CTP	Propeller thrust coefficient
$C_{TD}$	CTD	Duct thrust coefficient
$C_V$	CV	Specific total viscous resistance coefficient
$C_W$	CW	Specific wavemaking resistance coefficient
$C_X$	CX	Specific air resistance coefficient
Ⓒ	CIRCC	R.E. Froude's resistance coefficient
F	F	Towing force in propulsion test
$F_D$	FD	Viscous scale effect on resistance
$F_n$	FN	Froude number
$F_P$	PULL	Pull of ship
$F_{PO}$	PULL	Pull of ship in bollard condition
Ⓕ	CIRCF	R.E. Froude's frictional resistance coefficient
g		Acceleration due to gravity
J	J	Advance coefficient
$J_V$	JV	Apparent advance coefficient
1+k	1+K	Three-dimensional form factor on flat plate friction

Symbol	Symbol in computer print	Title
$K_p$		Equivalent sandroughness of propeller blade surface
$K_s$		Roughness height of hull surface
$K_{siP}$	$K_{siP}$	Dependency of propulsive efficiency with resistance increase
$K_{siN}$	$K_{siN}$	Dependency of propeller shaft speed with power increase
$K_{siV}$	$K_{siV}$	Dependency of propeller shaft speed with speed change
$K_Q$	$K_Q$	Torque coefficient
$K_T$	$K_T$	Thrust coefficient
$K_{TD}$	$K_{T-D}$	Duct thrust coefficient
$K_{TP}$	$K_{T-P}$	Propeller thrust coefficient
$K_{TS}$	$K_{T-S}$	Stator thrust coefficient
$\textcircled{K}$	CIRCK	R.E. Froude's speed-displacement coefficient
MCR		Maximum continuous rating
SMCR		Specified maximum continuous rating
NCR		Normal continuous rating
$n$	$N$	Rate of revolutions
$P_B$		Brake power
$P_D$	$PD$	Power delivered to the propeller(s)
$P_E$	$PE$	Effective power
$P_I$		Indicated power
$P_S$	$PS$	Shaft power
$Q$	$Q$	Torque
$R$	$R$	Resistance in general
$R_n$	$RN$	Reynolds number
$R_A$		Model-ship correlation resistance
$R_F$	$RF$	Frictional resistance
$R_V$	$RV$	Total viscous resistance
$R_W$	$RW$	Wavemaking resistance
$s_A$		Apparent slip ratio
$s_R$		Real slip ratio
$t$	$THDF$	Thrust deduction fraction
$t^*$		Thrust deduction fraction from load variation test
$T$	$TH$	Thrust
$T_D$	$TH-D$	Duct thrust
$T_P$	$TH-P$	Propeller thrust
$T_S$	$TH-S$	Stator thrust
$T_U$	$TH-U$	Azimuthing thruster unit thrust
$t_v$	$TV$	Running trim

Symbol	Symbol in computer print	Title
$V$	$V$	Speed of ship or ship model
$V_r$	$V_r$	Radial flow velocity component in the direction of the z-axis of the Pitot tube, and is positive if directed down for strut orientation tests or outward in a wake survey
$V_t$	$V_t$	Tangential flow velocity component in the direction of the y-axis of the Pitot tube, and is positive if directed to port for strut orientation tests or in clockwise direction in a wake survey
$V_x$	$V_x$	Longitudinal flow velocity component in the direction of the x-axis of the Pitot tube, and is positive if directed aft
$V_A$	$V_A$	Advance speed of propeller relative to water flow
$w_T$	$W_T$	Effective wake fraction on thrust identity
$w_Q$	$W_Q$	Effective wake fraction on torque identity
$\beta$		Advance angle of propeller blade section
$\beta_h$		Angle of the flow in the x-y plane of the Pitot tube co-ordinate system, and is positive if the flow is directed to port for strut orientation tests
$\beta_v$		Angle of the flow in the x-z plane of the Pitot tube co-ordinate system, and is positive if the flow is directed to the hub for strut orientation tests
$\eta_B$		Propeller efficiency behind ship
$\eta_D$	ETA-D	Propulsive efficiency
$\eta_E$	ETA- $\epsilon$	Merit coefficient
$\eta_G$		Gearing efficiency
$\eta_H$	ETA-H	Hull efficiency
$\eta_M$		Mechanical efficiency
$\eta_o$	ETA-O	Propeller efficiency in open water
$\eta_R$	ETA-R	Relative-rotative efficiency on thrust or torque identity
$\eta_S$		Shafting efficiency

Symbol	Symbol in computer print	Title
<b>CAVITATION, HULL PRESSURES, SHAFT FORCES AND NOISE</b>		
$a_{x0.8}$		Longitudinal clearance from propeller clearance curve to stern frame at a height of 0.8 R above propeller shaft axis
$a_z$		Vertical clearance of propeller tip in top position to the hull
$A_i$		Single amplitude of i-th harmonic component of periodic pressure signal
$B_s$		Waterline beam at station at most forward point of screw aperture
$c$		Speed of sound
$C$		Empirical constant
$C_p$		Pressure coefficient
$D_M$		Depth moulded
$E_{H,V}$		Thrust eccentricity
$f$		Frequency in general
$f_1$		Blade passage frequency
$f(\Theta)$		Function of mean periodic pressure signal
$F_{H,V}$		Propeller-induced dynamic force acting on the shaft
$F_{x,y,z}$	FX,FY,FZ	Propeller-induced dynamic force acting on the hull
$F_{z\ eq}$		Equivalent vertical excitation force
$g$		Acceleration due to gravity
$h$		Immersion in general
$J$	J	Advance coefficient
$M_{H,V}$		Propeller-induced dynamic moment acting on the shaft
$M_{x,y,z}$	MX,MY,MZ	Propeller-induced dynamic moment acting on the hull
$n$	N	Rate of revolutions
$p$		Sound pressure
$p_o$		Ambient pressure
$p_v$		Vapour pressure of water
$r$		Distance to cavitating propeller
$R_n$	RN	Reynolds number
$V$	V	Speed of ship or model
$V_A$	VA	Advance speed of propeller relative to water flow
$\alpha_i$		Phase angle of i-th component in harmonic function
$\Theta$		Angular propeller blade position
$\rho$		Mass density of water

---

Symbol	Symbol in computer print	Title
$\sigma_f$		Non-dimensional parameter for frequency
$\sigma_n$		Cavitation number related to rotation rate
$\sigma_p$		Non-dimensional parameter for sound pressure
$\sigma_v$		Cavitation number related to flow velocity

---

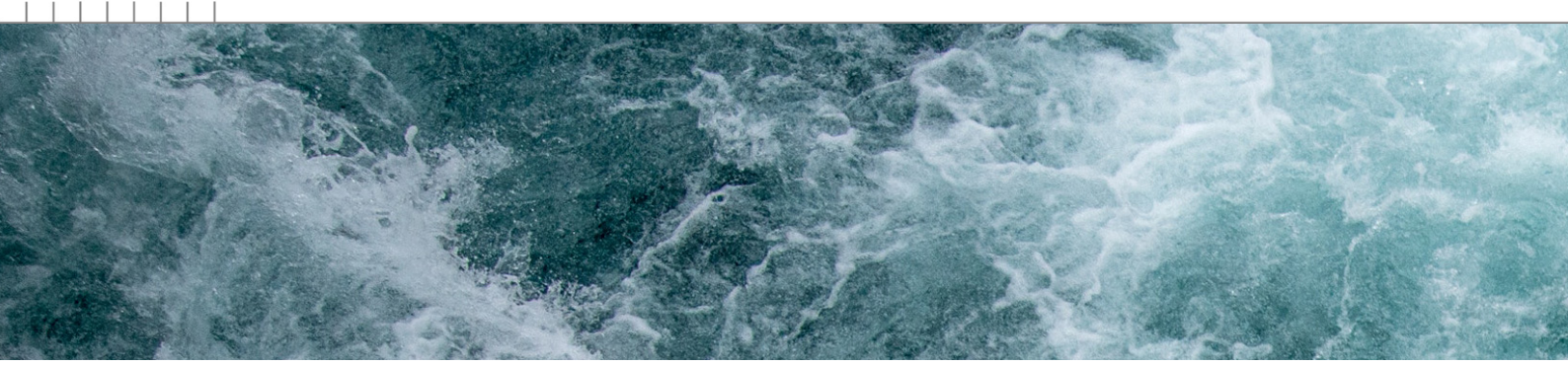
-H	-H	Subscript for horizontal
-m	-M	Subscript for model
-s	-S	Subscript for ship
-v	-V	Subscript for vertical



Report No. 33418-2-POW

# **DOCUMENTATION SHEETS**





# DESP

## Prediction of propulsive performance

The computer program DESP predicts the resistance and propulsion characteristics of displacement ships. The predictions are based on formulas obtained from a regression analysis on results of model experiments and sea trials.

### References

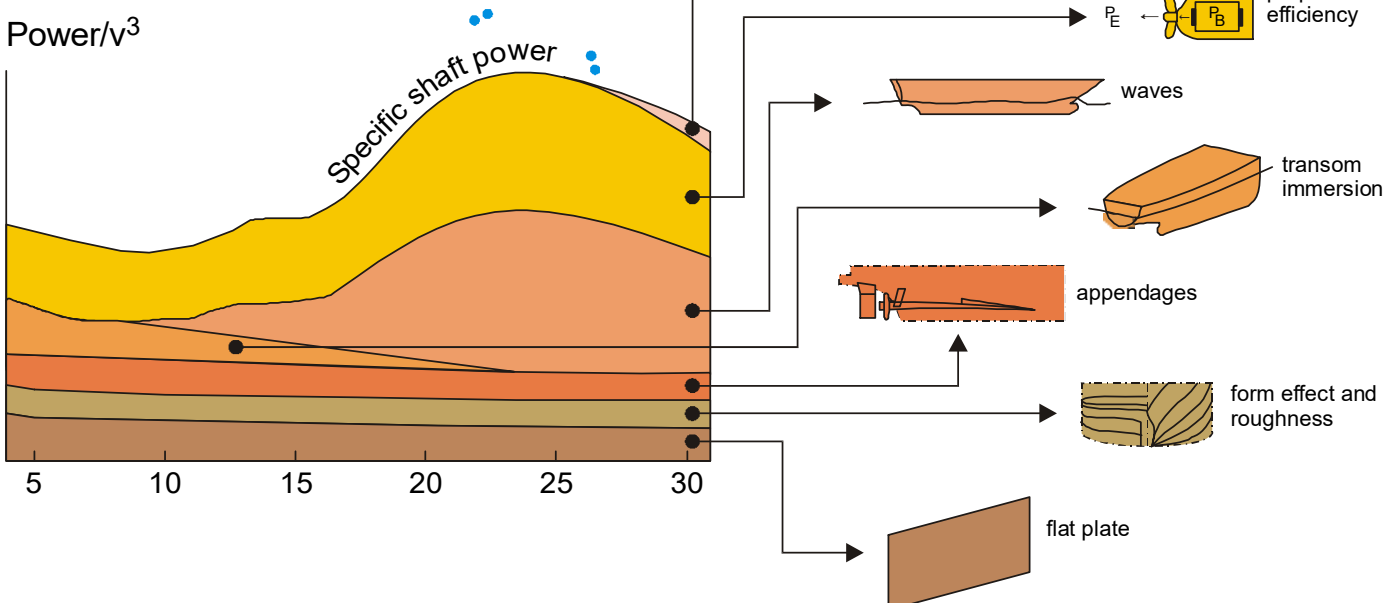
- Holtrop, J.; "A Statistical Resistance Prediction Method with a Speed Dependent Form Factor", SMSSH 88, Varna, October 1988.
- Holtrop, J.; "A Statistical Re-analysis of Resistance and Propulsion Data", International Shipbuilding Progress 31, November 1984.

### Applications

DESP can be used to estimate the speed and power in the early design stage. The level of confidence in the results can be improved by correlation with test or trial data of similar ships. These data can be used to derive an addition to the Correlation Allowance to be applied as input for the new design.

Example of statistical power prediction

- Full-scale trials



For more information contact MARIN:  
SOSC  
T + 31 317 49 32 37  
E [sosc@marin.nl](mailto:sosc@marin.nl)

## Input

The input of DESP consists of the main dimensions of the ship, the displacement volume, the form coefficients CM, CWP LCB, the bulb particulars, the immersed transom area when at rest and various parameters related to the propeller arrangement. For the calculation of the drag of stream-lined, flow oriented appendages either the equivalent appendage drag factor and wetted surface area or a detailed description of the various appendages can be provided.

## Output

The output consists of the resistance and efficiency components for the design speed or the design power, a review of the resistance, the thrust and the propulsive power as a function of the speed and tables of the pulling performance at both constant torque and at constant power.

## Accuracy

As to the accuracy of DESP it is noted that both systematic and random deviations occur. The latter are about 8 per cent of the delivered power for large comparatively slow ships ( $F_n < 0.25$ ) and tend to be larger in the steep, pre-hump range around  $F_n = 0.3$ .

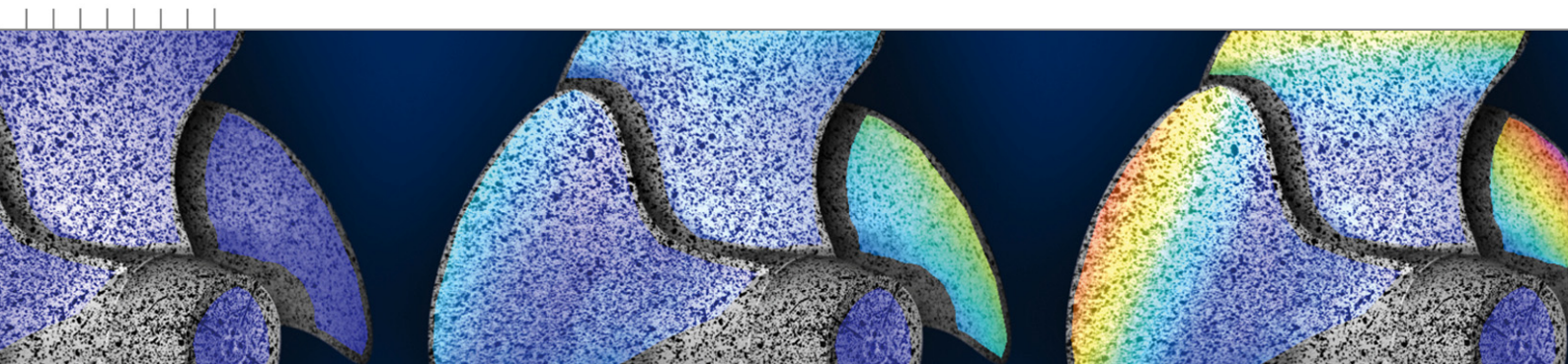
The accuracy in the post hump range is comparable with the accuracy at low speeds. Only when DESP is correlated with relevant model test data, an accuracy similar to model tests can be achieved.

Regarding the systematic deviations it is noted that DESP represents 'the average ship'. Optimised hull forms can perform 5-10 percent better than predicted by DESP. For special hull forms such as dredgers and barges DESP can be used only when checked first against results of similar ships. DESP cannot be used for planing craft.

## Computational approach

DESP applies a simple hydrodynamic model for the resistance components according to the form factor method. As to the propeller-hull interaction statistical formulas were derived for the wake fraction, the thrust deduction factor and the relative-rotative efficiency. A propeller is preliminary designed by using the Wageningen B-series or Ka-series polynomials. The propeller can be designed either for a fixed speed or for a fixed power.

In addition, either the diameter or the rotation rate can be optimised within given constraints. Effects of cavitation on the propulsion, if any, are approximated. Applying DESP for optimising hull forms or hull form details is advised against since the performance effects of various parameters are modelled with limited accuracy.

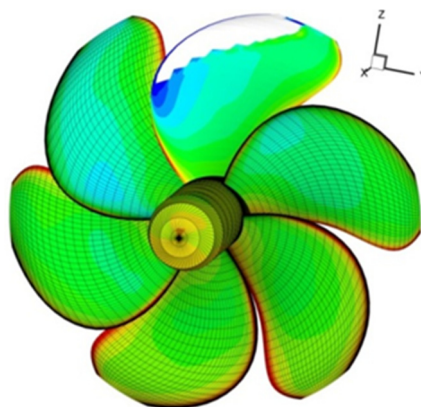


# PROCAL

## Calculating propeller performance in potential flow

MARIN internal use only

The computer program PROCAL calculates the unsteady inviscid flow including sheet cavitation around a propeller geometry using a boundary element method. It is used for the analysis of the propeller performance operating in open water or in a wake field of a ship hull. For the analysis of the hull pressure fluctuations of the non-cavitating and cavitating propeller, a coupling is made with the boundary element method EXCALIBUR, which solves the acoustic wave equation and takes the diffraction of the ship hull and the free surface into account. PROCAL has been developed in the period 2003-2008 within the Cooperative Research Ships organisation (CRS). Extensive use has been made of MARIN's experience in the implementation and application of boundary element methods for propeller analysis.



### Applications

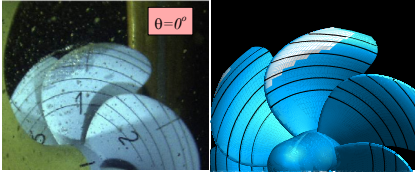
The PROCAL code has been applied to a wide variety of propeller geometries to analyse:

- Open water performance (shaft thrust and torque)
- Behind-hull performance (blade and shaft forces and moments)
- Sheet cavitation inception, extent and volume
- Field velocities and propeller-induced pressure fluctuations

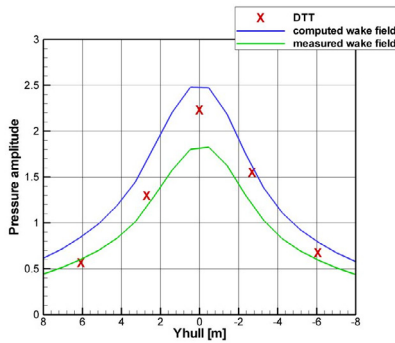
The code is capable of analysing multi-component propulsors and its application for podded propellers, propeller-rudder combinations and ducted propellers is currently being investigated. The code has also been applied for the analysis of wings at varying angles of attack.

### Accuracy

The code has been validated for a large number of different propeller geometries and it gives, in general, good results. The accuracy depends somewhat on the propeller geometry and the operating point, but PROCAL results are very consistent making it a reliable propeller analysis tool for a wide range of propeller geometries. The sheet cavitation model shows very realistic patterns and good correlation with model scale and full-scale observations while predicting only a small phase lead in the growth of the cavity compared to experiments. An acceptable prediction of the pressure pulses on the hull for the first blade passage frequency is obtained.



Comparison between cavitation extents observed during experiments in the Depressurised Towing Tank (DTT) and computed by PROCAL.



Variation of pressure fluctuations on the hull in the propeller plane. PROCAL results are shown using a measured wake field and a PARNASSOS computed ship wake and compared with model scale measurements in the DTT.

## References

- Vaz, G. and Bosschers, J.; “Modelling Three-dimensional Sheet Cavitation on Marine Propellers Using a Boundary Element Method”, Sixth international symposium on Cavitation, CAV2006, Wageningen, 2006.
- Bosschers, J., Vaz, G., Starke, A.R., Wijngaarden, E. van; “Computational Analysis of Propeller Sheet Cavitation and Propeller-ship interaction”, RINA conference MARINE CFD2008, Southampton, 2008.

For more information contact MARIN:  
 SOSC  
 T +31 317 49 32 37  
 E [sosc@marin.nl](mailto:sosc@marin.nl)

## Input

The graphical user interface PROVICE, developed by DRDC Atlantic within the CRS, helps to generate and visualise the panel distribution for the propeller and the hub, to generate the other input files and to analyse the results. The propeller geometry needs to be described by a propeller description file using tabular offset data for the foil sections and radial distribution data of pitch, chord, skew and rake. A hub geometry of arbitrary shape can be generated in PROVICE. The propeller inflow velocity field, representing the effective wake field of the hull, is specified in a ship wake file. Finally, the coordinates where field point velocities and pressures are to be calculated need to be selected. The wake field of the ship hull can be obtained from model tests or from computations using MARIN's RANS solvers PARNASSOS and REFRESCO. These computations can be made for model scale and full-scale conditions. Several methods are available for obtaining effective wake fields from nominal or total wake fields.

## Output

A large variety of output files are generated, showing pressure, cavity thickness and velocity distributions on the propeller and hub geometry, pressure and velocities in field points and hull points, radial distribution of loading, cavity length and volume on the propeller blade, and the integrated forces and moments for each blade and as transmitted to the propeller shaft. All results can easily be visualised using PROVICE.

## Computational approach

PROCAL uses the Morino formulation to solve for the velocity potential. The geometry of the propeller wake is modelled by either an empirical formulation or by an iterative approach computing the wake pitch and tip vortex roll-up. An iterative procedure is applied to satisfy the pressure Kutta condition at the propeller blade trailing edge. The cavitation model iteratively solves the non-linear boundary conditions assuming that the cavity thickness remains small. The analysis of the propeller in a wake field is performed in the time domain for a number of shaft revolutions until the change in propeller wake strength and blade loading between subsequent revolutions is sufficiently small.

## Restrictions

As the code is based on inviscid flow theory, the influence of boundary layers, flow separation and vortex formation is not included. These effects may become important for the analysis of high skew propellers and propellers operating in off-design conditions. The cavitation model is restricted to sheet cavitation and therefore does not include vortex cavitation and cloud cavitation that can be generated from the aft end of the sheet.

MARIN  
P.O. Box 28

6700 AA Wageningen  
The Netherlands

T +31 317 49 39 11  
E [info@marin.nl](mailto:info@marin.nl)

I [www.marin.nl](http://www.marin.nl)  
   



**Contact person**

Tamunoyala S. Koko  
Team Leader, Risk & Reliability  
237 Brownlow Ave, Suite 200  
Dartmouth, NS  
Canada  
B3B 2C7

Registered name    Martec Limited

t: +1 902 407 9815  
e: tamunoyala.koko@lr.org  
w: **lr.org**

Lloyd's Register Group Limited, its subsidiaries and affiliates and their respective officers, employees or agents are, individually and collectively, referred to in this clause as 'Lloyd's Register'. Lloyd's Register assumes no responsibility and shall not be liable to any person for any loss, damage or expense caused by reliance on the information or advice in this document or howsoever provided, unless that person has signed a contract with the relevant Lloyd's Register entity for the provision of this information or advice and in that case any responsibility or liability is exclusively on the terms and conditions set out in that contract.

Lloyd's Register and variants of it are trading names of Lloyd's Register Group Limited, its subsidiaries and affiliates. Copyright © Martec Limited. 2021. Martec Limited is registered under the Corporations Registration Act of Nova Scotia, Canada, doing business as Lloyd's Register Applied Technology Group (ATG). A member of the Lloyd's Register group.

**DOCUMENT CONTROL DATA**

\*Security markings for the title, authors, abstract and keywords must be entered when the document is sensitive

1. ORIGINATOR (Name and address of the organization preparing the document. A DRDC Centre sponsoring a contractor's report, or tasking agency, is entered in Section 8.)  Lloyd's Register Applied Technology Group 237 Brownlow Ave. Suite 200 Dartmouth (Nova Scotia) B3B 2C7 Canada		2a. SECURITY MARKING (Overall security marking of the document including special supplemental markings if applicable.)  CAN UNCLASSIFIED
		2b. CONTROLLED GOODS  NON-CONTROLLED GOODS DMC A
3. TITLE (The document title and sub-title as indicated on the title page.)  Propeller Optimization for Noise Reduction		
4. AUTHORS (Last name, followed by initials – ranks, titles, etc., not to be used)  Arisman, C.		
5. DATE OF PUBLICATION (Month and year of publication of document.)  February 2022	6a. NO. OF PAGES (Total pages, including Annexes, excluding DCD, covering and verso pages.)  172	6b. NO. OF REFS (Total references cited.)  6
7. DOCUMENT CATEGORY (e.g., Scientific Report, Contract Report, Scientific Letter.)  Contract Report		
8. SPONSORING CENTRE (The name and address of the department project office or laboratory sponsoring the research and development.)  DRDC – Atlantic Research Centre Defence Research and Development Canada 9 Grove Street P.O. Box 1012 Dartmouth, Nova Scotia B2Y 3Z7 Canada		
9a. PROJECT OR GRANT NO. (If appropriate, the applicable research and development project or grant number under which the document was written. Please specify whether project or grant.)  Naval Signature Management	9b. CONTRACT NO. (If appropriate, the applicable number under which the document was written.)  W7707-186266/001/HAL	
10a. DRDC PUBLICATION NUMBER (The official document number by which the document is identified by the originating activity. This number must be unique to this document.)  DRDC-RDDC-2022-C195	10b. OTHER DOCUMENT NO(s). (Any other numbers which may be assigned this document either by the originator or by the sponsor.)  TR-21-24-REV03, 19.28074.1125	
11a. FUTURE DISTRIBUTION WITHIN CANADA (Approval for further dissemination of the document. Security classification must also be considered.)  Public release		
11b. FUTURE DISTRIBUTION OUTSIDE CANADA (Approval for further dissemination of the document. Security classification must also be considered.)		

12. KEYWORDS, DESCRIPTORS or IDENTIFIERS (Use semi-colon as a delimiter.)

optimization; propellers; underwater radiated noise; computational fluid dynamics; modelling & simulation; RANS-BEM coupling

13. ABSTRACT/RÉSUMÉ (When available in the document, the French version of the abstract must be included here.)

It is of interest to Transport Canada and Defense Research and Development Canada (DRDC) Atlantic to show a general approach for reducing the noise radiated by commercial shipping vessels. The objective of this task is to undertake propeller optimization design studies for two typical commercial vessels, operating in the west coast of Canada, to determine potential underwater radiated noise reduction benefits.

This report details the calculation methodology used to obtain the ship wake fields for both ships: a 159,000 DWT tanker and a ferry. The ship wake fields are required to account for the effect of the ship wake on the propeller noise calculation and are an integral component in the optimization routine. The ship wake fields are calculated using a coupled Computational Fluid Dynamics (CFD) and a potential flow approach. Results of the optimization study for both vessels are included in Appendix A and B for the 159,000 DWT tanker and the ferry respectively.

In addition to the optimization, CFD simulations of the vessels are conducted for comparison to speed-power predictions. These simulations utilize a sliding mesh methodology for the propeller. The ferry shows better agreement between the CFD and the speed power predictions, with a difference of 8% for the shaft power. The tanker shows a difference of 20% in the shaft power, but the results show oscillations in the forward speed and free surface wake, suggesting that simulation setup refinements may be required to achieve better predictions.

Il est intéressant pour Transports Canada et Recherche et développement pour la défense Canada (RDDC) Atlantique de montrer une approche générale pour réduire le bruit rayonné par les navires commerciaux. L'objectif de cette tâche est d'entreprendre des études de conception d'optimisation des hélices pour deux navires commerciaux typiques, opérant sur la côte ouest du Canada, afin de déterminer les avantages potentiels de la réduction du bruit rayonné.

Ce rapport détaille la méthodologie de calcul utilisée pour obtenir les champs de sillage des deux navires: un pétrolier et un ferry. Les champs de sillage sont nécessaires pour tenir compte de l'effet du sillage du navire sur le calcul du bruit de l'hélice et font partie intégrante de la routine d'optimisation. Les champs de sillage des navires sont calculés au moyen d'analyses numériques de la dynamique des fluides couplée (CFD) et d'une approche des méthodes des intégrales frontières (BEM). Les résultats de l'étude d'optimisation pour les deux navires sont inclus dans les annexes A et B pour le pétrolier et le ferry respectivement.

En plus de l'optimisation, des simulations CFD des navires sont effectuées à des fins de comparaison avec les prédictions vitesse-puissance. Ces simulations utilisent une méthodologie de maillage glissant pour l'hélice. Le ferry montre un meilleur accord entre le CFD et les prédictions de puissance vitesse, avec une différence de 8% pour la puissance à l'arbre. Le pétrolier montre une différence de 20 % dans la puissance à l'arbre, mais les résultats montrent des oscillations dans la vitesse d'avancement et le sillage de surface libre, ce qui suggère que des améliorations de la configuration de la simulation peuvent être nécessaires pour obtenir de meilleures prédictions.